

**Use of carbonaceous materials for the
improvement of agriculture resilience**

By James Michael Shannon

Doctor of Philosophy

Department of Chemistry

University of York

April 2019

Abstract

As global population increases, new methods for more reliant seed germination will play an important role in securing enhanced agri-resilience and, hence, improved crop yields. Seed coatings are commonly used to protect and promote seed germination which often comprise impermeable polymers or microporous materials, e.g., activated carbon (AC), to adsorb chemicals.

Herein, the use of Starbons, carbonaceous mesoporous materials derived from polysaccharides, as novel seed coatings to replace AC is reported. Unlike AC, the mesoporous nature of Starbon allows for both adsorption and desorption. The physico-chemical properties of Starbons are tuneable such that their porosity and surface chemistry can be changed dependent on its carbonisation temperature.

A range of Starbons derived from alginic acid (A300, A500 and A800, where A signifies alginic acid and the three number suffix denotes carbonisation temperature) were prepared via gelation, retrogradation, solvent exchange and, subsequent, carbonisation of alginic acid. Their structural and physico-chemical properties were examined using a range of techniques followed by specific adsorption/desorption, thermodynamic and, kinetic studies with respect to three plant growth hormones (gibberellic acid (GA), indole-3-acetic acid (IAA), kinetin (KI) and one growth inhibitor (abscisic acid (ABA))). The adsorption capacity increased at higher temperatures of carbonisation and was dependent on hormone type; GA possesses a lower capacity than IAA which was attributed to its size and interaction with the surface. Kinetic studies showed evidence of a pseudo-second order rate of adsorption in all cases with a prevalence for multilayers forming in Starbon. Starbon surface area increased with carbonisation temperature due to increasing microporosity. Germination studies showed that Starbon materials improve germination rates and at a greater effect than AC.

This is the first study to show the use of Starbons as seed coatings for improved agri-resilience.

Table of Contents

Abstract	i
Table of contents	ii
List of tables	vi
List of figures	viii
Acknowledgements	xiii
Declaration of interests	xiv
Publications and conference presentations	xiv
1 Aims and Contextualisation.....	1
1.1 Aims	1
1.2 Contextualisation.....	5
1.2.1 Carbonaceous materials and porosity	5
1.2.2 Porosimetry and surface chemistry	12
1.2.3 Adsorption	16
1.2.4 Seed germination	19
1.2.5 Seed treatments	22
2 Experimental	25
2.1 Materials and chemicals.....	25
2.2 Procedures.....	25
2.2.1 Preparation of Starbons: A00; A300; A500, and A800.....	25
2.2.1 Batch mode adsorption capacity testing	27

2.2.2	Thermogravimetric analysis.....	27
2.2.3	UV-vis Spectroscopy.....	27
2.2.4	Light optical Microscopy.....	27
2.2.5	Scanning electron microscopy.....	28
2.2.6	Transmission electron microscopy.....	28
2.2.7	Solid state ¹³ C CP-MAS Nuclear Magnetic resonance (SSNMR)	28
2.2.8	Elemental analysis and XPS analysis.....	28
2.2.9	pH drift measurement.....	29
2.2.10	Boehm titration.....	29
2.2.11	N ₂ Adsorption Porosimetry.....	30
2.2.12	N ₂ Adsorption Porosimetry of materials after adsorption and desorption process.....	31
2.2.13	Determination of adsorption isotherms and kinetics.....	31
2.2.14	Thermodynamic analysis.....	31
2.2.15	SPE Adsorption and desorption testing of plant hormones ...	32
2.2.16	High-performance liquid chromatography analysis (HPLC) ..	33
2.2.17	Long term desorption.....	33
2.2.18	Water holding and retention value.....	33
2.2.19	Liquid chromatography-mass spectrometry (LC-MS).....	34
2.2.20	Seed Germination testing.....	34
2.2.21	Seed Germination testing of seeds using doped materials ...	35
2.2.22	Statistical analysis of germination data.....	35
3	Results and Discussion.....	36
3.1	Preparation and physical characterisation of materials.....	36
3.1.1	Preparation.....	36
3.1.2	Thermogravimetric analysis (TGA).....	36

3.1.3	Inductively coupled plasma (ICP)	39
3.1.4	Carbon-13 nuclear magnetic resonance (¹³ C NMR) of Starbons	39
3.1.5	Microscopic Analysis	40
3.1.6	Optical microscopy	41
3.1.7	Scanning electron microscopy (SEM).....	43
3.1.8	Transmission electron microscopy (TEM).....	48
3.1.9	X-ray photoelectron spectroscopy (XPS).....	49
3.1.10	pH drift and Boehm titration of materials	54
3.1.11	Porosimetry	58
3.1.12	Analysis of Starbon surface via porosimetry.....	60
3.1.13	Porosimetry during adsorption and desorption experiments Error! Bookmark not defined.	
3.1.14	Adsorption capacity	65
3.2	Kinetic adsorption studies	71
3.2.1	Rate of reaction: a kinetic modelling study	71
3.2.2	Pseudo-first order model	71
3.2.3	Pseudo-second order model.....	72
3.2.4	Bangham equation	76
3.2.5	Elovich equation	80
3.2.6	Adsorption kinetic isotherms.....	85
3.2.7	Langmuir isotherm.....	85
3.2.8	Freundlich isotherm	89
3.2.9	Temkin isotherm	93
3.2.10	Dubinin Radushkevich isotherm.....	96
3.2.11	Thermodynamic study of adsorption	105
3.2.12	Intermolecular forces of bioactives.....	114

3.3	Adsorption and desorption studies.....	120
3.3.1	Adsorption and desorption on commercial activated carbon ..	121
3.3.2	Adsorption and desorption on Starbon A300.....	125
3.3.3	Adsorption and desorption on Starbon A500.....	128
3.3.4	Adsorption and desorption on Starbon A800.....	130
3.3.5	In flow and static desorption of leachates.....	133
3.3.6	Water holding capacity (WHC) and Water retention value (WRV)	140
3.3.7	Extended study: influence of seed exudates	142
3.4	Batch germination testing	149
3.4.1	Plant hormone testing (tomato seeds).....	149
3.4.2	Lettuce seed germination	153
3.4.3	Tomato seed germination.....	156
3.4.4	Tomato seed germination using Starch and A00.....	163
3.4.5	Statistical analysis of tomato seed germination	167
4	Summary and future work.....	172
5	Conclusions	175
6	Appendix.....	177
7	Abbreviations	190
7.1	References	192

List of Tables

Table 1. A summary of the differences between physisorption and chemisorption.....	17
Table 2. Elemental analysis of Starbon materials	38
Table 3. XPS analysis of AC.	50
Table 4. XPS analysis of AA.	51
Table 5. XPS analysis of A00.....	51
Table 6. XPS analysis of A300.....	52
Table 7. XPS analysis of A500.....	53
Table 8. XPS analysis of A800.....	54
Table 9. pH _{pzc} of Starbons, precursor and AC.....	56
Table 10. Boehm titration results of materials tested.....	58
Table 11. Porosity data for activated carbon (AC) and Starbons (A300, A500 and A800).....	60
Table 12. Adsorption and Desorption porosimetry analysis of materials.	64
Table 13. Adsorption capacity of hormones adsorbed onto Starbons and activated carbons (at equilibrium).....	67
Table 14. Modelling of pseudo first and second order reaction. (2 repetitions)	73
Table 15. Modelling of the Bangham equation (2 repetitions)	78
Table 16. Modelling of the Elovich equation (2 repetitions)	82
Table 17. Modelling of the Langmuir isotherm (2 repetitions).....	86
Table 18. Modelling of the Freundlich isotherm (2 repetitions).....	90
Table 19. Modelling of the Temkin isotherm. (2 repetitions)	94
Table 20. Modelling of the Dubinin Radushkevich isotherm (2 repetitions)	100
Table 21. Thermodynamic parameters of Gibberellic acid.	107
Table 22. Thermodynamic parameters of Indole-3-acetic acid.....	108
Table 23. Thermodynamic parameters of Kinetin.....	109
Table 24. Thermodynamic parameters of abscisic acid.	110
Table 25. Equilibrium point of ΔG	114
Table 26. Computational analysis (MM2) of bioactives tested.	115
Table 27. A closer look at bioactives.....	118

Table 28. Water holding capacity (WHC) of selected materials.	140
Table 29. Water retention value (WRV) of selected materials.....	141
Table 30. LC-MS adsorption and desorption results for tomato seeds.	145
Table 31. T50 % values for increasing dosages of Gibberellic acid.	150
Table 32. T50% points of tomato seeds with doped and non-doped material.	158
Table 33. Porosimeter comparison between AC, A300, A00, Alginic acid .	163
Table 34. T50 % of all tomato seeds with all tested materials.....	164
Table 35. One-way factor ANOVA of T50% for both material testing and control doping.	169
Table 36. Post hoc t test of non-doped materials.....	169
Table 37. Two-way ANOVA of doped materials.	170
Table 38. Post hoc t-test of doped materials.....	170
Table 39. ICP analysis of Alginic acid. (Values below 1 ppm not included).	177
Table 40. ICP analysis of Starbon precursor. (Values below 1 ppm not included).	178

List of Figures

Figure 1. An exemplar seed coating.....	1
Figure 2. A) Gibberellic acid, B) Indole-3-acetic acid, C) Kinetin and, D) Abscisic acid.	3
Figure 3. Methodology of SPE: 1. Preparation of cartridge; 2. Condition with selected solvent; 3. Washings with deionised water; 4. Loading of Adsorbate, and; 5. Desorption of adsorbate.	4
Figure 4. Representation of a germination experiment with a layer of Starbon and seeds placed over them.	5
Figure 5. Schematic showing the difference of Starbon functionality with respect to the carbonisation processing temperature. ¹⁵	6
Figure 6. Adsorption isotherms I, II and III.....	8
Figure 7. Adsorption isotherms IV, V and VI	8
Figure 8. An illustration of capillary condensation, note pore filling (A and B) followed by a slowed overall desorption (C, D and E)	10
Figure 9. An illustration of the five most common hysteresis loops.	11
Figure 10. A summary of pores. A. Open pore, B. Pore channel, C. Blind pore and D. Closed pore	13
Figure 11. Movement through pores, A. Free diffusion, B. Knudsons diffusion, C. Surface diffusion, D. Activated diffusion.	14
Figure 12. Three different methods a porosimeter may use to determine surface adsorption on an adsorbate. A. Molecular model, B. Molecular surface. C. Perfected model.....	16
Figure 13. A summary of diffusion, A. Mass transport, B. Film diffusion (external) and C. Pore diffusion (internal).....	19
Figure 14. Stages of germination and early seed development (note the emergence of the radicle. ⁵¹	20
Figure 15. Three methods used in the seed pelletisation process. ⁴	23
Figure 16. The stages of creating Starbon precursor from Alginic acid. A. initial, B. Gelation, C. Retrogradation, D. Freeze drying	26
Figure 17. Alginic acid monomer.	36
Figure 18. Thermogravimetric of Starbons	37

Figure 19. Optical microscope of A. Alginic acid. B. A00. C. Activated carbon. D. Starbon A300. E. Starbon A500 and F. Starbon A800. (x 200 magnification)	42
Figure 20. A+B. Alginic acid at x 250 and x 10k magnification. C+D. A00 at x 250 and x 10k magnification	44
Figure 21. SEM images at x 750 magnification. A.AC, B. A300, C. A500 and D A800.....	45
Figure 22. SEM image of AC at x 6000 magnification.....	46
Figure 23. SEM image of A300 at x 6000 magnification.	46
Figure 24. SEM image of A500 at x 2500 magnification.	47
Figure 25. SEM images of A800 at x 2000 and x 15,000 magnification.	47
Figure 26. A, B, Alginic acid at 30x and 98x magnification. C, D, A00 at x30 and x98 magnification.	48
Figure 27. TEM images of A. AC. B. A300. C. A500 and D. A800 (x 98k magnification).....	49
Figure 28. pH drift and determination of pH_{pzc}	56
Figure 29. Porosimetry data of mesoporous materials.....	59
Figure 30. A. ink bottle and B. capillary shaped pore.....	60
Figure 31. Total surface area ($m^2 g^{-1}$) of AC and Starbon materials.....	61
Figure 32. Total pore volume ($cm^3 g^{-1}$) of AC and Starbon materials.....	61
Figure 33. Adsorption capacity of bioactives for each material. (A) AC (B) A300 (C) A500 and (D) A800.	69
Figure 34. Pseudo second order for all tested materials and hormones. A. AC, B. A300, C. A500, D. A800 (four repetitions).	76
Figure 35. Bangham equation for all tested hormones and materials. A. AC, B. A300, C. A500, D. A800 (four repetitions).....	80
Figure 36. Elovich equation for all tested hormones and materials. A. AC, B. A300, C. A500, D. A800 (four repetitions).....	84
Figure 37. A representation of the Langmuir model, note the homogenous surface and monolayer.....	86
Figure 38. Langmuir Isotherm for all tested hormones and materials. A. AC, B. A300, C. A500, D. A800 (four repetitions).....	88

Figure 39. Model of Freundlich, note the multilayer and heterogenous surface.	89
Figure 40. Freundlich Isotherm for all tested hormones and materials. A. AC, B. A300, C. A500, D. A800 (four repetitions).....	92
Figure 41. Model of Temkin, note the multilayer and heterogenous surface.	93
Figure 42. Temkin Isotherm for all tested hormones and materials.....	96
Figure 43. Pore distribution as theorised by the Dubinin-Radushkevich isotherm. (One variation of the isotherm model).	98
Figure 44. Model of the Dubinin-Radushkevich isotherm. Note the homogenous surface and multilayer formed.	99
Figure 45. Dubinin Radushkevich Isotherm for all tested hormones and materials showing full set of data and zoomed in of initial points.	103
Figure 46. Thermodynamics for all tested hormones and materials. A. AC. B. A300. C. A500 and D. A800 (average over four repetitions).	112
Figure 47. Potential energy interactions, A. Bond stretching, B. Bend stretching, C. Torsion and D non-bonded interactions.	115
Figure 48. Adsorption and desorption of plant hormones through AC in water. (Results show average over 4 repetitions).	122
Figure 49. Adsorption and desorption of plant hormones through activated carbon in ethanol. (Results show average over 4 repetitions).....	123
Figure 50. Adsorption and desorption of plant hormones through activated carbon in mixed solvents (water and ethanol in a 50:50 mix. (Results show average over 4 repetitions).....	124
Figure 51. Adsorption and desorption of plant hormones through A300 in water. (Results show average over 4 repetitions).....	125
Figure 52. Adsorption and desorption of plant hormones through A300 in ethanol. (Results show average over 4 repetitions).....	126
Figure 53. Adsorption and desorption of plant hormones through A300 in mixed solvents (water and ethanol 50:50 mix). (Results show average over 4 repetitions)	127
Figure 54. Adsorption and desorption of hormones through A500 in water. (Results show average over 4 repetitions)	128

Figure 55. Adsorption and desorption of hormones through A500 in ethanol. (Results show average over 4 repetitions).....	129
Figure 56. Adsorption and desorption of hormones through A500 in mixed solvents. (Results show average over 4 repetitions).....	130
Figure 57. Adsorption and desorption of hormones through A800 in water. (Results show average over 4 repetitions).....	131
Figure 58. Adsorption and desorption of hormones through A800 in ethanol. (Results show average over 4 repetitions).....	132
Figure 59. Adsorption and desorption of hormones through A800 in mixed solvents (water and ethanol 50:50 mix). (Results show average over 4 repetitions).....	133
Figure 60. Long term leachate experiment with both agitated and still conditions.....	138
Figure 61. A. Plant exudates tested. A. Salicylic acid. B. Indole-3-acetic acid. C. Jasmonic acid. D. Zeatin. E. Kinetin. F. Abscisic acid and G. Gibberellic acid.	143
Figure 62. LC-MS of two separate tomato seed batches.	144
Figure 63. Adsorption and desorption of bioactives via LCMS (results over 4 repetitions).	148
Figure 64. Germination rate of tomato seeds with increasing doses of Gibberellic acid.	150
Figure 65. Seed germination when doped with GA after 168 hours. A. 100 mg / L, B. 300 mg / L, C. 500 mg / L, D. 1000 mg / L and E. 3000 mg / L.....	152
Figure 66. Total germination of lettuce seeds with both doped materials and non-doped materials over 86 hours. (8 sets of 50 seeds per experiment). Note the overlap for all Starbon results.	153
Figure 67. Lettuce seedling germination testing of control after 48 hours, AC, A300, A500 and A800 after 48 hours.	155
Figure 68. Lettuce seedlings germinated with doped materials at seven days A. Control, B. Activated carbon, C. A300, D. A500 and E. A500.....	156
Figure 69. Total germination of tomato seeds with both doped materials and non-doped materials over 168 hours. (8 repeats per experiment)	157

Figure 70. Tomato seedlings with non-doped materials at 7 days A. Control, B. Activated carbon, C. A300, D. A500 and E. A500.....	161
Figure 71. Tomato seedlings with doped materials at 7 days A. Control, B. Activated carbon, C. A300, D. A500 and E. A800.	162
Figure 72. Total Germination of tomato seedlings with both doped materials and non-doped materials over 7 days. (8 sets per experiment)	164
Figure 73. Tomato seedlings after 7 days for non-doped and doped Starch and A00.....	166
Figure 74. A conceptual model of the film-pore diffusion. ¹³⁸	173
Figure 75. Four derivatives of abscisic acid, A. α -lonylidene acetic acid, B. 1-deoxy- ABA, C. α -lonone and D. ABA methyl ester.....	175
Figure 76. Pore distribution of AC and Starbon materials.	179
Figure 77. Pseudo first order reaction for all tested materials and hormones. A. AC, B. A300, C. A500, D. A800. (four repetitions)	181
Figure 78. ¹³ C NMR of AC.....	186
Figure 79. ¹³ C NMR of A00.....	187
Figure 80. C13 NMR of A300.	187
Figure 81. C13 NMR of A500.	188
Figure 82. C13 NMR of A800.	188
Figure 83. Identification of key plant hormone peaks	189

Acknowledgments

I would like to thank my Academic supervisors Prof James Clark and Dr Avtar Matharu for all their help during my PhD. In particular Dr Matharu whose encouragement, guidance and support from the initial to the final level enabled me to develop an understanding of the subject.

This project would not be possible without the support from Syngenta who not only provided funding but also allowing me to work on such an interesting project but allowed me to visit numerous sites and learn about the project from both an industrial and scientific view.

In particular from Syngenta I am thankful to Dr Martine Deheer, Dr Jeroen Hoffer, Dr Tobias Eckblad, Dr Andro Tjin and Dr Chris Lindsey who have through different stages of the project provided considerable knowledge and expertise to the project whilst ensuring that I was always supported even as the company went through major changes.

Of course I am thankful to my parents and brother who put up with me when I was stressed and pushed me to leave the safety of the Channel Islands and chase my dreams of returning to academia.

To all the friends I have made over the course I say thank you, in particular Jenny and Katie, two housemates I am so grateful to have met and to Jonny who is worth a 5 star review and not the 2 1/2 I gave him.

Finally to Fruzsina, since we have been together you have been given me so much emotional and moral support. Köszönök mindent, szeretlek.

Declaration of Interests

I declare that this thesis was composed by myself, that the work contained herein is my own except where explicitly stated otherwise in the text, and that this work has not been submitted for any other degree or professional qualification except as specified.

Parts of this work have been published in Kinetic and Desorption Study of Selected Bioactive Compounds on Mesoporous Starbons: A Comparison with Microporous-Activated Carbon, *ACS Omega*, **2018**, 3 (12), pp 18361–18369

Publications and Conference Presentations

Kinetic and Desorption Study of Selected Bioactive Compounds on Mesoporous Starbons: A Comparison with Microporous-Activated Carbon, *ACS Omega*, **2018**, 3 (12), pp 18361–18369

Winner of the annual Syngenta Research Conference 2018

1 Aims and Contextualisation

1.1 Aims

Food security, agri-resilience and ensuring sustainable supplies of food is a global grand challenge as global population is set to increase to approximately 8.5 billion by 2030.¹ The UN has released a list of sustainability targets, i.e., Sustainable Development Goals, that governments and industries should aim for in order to sustain and improve life on the planet.² Alleviating hunger or the threat of hunger, improving sustainable consumption and production patterns and improving food security are some of the many key targets.

The primary aim of this research is to investigate alginic acid-derived Starbon materials, as a replacement for activated carbon (AC) in seed coatings for enhanced agri-resilience, i.e., germination.

Seed coatings are multilayer coatings (see Figure 1) that protect the seed from harm, promote germination and are applied in such a way that a near spherical pellet is ultimately produced which aids precision farming practices.³⁻⁶

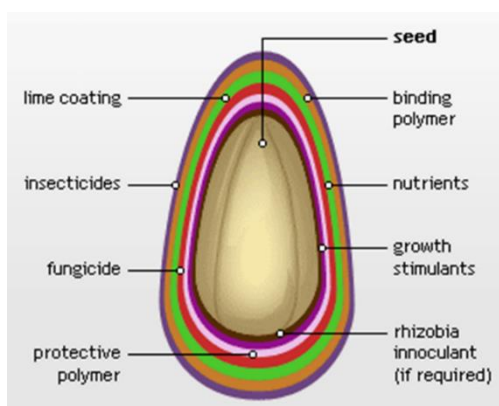


Figure 1. An exemplar seed coating.⁶

Plant hormones (e.g. Gibberellic acid) and other bioactives are added to seed coatings to promote germination or inhibit germination until conditions are suitable for growth. Plant growth promoters work to promote early stage growth of plants by activating different aspects / stages of growth from

germination to cell wall lengthening and cell mitosis. Plant growth inhibitors (e.g. Abscisic acid) work to prevent plant germination and growth while under adverse conditions, e.g., conditions are too cold or there are toxins in the environment which may prevent growth. The final step in manufacturing a seed coating is application of a “pelletising” layer which usually comprises applying a biodegradable material such as activated carbon or wood pulp, or pumice stone which increases seed weight and improves precise seed-drilling in field.⁷⁻¹⁰

Herein, this research specifically aims to:

- i. Synthesise and characterise a range of Starbons derived from alginic acid using standard methodology developed in-house involving: i. gelation; ii. retro gradation; iii. solvent exchange, and; iv. controlled carbonisation. Steps i-iii yield expanded alginic acid which herein will be coded A00. Controlled carbonisation (step iv) will be effected at three different temperatures: 300°C (A300); 500°C (A500), and; 800°C (A800). All Starbon materials (A00, A300, A500 and A800) will be characterised appropriately that reflects chemical and physical changes occurring because of expansion and subsequent carbonisation. For example, nitrogen porosimetry will be an important technique providing information with respect to porosity, pore type, surface area and pore volume. Whereas, XPS and Boehm titrations will evidence surface chemical composition. It is well-known that as the carbonisation temperature increases the surface changes from hydrophilic-like to hydrophobic-like. Surface area also increases with increasing temperature as the mesopore: micropore ratio decreases;
- ii. Determine the adsorption-desorption propensity of the prepared Starbons (A00, A300, A500 and A800) with respect to four bioactives (see Figure 2), three of which are plant growth hormones (gibberellic acid (GA), indole-3-acetic acid (IAA) and kinetin (KI)), and the fourth is a plant growth inhibitor (abscisic acid (ABA)).

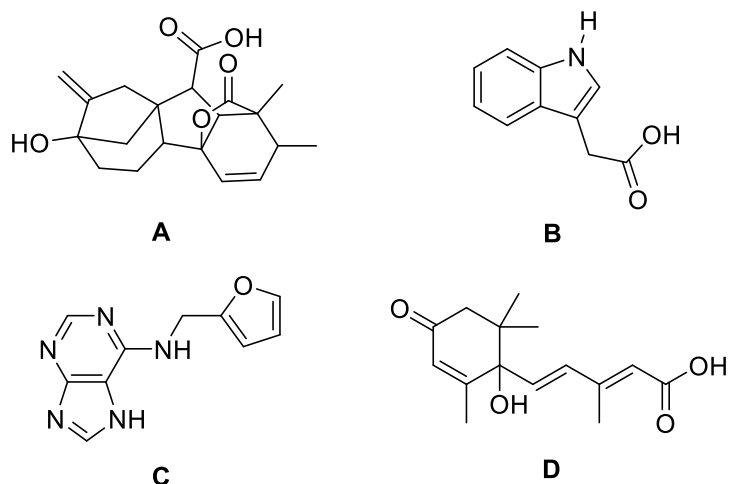


Figure 2. A) Gibberellic acid, B) Indole-3-acetic acid, C) Kinetin and, D) Abscisic acid.

- iii. Solid phase extraction (SPE) methodology will be employed whereby a small plug of Starbon material will be loaded in to a cartridge and conditioned with deionised water and the selected solvent for adsorption experimentation (see Figure 3). A fixed concentration of each bioactive will be passed through the Starbon and the eluate will be analysed by HPLC. The maximum amount of retained material will be the loading capacity (mg g^{-1}). Thereafter, desorption studies will be conducted by passing through solvent (10 ml aliquots) and analysing the eluate by HPLC to develop an initial understanding of desorption characteristics of materials. Multiple

aliquots will be used to observe desorption over multiple washings to determine consistency of desorption (see Figure 3).

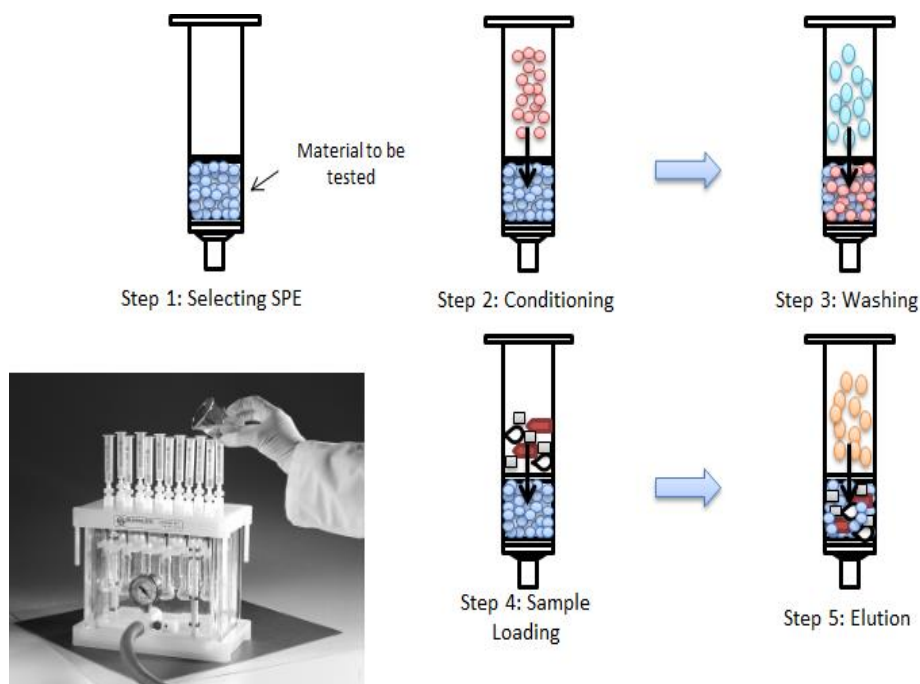


Figure 3. Methodology of SPE: 1. Preparation of cartridge; 2. Condition with selected solvent; 3. Multiple washings with deionised water; 4. Loading of Adsorbate, and; 5. Desorption of adsorbate.

- iv. Determine the kinetics of adsorption and the likely method of adsorption by modelling experimental data on selected adsorption isotherm models. Experiments will be conducted in which adsorption onto Starbons will be analysed at set time intervals (between 0 and 1440 minutes) for kinetic experiments and with varying concentrations for the adsorption isotherms (between 10 and 500 ppm). Results will be analysed via UV-Vis spectroscopy. Once results are obtained kinetic models will be used to understand the kinetics of adsorption as well as modelling to determine the most suitable adsorption isotherms.

- v. Evaluate the materials for their effectiveness as *pseudo* seed coatings by conducting germination experiments. It is important for any experiments conducted to have a set point to determine whether a seed can be counted as germinated or not. In this research, the point at which a seed clearly show a radicle will be deemed as onset of germination. A set number of seeds will be placed in to a pre-prepared petri dish containing Starbon (see Figure 4). Seed counting will be conducted at set times to observe and record seed germination. Eight sets for each experiment will be conducted simultaneously to reduce the potential for error. At this point the T50% (time point at which 50 % of the seeds have germinated) will be determined and the results evaluated via statistical analysis.

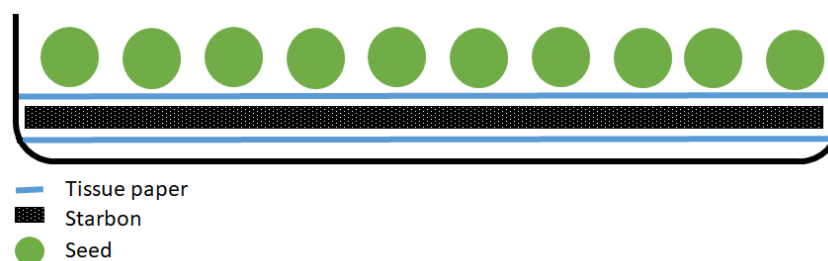


Figure 4. Representation of a germination experiment with a layer of Starbon and seeds placed over them.

1.2 Contextualisation

1.2.1 Carbonaceous materials and porosity

One important factor used to distinguish between different adsorbates is the adsorbate average pore size. IUPAC defines three categories: i. microporous (<2 nm in diameter); ii. mesoporous (>2-<50 nm in diameter), and; macroporous (>50 nm).

Starbons are a mesoporous carbonaceous material derived from polysaccharides such as starch, AA or pectin. Unlike AC which is highly microporous, the mesoporous nature of Starbon allows for both adsorption and desorption of *larger* molecules. The chemical surface of Starbon is tuneable and dependent on its carbonisation temperature (see Figure 5).

Starbons carbonised at low temperatures, such as 300 °C, have a similar structure and functionality to its expanded precursor polysaccharide, i.e., essentially hydrophilic with high oxygen content. At higher temperatures, e.g., 800 °C, similar attributes to activated carbon with high carbon content and hydrophobicity are noted. However, Starbons still retain a partially oxygenated surface compared to activated carbon even at high temperatures.¹¹⁻¹⁴

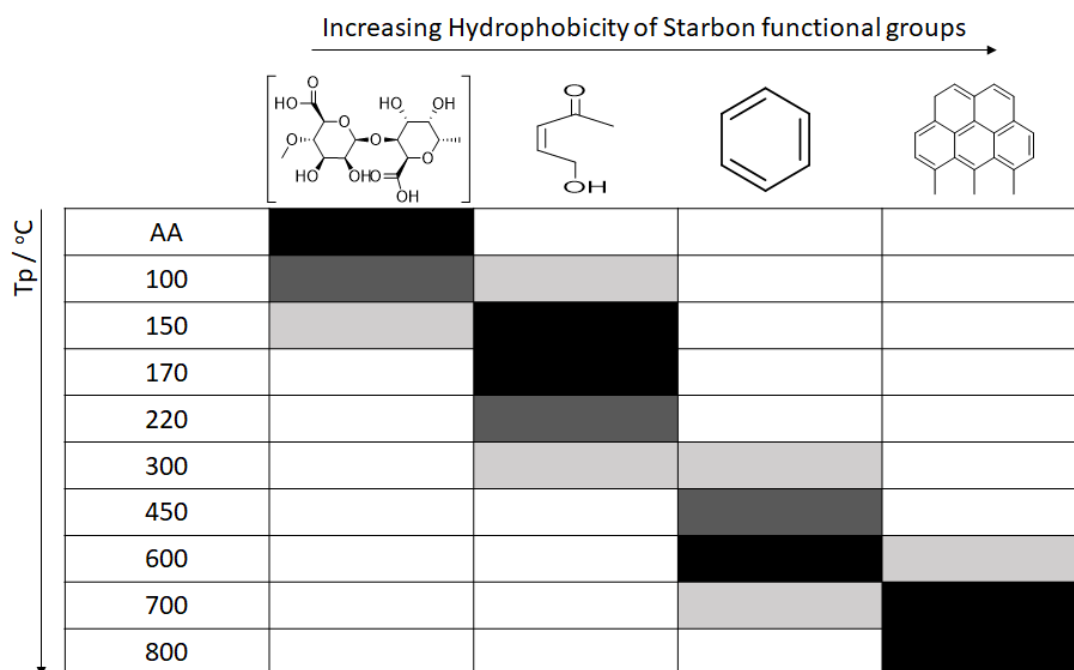


Figure 5. Schematic showing the difference of Starbon functionality with respect to the carbonisation processing temperature.¹⁵

Activated carbon is a carbonaceous material which has been acid treated (washed with an acid before carbonisation) and carbonised at very high temperatures yielding a microporous structure (pore size <2 nm) with high surface area (e.g. over 500 m² g⁻¹). However, a weakness of activated carbon as a desorbent is that, due to its microporosity, certain *large* bioactive compounds can block pores, i.e., they are unable to travel through the structure, reducing the effective surface area available for adsorption. The structure of activated carbon is such that it is classed as a heterogenous material (not uniform along the surface due to defects and uneven pore opening) with its chemical composition primarily made up of carbon with a smaller proportion of oxygen. The structure mostly comprises C-C and C=C

bonds along with aromatic rings which can cause a graphitic like structure to form. This mix of aromatic, aliphatic and alkenic structure allows for a very high degree of interaction with adsorbates. The surface of AC would suggest that due to the mostly carbon surface, polar materials would not interact as strongly to the surface however, the aromaticity found on AC results in greater than expected interactions with polar material based on the primarily non-polar functional groups found on the surface. This effect is known as the polar retention effect. ¹⁶

The high surface area of AC and consequent, very high adsorption capacity per gram, makes it an excellent material in cleaning and removing impurities such as waste dyes from the environment. ¹⁷⁻¹⁹

Adsorption isotherms are used commonly to understand the shape of the surface of an adsorbent. ^{21,22} Adsorption isotherms examine the relationship between gaseous pressure (or liquid concentration) and adsorption on the adsorbent surface with the maximum adsorption amount being achieved at the saturation equilibrium pressure. The six most commonly observed isotherms are shown in Figure 6 and Figure 7.

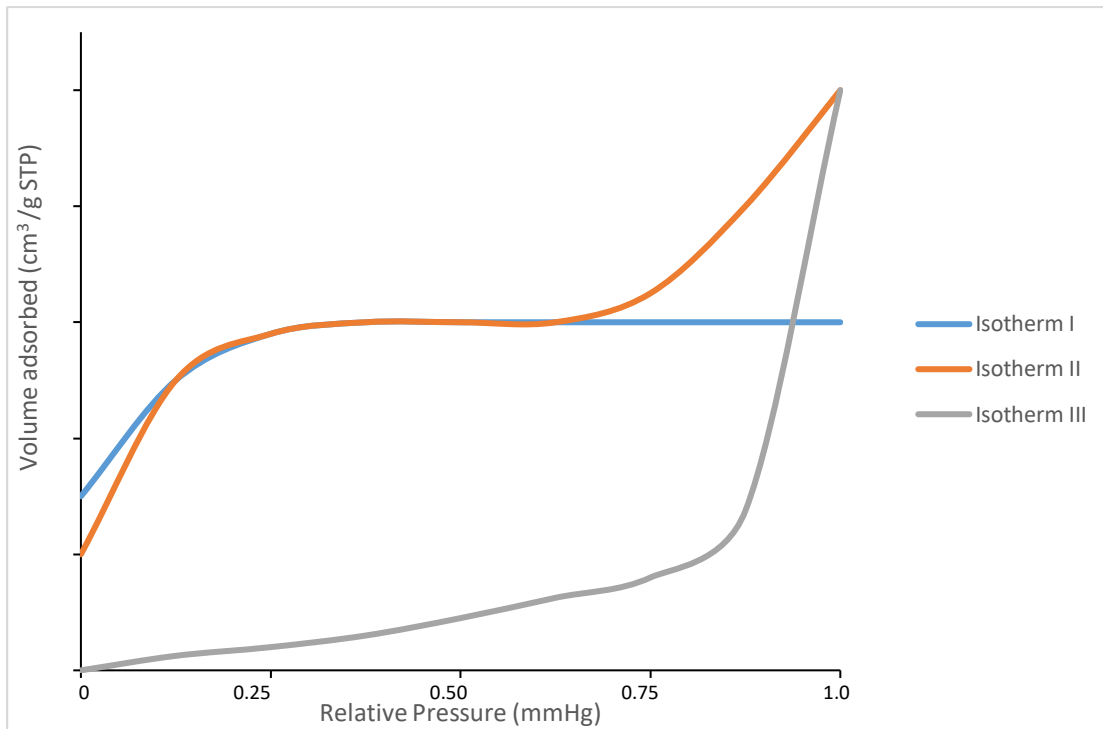


Figure 6. Adsorption isotherms I, II and III

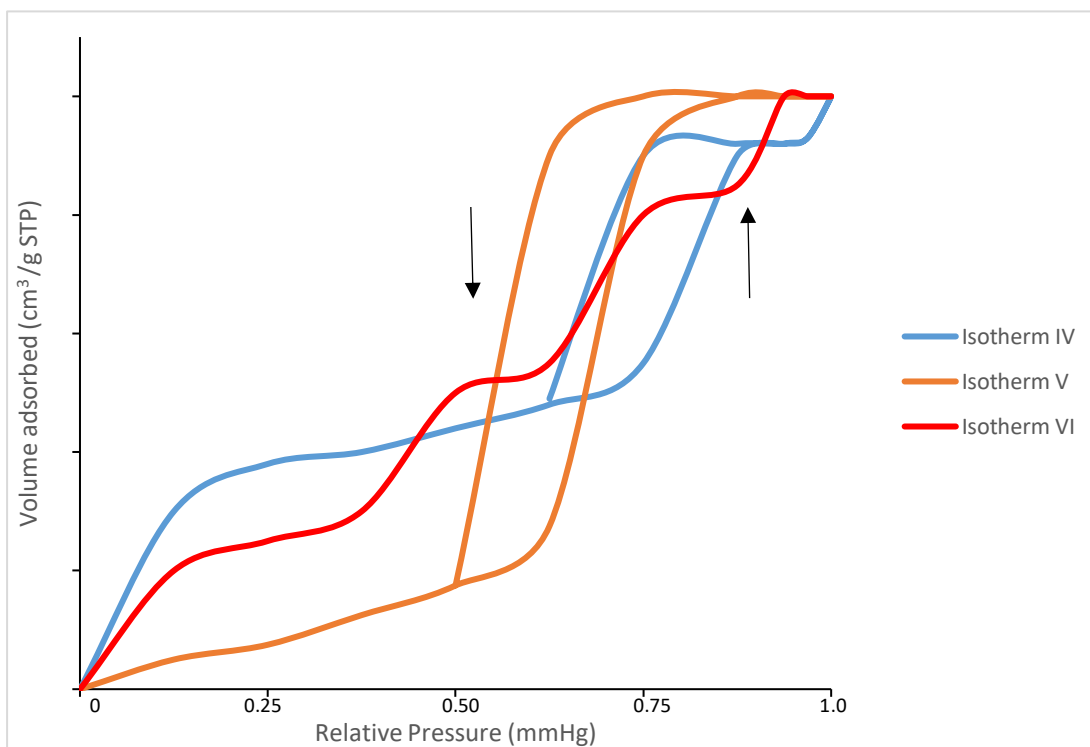


Figure 7. Adsorption isotherms IV, V and VI

Isotherm I (Figure 6) occurs when adsorption occurs up to a saturation point, most commonly occurs when a single monolayer forms on the adsorbent and then stops as all possible pore space has been occupied.

Isotherm II (Figure 6), like isotherm I, shows adsorption up to a saturation point before further adsorption occurs after a period of stability as pressure increases. This occurs due to a monolayer forming during the initial stages of the adsorption process (see the flat section of the isotherm) followed by a second layer of adsorption occurs on top of the initial monolayer forming a multilayer.

The key difference in isotherm III (Figure 6) with respect to isotherms I and II is the lack of monolayer formation at low pressures showing that a multilayer is formed rapidly at higher pressures. The sharp increase in adsorption is due to multilayer formation occurring at a rapid rate as the larger pores are filled as pressure increases. The initial low rate of adsorption may also be a sign of poor interaction between the adsorbate and surface. The increased pressure is then required in order for the rapid multilayer formation.

Isotherm IV (Figure 7) shows adsorption characteristics similar to isotherm II but includes a “hysteresis loop”. Rather than showing identical adsorption/desorption, adsorption remains high at lower pressures but as the pressure decreases it slowly drops to previously observed levels.

Isotherm V (Figure 7) is similar to isotherm IV but shows a rapid decrease in adsorption. This is due to the adsorbate and adsorbent experiencing weak interactions with one another. An example of this is the adsorption of water onto AC.²²

Isotherm VI (Figure 7) shows a few steep increases in adsorption before levelling off. In this case, a monolayer is initially formed and completely covers the adsorbate surface before multilayers form on top of the monolayer and then continually repeats to form an ever-increasing multilayer.

The presence of a hysteresis loop in an adsorption isotherm is an indication of mesoporosity and occurs due to the capillary condensation effect. Capillary

condensation is the mechanism by which an adsorbate is condensed within and then fills the pores of the adsorbate (Figure 8). This condensation occurs at a pressure lower than the saturation equilibrium pressure due to the increased interaction of van der Waals forces from all sides.²³⁻²⁵

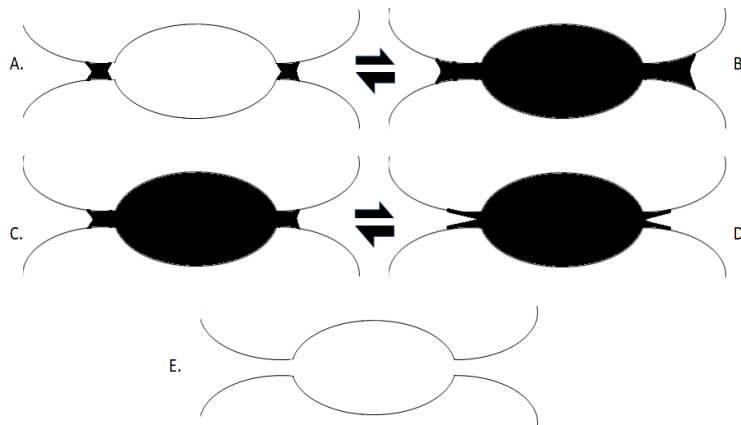


Figure 8. An illustration of capillary condensation, note pore filling (A and B) followed by a slowed overall desorption (C, D and E)

Mesoporous materials have wider pores than microporous materials and are subject to the capillary condensation effect which prevents the pores from filling to adsorption capacity at low pressures as the pores are not completely filled. At higher pressures, an equilibrium pressure (the point in which the pressure has opened for them to be filled (see Figure 8, A-B)) is required before mesoporous pores are filled. In the reverse process, the material does not fully desorb until the pressure returns to a lower pressure than the saturation equilibrium point, which results in slow desorption and thus creates a hysteresis loop (Figure 8, C-E). By determining the shape of the hysteresis loop, an approximation of the mesopore shape can be determined, as they can be classified into 5 sub categories (on the assumption that the hysteresis loop is only due to the presence of mesopores) (Figure 9).^{26,27}

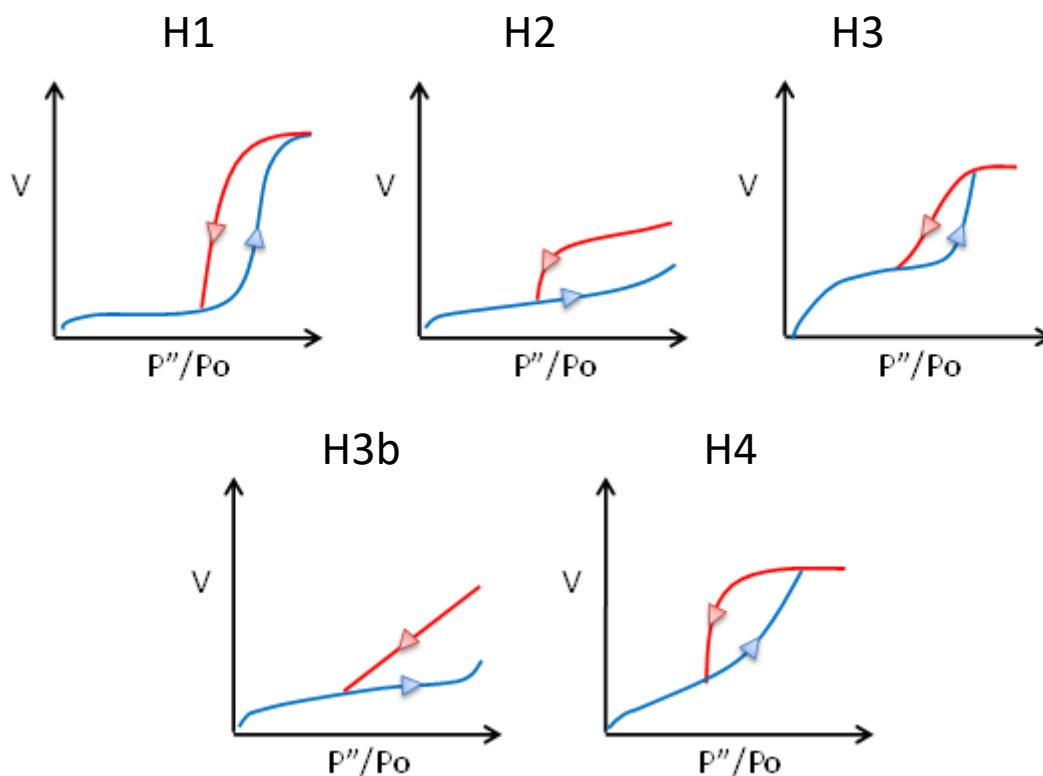


Figure 9. An illustration of the five most common hysteresis loops.

These hysteresis loops were originally known as De Boer's loops, and are now classed via IUPAC as H1-4.^{28,29} H1, shows a rapid rise and decrease in adsorption which indicates ink bottle shaped pores along with expanding capillaries, or consists of cylindrical pores where desorption is decreased due to a bottleneck at a narrow opening. H2 shows a steady decrease in the adsorbed material which is a sign of capillary pores but with narrower capillaries, which results in desorption occurring at a slow but steady rate until pressure decreases enough to allow a rapid desorption through the pores. H3 and H3 (b) suggests that only capillary tubes are formed and are like H2 as both their hysteresis loops indicate that narrow necked capillary tubes are present which results in slow desorption. H4 shows no desorption for a long period followed by rapid desorption, which suggests ink bottle pores along interconnected capillaries are present. This means desorption is difficult until the pressure drops below the capillary condensation pressure, which leads to rapid desorption.

1.2.2 Porosimetry

Adsorption is the scientific principle in which a material (the adsorbent) will bind to the surface of other materials (adsorbate). Adsorption is a method in environmental science used to remove/clean impurities from solutions with activated carbon being one of the more commonly used materials.^{30,31} There have been many mathematical theories developed in order to explain how adsorption occurs ranging from the monolayer formed via the Langmuir isotherm to the Freundlich isotherm which takes into account issues such as multilayers.^{32,33} By using a material with a high surface area to mass ratio it is possible to adsorb substantial amounts of material onto its surface, it is for this reason AC is so commonly used due to its high surface area. By understanding how the adsorption and desorption interactions occur at the surface of the material it becomes possible to predict which materials will be able to adsorb and which will become desorbed back into the environment.^{34,35,36}

Surfaces are in general never perfectly smooth, there are defects and depressions that form throughout the surface of the material. There are two classes of depressions on a surface, “external” and “internal”. External depressions have a width greater than depth and are seen closer to defects on the surface. Internal depressions have a lower width than depth and these internal depressions are commonly known as pores. Porosity is defined as the pores and channels that form throughout a solid and being further placed into sub categories (Figure 10).³⁷

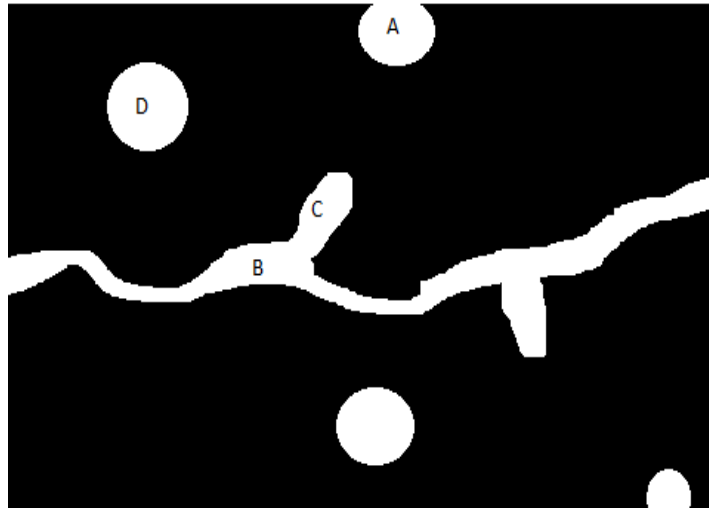


Figure 10. A summary of pores. A. Open pore, B. Pore channel, C. Blind pore and D. Closed pore

Open pores have only one entrance to the surface of the material and can have a large depth into the structure if there is only one opening to the surface. A pore channel is comparable to open pores but with multiple openings on the surface essentially forming a pathway or channel throughout the pore. A blind pore is a pore that forms off an open or pore channel with no direct access to the surface. Finally, a closed pore has no opening and merely an empty space within the solid structure. This is not used in surface area calculation or surface science unless it is opened through changing the material to make it accessible.

There are four forms of diffusion that are observed through pores. It is important to note that while all forms of diffusion may occur, the size of the pore has a significant effect on what the most common form of diffusion observed would be (Figure 11).

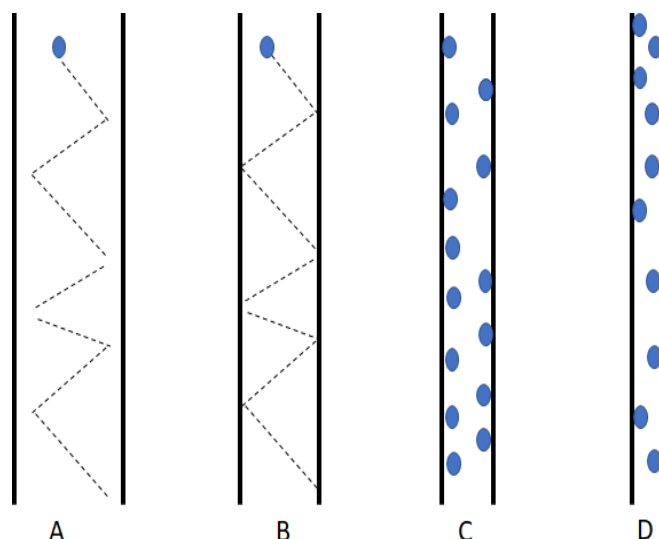


Figure 11. Movement through pores, A. Free diffusion, B. Knudson diffusion (too narrow for complete free diffusion), C. Surface diffusion (little room for free diffusion), D. Activated diffusion (narrowest pores).

Free diffusion is observed in macro and mesopores normally, in which the adsorbate can freely move within the pore but micropores are too narrow for this to occur. Knudson diffusion is when the pore is slightly narrower, and the free movement of the adsorbate is restricted, increasing the potential for interaction between adsorbate and adsorbent which may result in adsorption. Surface diffusion occurs with very narrow pores where adsorbate movement is significantly reduced. Diffusion now occurs due to the adsorbate interacting with the adsorbent and before the prevailing concentration causes diffusion, so the adsorbate will slowly move from adsorbate site to adsorbate site, of note is that there is still some potential for movement away from the adsorbent. Finally, activated diffusion is when the narrowest pores form and the only diffusion or movement through the pore is through active diffusion through the available adsorption sites. This is the slowest form of diffusion and can result in blocking of the pores which reduces the overall potential surface area and reduces desorption potential.^{38,39}

Porosimetry allows Starbons to be examined with mathematical models to calculate overall surface area, as well as microporous and mesoporous area. The BET (Brunauer Emmett and Teller) isotherm was developed in 1938 and

uses an inert gas such as nitrogen to form a multilayer over the adsorbate surface to then calculate the surface area by determining the overall adsorption and then calculating overall surface area from this.⁴⁰ This calculation however is known to result in high deviations from the specific surface area at extreme ranges of pressure in particular at lower pressures where microporosity is usually determined (gives lower results at low pressure and higher than expected for high pressures). The other issue is that it assumes that a multilayer has formed in its calculations which may result from differences to the actual surface area.⁴¹ The Langmuir isotherm assumes that in all cases the adsorbate acts as an ideal gas, and that during the adsorption process there are no deviations on the surface, from this it is possible to determine an idealised surface area. The actual surface area is usually between the BET and Langmuir values. This value is almost always higher than the BET value and the actual surface area but once calculated does allow a comparison to see how close the surface and adsorbate may fit these idealised values. From these methods the mesopore and micropore volume may be calculated based on these assumptions. These methods were selected to reduce the potential error that occurs when using a porosimeter to calculate surface and pore area. However, while error may be reduced there is an inherent risk when using models to calculate surface area due to their assumptions used and the method of calculating the surface area as observed in Figure 12.

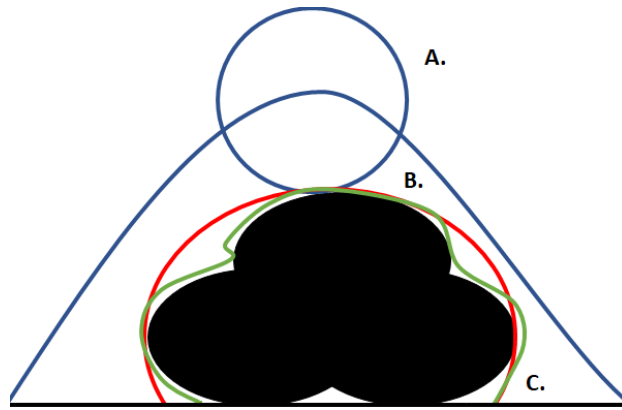


Figure 12. Three different methods a porosimeter may use to determine surface adsorption on an adsorbate. A. Molecular model, B. Molecular surface. C. Perfected model.

From Figure 12, A (molecular model), represents the most commonly used characterise the surface where the molecule (typically nitrogen) is adsorbed on the surface and surface area is calculated based on the molecule coverage which may result in defects not being detected affecting the surface area. B (Molecular surface), takes this further and tries to look at the specific interaction between adsorbate and adsorbent which allows a more accurate representation of surface area, though still not completely accurate due to potential gaps in the surface not detected as most surfaces are not homogenous. Finally, C, is the most accurate characterisation method considering almost all deviations on the surface to calculate surface area. However, C, as a method is very energy and time intensive to run and requires specialised equipment.

1.2.3 Adsorption

There are two known methods in which adsorption occurs, physisorption and chemisorption. Physisorption is the process in which the adsorbate and adsorbent interact with one another via intermolecular interactions such as from Van der Waals forces.^{42,43} This is a weak attraction which can normally be easily broken upon application of external factors such as heating. Physisorption occurs in lower temperatures so must be considered during practical applications such as a seed coating which would be used in soil which generally has a cooler environment (e.g. less than 298 K). Chemisorption is

the adsorption process in which a chemical bond is formed between the adsorbate and surface.^{44,45} This form of adsorption results in stronger bonds which can prevent desorption occurring unless an outside force results in the bond breaking. Chemisorption has been used in a number of well-known catalytic reactions including the Haber process.^{46,47}

The adsorption characteristics between physisorption and chemisorption as two processes are very different and would have a significant effect on the adsorption and more importantly for this project the desorption capabilities of the project (Table 1).

Table 1. A summary of the differences between physisorption and chemisorption

	Physisorption	Chemisorption
Heat of adsorption / kJ mol⁻¹	Below 40 e.g. quite low	Over 80 due to the bulk phase chemical reaction
Rate of adsorption at 273 K	Fast	Slow
Temperature dependence of uptake	Reduces as temperature increases	Increases as temperature increases
Desorption	Easy to occur	Difficult – high energy required to
Desorbed species	Unchanged	Maybe different to original adsorbate
Specificity	Non-specific	Specific
Monolayer coverage	Mono or multi-layered	Monolayered only

Physisorption is made up of weak attractive forces and as such are easily broken when the pressure or temperature changes. Physisorption is inverse to the temperature resulting in adsorption being favoured at lower temperatures and desorption at higher temperatures.

Within this project, physisorption is the preferred adsorption process as desorption of plant growth promoters is preferred. The conditions that would be naturally occurring for a seed coating would be below 298 K with the solvent being water as the primary means for desorption. Chemisorption would require significantly higher energy requirements for desorption to occur. Another issue is that with chemisorption only a monolayer (single layer on the surface) would form, while as if physisorption occurs then a multilayer (multiple layers over the surface) may form which would increase the overall adsorption capacity.

The rate determining step of the adsorption process was also investigated. For adsorption to occur it is first necessary for the adsorbate to be able to reach the adsorbent. This occurs through the adsorbent diffusing through the solution to move through the pores. Movement through the pores was discussed earlier (Section 1.2.2). However, this can be further expanded upon to include diffusion from the bulk solution to the surface. These individual steps are known as mass transport, pore diffusion and film diffusion. Mass transport is the movement of the adsorbate through the bulk solution towards the surface of the adsorbent, pore diffusion is the movement through the pores towards the surface film of the adsorption sites and finally film diffusion which is diffusion through the immobile solution found coating the surface to the adsorption sites.^{19,27,48} Finally, there is the adsorption process itself which may also act as the rate determining step. A demonstration of the diffusion steps can be observed below (Figure 13).

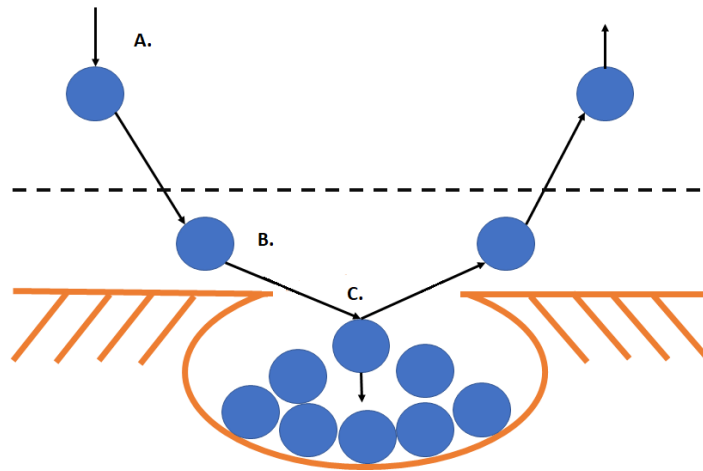


Figure 13. A summary of diffusion, A. Mass transport, B. Film diffusion (external) and C. Pore diffusion (internal).

Generally, there are three cases from these diffusion models which affect the rate determining step;

Case 1: External transport > internal transport (Film diffusion is rate determining step)

Case 2: External transport < internal transport (Pore diffusion is the rate determining step)

Case 3: External transport \approx internal transport

With case 3 diffusion from the bulk of solution to the adsorption sites is not occurring at a significant rate. This can lead to a film forming over the surface with a concentration gradient forming around the particle.⁴⁹

Usually this film diffusion is the rate determining step when there are; small particle sizes, poor phase mixing, low concentration of adsorbate or high affinity for adsorbate and adsorbent. Pore diffusion however is the rate determining step when there are; larger particulate size, good phase mixing, high concentration of adsorbate or a low affinity for adsorbate and adsorbent.^{39,50}

1.2.4 Seed germination

Germination is defined as the process in which dormancy ends and the seed takes in water and nutrients officially ending when penetration of the seed has

occurred with an extrusion emerging from the seed itself. Seeds go through several stages of growth to become the mature plant that can be seen above the soil and eventually harvested (see Figure 5). In this work, only the early stages of plant growth will be considered, namely: i. Imbibition, the seed draws in large amounts of water and nutrients from the environment which initiates growth; ii. Interim, water intake is reduced, and the seed starts to metabolise the stored food, and; iii. Radicule emergence, cells within the seed start to grow and elongate pushing the radicle root out of the seed.



Figure 14. Stages of germination and early seed development (note the emergence of the radicle).⁵¹

At this point it can be stated that the seed has germinated and is now in the early seedling stages. The radicle can now be seen and acts as the primary root required for the seed to anchor into the ground and from which other roots will emerge and grow. The hypocotyl will begin to form between the seed and radicle which will eventually become the stem of the seed as the shell of the seed starts to decompose as its use ends. During the emergence step the hypocotyl appears from the ground and the remainder of the seed will become loose and falls away from the plant. The final stage of a seedling is as foliage leaves start to emerge signifying that the plant is now drawing nutrients from the environment and is no longer dependent on the seed itself to assist in growth.

Within industry one of the key aspects of what makes for an effective crop is that the crop germinates and grows at a consistent rate. This allows for ease of farming, as once planted it can then be assumed that the plant can be harvested after a set date with consistent maturity throughout the crop. To take this consistency into account, when looking at germination rates a set point is used of when the number of seeds which have germinated is selected, with the time for 50 % of the total number of seeds to have germinated being the most commonly used data point. This value is known as the T50 % and is very important for comparing germination experiments as it allows a clear comparison of variables at a set point. This statistical result is commonly used over “total germination” as most germination rates slow down, and variables are less distinct as 100% germination approaches.

Multiple seed crop varieties were investigated for use in the project including sugar beet, arabidopsis, lettuce and tomato. Arabidopsis was considered as it is a staple crop for biological studies as a model organism, due to its fully mapped genome and having a low proportion of “junk DNA” allowing easy analysis during biological testing.⁵²⁻⁵⁴ However as the aim for this project was to focus on the potential improvement of agricultural crops it was decided that arabidopsis would not be a suitable crop as it is not widely grown for agricultural reasons. Another seed considered was sugar beet, as it is widely grown throughout the world particularly in the United States of America, Russia and Europe as a replacement to sugar cane due to its growth conditions requiring merely temperate conditions (below 18 °C and above -3 °C) rather than the tropical conditions required by sugar cane. Sugar beet was found to account up to 20 % of the world’s sugar in 2009 so is an important agricultural crop.⁵⁵ Unfortunately, sugar beet has a very robust germination cycle and as such any variation in germination due to the use of Starbons doped or non-doped would likely be too small to be statistically significant.^{56,57} As such, other commonly grown crops were looked at and lettuce and tomato seeds were selected for germination testing. Lettuce is one of the most commonly grown crops in Europe and due to its fast germination rates and sensitivity to the environment would be one of the test crops. Lettuce has an increased

dependence on temperature compared to many other crops including tomato and sugar beet and has been found to be strongly affected by plant growth inhibitors compared to a number of other test crops such as tomato.^{58,59} During observation, seeds were counted and marked if signs of germination had been detected with a calculation for when the T50 % value had been achieved for that batch. Tomato seeds were selected due to their robustness, being able to grow under a variety of unfavourable conditions including temperature changes and soil makeup, whilst still being sensitive enough to the environment to clearly see differences in growth when these factors change.⁶⁰⁻⁶²

1.2.5 Seed treatments

Within the agricultural industry a common way to improve plant germination and distinguish the brand is to use seed treatments. Seed treatments such as coating the seed in varying pesticides can significantly improve the plants chances of growing and improving overall yields.^{63,64}

Seed coating and pelleting is a method in which materials are coated onto the seed that promote seed germination and growth or protect the seed from germination and growth inhibitors. Seed pellets are created by covering the material with multiple coatings of varying thickness using the selected material, binding agent and active ingredients to affect the seed growth. With the initial thinnest layer being the film coating. After the film coating the seed is encrusted with the selected material and finally the largest layer on the outside creates the final pellet. This methodology has been advanced over the years to allow for improved mechanisation.⁶⁵ There are 3 common methods of the seed pelletisation process (Figure 15).

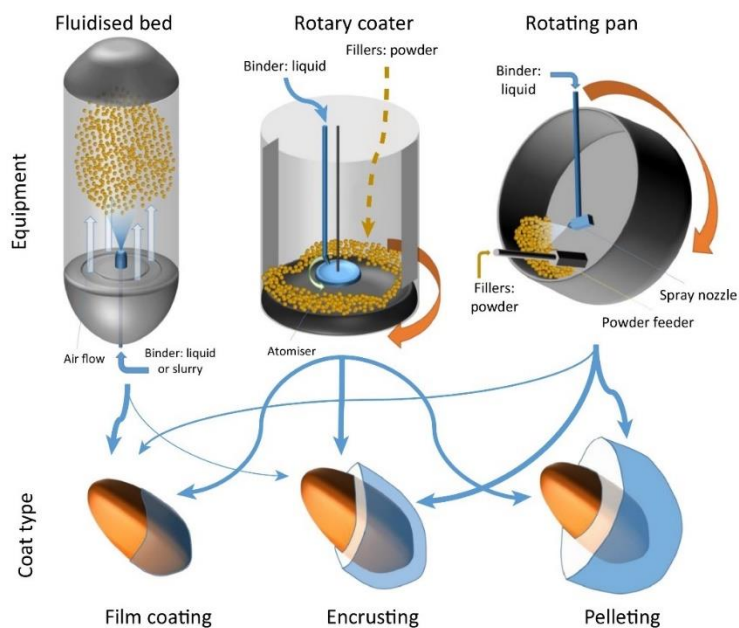


Figure 15. Three methods used in the seed pelletisation process.⁶⁶

A fluidised bed uses strong airflow to keep the seeds buoyant in the air while a spray is used to coat them equally. This machine is commonly used in the earlier stages of coating a seed as it is difficult to ensure the seed remain buoyant as its mass increases due to the increasing coating size.⁶⁵

A rotary coater uses multiple rotating portions of the machine to allow the seeds to be flowed in one direction whereas the binder and active ingredients flow in another direction. This opposing force results in the seeds obtaining an even and more spherical/oval shape. This machine can be set up so that it can be used throughout the entire seed pelletisation process.^{67,68}

Finally, there is the rotating pan, the seeds and active ingredient mix are continuously rotated and mixed but remain concentrated into one area of the pan. This continuous friction and mixing results in a rapid but even build-up of the seed pellet.⁶⁹

A seed pellet will normally have multiple layers of coating materials (see Figure 1 earlier). Each coating will have a different purpose (from binding other coatings together to covering with selected herbicides) with the final aim of increasing the seed's chances of germination as well as the rate and quality of seedling growth.

Figure 1 shows an idealised multilayer seed coating which contains specific compounds to assist in the life cycle of the plant. Growth stimulants, such as plant hormones, are required in the early germination stages and so are found closer to the seed itself. Plant hormones must be desorbed to be bioavailable for the seed, but the seed coating also acts to adsorb compounds that may inhibit plant growth. Then, there are several protective layers and binding polymers which prevent potentially harmful chemicals, such as pesticides and fungicides, reaching the seed. An additional layer that is included is a “pelletising” layer usually consisting of biodegradable material such as activated carbon or wood pulp. Pelletising is one of the major benefits of a seed coating as it generates a more uniform shape which helps mechanisation and increases the seed weight which also makes planting the seeds easier which improves the process sowing.⁷⁰⁻⁷⁴ One of the uses of Seed treatments is by using pesticides such as neonicotinoids to protect the seed and plant from pests for up to 10 weeks after planting.⁷⁵

One of the layers of seed coatings use porous materials to adsorb plant growth inhibitors from the environment. Normally, materials such as powdered pumice stone or more commonly activated carbon are used though in recent years more materials have been developed including biodegradable cellulose based materials.^{10,76-84}

2 Experimental

2.1 Materials and chemicals

Alginic acid derived from brown algae (*Macrocystis pyrifera*, CAS-9005-32-7) was purchased from Bright Moon Seaweed Group, (China). Analytical grade ethanol was supplied by VWR Chemicals (UK). Activated carbon was supplied by Syngenta, Netherlands and was produced by Carbotech. Calcium chloride, kinetin, indole-3-acetic acid, gibberellic acid, and abscisic acid were purchased from Sigma-Aldrich (now known as Merck). Tomato and lettuce seeds were supplied by Syngenta. All materials and chemicals were used as supplied unless specified otherwise.

2.2 Procedures

2.2.1 Preparation of Starbons: A00; A300; A500, and A800

A stirred mixture of AA (500 g) and water (2 L) contained in a 5-L glass vessel was heated at 90 °C for 6 h to effect gelation. The resultant gel was cooled and allowed to settle for 24 h. The gel was then centrifuged (3500 rpm, 10 mins) to remove excess water and the pellet was treated with *tert*-butanol (230 g) to create a slurry of expanded alginic acid. The latter was freeze-dried (Ramped to -50 °C at a rate of 80 °C a minute and then held for 360 minutes before being heating back to 10 °C over the course of 24 hours, pressure would begin at 720 Torr before decreasing to 170 Torr over the course of the experiment) to yield A00 (expanded alginic acid), 250 g (50 %), as a white powder. A summary of the process at the molecular level is shown (Figure 16).

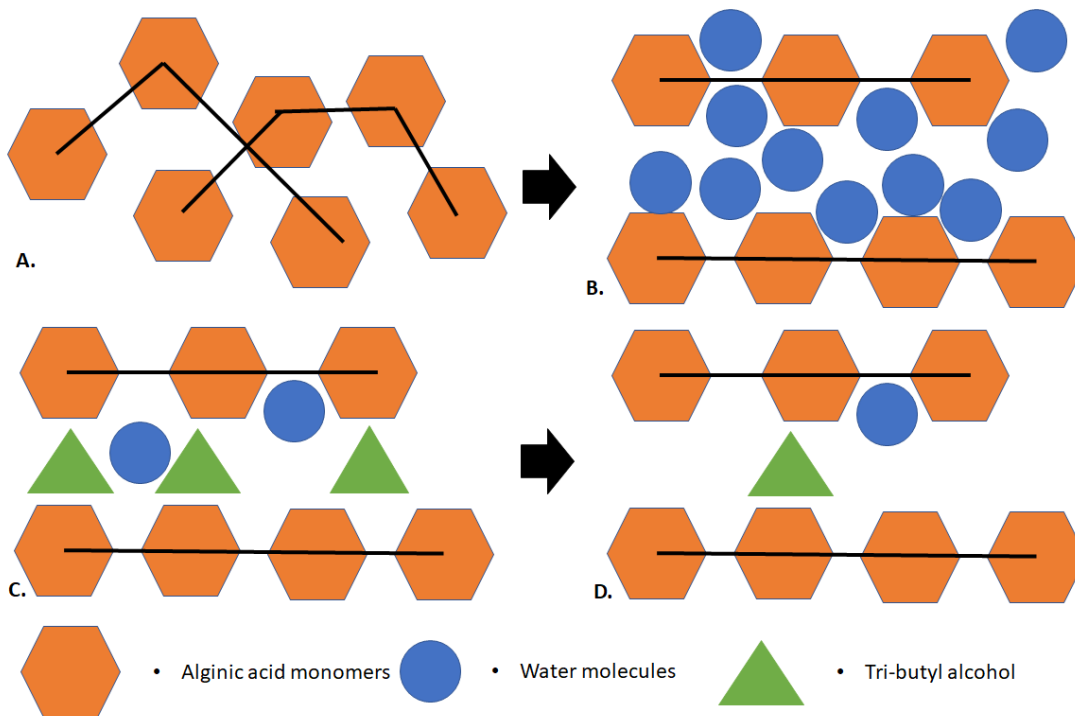


Figure 16. The stages of creating Starbon precursor from Alginic acid. A. initial, B. Gelation, C. Retrogradation, D. Freeze drying

The expanded alginic acid was then stored at room temperature prior to carbonisation (Thermolyne 6000 furnace under vacuum conditions) at the desired temperature (300, 500 and 800 °C). For example, the temperature programme setting for A800 (expanded alginic acid carbonised at 800 °C) was: ramp to 100 °C at 5 °C per min; hold for 1 h; Ramp to 210 °C at 0.3 °C per min; hold for 1 h; ramp to 400 °C at 0.3 °C per min; ramp to 600 °C at 1 °C per min, and; ramp to 800 °C at 3 °C per min with no dwell time at the end with average yield shown below in Table 2.

Table 2. Average yield of Starbons produced.

Material	Average Yield (%)
A300	50 ± 10
A500	42 ± 10
A800	18 ± 6

2.2.1 Batch mode adsorption capacity testing

The appropriate Starbon (50 mg) was mixed with deionised water (50 ml) containing increasing concentrations of the selected hormone (GA, IAA, KI or ABA) (50, 100, 150, 200, 250, 300, 350, 400, 500 mg L⁻¹) at stirred for 48 h at room temperature (17-19 °C). The Initial concentration of the hormone to be tested was determined by UV adsorption before the addition of material and agitated for 48 h. The stirred mixture was filtered and the concentration of the hormone in the filtrate was determined using a Jasco V-550 UV-vis spectrophotometer as detailed in section 2.2.3.

2.2.2 Thermogravimetric analysis

The appropriate material was placed into a Netzsch STA 409 and purged of air. Nitrogen flow was kept steady at 50 ml per minute. Heating was at a rate of 10 °C per minute and stopped at 1000 °C with a transfer pipe at 180 °C to prevent condensation. Readings were taken after the first 10 minutes to ensure all water was removed before analysis.

2.2.3 UV-vis Spectroscopy

A standard of the required solvent (1 ml; water, ethanol or a 50:50 mix) was used to determine the background between 200 and 800 cm⁻¹. An aliquot of each sample containing the plant hormone was created (1 ml) and analysed compared to the standard solution. Concentration was determined by comparing results of specific peak heights created by the plant hormones. When concentration was found to exceed the parameters of the Jasco V-550 UV-vis spectrophotometer solutions were diluted up to 10x in order to get a clear and consistent reading. Background samples were re-examined every 4 samples in order to recalibrate the UV-Vis.

2.2.4 Light optical Microscopy

For light optical microscopy (Leica microscope), the appropriate Starbon (approx. 10 mg) was placed onto a clean optical glass slide and viewed in reflectance mode at 200 x magnification. Images were captured analysed using Spectrum software as supplied by the manufacture.

2.2.5 Scanning electron microscopy

Micrographs were recorded with JEOL JSM-6490LV scanning electron microscope. The samples, mounted on an aluminium plate, were coated with Au-Pd prior to analysis. The acceleration voltage beam energy was 5 kV. The analysis was performed by Meg Stark (Biology Department, University of York) and analysed between x 750 and x 15 k magnification.

2.2.6 Transmission electron microscopy

A mixture of the appropriate Starbon (approximately 2 mg in ethanol (2 ml) was applied to a transmission electron microscope slide. The solution was allowed to dry (evaporate) at room temperature over a 1 h period. The resultant residue was subjected to TEM using a Tecnai 12 BioTWIN (manufactured by FEI) instrument coupled to a SIS Megaview 3 camera at acceleration voltage of 120 kV.

2.2.7 Solid state ¹³C CP-MAS Nuclear Magnetic resonance (SSNMR)

Solid State ¹³C Cross Polarization Magic Angle Spinning (CP-MAS) NMR (SSNMR) spectra were acquired using a 400 MHz Bruker Avance III HD Spectrometer equipped with a Bruker 4 mm H(F)/X/Y triple-resonance probe and a 9.4T Ascend® superconducting magnet. CP experiments employed a 1 ms linearly-ramped contact pulse, spinning rates of 10,000 ± 2 Hz, optimized recycle delays of 5 s, and number of scans varying from 200 - 300 for AC and Starbon varieties. Chemical shifts were reported and were referenced using adamantane (29.5 ppm) as an external secondary reference.

2.2.8 Elemental analysis and XPS analysis

All materials were analysed by the XPS analysis service provided by the University of Cardiff XPS service. A Kratos Axis Ultra DLD system was used to collect XPS spectra using monochromatic Al K α X-ray source operating at 120 W (10 mA x 12 kV). Data was collected with pass energies of 160 eV for survey spectra, and 40 eV for the high-resolution scans with step sizes of 1 eV and 0.1 eV, respectively. The system was operated in the Hybrid mode, using a combination of magnetic immersion and electrostatic lenses and acquired over an area approximately 300 x 700 μm^2 . A magnetically confined

charge compensation system was used to minimize charging of the sample surface, and all spectra were taken with a 90° take of angle. A base pressure of $\sim 1 \times 10^{-9}$ torr was maintained during collection of the spectra. Data was analysed using Casa XPS software (v2.3.19rev1.1l) after subtraction of a Shirley background and using modified Wagner sensitivity factors as supplied by the manufacturer.

2.2.9 pH drift measurement

The pH of eight batches of degassed (nitrogen and bubbling) pH solution (50 ml) (pH 3 – 12; achieved by appropriate mixing of calcium chloride solution (0.1 M); hydrochloric acid (0.1 M), and sodium hydroxide (0.1 M)) placed in to glass powder jars were measured using a calibrated pH probe (Jenway model 6505). Once analysed, a portion of the appropriate material (50 mg; AC or A00 or A300 or A500 or A800) was added to one powder jar, sealed and stirred for 24 h. Thereafter, stirring was stopped, the mixture was allowed to settle for 1 h prior to its pH determination. Each experiment was repeated in quadruplicate.

2.2.10 Boehm titration

For acidic surfaces, three basic solutions (50 ml; 0.05 M NaOH, NaHCO₃ and Na₂CO₃ (50 ml) were prepared. To each, the appropriate test material (1 g) was added, purged with nitrogen and agitated for 12 h. The resultant mixture was filtered and the filtrate was separated into five equal aliquots (10 ml each). Each aliquot was acidified with 0.05 M aqueous-HCl (20 ml for NaOH and NaHCO₃, 30 ml for Na₂CO₃), basified with an excess of NaOH (40 ml; 0.05 M) before and back titrated with acid solution HCl (0.05 M aqueous). For basic surfaces the same methodology was used but the material was mixed with 0.05 M HCl solution and treated with 0.05 M NaOH solution, treated with an excess of HCl and back titrated with 0.05 M NaOH solution.

Titration were conducted with a 907 titrando auto titrator with an 804 titrando stirrer set up and using a set endpoint pH (pH 4 and 10 respectively). The first titration would be set to pH 5 with an addition rate of 0.1 ml / min following a

second titration with the set endpoint of pH 7.1 with a drift of 0.1 pH and a slow set addition (0.10 µl per min).

2.2.11 N₂ Adsorption Porosimetry

Prior to analysis, the appropriate Starbon (approximately 100 mg) was degassed (90 °C for 8 h) and then porosity determined using a Tristar porosimeter. The data collected via N₂ adsorption was then processed via the Langmuir and BET isotherms to determine the overall surface area.

Equation 1. Langmuir isotherm

$$\frac{C_e}{Q_e} = \frac{1}{K_L} + \frac{A_L}{K_L} C_e$$

$$Q_0 = \frac{K_L}{A_L}$$

C_e = concentration at equilibrium (mg L⁻¹),

Q_e = adsorption capacity at equilibrium

a_L (L mg⁻¹) and K_L (L g⁻¹) = Langmuir adsorption constants.

Q₀ is the monolayer adsorption capacity of the solid (mg g⁻¹).

Equation 2. BET isotherm.

$$\frac{1}{V[(P_0/P) - 1]} = \frac{C - 1}{VmC} \left(\frac{P}{P_0}\right) + \frac{1}{VmC}$$

V = Adsorption gas quantity

P₀ = Saturation pressure

P = Equilibrium pressure

V_m = Monolayer adsorption capacity

C = BET constant

2.2.12 N₂ Adsorption Porosimetry of materials after adsorption and desorption process

Deionised water (10 ml) was drained through the expanded material to condition the cartridge (consisting of a 2 filters and expanded material between them). Water (50 ml) mixed with 200 mg g⁻¹ gibberellic acid was drained through the SPE cartridge to complete the adsorption process and ensure maximum surface coverage. The Starbon material was left under vacuum for 4 h to dry. Once dry, the Starbon underwent degassing under identical conditions to those previously stated and was analysed by porosimetry. Finally, the material was loaded onto an SPE cartridge and water (50 ml) was drained through the SPE cartridge for desorption to take place. The Starbon material was then left under vacuum for 4 hours to dry. Once dry, the Starbon underwent degassing and analysed via porosimetry. Each experiment was conducted twice.

2.2.13 Determination of adsorption isotherms and kinetics

To determine adsorption kinetics, the appropriate Starbon (50 mg) was added to a glass powder jar containing a set concentration of plant hormones (20, 50, 100, 150, 200, 250, 300 mg L⁻¹) in deionised water (50 ml). The resultant mixture was agitated for 24 h to reach equilibrium and was then analysed using a Jasco UV-vis spectrophotometer V-550. For kinetic analysis, the same process was repeated, and UV-vis measurements were taken after 0, 5, 10, 15, 30, 60 and 240 minutes and analysed as before. Each experiment was repeated in quadruplicate.

2.2.14 Thermodynamic analysis

A hormone solution was prepared (200 mg L⁻¹) and added to a centrifuge tube. The solution was then heated in a water bath at a set temperature (25, 30, 35, 40 and 45 °C). After 24 h samples were taken for analysis and 50 mg of material was added to the remaining solution. The solution was returned to the water bath and agitated for 24 h. The samples were then analysed using a Jasco UV-vis spectrometer V-550. Each experiment was conducted twice and analysed using the Van't Hoff equation and the Gibbs free energy equation;

Equation 3. Van't Hoff equation

$$\ln k = \frac{\Delta S}{R} - \frac{\Delta H}{RT}$$

Where k = the equilibrium constant at

T = temperature (K)

R = the gas constant

ΔH = Change in enthalpy

ΔS = Change in entropy

The Gibbs free energy was also calculated to determine the adsorption feasibility:

Equation 4. Gibbs free energy.

$$\Delta G = -RT \ln k$$

Or

Equation 5. Alternative for Gibbs free energy.

$$\Delta G = \Delta H - T\Delta S$$

2.2.15 SPE Adsorption and desorption testing of plant hormones

To test adsorption and desorption all experiments were conducted at room temperature (17-19 °C). The appropriate Starbon (80 mg) was placed in an SPE cartridge and sealed. The selected solvent (deionised water, ethanol or aqueous ethanol (50:50 mix)) (10 ml) was drained through the cartridge for conditioning purposes and then washed using deionised water (10 ml). A solution of the desired plant hormone (375 μ l in deionised water (50 ml) containing calcium chloride (0.1 mol) was passed through the cartridge and the run off collected for HPLC analysis. Finally, to collect data of desorption, the appropriate desorption solvent (5 ml) was drained through the SPE cartridge and collected for HPLC analysis. This process was repeated 10x to

obtain a total of 10 run-off samples (10 x 5 ml). Each experiment was repeated in quadruplicate.

2.2.16 High-performance liquid chromatography analysis (HPLC)

HPLC analysis was conducted using a Shimadzu Prominence HPLC with an Athena C18-WP 250 x 4.6 mm, 5 µm column. Initial equilibration was conducted using a deionised water (0.1 % formic acid): acetonitrile at a 90:10 mixes and was run for 5 minutes and repeated a minimum of three times. The primary run was deionised water (0.1 % formic acid): acetonitrile at 90:10 mixes shifting to 10: 90 over the course of a 30-minute run. The software used in analysis was LC Solutions.

2.2.17 Long term desorption

To observe long term desorption effects, 50 mg of material was added to a glass jar with water (50 mL) and 200 mg L⁻¹ of plant hormone. Material was then stirred for 24 hours to equilibrate, water was replaced and analysed via HPLC, and this was repeated for 7 days. Each experiment repeated for a total of four replicas.

2.2.18 Water holding and retention value

The appropriate Starbon (1 g) was placed into a pre-weighed sinter adapter and the total weighed. Calcium chloride solution (0.4 %, 20 ml) was passed through the sinter under vacuum. The sinter was placed in a centrifuge tube and centrifuged (3500 rpm for 15 mins) to remove any excess moisture. The remaining solid on the sinter was re weighed and dried overnight at 110 °C before cooling in a desiccator. A final weighing was conducted to determine the dry mass. Each experiment was conducted in duplicate. Water holding capacity was calculated using Equation 63.

Equation 6. Water holding and retention capacity

$$WHC = \frac{m_1}{m_2} - 1$$

M1 = wet mass g

M2 = mass after gravimetric filtration g

Water retention value was also calculated using Equation 6 but where M2 = dry mass after heating in oven for 24 h.

2.2.19 Liquid chromatography-mass spectrometry (LC-MS)

For LCMS testing 100 mg of selected seeds (tomato or lettuce) were placed into a test tube along with 2 mL of deionised water and sealed. This was placed into a germination bay at 5 °C with a 24 h night cycle for 3 days at ambient humidity. The seeds were removed via centrifugation and gravity filtered to remove any remaining solids. The liquid sample was flash frozen at -80 °C and freeze dried to remove moisture from the sample. Methanol (50 µL) was used to dissolve the solid sample, which was then analysed via a triple core, “Endura” LC-MS. The sample was then mixed with 2 mL deionised water. A sample of 10 mg Starbon material was placed into an SPE cartridge containing seed hormones. The cartridge was conditioned with deionised water (5 ml) beforehand. The resultant run off was then analysed via LC-MS using the preparation method. Plant hormones were desorbed using deionised water (2 mL) and analysed via LC MS. Comparisons were conducted to analyse the effects of adsorption and desorption. Controls were analysed at the same time as adsorption and desorption to observe natural degradation. A total of 2 controls and 4 samples were run at a time per material. Results were run in a randomly selected order as decided by a random number generator with control samples analysed

2.2.20 Seed Germination testing

A petri dish (120 x 120 mm) was set up with a base layer of filter paper. Material (100 mg) was spread onto the filter paper to create an equal sized layer and covered with another layer of filter paper. Water (10 mL) was used to wet the Starbon and filter paper equally and 50 seeds (tomato or lettuce) were arranged on the filter paper in a grid system so that none were touching. The petri dish lid was then covered and placed into a germination bay. Tomato (humidity 80%, 12-hour light cycle, 100 lumens, 18 – 20 °C) was examined for signs of seed germination for a total of 7 counting's and analysed every 24 hours over the course of a week. Lettuce (humidity 80%, 12-hour light cycle, 100 lumens, 12 – 14 °C) analysis was done every 12 hours for a total of 7

counting's over the course of 3.5 days. Each experiment was repeated for a total of 8 batches for a total of 400 seeds analysed.

2.2.21 Seed Germination testing of seeds using doped materials

For initial testing Starbon material (100 mg) was placed onto the filter paper and covered with another layer of filter paper. Water (10 mL) containing varying amounts of hormone (20, 60, 100, 200, 600 µg / seed) was used to cover the filter paper and 50 seeds (tomato or lettuce) were arranged on top of the filter paper. The petri dish was placed into a germination bay under the conditions discussed in Figure 4. For testing with Starbon or AC 100 mg of material was placed into an SPE cartridge and sealed.

Deionised water (10 mL) was drained through the expanded material to condition the cartridge. Plant hormone solution (gibberellic acid was selected as the hormone to have the most prominent initial effect 100 µg / seed) was mixed with deionised water (50 mL) and drained through the SPE cartridge. The material was then collected and a petri dish (120 x 120 mm) was set up with the base layered with filter paper. The petri dish was placed into a germination bay under the conditions discussed in 3.6 for a total of 7 counting's. In the case of tomato seeds this was every 24 hours for a period of 7 days, and for lettuce seeds every 12 hours for 3.5 days. Each experiment was replicated for a total of 8 times for a total of 400 seeds analysed.

2.2.22 Statistical analysis of germination data

Statistical analysis was conducted using Microsoft Excel 2013 to calculate the "F" critical test and ANOVA testing. Each experiment was compared to previous results to determine which experiments were found to be statistically significant to one another.

Equation 7. "F" critical test

$$F = \textit{explained} \frac{\textit{variance}}{\textit{unexplained variance}}$$

3 Results and Discussion

This chapter is subdivided in to four parts, namely;

- i. Preparation and physical characterisation of materials;
- ii. Physical and kinetic studies;
- iii. Adsorption and desorption studies, and;
- iv. Batch germination testing

3.1 Preparation and physical characterisation of materials

3.1.1 Preparation

All Starbons were prepared from commercial grade AA (Figure 7), which is a linear copolymer commonly found in algae and seaweed. Alginic acid is a biobased renewable feedstock and thus conforms with one of the core tenets of green chemistry, i.e. Principle 7: use of renewable feedstocks.^{85,86}

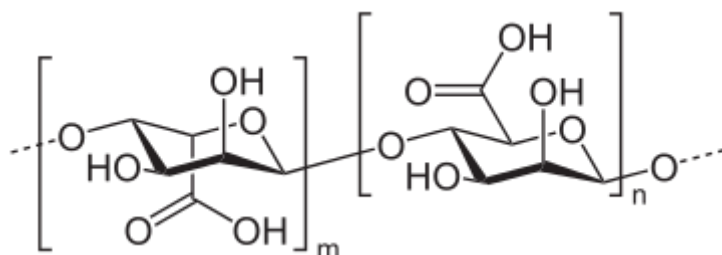


Figure 17. Alginic acid monomers (mannuronic acid and guluronate acid).

3.1.2 Thermogravimetric analysis (TGA)

Thermogravimetric analysis was used to determine the mass loss during the carbonisation process of Starbon materials (whilst heated under N₂)

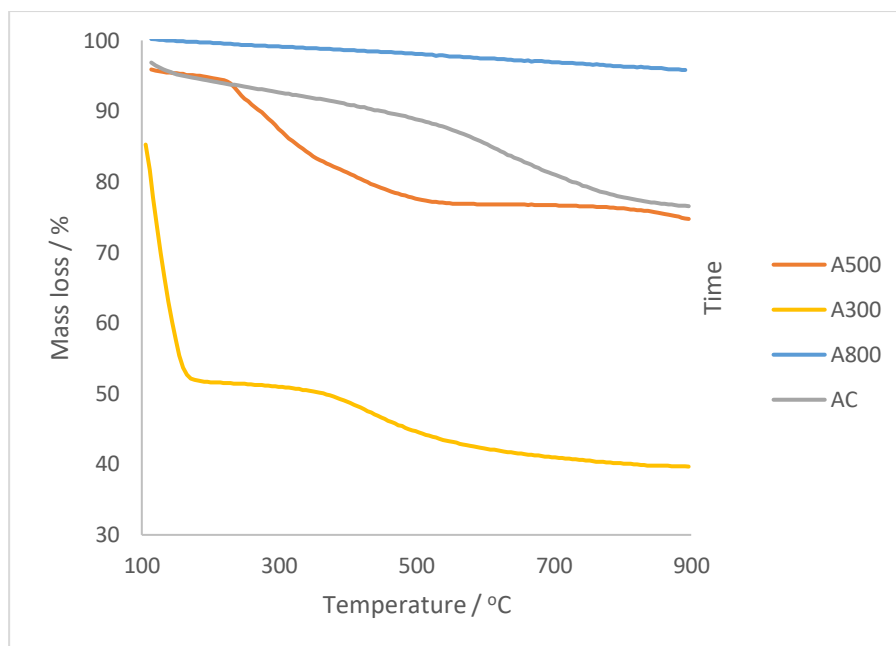


Figure 18. Thermogravimetric analysis of Starbons

The results were recorded after 10 minutes in order to remove initial water loss during initial heating. Starbon A300 shows a steep decrease in mass at the early stages of the experiment indicating further loss of water to just over 40% of the original mass recorded, suggesting that A300 can retain a large amount of water. After 300 °C there is a further drop in mass, indicating further carbonisation occurring as the A300 is further carbonised into A500 and the surface of the Starbon changes. There is a decrease in mass as the material is heated up to 900°C showing that material is still being carbonised but to a lesser degree. Starbon A500 shows a similar trend to A300 but instead shows a decrease in mass between 300 and 500 °C suggesting that the A500 has not been fully carbonised and may contain traces of A00 and A300. This is unusual as it shows that A500 loses approximately 15 % of its mass before reaching 500 °C while as A300 loses approximately 10 % mass indicating that there is a continuous loss of material even at higher temperatures as more material is exposed to higher temperatures. Starbon A800 shows a very minor (ca 3 %) decrease in mass over the course of the experiment showing that most of the material has fully carbonised. Activated carbon however, shows a steady decrease in mass as temperature increases up to 600 °C followed by further decrease in mass to the 900 °C showing that as the Starbon material

is heated above its carbonisation temperature, further material is removed from the Starbon.

3.1.2. Elemental analysis

Elemental analysis highlights the change in carbon, nitrogen and oxygen content of the Starbons as carbonisation temperature increases (Table 3). Activated carbon shows the highest carbon content and lowest hydrogen content compared to the Starbon materials. Both A300 and A500 showed hydrogen content of over 3% with A800 showing just over 1%. It was noticed that all the Starbons tested showed an increasing carbon percentage with increasing temperature of carbonisation, due to the thermal degradation removing most of the non-carbonaceous material. Finally, the “other” elements detected is higher for Starbon materials compared to the AC indicating that Starbons contain several other elements in much higher quantities. Based on the precursor structure of alginic acid much of this is likely to be oxygen, meaning that Starbons would contain a much higher oxygen content than AC though other trace elements may also be observed such as sodium and calcium. Though it should also be noted that compared to the theoretical elemental analysis it suggest that the AA used does have additional elements other than the expected C, H and O most likely Ca. This is further discussed when analysing via inductively coupled plasma.

Table 3. Elemental analysis of Starbon materials

	C %	H %	N %	Other %
AA (theoretical)	42.22	5.57	-	52.21
AA	36.98	4.96	-	58.06
AC	86.79	0.80	0.16	12.26
A00	31.29	4.80	-	63.91
A300	63.41	3.85	-	32.74
A500	75.00	3.01	0.14	21.85
A800	75.19	1.28	-	23.54

3.1.3 Inductively coupled plasma (ICP)

Inductively coupled plasma was employed to analyse and quantify the other elements which were recorded during CHN analysis.⁸⁷ While Starbons and AC cannot be analysed via ICP due to their insolubility, both AA (Table 40) and A00 (Table 41) could be analysed (results found in appendix).

In both tables a large amount of calcium and sodium were detected. Alginic acid and all Starbons were derived from biological material processed from seaweed. The presence of calcium suggests that calcium alginate was used instead of pure AA. The original form of AA is sodium alginate collected from the brown seaweed feed stock, hence the presence of sodium. The material also readily reacts with calcium to form calcium alginate. The results suggest that both the A00 and AA contains a larger amount of calcium alginate than expected, with A00 showing a much higher proportion than AA which explains the discrepancies in Table 3 with A00 showing a higher proportion of Other elements than AA. It is important to note though that while there is a high proportion of calcium and sodium within the structure, once carbonised this would likely mostly be removed and have little effect on the adsorption or desorption of plant hormones.

3.1.4 Carbon-13 nuclear magnetic resonance (¹³C NMR) of Starbons

From the ¹³C NMR analysis and break down of the Starbons (Figure 79, Figure 80, Figure 81 and Figure 82 in the appendix) it is clearly visible from the offset is that as the temperature of carbonisation increases, a decrease in surface functionality was observed, for example, A00 shows clear distinct resonances showing each of the four carbon containing groups (C-O, C=O, C-C-C and O-C-O). On the other hand, A800 shows only one small resonance. As temperature of carbonisation increases it becomes clear that the ability for the ¹³C NMR analysis becomes more difficult to cleanly register functional groups. This does not mean that there are no functional groups which may be analysed as this they are clearly observed in section 3.1.9 (S-ray photoelectron spectroscopy), the difference in intensity of detected peaks suggests that there is considerably more hydrogen attached to the functional groups of A00 than the carbonised material which is what would be expected

based on the elemental analysis. This makes it considerably easier for analysis to occur while as the higher carbonisation materials are mostly carbonaceous already do it becomes more difficult to analyse the differing groups as they are much less abundant.

There is a decrease in observable functional groups when temperature of carbonisation increases, with the only functional peaks being observed at 150– 30 ppm for A800 signifying aromatic structures. It was interesting to see how similar A800 and AC were to one another with AC showing only a small peak for aromaticity. These materials are treated at the highest temperatures which would suggest that there is reduced functionality due the decrease in functional groups. Starbon A300 and A500 both show multiple functional groups meaning that based on results seen in Table 14. This decreasing trend in recordable functionality suggests that the carbonisation of the Starbon material has a considerable effect on the functionality elements are removed and form more volatile compounds which are removed from the surface and the Starbon becomes more carbonaceous and develops more aromatic characteristics as observed with the A800 NMR. This change in functionality and along with the increasing surface area would explain why both AC and A800 show the greatest adsorption capacity, but also have the smallest variety in surface functionality, as they only show one functional group while as A300 and A500 both show multiple functional groups meaning that based on results seen in Table 14. Overall adsorption capacity appears to be influenced more heavily by surface area than the surface functionality. Surface functionality and its interactions though will likely have a greater affect when desorption is considered the strength of these interactions may affect removal from the surface. It would also suggest that as the surface functionality decreases and becomes more aromatic that desorption will become more favoured for some hormones due to the decreased interactions.³⁸

3.1.5 Microscopic Analysis

By examining Starbon materials at a microscopic level, using scanning electron microscopy (SEM) and transmission electron microscopy (TEM), key differences between each material are observed and provide further

understanding as to how the adsorption and desorption of the plant hormones may be taking place. As the level of magnification increases more data may be analysed, with TEM commonly used in porous materials studies to analyse the surface interface and determine if there is any structural ordering to the pores.⁸⁸⁻⁹⁰

3.1.6 Optical microscopy

Optical microscopy allowed a microscopic (up to x 200 magnification) view of the materials allowing a visual method to see key differences with the structure of the Starbons compared to activated carbon. The most important points of discussion were the particle size, uniformity of the material and differences in colour (Figure 19).

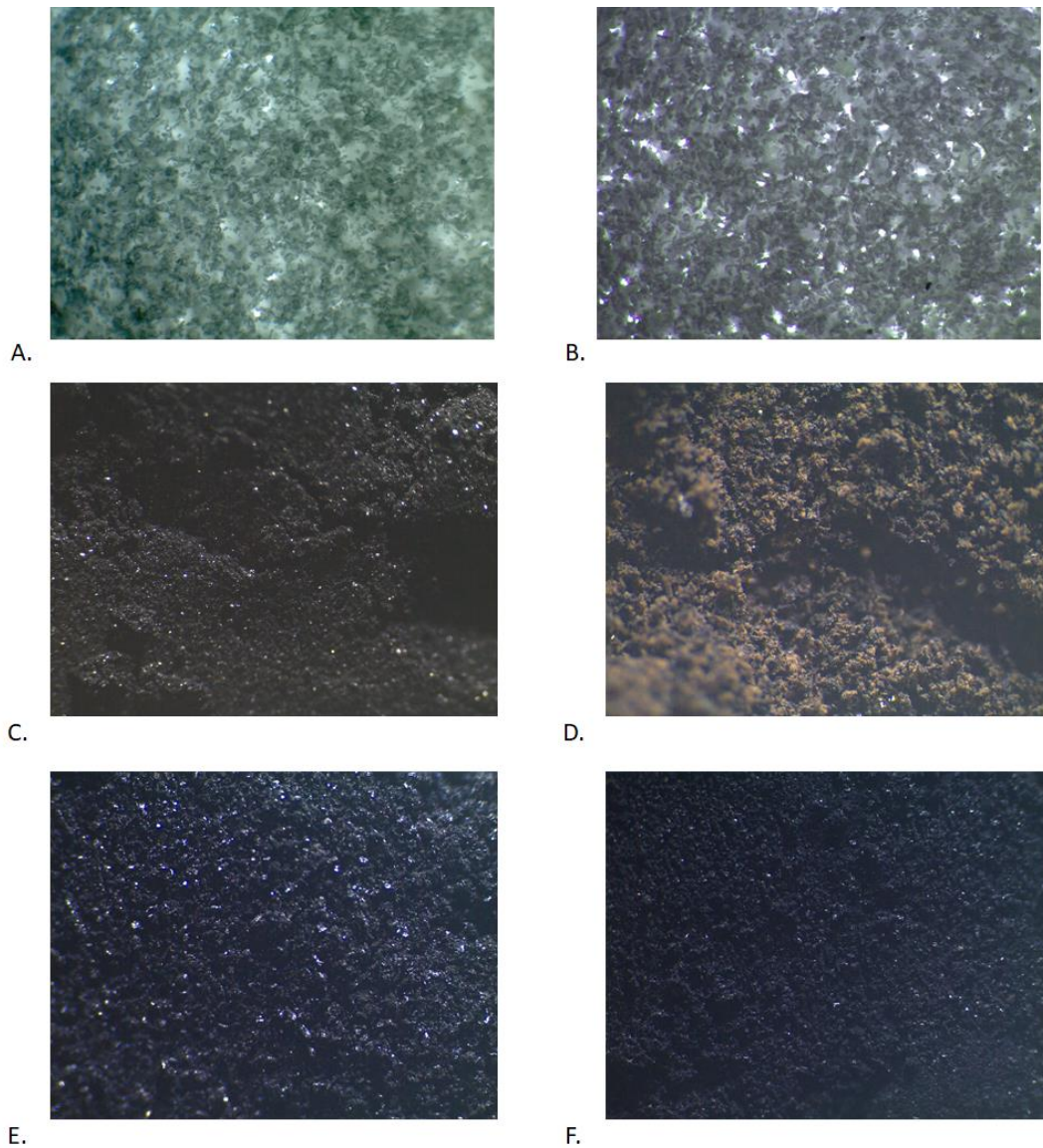


Figure 19. Optical microscopy of A. Alginic acid. B. A00. C. Activated carbon. D. Starbon A300. E. Starbon A500 and F. Starbon A800. (x 200 magnification)

Both AC and A800 show material of a uniform shape and colour (Figure 19) under an optical microscope. Starbon A300 showed two varied materials with differing physical consistency, one appears to be the Starbon material and the other is uncarbonized A00 meaning that A300 is a mix of both carbonised and uncarbonized material. This mixture of both precursor and Starbon material for A300 suggest that A300 has a high level of mesoporosity due to this mix of uncarbonized material which produce more micropores, this would also give an explanation sue to why there is such a significant difference in

mesoporosity between Starbon 300 and 500 (Table 12) as it would appear in Figure 19 that A500 has fully carbonised all the A00 at that temperature. This mixture of A300 and A00 would also explain why there was a lower than expected adsorption capacity of A300 along with the high percentage of unknown recorded elements in Table 3 as the presence of A00 would skew the results to show significantly higher mesoporosity (as observed in A00) along with a higher concentration of other elements (most likely Oxygen and Calcium as discussed earlier). Finally, A500 showed comparable colour and structure to A800 but it lacks a consistent particle size showing that the Starbon material is still degrading further to A800. No amount of precursor was observed showing that the precursor has been fully carbonised at this point. Alginic acid and A00 show similar results with inconsistent particle sizes and with A00 particles being a lighter colour to AA due to the process of creating it suggesting the removal of trace chemicals.

3.1.7 Scanning electron microscopy (SEM)

Scanning electron microscopy uses highly focused electron beams to excite the surface of the selected material resulting in electron scattering from the surface. This scattering is then detected, and an image can be created by the computer giving an image of the surface of the material. It is necessary with Starbons and AC as nonconductive materials to initially coat them in a conductive material such as tungsten, chromium or in this case gold to allow detection. One major issue with the use of SEM is that magnification is dependent on the focus of the electron beam rather than the lenses involved, this means that at higher magnification it can result in damaged material if focused on one point for too long preventing a clear image being formed. As such, for this experiment, images were taken at x 750 magnification for all materials and then images were taken individually for each material at the highest magnification possible before the material was damaged (Figure 20).

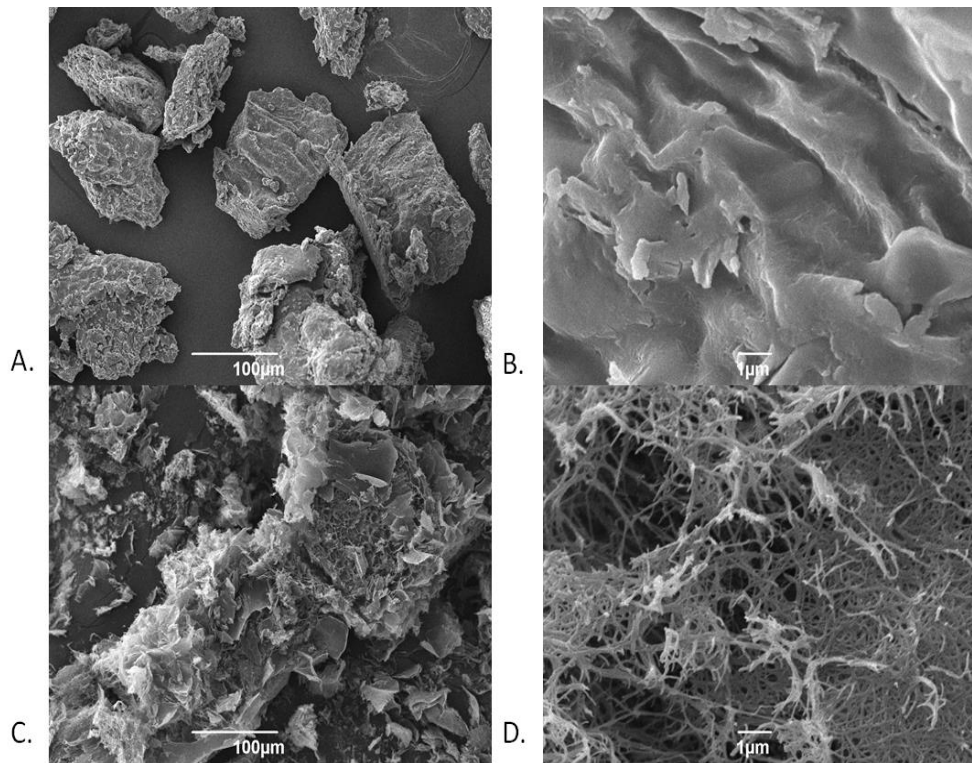


Figure 20. A+B. Alginic acid at x 250 and x 10k magnification. C+D. A00 at x 250 and x 10k magnification

Figure 20 above shows the change in structure between AA and A00. Starbon A00 has many more surface defects compared to AA as expected for untreated material. It can also be seen between images A and C that the overall trend for particle size changes with A00 and is showing a greater variance in size. Image D also shows that the material has a more fibrous quality compared to the AA due to the gelation and freeze-drying step. On comparing these particle sizes A00 were being considerably larger than observed with the Starbon material.

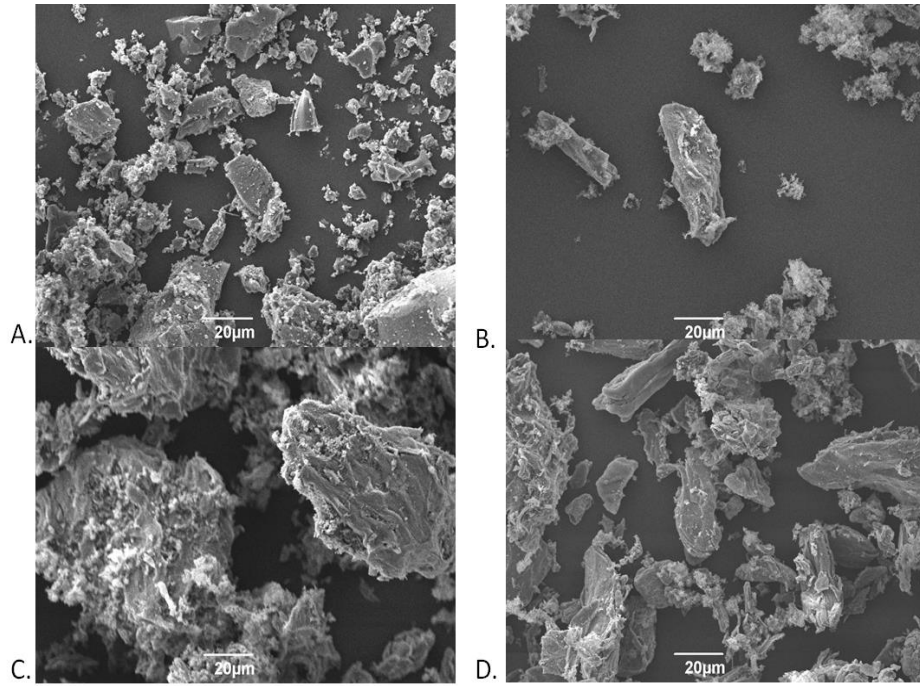


Figure 21. SEM images at x 750 magnification. A.AC, B. A300, C. A500 and D A800.

At 20µml, the Starbons do not show a smooth surface particularly for A300 and A500 (Figure 21). Activated carbon and A800 show smoother surfaces, showing that these surface defects thermally decompose at higher temperatures resulting in a smoother surface. The variation in sizes of the materials is also highlighted, showing a high variety in particle size. This overall shows that AC has a much greater variety in particle size than may have been expected which may also account for the increased surface area due to the smaller particulate size compared to the Starbons. A500 showed particles with a much larger size compared to A800. At higher temperatures the Starbon material is further carbonised and decomposes into smaller particulates.⁹¹

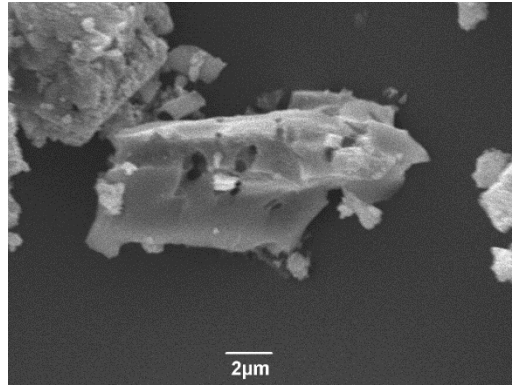


Figure 22. SEM image of AC at x 6000 magnification.

At 2 µm scale of AC (Figure 22), it is easier to see the largest macropores forming on the surface and the macropore channels throughout the material. Only a few additional bumps and protrusions on the surface of the particle are visible on the surface, suggesting that most surface defects are much smaller than the SEM detection limits which cannot go much further than 1 µm.

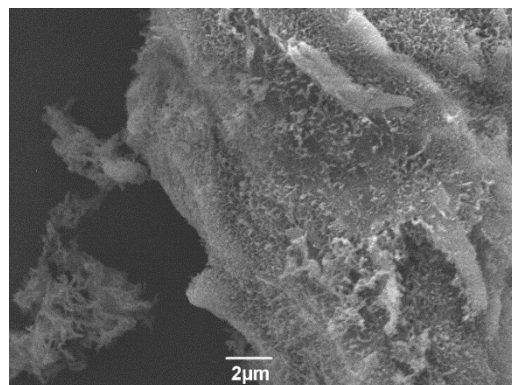


Figure 23. SEM image of A300 at x 6000 magnification.

At 2 µm magnification of A300 (Figure 23), the surface is much rougher than observed with the AC. It showed that the surface contains many surface “defects” which may affect overall adsorption and desorption. These defects are larger than many of the defects observed with other Starbon materials.

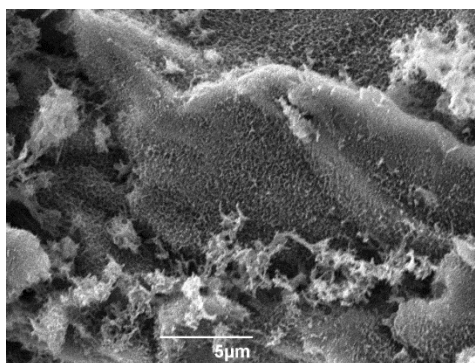


Figure 24. SEM image of A500 at x 2500 magnification.

Unfortunately, it was not possible to get closer magnification of A500 (Figure 24) as the sample was damaged at closer magnification. Like A300 the surface protrusions are again visible.

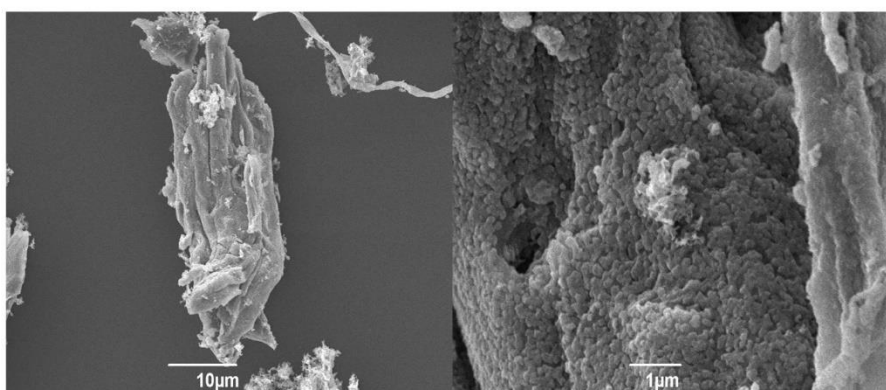


Figure 25. SEM images of A800 at x 2000 and x 15,000 magnification.

SEM analysis of A800 at 10µm and 1µm (Figure 25) showed that while the particle is smoother than A300 and A500, there are more defects than observed with AC and large channels on the surface. This agrees with what has been observed in previous experiment which shows that AC and A800 have similar surface area but A800 has a greater mesoporous and macroporous volume. At x 15,000 magnification, the highest magnification achievable for this experiment, clearly showed the macropores covering the surface of the particle and forming channels in the particle also with smaller pores within them.

3.1.8 Transmission electron microscopy (TEM)

Transmission electron microscope was used to obtain a higher magnification of the Starbon materials and allows the imaging of the porosity within the Starbon materials (Figure 26).

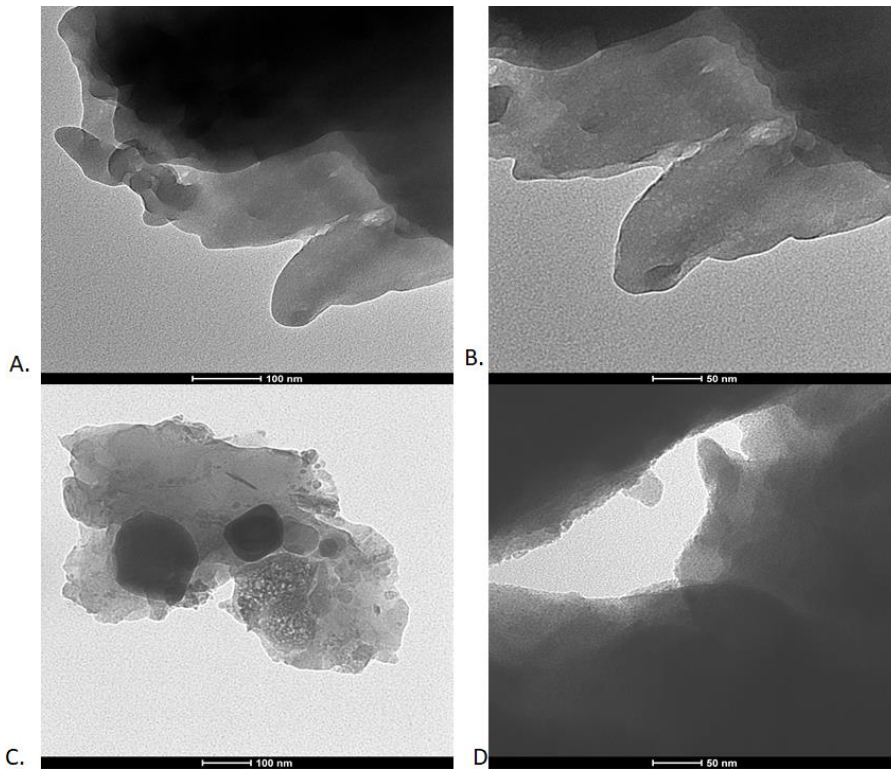


Figure 26. A, B, Alginic acid at 30x and 98x magnification. C, D, A00 at x30 and x98 magnification.

The primary difference between the materials analysis (Figure 26) that can be determined is that it due to the particle size there is little detail that can be observed at higher magnification. It is possible to see some meso and micropore channels within the material.

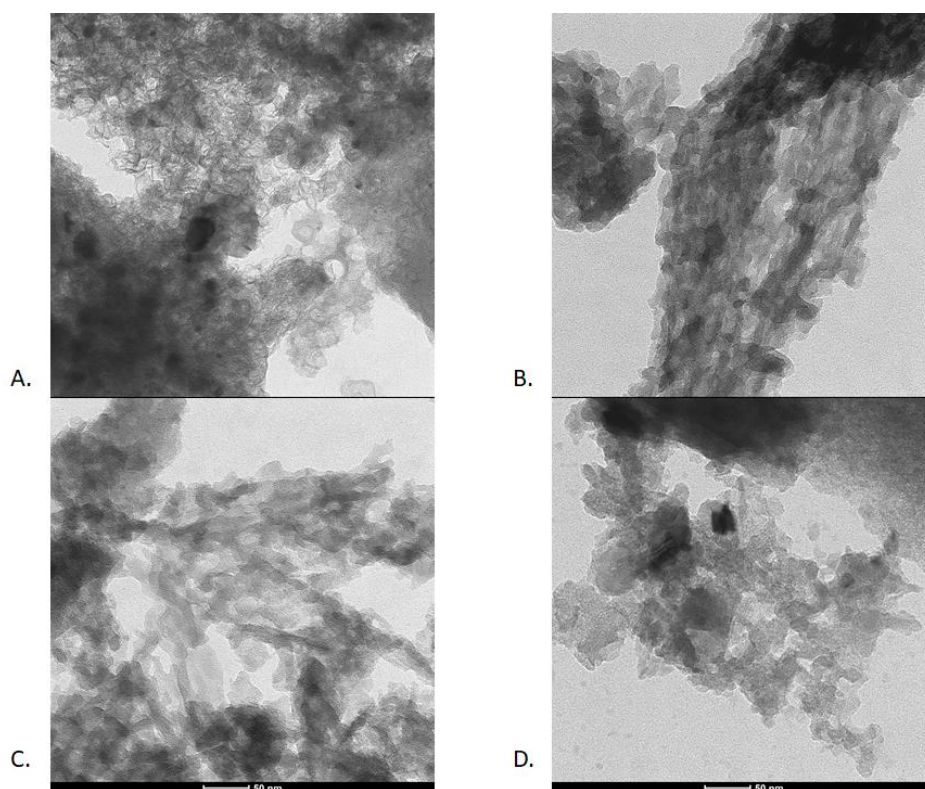


Figure 27. TEM images of A. AC. B. A300. C. A500 and D. A800 (x 98k magnification)

In the TEM images of AC and the Starbon materials (Figure 27), both A300 and A500 show similar structures with macro and mesopore channels running through the structure. Activated carbon shows much smaller and thinner channels that are from micropores. Starbon A800 highlighted that mesopores and micropores are within the structure.

3.1.9 X-ray photoelectron spectroscopy (XPS)

X-ray photoelectron spectroscopy uses the methodology of mono energetic X-rays which excite the surface of the material releasing excited photons to analyse the core binding energies at the surface of a material. By investigating the binding energies released it becomes possible to understand the bonding that is occurring at the surface, allowing an comprehension of how the key compounds are binding to the surface of the Starbons.^{92–95}

It is likely that adsorption may be influenced by surface functionality so It is important to compare the surface of the Starbon material for this project to the

surface of AC (Table 4) (if concentration is below 0.1 % then it has not been included in the tables).

Table 4. XPS analysis of AC.

Activated Carbon		
Name	Binding energy, eV	%At Conc
Na 1s	1,071	0.2
O 1s	533.5	4.1
O 1s	531.9	3.8
O 1s	534.8	1.5
Ca 2p	350.9	0.1
Ca 2p	354.5	0.1
Ca 2p	348.1	0.2
Ca 2p	351.7	0.1
C Sp²	284.4	65
π- π*	291.2	4.1
π- π*	293.9	1.3
C=O	288.1	2.8
C-O	286.8	4.7
C sp³	285.9	8.5
O-C=O	289.8	3.3
Si 2p	101.8	0.4

Several functional groups are found on the surface of the AC via XPS analysis. Interestingly several additional elements were detected at low concentrations that were unexpected, including calcium, chlorine and silicon. As the AC was derived from biomass it is likely that they were trace elements in the initial biomass and the very low percentage detected in the XPS suggests that this is the case. It was found that most of the AC surface consisted of C Sp² which is observed with C=C bonds. Other groups detected were oxygen based functional groups including carbonyl and carboxylic acids. Finally, π- π* bonds were also detected showing with C sp³ which would mean that most likely methyl groups would also be on the surface. The remaining functional groups were oxygen based including carboxylic acids.

Table 5. XPS analysis of AA.

Alginic Acid		
Name	Binding energy, eV	%At Conc
Na 1s	1,072	0.2
O 1s	533.1	37
N 1s	400.3	0.6
N 1s	402.1	0.2
Ca 2p	347.9	0.1
C 1s	285.1	18
C 1s	286.8	28
C 1s	288.2	9.6
C 1s	289.5	6.6
Cl 2p st 1	200.4	0.3
Cl 2p st 1	202.0	0.2
Si 2p	102.0	0.1

The results for AA confirms the presence of calcium, chlorine and sodium compounds in low quantities, which confirms what was detected previously in Table 40. The surface shows a high proportion of oxygen on the surface along with multiple C-C bonds. This XPS was used as the control as the surface of the structure is known, (Figure 17).

Table 6. XPS analysis of A00.

A00		
Name	Position	%At Conc
O 1s	533.2	26
O 1s	531.8	12
N 1s	400.2	0.4
Ca 2p	347.9	1.7
Ca 2p	351.5	0.8
C 1s	285.1	16
C 1s	286.8	27
C 1s	288.1	6.8
C 1s	288.8	9.4
Cl 2p st 1	200.4	0.1
Cl 2p st 1	202.0	0.1
Si 2p	103.7	0.2

Table 6 shows results like Table 5 with the same functional groups detected which would be expected due to the lack of chemical change to the material. The main difference being that more distinct peaks for O 1s were detected suggesting that more oxygen species can be detected on the surface. Unusually no carboxylic acid carbon at 289 was detected which is unusual as this is known to be present in AA and A00 so should have been observed.

Table 7. XPS analysis of A300.

Starbon A300		
Name	Position	%At Conc
Na 1s	1,071	0.3
O 1s	531.7	28.5
O 1s	533.4	17.0
O 1s	536.5	0.7
N 1s	400.4	1.1
Ca 2p	347.5	2.0
C Sp²	284.5	39
π- π*	291.2	0.1
C=O	288.4	1.7
C-O	287.2	1.8
C sp³	286.0	6.4
O-C=O	289.5	0.7
Cl 2p	200.7	0.1
Si 2p	102.1	1.0

Table 7 shows the changes at the surface of the Starbon as carbonisation takes place. π- π* bonding can now be detected though at low concentrations. Cleaner distinctions for the carbon to oxygen binding energies were reported, hence it was deduced that carbonyls and carboxylic acid functional groups are on the surface. The presence of C sp³ groups suggests that either CH₂ or methyl groups are now on the surface of the material though based on the NMR data it is most likely CH₂. The results show that A300 had similar functional groups to AC but with a higher proportion of oxygen based functional groups.

Table 8. XPS analysis of A500.

Starbon A500		
Name	Position	%At Conc
Na 1s	1,071	0.7
O 1s	531.4	24
O 1s	533.3	12
O 1s	535.8	0.9
O 1s	537.8	0.5
N 1s	400.7	1.4
Ca 2p	347.3	2.8
C Sp²	284.3	48
π- π*	290.8	1.5
π- π*	293.9	0.0
C=O	288.3	1.4
C-O	286.8	1.6
C sp³	285.6	3.5
O-C=O	289.2	1.2
Cl 2p	199.8	0.2
Si 2p	101.7	0.2

Table 8 shows the XPS for A500 and the results show similarities to Table 7 but with an increasing proportion of aromatic π- π* character and a decreasing amount of oxygen-based functional groups as the oxygen begins to be removed from the material. These results are expected with increasing carbonisation temperature and agree with including elemental analysis. The concentration of C Sp² peaks increased, showing that there was a greater proportion of C=C and C=O functional groups on the surface.

Table 9. XPS analysis of A800.

Starbon A800		
Name	Position	%At Conc
O 1s	531.63	2.2
O 1s	533.51	0.6
O 1s	535.49	0.2
O 1s	537.29	0.1
N 1s	400.55	0.3
Ca 2p	347.35	2.3
C Sp2	284.35	68.2
π - π^*	291.04	6.0
π - π^*	293.98	1.5
C=O	287.95	4.0
C-O	286.55	3.7
C sp ³	285.65	5.6
O-C=O	289.28	2.7
O-C=O	289.96	2.2

The results of Table 9 shows that much of the surface consists of Carbon based functional groups. An increased presence of π - π^* was also detected compared to A500 showing the increasing aromaticity being formed as the carbonisation temperature increases. A decrease in the overall oxygen based functional groups was also observed. These results show the continued change in the surface functionality of the Starbon surface to a more hydrophobic surface as the carbonisation temperature increases and oxygen and other functional groups are removed from the Starbons.

3.1.10 pH drift and Boehm titration of materials

The surface of the material has a differing chemistry to the bulk of the material and which influences the adsorption chemistry. Further, the elemental composition and surface chemistry differs depending on carbonisation temperature. This changing surface functionality has a significant effect on the pH at the surface and therefore adsorption. A pH slurry method was conducted and compared to previous experiments conducted to determine surface pH when in an aqueous environment. A Boehm titration was also conducted to

provide information regarding the surface functionality along with determining surface functionality density.

Within an aqueous environment the surface can interact with both the hydroxyl groups (-OH^-) and the hydrogen groups (-H^+) in the solution. This interaction can have a significant impact on the potential uses of the material e.g. catalysis or filtration and adsorption etc.^{96,97} The most important interaction to understand is known as the point of zero charge (pH_{pzc}), which is defined as the pH of a solution at which net surface charge is zero of the material has a net neutral charge. If a pH_{pzc} is found to be a low pH, then it indicates a more acidic surface while a high pH_{pzc} indicates the surface has more basic surface. These results can be compared to both the elemental analysis and the Boehm results to further understand the surface functionality of the material and how this may affect adsorption. Once the pH_{pzc} is known it can also be compared to the calculated pH in aqueous solutions (what it should be based on experimental design)) to also show the hydrophilicity of the surface with a lower value meaning increased hydrophilicity and a higher value indicating hydrophobicity.⁹⁸⁻¹⁰⁰

A Boehm titration (see Section 2.2.10) takes the pH drift further to determine what proportion of the surface of a material is acidic and basic. The acidic groups primarily consist of carboxylic acids, lactones and phenolic groups, while as the basic groups If detected would consist of ketones, pyrones, chromones and π - π bonds. Surface acidity has a connection with oxygen content in particular functional groups such as carbonyl, carboxyl and hydroxyl groups. These combined influences result in the point of zero charge (pH_{pzc}).

Experiments conducted in previous work and done for this project showed that the pH_{pzc} was calculated as the point where the final pH intersects with the initial pH (Figure 28).^{101,102}

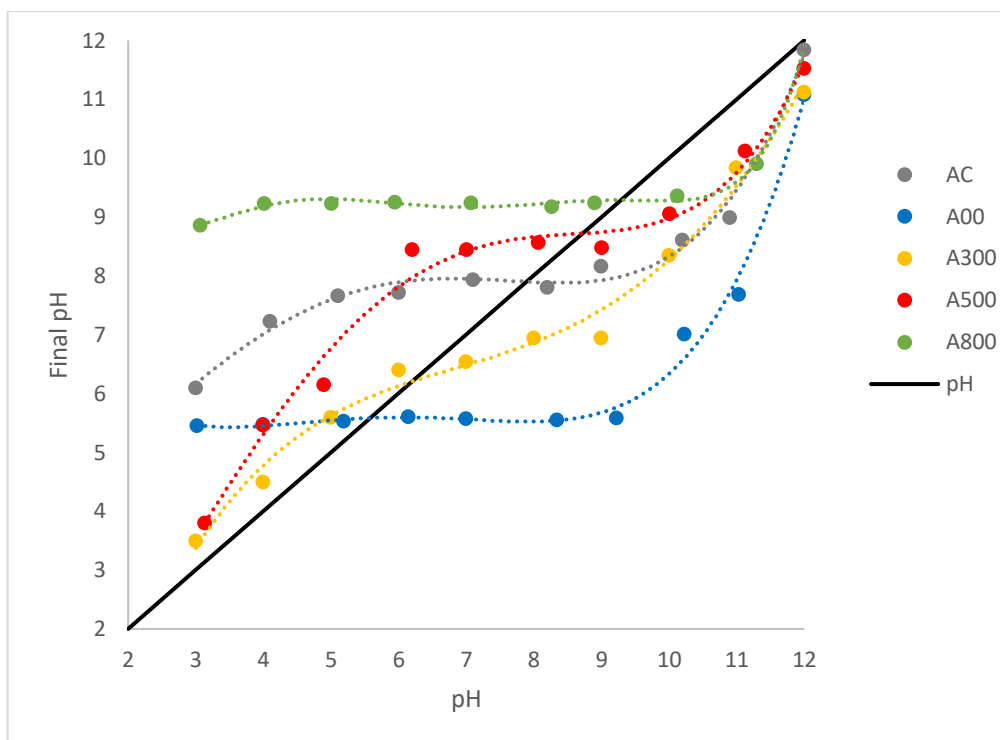


Figure 28. pH drift and determination of pH_{pzc} (see Section 2.2.9)

Table 10. pH_{pzc} of Starbons, precursor and AC.

Material	pH_{pzc}
AC	7.9 ± 0.1
A00	5.5 ± 0.2
A300	6.1 ± 0.2
A500	8.7 ± 0.1
A800	9.2 ± 0.3

The results show (Figure 28 and Table 10) similarities to previously established work conducted on Starbons with only A800 showing a variational difference.³⁶ Both A00 and A300 have an acidic surface. This acidity was to be expected as A00 is treated alginic acid which is very acidic in nature (pH 2.0 – 3.5). Section 3.1.3, confirmed that A300 is structurally similar to A00 and in fact has not been fully carbonised to A300 so would also have an acidic surface. This acidic nature is due to the oxygen based functional groups (carbonyls and alcohol groups found on the surface). There is a significant

shift in pH_{pzc} between A300 and A500 going from 5.4 to 8.7 going from acidic to basic in nature, due to the loss of oxygen-based groups and the shift of the remaining functional groups to more anionic structures on the surface as the carbonisation temperature increases. A800 shows a higher pH_{pzc} than A500 of 9.2 indicating that there has been a continued change to the surface acidity and functionality as carbonisation increases. This correlates to the information gained in Section 1.2.2 showing that further carbonisation to A800 continues to remove material from the Starbons and further changing the surface chemistry to a graphitic like nature with strong basicity. Activated carbon shows a basic pH_{pzc} of 7.9 which indicates that much of its surface contains more neutral functional groups such as aromatic rings and basic groups which is in line with the analysis via XPS.

Boehm titration works by saturating the materials in solutions of varying bases and acids so that each solution will react with specific surface functional groups.^{103,104} Typically, sodium hydroxide is used to neutralise the most acidic groups such as phenols, lactones and carboxylic acids, sodium carbonate will only remove carboxylic and lactonic groups. Finally, sodium bicarbonate is used for the removal of just carboxylic groups. By testing the material with each base it becomes possible to identify and further quantify the acidic oxygen groups found on the surface. It is more difficult to determine the specific basic functional groups found on the surface of the material. Generally hydrochloric acid is used to neutralise all of the basic surface groups which can then be analysed via back titration to determine the total basic groups in the same way it can be done for the acidic groups.¹⁰⁵⁻¹⁰⁷

Results show that acidic groups were detected on all Starbon materials though in decreasing quantities as the temperature of carbonisation increased. This is in line with what was observed in Figure 28 which showed that A300 was acidic in nature while as both A500 and A800 were basic in nature. The results also allow comparison to the results observed in 3.8 which determined the potential functional groups on the surface. By comparing the results, a more precise understanding of the surface can be obtained.

Table 11. Boehm titration results of materials tested.

Material	Total Acidic Groups / mmol			Total	Total Basic Groups/ mmol
	Carboxylic groups	Lactonic groups	Phenolic groups		
AC	0.58	0.41	0.70	1.69	2.02
A300	1.44	0.24	0.62	2.39	1.42
A500	0.02	0.19	0.56	0.77	2.75
A800	0.05	0.20	0.51	0.75	3.10

Based on the results shown in Table 11 the results show that with A300 most of the acidic groups are carboxylic groups and that there are significantly more acidic groups compared to the total number of basic groups, which is in line with the pH drift results. For A500 and A800 there is an observable decrease in the total number of acidic groups mostly due to the decrease in the number of carboxylic groups in A500 and A800. This confirms the results observed via XPS and pH drift which shows that the surface pH becomes more basic at higher carbonisation temperatures and this is most likely due to de-carboxylation which is confirmed via XPS. The results show that overall A500 and A800 have similar overall total number of acidic groups but the primary difference between them is the change in total basic groups with A800 having more basic groups on the surface.

3.1.11 Porosimetry

N₂ adsorption isotherms for native AA, Starbons (A000, A300, A500 and A800) and commercial activated carbon are displayed in Figure 29 and the resultant, derived, porosity data is listed in Table 12.

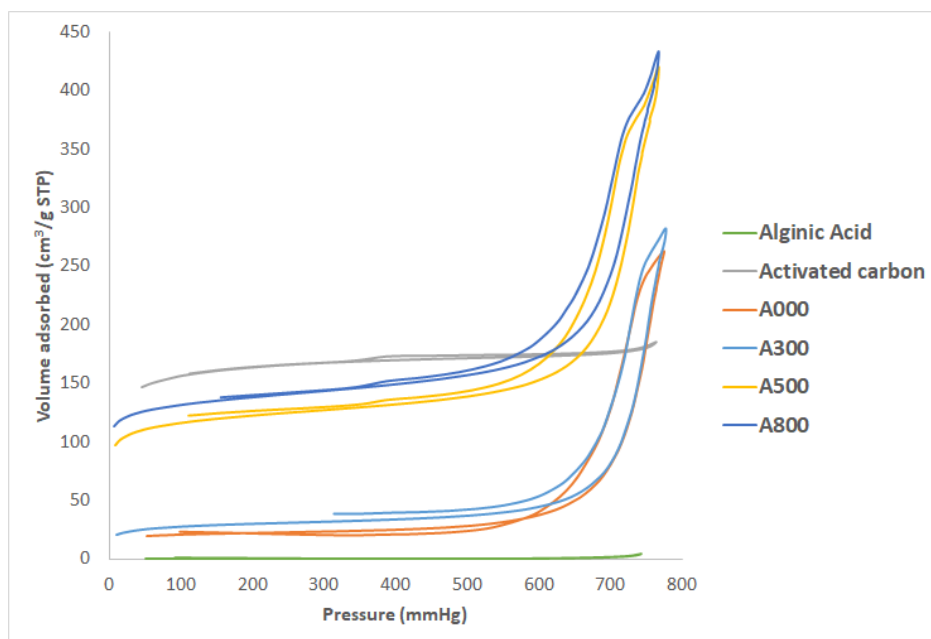


Figure 29. Porosimetry data of mesoporous materials.

All of the Starbon materials show similar hysteresis loops and, as expected, native alginic acid showed no porosity. The nature and shape of the isotherm for AC depicts a type B/H2 loop with minimal mesoporosity and pores resembling an ink bottle but with a narrow capillary (see Figure 30).^{108,109} The isotherms for all the Starbons follow a H1 pattern, as discussed previously in Chapter 1 (p. 22, Figure 9), are primarily mesoporous and are cylindrical or ink-bottle in shape (see Figure 9). The Starbons show a marked increase in total adsorption when the pressure rises with A500 and A800 having the highest recorded adsorption at high pressures.

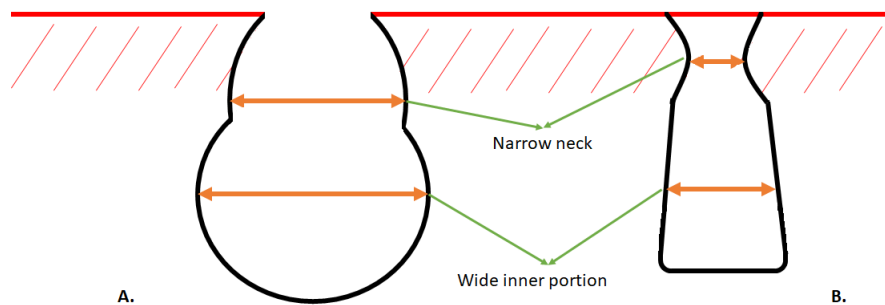


Figure 30. A. ink bottle and B. capillary shaped pore.

3.1.12 Analysis of Starbon surface via porosimetry

Table 12 below shows the change in calculated surface area and how the change in micro and mesopore area has an effect on surface area.

Table 12. Porosity data for activated carbon (AC) and Starbons (A300, A500 and A800)

Parameter	AC	A300	A500	A800
BET surface area (m ² /g)	525.8 ± 1.8	100.1 ± 15.6	408.9 ± 41.3	459.4 ± 16.4
Langmuir surface area (m ² /g)	730.4 ± 2.8	136.0 ± 21.3	545.1 ± 47.5	610.4 ± 34.4
Micropore area (m ² /g)	497.1 ± 7.1	63.4 ± 1.3	330.1 ± 43.2	368.1 ± 12.8
Micropore volume (cm ³ /g)	0.24 ± 0.0	0.0 ± 0.0	0.2 ± 0.0	0.2 ± 0.0
mesopore volume (cm ³ /g)	0.04 ± 0.0	0.42 ± 0.3	0.5 ± 0.1	0.3 ± 0.2
Ratio of micro to mesopore	1:0.16	1:15	1:30	1:20
Mesoporosity factors (%) (mesopores / total pores * 100)	14	93	75	79

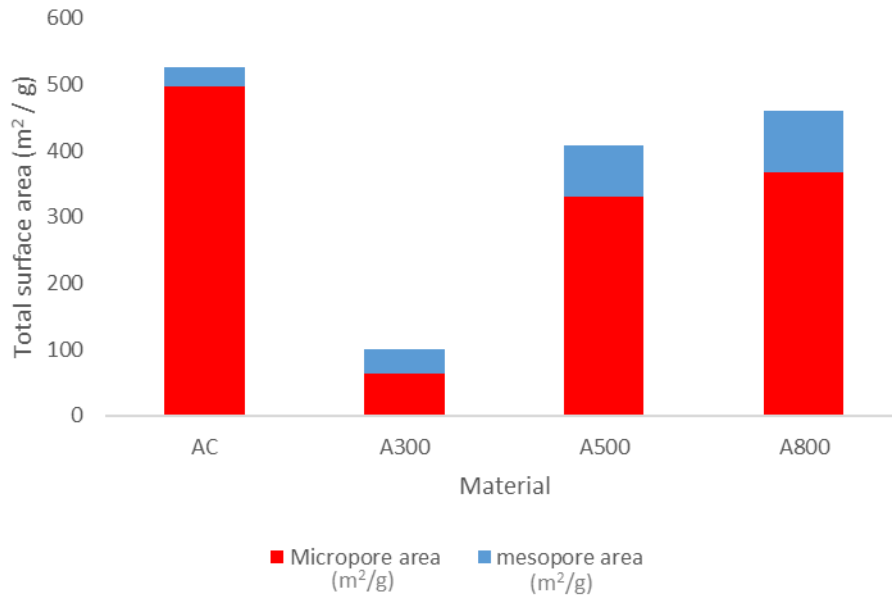


Figure 31. Total surface area (m² g⁻¹) of AC and Starbon materials

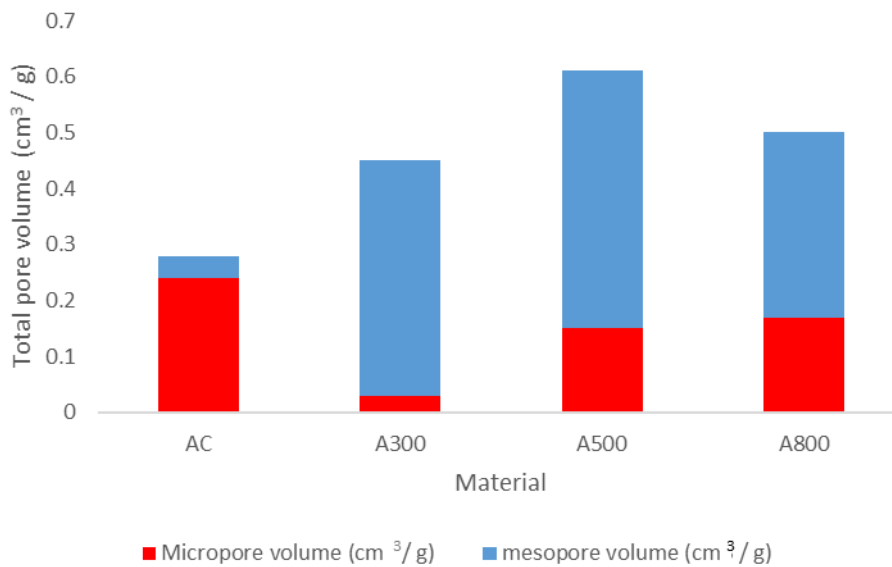


Figure 32. Total pore volume (cm³ g⁻¹) of AC and Starbon materials.

Figure 31 and Figure 32 shows the total surface area and pore volume of the materials and the contribution of micro- and meso-pores. Activated carbon has the largest surface area with the largest concentration of micropores followed by A800, suggesting that both will have the highest adsorption capacity as more material can adsorb onto the surface. Activated carbon has a very high surface area but a very low ratio of micro- to meso-pores, highlighting that it is

mainly microporous. The overall surface area of the Starbon materials increases as the temperature of carbonisation increases, which is due to the increase in microporosity (Figure 31). When comparing A800 and AC, although they are expected to show structural similarities, reveals that the surface area for the latter is only slightly larger than A800. However, there is a clear difference between the micro- to meso-pore ratio. A800 is still mesoporous in nature and activated carbon is very much microporous. The greatest change of surface area was between A300 and A500 (136 to 545 m²/g) in which the surface area of A500 is roughly 4 times greater than A300 with A500 and the mesoporosity factor showing a change from 1:15 to 1:3. Between these temperatures (300 and 500°C) the micropores are chemically generated. A smaller difference between A500 and A800 surface area was recorded (545 to 610 m²/g) though with an increase in overall microporosity. Figure 29 shows the volume adsorbed for A300, was lower than A500 though similar to A800 which though it had a slightly lower number of mesopores the increasing microporosity increased overall pore volume. Figure 32 shows that while the micropores make up most of the surface area, overall pore volume for the Starbons is due to the mesoporous nature of the material.

By comparing the pore volume and diameter, it was possible to create a model to determine the mesopore diameter and volume and estimate the proportion of micropores (Figure 76). It should be noted this does not show the average pore distribution but the overall pore volumes at each diameter. The results show that AA is essentially non porous (based on the data primarily looking at pores below 50 nm in diameter) showing only minor microporosity and that as the diameter increases overall pore volume increases. Starbon A00 shows a more mesoporous nature than most of the material averaging between 20-40 nm showing the change in structure from AA to the Starbon precursor leads to more mesoporosity due to the templating process. Activated carbon shows that most of its pores are microporous, with pore diameter <2 nm. This is in line with the analysis which showed that AC is primarily microporous (Table 12). Starbon A300 is primarily mesoporous with almost no microporosity but with some similarities to A00. Starbon 500 shows an overall smoother pore

diameter, of 25 nm in diameter. Finally, A800 shows a similar model to activated carbon showing a high number of micropores but with a clear increase in pore volume at 20 nm showing the mesoporosity of the material.

3.1.13 Effect of bioactive adsorption on porosity

By analysing porosity during the adsorption and desorption process, a greater understanding of how bioactives, adsorb and desorb to the Starbon material and which pores are being filled at those times. This allows a comparison to determine if either meso or micropores are favoured for the adsorption and desorption process (Table 13).

Table 13. Adsorption and Desorption porosimetry analysis of materials.

AC	Pre	Ads	Des
BET surface area (m ² /g)	498.78	349.28	365.11
Langmuir surface area (m ² /g)	691.23	486.22	508.73
Micropore area (m ² /g)	467.10	310.59	323.52
Micropore volume (cm ³ /g)	0.23	0.15	0.16
mesopore volume (cm ³ /g)	0.20	0.13	0.13
Ratio of micro to mesopore	2.6:1	1.7:1	1.7:1
Mesoporosity factors (%) (mesopores / total pores * 100)	28.52	41.27	42.56
Average adsorption pore diameter	2.29	2.50	2.50

A300	Pre	Ads	Des
BET surface area (m ² /g)	226.74	100.13	115.09
Langmuir surface area (m ² /g)	454.28	135.95	160.86
Micropore area (m ² /g)	144.94	63.40	42.16
Micropore volume (cm ³ /g)	0.06	0.03	0.04
mesopore volume (cm ³ /g)	0.64	0.42	0.47
Ratio of micro to mesopore	1:10.5	1:14	1:10
Mesoporosity factors (%) (mesopores / total pores * 100)	90.14	93.25	92.47
Average adsorption pore diameter	12.30	21.96	18.87

A500	Pre	Ads	Des
BET surface area (m ² /g)	321.36	106.03	129.68
Langmuir surface area (m ² /g)	444.75	104.96	180.06
Micropore area (m ² /g)	238.43	74.86	105.95
Micropore volume (cm ³ /g)	0.12	0.04	0.05
mesopore volume (cm ³ /g)	0.40	0.14	0.15
Ratio of micro to mesopore	1.3.8	1.3.1	1.3.0
Mesoporosity factors (%) (mesopores / total pores * 100)	28.52	76.32	71.51
Average adsorption pore diameter	2.29	6.55	5.52

A800	Pre	Ads	Des
BET surface area (m ² /g)	366.97	177.06	182.89
Langmuir surface area (m ² /g)	506.99	246.55	255.41
Micropore area (m ² /g)	231.79	171.67	173.73
Micropore volume (cm ³ /g)	0.11	0.08	0.09
mesopore volume (cm ³ /g)	0.45	0.03	0.06
Ratio of micro to mesopore	1:4.1	2.75:1	1:0.75
Mesoporosity factors (%) (mesopores / total pores * 100)	79.75	24.55	44.14
Average adsorption pore diameter	6.09	2.49	2.49

Porosimetry analysis shows that, AC shows similar results with roughly equal percentage of the micro and mesopores being filled during adsorption. It was observed that there was very little difference between the adsorbed materials porosimetry and the desorbed materials porosimetry which suggests that very little desorption occurs with activated carbon, this result was confirmed in Section 3.3.1. Starbon A300 decreases in surface area during adsorption but once desorption occurs there is only a slight increase in overall volume. This suggests that desorption has only removed a small proportion of the adsorbed plant hormone. Interestingly, once desorption takes place, the ratio of micro- to mesopores returns to similar pre-adsorption results, meaning that as desorption is taking place, the primary point of desorption is at the mesopores rather than the micropores. Desorption was also observed from the micropores but at a much lower amount than the mesopores. Starbon A500 material shows that both the micro and mesopores showed changes during the adsorption process with the mesopores adsorbing the most material the desorption results show that while both micro and mesopores show some desorption overall desorption favoured the micropores as can be seen with the decrease in mesoporosity and the decrease in average pore diameter. Finally, A800 shows that high amounts of adsorption from micro and mesopores with a significant decrease in pore volume. Overall this shows that when desorption occurs most of the material is being desorbed and removed from the mesopores rather than micropores which would indicate that Starbons will desorb greater amounts of plant hormone than AC.

3.1.14 Adsorption capacity

To understand the benefit of using Starbons as an additive to seed coatings, it is important to look at the surface of the adsorbate and how this will affect adsorption and desorption. Adsorption capacity of the adsorbents is affected by the morphology of the material.¹¹⁰ Finally, adsorption is affected by the interaction between the adsorbate, adsorbent and the environment including:

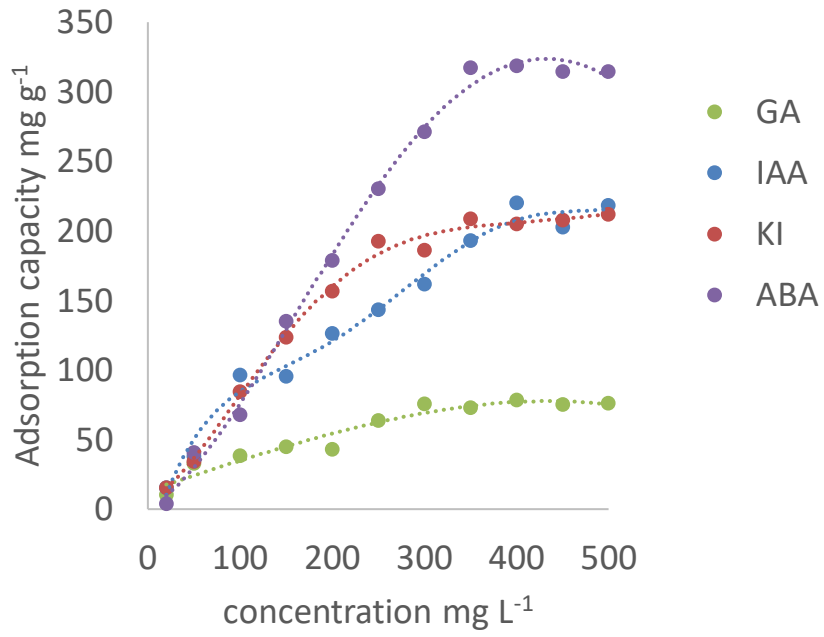
- i. Solvent on the adsorbate and adsorbent. Water was the primary solvent tested, which allows strong H-bonding to occur. This would influence adsorption as the water hinders adsorption from occurring if it can interact with the hormone or surface.
- ii. Intermolecular forces such as London dispersive forces and Van der Waals forces. These would influence the surface of the adsorbent and favourable interactions would lead to stronger adsorption.
- iii. Interaction between polarisable groups on the adsorbent and adsorbate. The adsorbent interaction is most likely to affect adsorption between the tested adsorbates as the selected plant hormones all differ significantly structurally and are the primary point of interaction with the adsorbent material.
- iv. The shape, orientation and functional groups of the adsorbate and adsorbent will influence adsorption. For example, a flat adsorbate would have more potential interaction points to interact with the surface than a large bulky compound and polar functional groups are attracted to other polar groups.

The adsorption capacity of each hormone with each tested material was recorded. From this a greater understanding of the adsorption process and the physical characteristics such as surface area could be obtained (

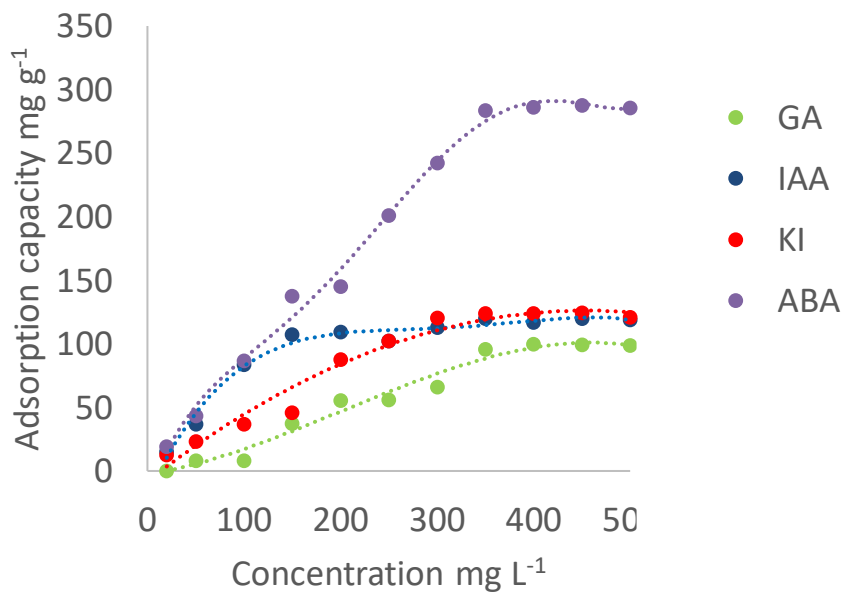
Table 14 and Figure 33).

Table 14. Adsorption capacity of hormones adsorbed onto Starbons and activated carbons (at equilibrium).

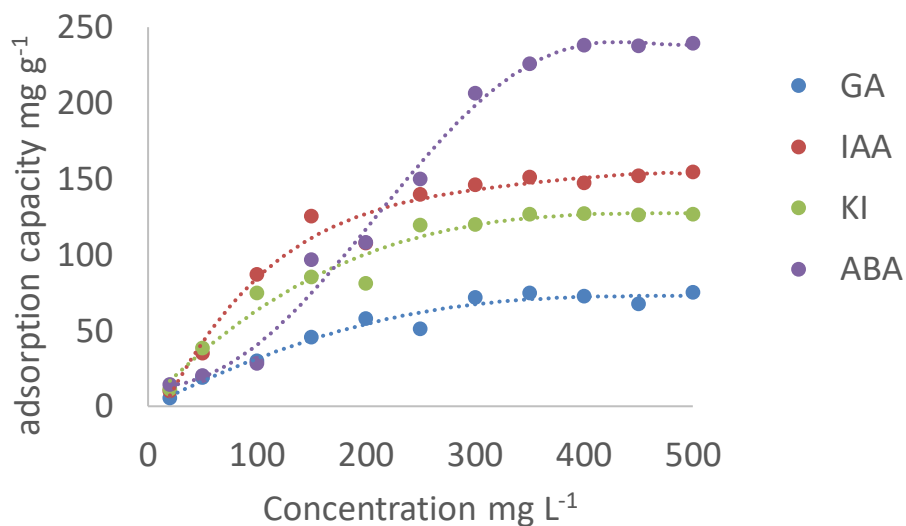
Hormone	Adsorption capacity at equilibrium (mg / g)			
	AC	A300	A500	A800
Gibberellic acid	72	98	76	118
Indole-3-acetic acid	210	115	150	157
Kinetin	205	120	125	121
Abscisic acid	314	282	239	370



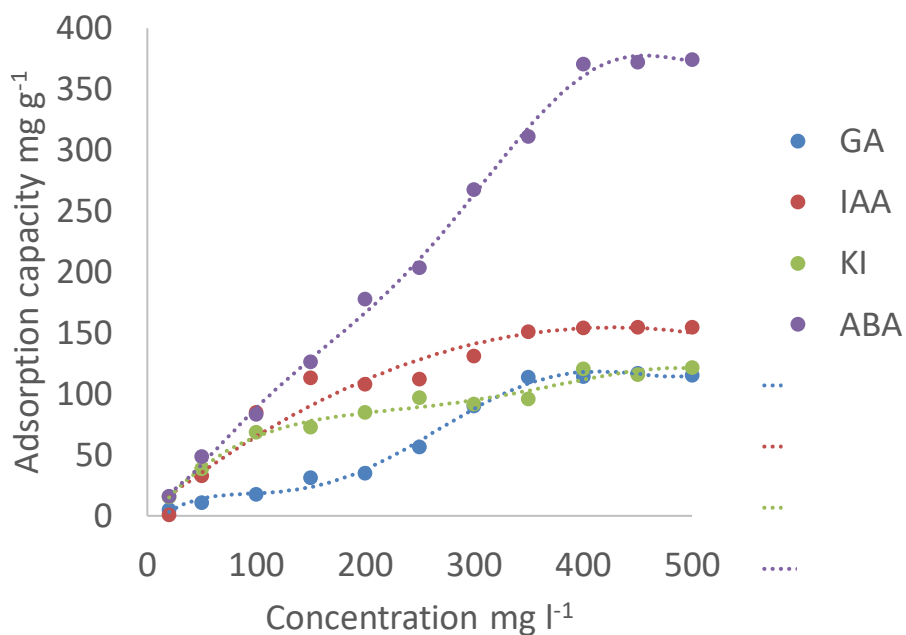
A.



B.



C.



D.

Figure 33. Adsorption capacity of bioactives for each material. (A) AC (B) A300 (C) A500 and (D) A800.

Activated carbon had highest adsorption capacity for both IAA and KI, (Figure 33, Table 14) which may be partially explained due to its high surface area though due to microporosity it may limit access to some larger hormones

(525.8 m² g⁻¹). There is also appears trend between Starbon adsorption capacity and temperature of carbonisation with increasing carbonisation temperature and increasing adsorption capacity. However, when looking at the capacity for each separate bioactive, there are differences, with GA showing the lowest adsorption capacity and ABA showing the highest adsorption capacity tested with each Starbon material. These results are due to the structural differences between each hormone and how they interact with the adsorbent (point iii) with GA being the bulkiest of the bioactives with multiple polarisable functional groups while as ABA has a tail structure with a polarisable functional group at the end which could affect adsorption. Abscisic acid shows a very high adsorption capacity in all cases, which indicates adsorption is favourable whereas desorption is unfavourable. This would also have an effect with the interaction of the adsorbent as the surface functional groups of the Starbons changes at higher temperatures as discussed in 3.1.10 with the acidic functional groups being less prominent at higher carbonisation temperature. Gibberellic acid is the largest and bulkiest of the bioactives tested with several alcohol groups which can promote hydrogen bonding around the structure. This can also explain why AC has a lower adsorption capacity compared to the Starbon materials, AC has fewer functional groups to interact with the bioactives, and its bulky shape reduces its overall potential area for adsorption to occur. Indole-3-acetic acid showed the greatest capacity of adsorption of all plant growth promoters tested (GA, KI and IAA), which may be due to its small, planar structure, which increases potential interaction at the adsorption surface area. The planar aromatic structure may also create a greater interaction between adsorbate and adsorbent due to π - π interactions. Kinetin showed similarities to IAA as it also has a planar structure, and a sterically hindered electron rich portion, which may hinder its adsorption. Abscisic acid is not planar but contains an accessible carboxylic group at the end. This allows increased interaction with the adsorbent as accessibility to the meso and micropores changes. There is also a possible trend based on the surface acidity as discussed in section 3.1.10 which shows that at lower temperature of carbonisation the Starbons are primarily acidic but at higher temperatures becomes more basic in nature. This again would have an effect

on adsorption as the more acidic hormones will interact more strongly with the more basic surfaces.

3.2 Kinetic adsorption studies

3.2.1 Rate of reaction: a kinetic modelling study

To understand the adsorption of the hormones it is necessary to find a suitable model to determine the rate of reaction of adsorption and the adsorption process that may be occurring. This requires understanding what additional factors may be involved during the adsorption process, for example mass transfer.

There are a wide variety of potential models that have been developed over the years to determine what form of adsorption was taking place. Mathematical models which were commonly used for this branch of experimentation were selected as the initial models, which in the case of liquid-solid phase experiments are the pseudo-first order and pseudo second order, The validity of the equation was determined from the correlation coefficient R^2 and the standard error calculated.¹¹¹⁻¹¹⁴

3.2.2 Pseudo-first order model

The linearized form of this model is shown in Equation 8:

Equation 8. Pseudo first order equation

$$\log(q_e - qt) = -\frac{k_1}{2.303}t + \log(q_e)$$

Where, q_e = amount of material adsorbed at equilibrium (mg g^{-1})

qt = amount of material adsorbed at time (mg g^{-1})

t = time (min)

k_1 = pseudo-first order rate constant (min^{-1})

Thus, plotting $\log(q_e - qt)$ vs time and analysing its' regression would show the applicability of this model.

3.2.3 Pseudo-second order model

Equation 9 can be used to determine if a reaction suits a pseudo-second order model:

Equation 9. Pseudo second order equation

$$\frac{t}{qt} = \frac{1}{k_2 q_e^2} + \frac{1}{q_e} t$$

Where, k_2 represents the pseudo second order rate constant.

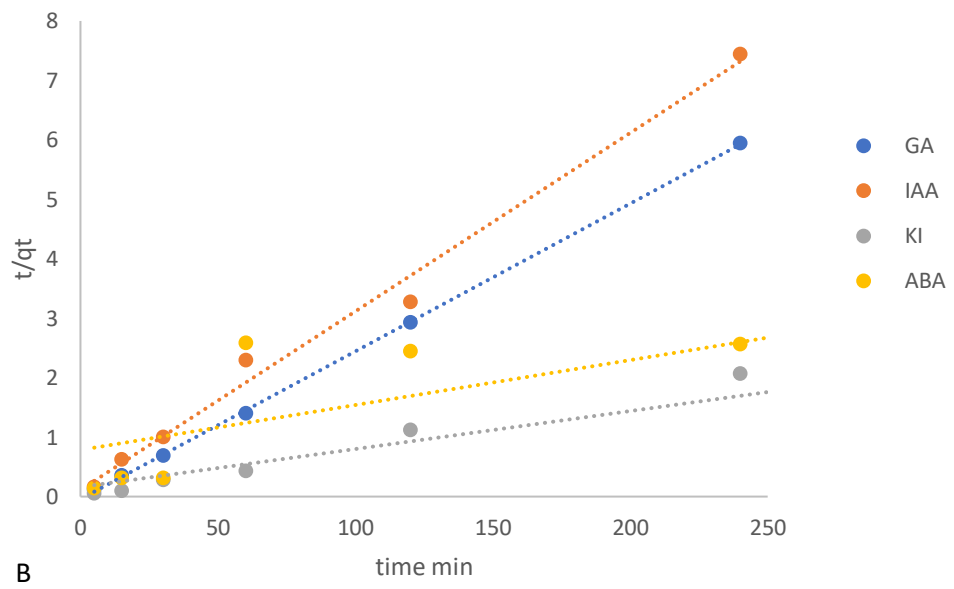
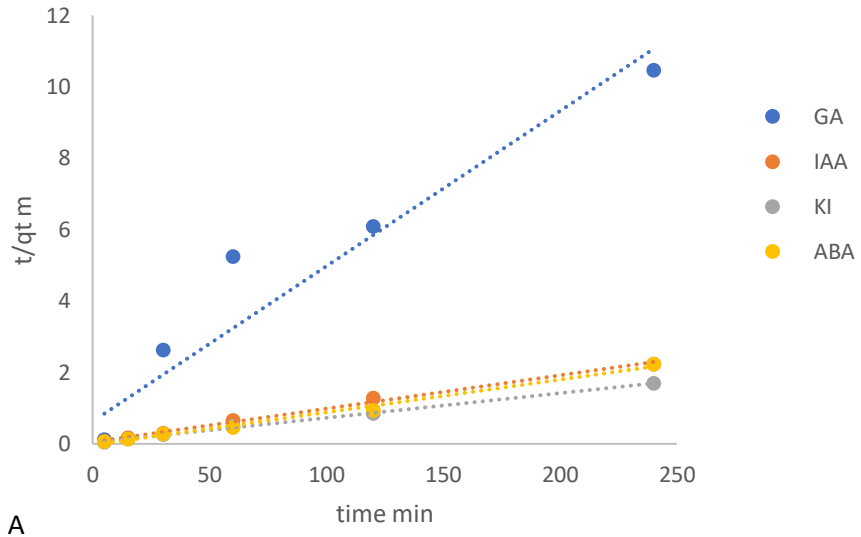
From inspection of the regression (r^2) data shown in Table 15 it is apparent that the hormones are likely to adsorb following pseudo-second order reaction kinetics, i.e., the internal transport and adsorption is occurring in multiple stages rather than one adsorption step, or that chemisorption is occurring via covalent forces.^{115,116}

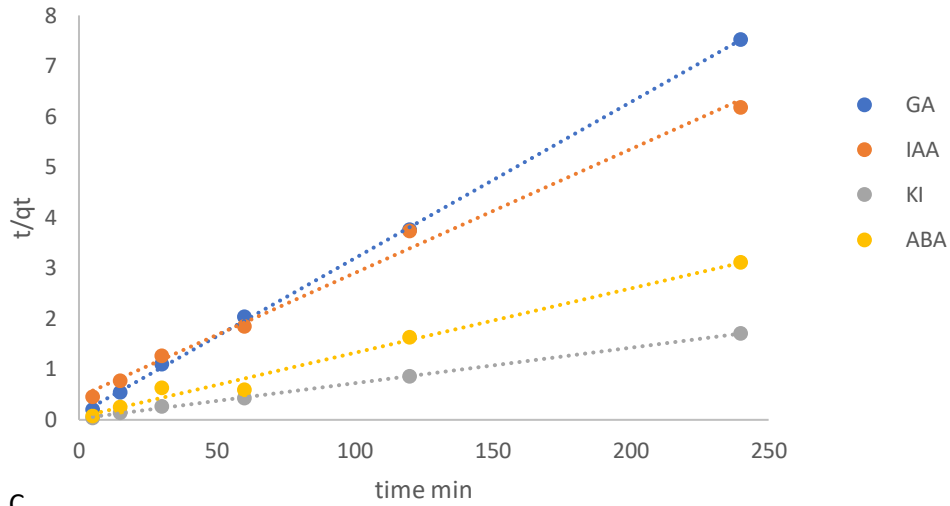
The rate constants for pseudo-second order reaction kinetics show that GA had the highest values for the plant growth promoters and showed a clear trend of increasing as the microporosity increases. The adsorption process for GA is very fast and likely affected by the porosity of the material. The rate constant for KI was found to remain low compared to the other tested hormones and was unchanged for each material it was tested on, meaning that it was adsorbing slowly onto the surface and the rate of adsorption was independent of the porosity. No such observable trend for IAA was observed, suggesting that further investigation may be required to understand what may have occurred. Abscisic acid closely follows pseudo-second order reaction kinetics with all materials tested and has the highest rate constant for AC but does not show a similar trend to GA (based on porosity) indicating that something other than porosity is affecting the rate of adsorption. The graphical data can be observed in Figure 34 and Figure 77 found in the appendix.

Table 15. Modelling of pseudo first and second order reaction. (2 repetitions)

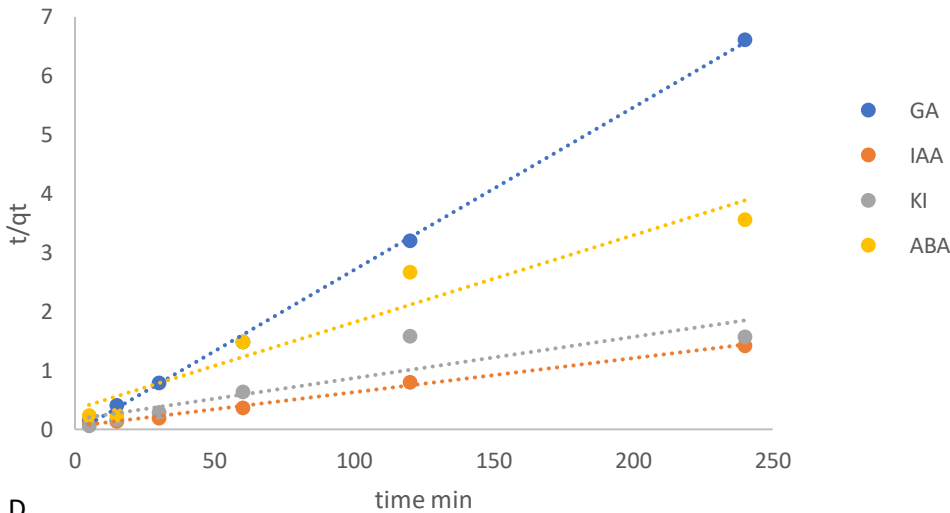
Pseudo first order			
Material	Hormone	K1 x10⁻³(min⁻¹)	R²
AC	GA	0.003	0.16 ± 0.00
	IAA	0.004	0.52 ± 0.03
	KI	1.997	0.80 ± 0.05
	ABA	0.130	0.01 ± 0.00
A300	GA	0.009	0.69 ± 0.00
	IAA	0.217	0.20 ± 0.01
	KI	2.953	0.87 ± 0.17
	ABA	0.651	0.23 ± 0.02
A500	GA	1.129	0.35 ± 0.08
	IAA	0.261	0.72 ± 0.00
	KI	4.255	0.91 ± 0.00
	ABA	0.868	0.22 ± 0.00
A800	GA	2.605	0.00 ± 0.00
	IAA	1.934	0.09 ± 0.00
	KI	4.125	0.35 ± 0.00
	ABA	0.564	0.13 ± 0.01

Pseudo second order			
Material	Hormone	K2 x10⁻³ (g mg⁻¹ min⁻¹)	R²
AC	GA	54.8	1.00 ± 0.00
	IAA	9.3	0.99 ± 0.00
	KI	6.9	0.99 ± 0.00
	ABA	61	0.99 ± 0.00
A300	GA	7.8	1.00 ± 0.00
	IAA	24.9	0.98 ± 0.00
	KI	6.4	0.99 ± 0.00
	ABA	29.9	0.99 ± 0.06
A500	GA	30.9	0.99 ± 0.00
	IAA	27.5	0.98 ± 0.00
	KI	6.9	0.99 ± 0.00
	ABA	12.5	0.94 ± 0.00
A800	GA	69.4	0.97 ± 0.00
	IAA	5.6	0.99 ± 0.01
	KI	6.9	0.81 ± 0.00
	ABA	14.3	0.92 ± 0.00





C



D

Figure 34. Pseudo second order for all tested materials and hormones. A. AC, B. A300, C. A500, D. A800 (four repetitions).

3.2.4 Bangham equation

The rate determining step during adsorption is an important point to be considered for understanding the adsorption process. There are several processes that occur that need to be investigated, such as mass transport, pore diffusion and film diffusion. To determine if pore diffusion is the primary rate determining step of adsorption the Bangham equation (Equation 10) is

used. Pore diffusion becomes more important as a diffusion method when the available space for movement is lower than the mean free path of the molecules (usually in mesoporous or smaller materials) resulting in numerous collisions with the adsorbate as it moves further through the Starbon materials. As such this can be one of the primary limiting factors for adsorption. The Bangham equation is a method used to further study the rate of reaction, specifically how much of the rate determining step is affected by pore diffusion through meso- and micropores.^{45,117,118} The equation is shown below:

Equation 10. Bangham equation

$$\log \log \left(\frac{q_e}{q_e - q_{tm}} \right) = \log \left(\frac{k_b m}{2.303 V} \right) + a \log t$$

In which

a and k_b are constants

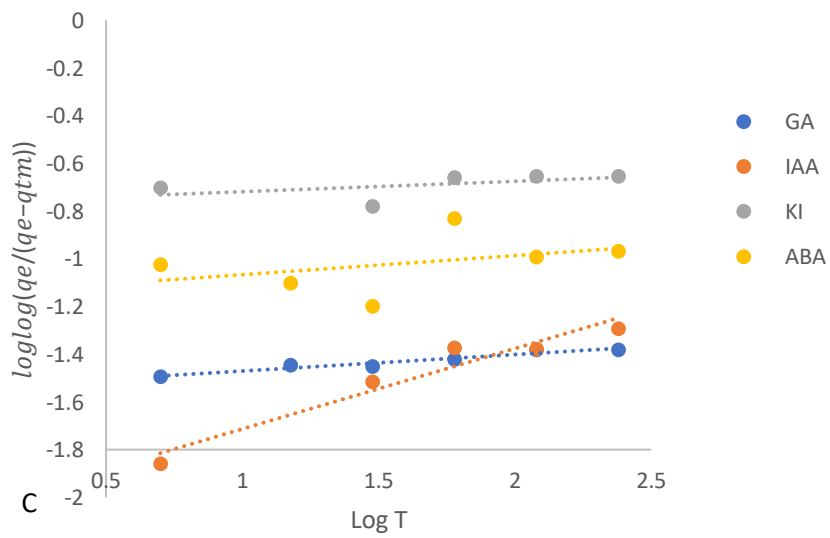
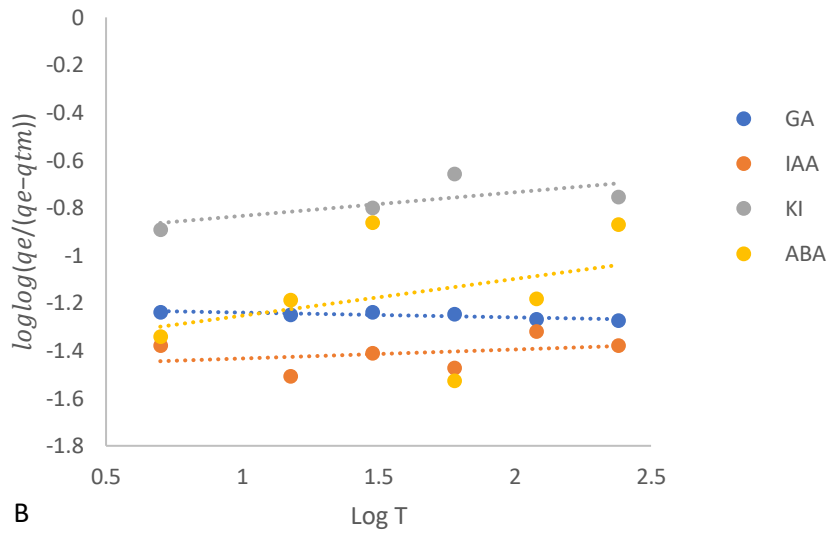
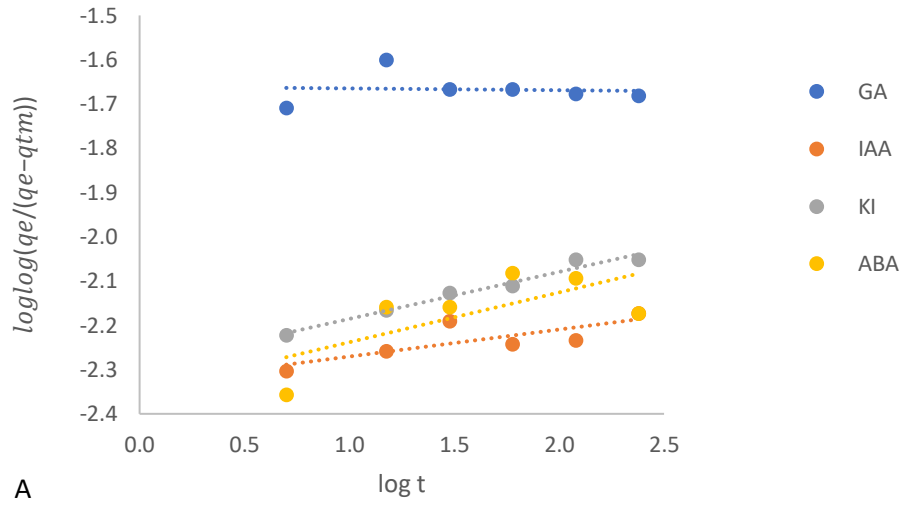
v = volume of solution (l) and,

m = mass of adsorbate (g l⁻¹).

The Bangham equation is predominantly used where it is observed that adsorption is a rapid process with capacity levelling off at a set point.

Table 16. Modelling of the Bangham equation (2 repetitions)

Material	Hormone	R²
AC	GA	0.94 ± 0.02
	IAA	0.89 ± 0.05
	KI	0.97 ± 0.02
	ABA	0.83 ± 0.00
A300	GA	0.71 ± 0.04
	IAA	0.85 ± 0.00
	KI	0.86 ± 0.03
	ABA	0.85 ± 0.00
A500	GA	0.84 ± 0.00
	IAA	0.81 ± 0.03
	KI	0.83 ± 0.00
	ABA	0.87 ± 0.00
A800	GA	0.90 ± 0.03
	IAA	0.88 ± 0.01
	KI	0.92 ± 0.02
	ABA	0.94 ± 0.03



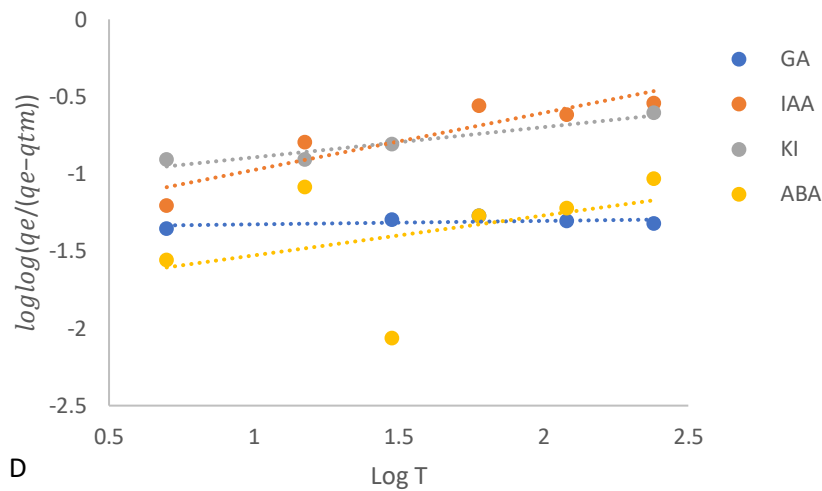


Figure 35. Bangham equation for all tested hormones and materials. A. AC, B. A300, C. A500, D. A800 (four repetitions).

Based off the results shown (Table 16 and Figure 35) most of the plant growth promoters fit the Bangham equation with the materials tested, except for A300 and to a lesser degree A500. Abscisic acid does not closely follow the Bangham equation for any of the materials tested bar A800 which would mean that there is another factor affecting the rate determining step. Table 16 also shows that the plant growth promoters fit the Bangham equation to a high order at higher temperatures of carbonisation which fits with results found in the literature.¹¹⁷ Overall the results show that as micro porosity increases, the rate of adsorption is increasingly affected by pore diffusion which would be expected due to the increasing number of smaller sized pore channels. The correlation coefficient of the plant growth promoters would suggest that pore diffusion is an important aspect in the rate determining step of adsorption but that there are other factors that affects the adsorption process.

3.2.5 Elovich equation

The use of the Elovich equation (Equation 11) adds to the understanding of the adsorption process. The Elovich equation is a model commonly used to confirm that the adsorption process taking place is chemisorption when the

evidence suggests that there is a heterogeneous surface which, based on what has been observed in 3.2.3 may be happening. The Elovich equation works on the assumptions that chemisorption is taking place and that as adsorption occurs an increasing number of adsorption sites becomes available. If followed, adsorption would be taking place via multilayer chemisorption and that the rate determining step is connected to the number of adsorption sites which would further confirm a pseudo second order reaction.¹¹⁹ Normally it has been used as a method for analysing gaseous adsorption but the equation can be adapted for use with liquid adsorption.

Equation 11. Elovich equation

$$\ln \frac{q_e}{c_e} = \ln K_e Q_m - \frac{q_e}{Q_m} \quad \text{Eq 6}$$

Where;

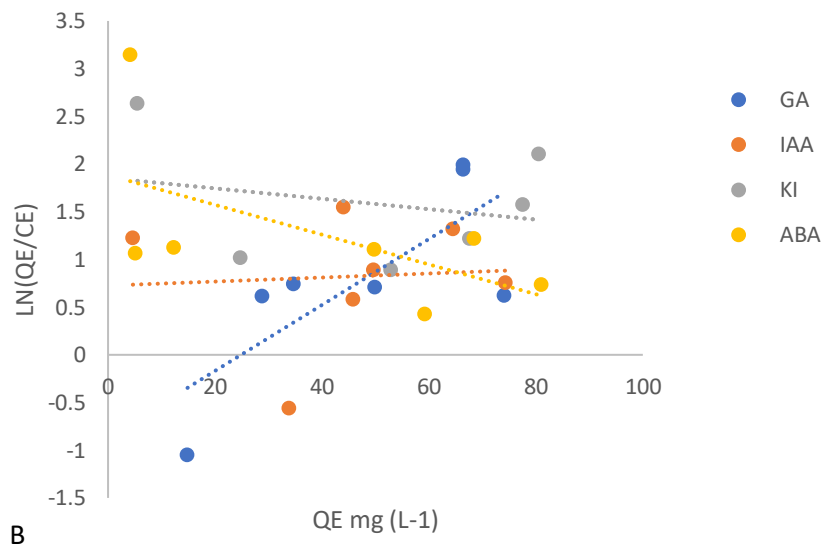
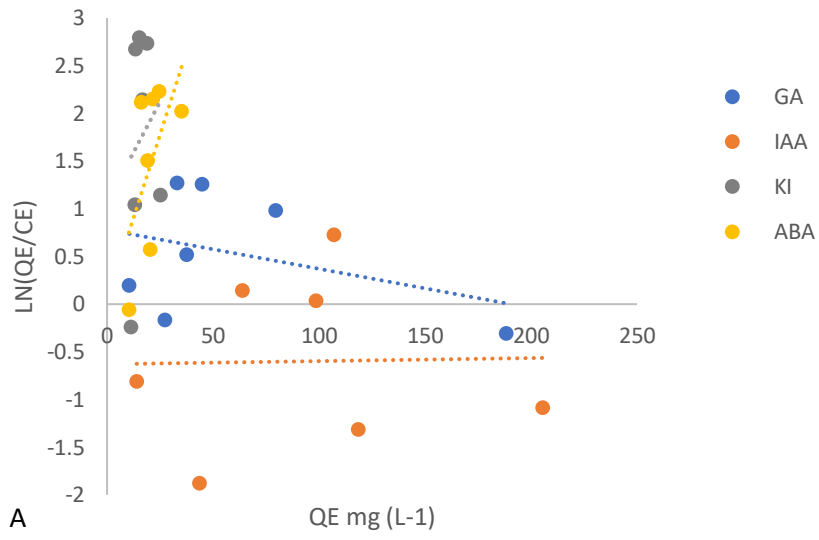
Ce = Concentration at equilibrium (mg L⁻¹)

Ke = Rate constant, and

Qm = Theoretical maximum adsorption capacity if there are no additional factors.

Table 17. Modelling of the Elovich equation (2 repetitions)

Elovich equation			
Material	Hormone	QM	R ²
AC	GA	19.96	0.11 ± 0.00
	IAA	9.84	0.19 ± 0.01
	KI	11.02	0.02 ± 0.00
	ABA	13.12	0.36 ± 0.05
A300	GA	7.12	0.58 ± 0.12
	IAA	23.78	0.18 ± 0.03
	KI	40.33	0.53 ± 0.00
	ABA	0.33	0.33 ± 0.04
A500	GA	60.17	0.61 ± 0.06
	IAA	3.89	0.10 ± 0.02
	KI	2.61	0.00 ± 0.00
	ABA	78.87	0.04 ± 0.02
A800	GA	10.31	0.12 ± 0.01
	IAA	6.48	0.23 ± 0.01
	KI	3.02	0.02 ± 0.00
	ABA	191.78	0.29 ± 0.06



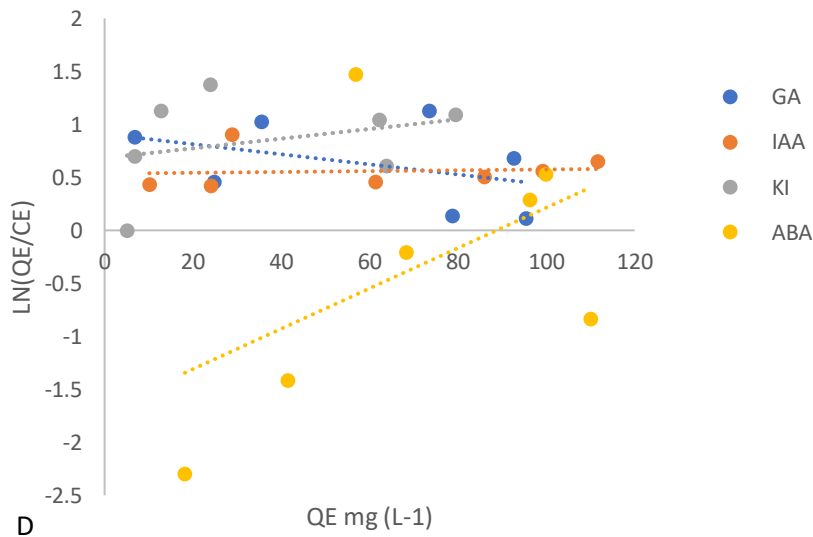
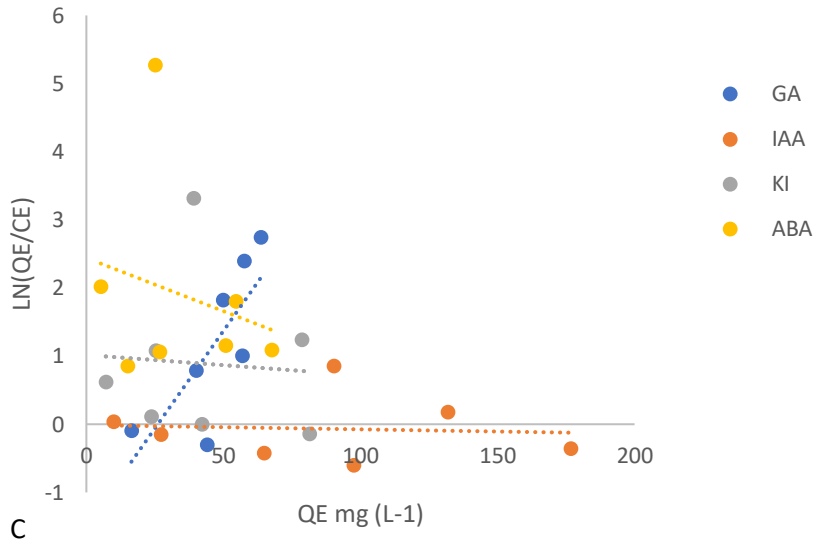


Figure 36. Elovich equation for all tested hormones and materials. A. AC, B. A300, C. A500, D. A800 (four repetitions).

It can be observed that no experiment conducted fit the Elovich model (Table 8 and Figure 36). From this a few insights can be gathered, one is that chemisorption is not occurring during adsorption which, if this is the case it means that while the experiments follow the pseudo second order it is not due to chemisorption but due to the multi-step adsorption process as expected. Looking at Figure 36, it can also be clearly seen that no hormone tested follows a linear model confirming the results seen in Table 17. Finally, results showed that the rate determining step is not connected to the number of adsorption

sites available which supports the results observed in Table 16. Overall both the data from the Elovich and Bangham equation showed that the rate determining step is primarily due to pore diffusion particularly with the materials with increasing microporosity, and that the rate determining step is not due to chemisorption but that there is a multi-step adsorption process going on and it is a physisorption process.

3.2.6 Adsorption isotherms

3.2.7 Langmuir isotherm.

Langmuir proposed an initial equation to determine the monolayer adsorption capacity of a solid.¹²⁰ The Langmuir adsorption isotherm is now commonly applied to adsorption processes due to its simplicity and many later isotherms are continuations of the Langmuir isotherm. The linear form of the isotherm is represented by the following Equation 12:

Equation 12. Langmuir isotherm

$$\frac{C_e}{Q_e} = \frac{1}{K_I} + \frac{A_I}{K_I} C_e$$

$$Q_0 = \frac{K_I}{A_I}$$

C_e = concentration at equilibrium (mg L^{-1}),

Q_e = adsorption capacity at equilibrium

A_I (L mg^{-1}) and K_I (L g^{-1}) = Langmuir adsorption constants.

Q_0 is the monolayer adsorption capacity of the solid (mg g^{-1}).

This model makes many assumptions, primarily that only a monolayer is formed from the adsorbate on to the homogeneous surface of the adsorbent. This isotherm makes the simple assumption that adsorption is occurring at specific sites within the adsorbent and once an adsorbate molecule is occupying this site no further adsorption can take place on it. This equation

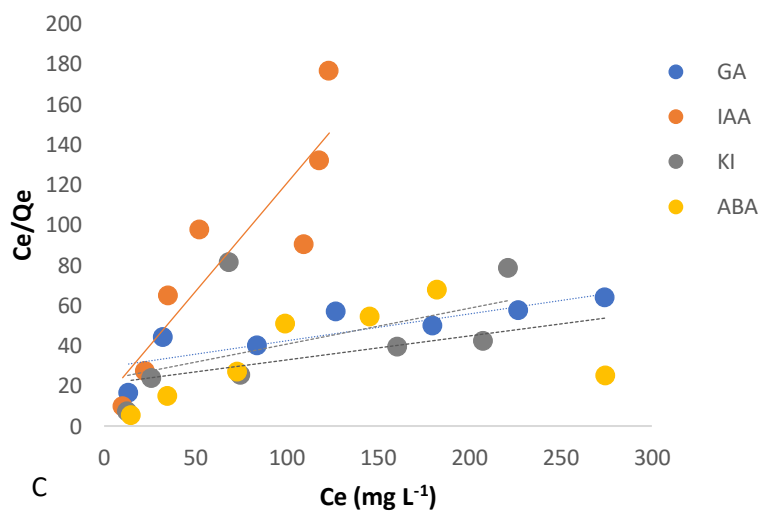
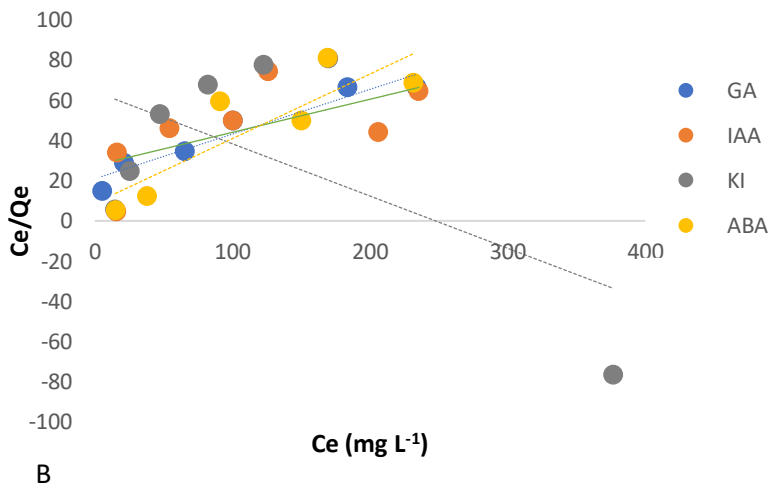
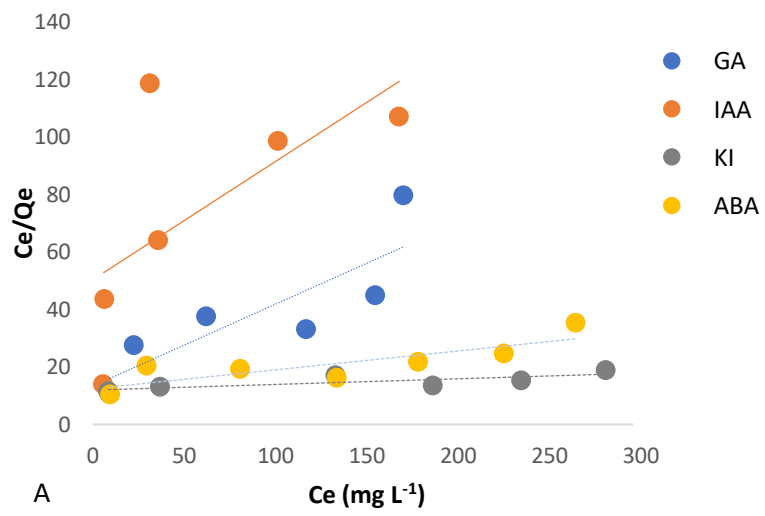
allows a basic calculation to see if the adsorption taking place is forming a full monolayer and the approximate capacity of this simplified monolayer.



Figure 37. A representation of the Langmuir model, note the homogenous surface and monolayer.

Table 18. Modelling of the Langmuir isotherm (2 repetitions)

Material	Hormone	Langmuir	
		$Q_0 \text{ mg g}^{-1}$	R^2
AC	GA	74.62	0.70 ± 0.04
	IAA	158.73	0.52 ± 0.05
	KI	16.03	0.93 ± 0.02
	ABA	15.22	0.69 ± 0.15
A300	GA	32.78	0.77 ± 0.09
	IAA	70.92	0.82 ± 0.02
	KI	24.57	0.76 ± 0.16
	ABA	3.11	0.75 ± 0.05
A500	GA	18.22	0.90 ± 0.01
	IAA	192.31	0.82 ± 0.21
	KI	68.97	0.61 ± 0.05
	ABA	2.74	0.97 ± 0.06
A800	GA	129.87	0.43 ± 0.03
	IAA	416.67	0.94 ± 0.16
	KI	153.85	0.25 ± 0.09
	ABA	2.26	0.52 ± 0.03



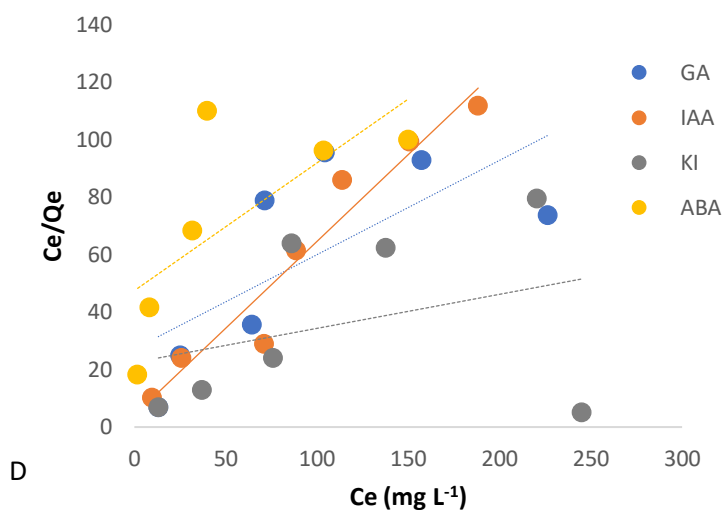


Figure 38. Langmuir Isotherm for all tested hormones and materials. A. AC, B. A300, C. A500, D. A800 (four repetitions).

It was deemed that any result with an R^2 below 0.8 was deemed to not fit the model for the purposes of this project. Based on the results plant hormones tested primarily do not follow the Langmuir isotherm with a few exceptions (Table 18). Q_0 calculated does not fit to the calculated values in (Table 14) for any of the results apart from GA and IAA with AC showing similar results. This suggests that overall while some show a closer fit to the Langmuir isotherm other factors are involved and most materials are not forming a monolayer. It was noted that ABA fits the Langmuir isotherm to a lower degree than the other tested hormones in most experiments and showed a very low Q_0 value in all experiments, which would mean that other influences are affecting the potential layer that was formed as seen earlier in section 3.1.14 ABA shows the highest amount of adsorption capacity. When looking at Figure 38 there is another story, with many of the hormones appearing to show a linear model with anomalous results for the hormones lowering the overall fit. For instance, IAA on AC showed an R^2 of 0.518 though looking at Figure 38 this was due to anomalous results, and the remaining results follow the Langmuir isotherm quite closely. It should be noted that the anomalous results should have been repeated in order to confirm the results are unreliable and should be

discounted. It suggests that all hormones tested have a closer fit Langmuir isotherm for AC, A300 and A500 but not A800. This would mean that there are aspects to the model which fit for the adsorption but that additional modifications are required to get a clearer understanding.

3.2.8 Freundlich isotherm

The Freundlich equation (Equation 13) is used to describe multilayer adsorption on heterogeneous surfaces (see Figure 39), which is characterised by the heterogeneity factor n .¹²¹

Equation 13. Freundlich equation

$$Q_e = K_f C_e^{\frac{1}{n}}$$

K_f = Freundlich constant and is linked to adsorption capacity of the solid.

n = heterogeneity factor, signifying the intensity of adsorption.

An n value of close to or greater than unity (1.0) indicates cooperative adsorption with greater values showing increasing heterogeneity. An n value below 1 indicates chemisorption at the surface.^{122,123} The Freundlich equation is related to the Langmuir equation, however it uses the assumption that adsorption will form a multilayer and/or onto an amorphous or heterogeneous surface rather than a homogeneous surface.³²

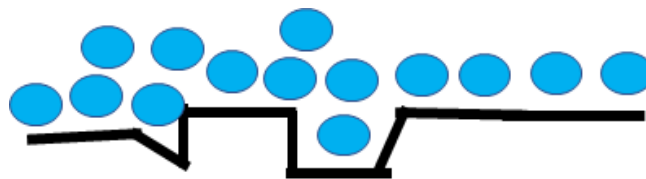
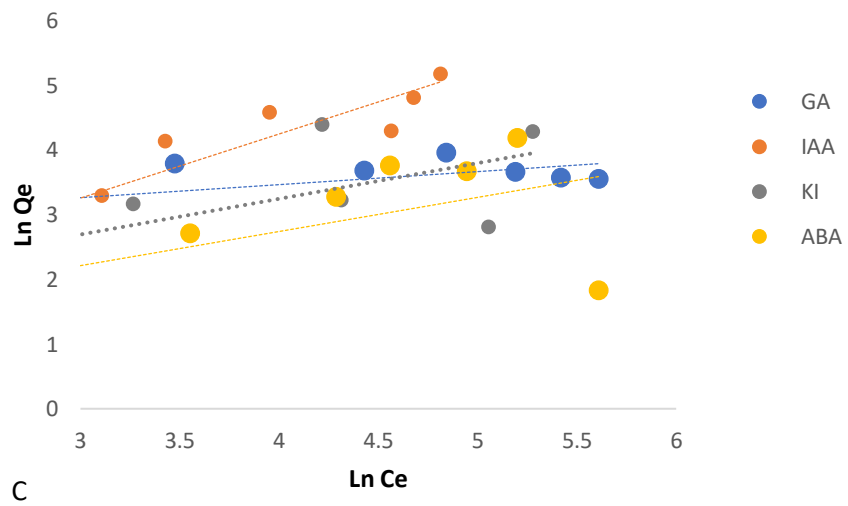
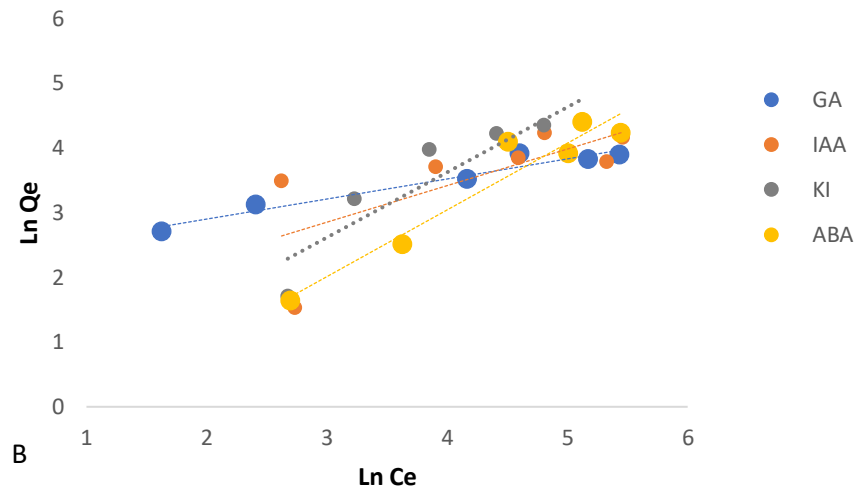
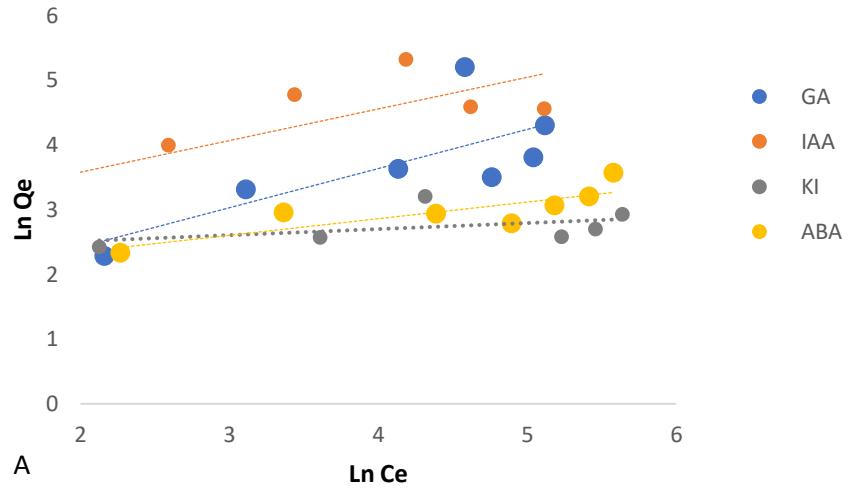
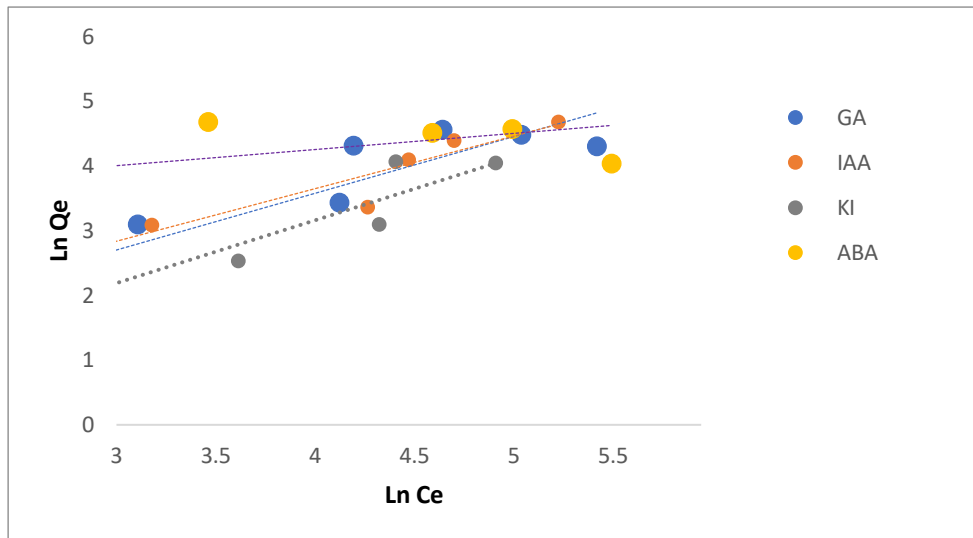


Figure 39. Model of Freundlich, note the multilayer and heterogeneous surface.

Table 19. Modelling of the Freundlich isotherm (2 repetitions)

Freundlich			
Material	Hormone	n	R²
AC	GA	1.65	0.56 ± 0.05
	IAA	1.61	0.20 ± 0.01
	KI	6.53	0.02 ± 0.00
	ABA	3.89	0.69 ± 0.07
A300	GA	3.90	0.28 ± 0.01
	IAA	2.18	0.65 ± 0.05
	KI	1.46	0.27 ± 0.01
	ABA	0.93	0.97 ± 0.13
A500	GA	5.01	0.33 ± 0.01
	IAA	1.01	0.88 ± 0.07
	KI	1.79	0.45 ± 0.00
	ABA	0.94	0.96 ± 0.03
A800	GA	1.56	0.84 ± 0.06
	IAA	1.11	0.95 ± 0.03
	KI	1.19	0.85 ± 0.02
	ABA	4.55	0.67 ± 0.15





D

Figure 40. Freundlich Isotherm for all tested hormones and materials. A. AC, B. A300, C. A500, D. A800 (four repetitions).

The plant growth promoters tested appear to fit the isotherm with A800 material (Table 19). Abscisic acid fits the Freundlich isotherm primarily with A300 and A500 but less so with A800 and AC. It was noted that with A300 there may be anomalous results for GA which may have resulted in a weaker fitting to the model however multiple repeats did not significantly improve the fitting. No hormones tested fit the isotherm when tested with AC which suggests that with AC a multilayer is unlikely to form or that the surface is primarily homogeneous. Results show that GA and KI both do not follow the Freundlich isotherm with A500. This would show that overall that the hormones form a multilayer on A500 and A800. The n values calculated are all above 1 for the plant growth promoters which confirms that instead of chemisorption occurring the primary adsorption process is physisorption. This was a very important confirmation as for the Starbons to be successful as a seed coating component the adsorbate would need to be physisorbed for desorption to occur at lower temperatures. Abscisic acid does show an n value below 1 for A300 and A500 (where it has the closest fit to the model) suggesting that stronger adsorption may be occurring for that hormone. Again, this is beneficial as if it is to be used as a seed coating a stronger bonding with the plant growth inhibitor would mean less material is desorbed.

3.2.9 Temkin isotherm

The Temkin isotherm (Equation 14) is used to determine the heterogeneity of the surface of the material. The isotherm assumes:

- i. There are adsorbent and adsorbate interactions;
- ii. The concentration of the solvent can be ignored, and;
- iii. Heat of adsorption will decrease on a linear model not on a logarithmic model as per the Langmuir model. A logarithmic model of heat of adsorption means that as more adsorbate is adsorbed there is an increased effect on the heat of adsorption but eventually levelling out as the multi-layer forms as and the interaction between the adsorbent and the adsorbate is weakened. The Temkin linear model means that there are an increasing number of interactions as more adsorbate binds to the surface and that the adsorbate adsorbent interactions are likely to be strong.

Equation 14. Temkin equation

$$Q_e = B \ln A + B \ln C_e$$

Where A = Temkin isotherm constant ($L g^{-1}$)

B = Heat of sorption ($kJ mol^{-1}$)

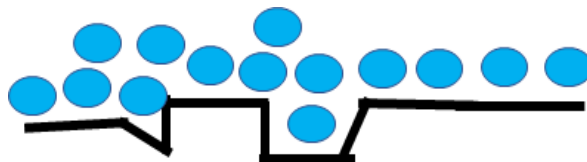
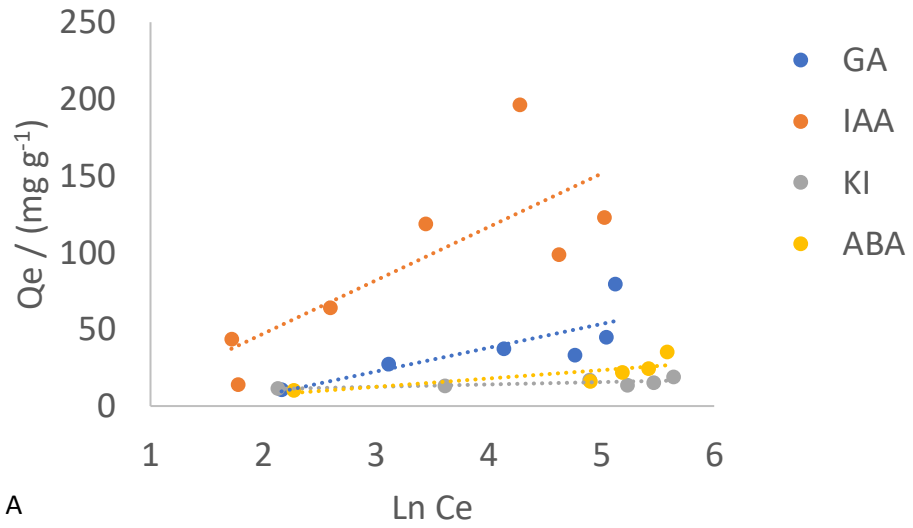


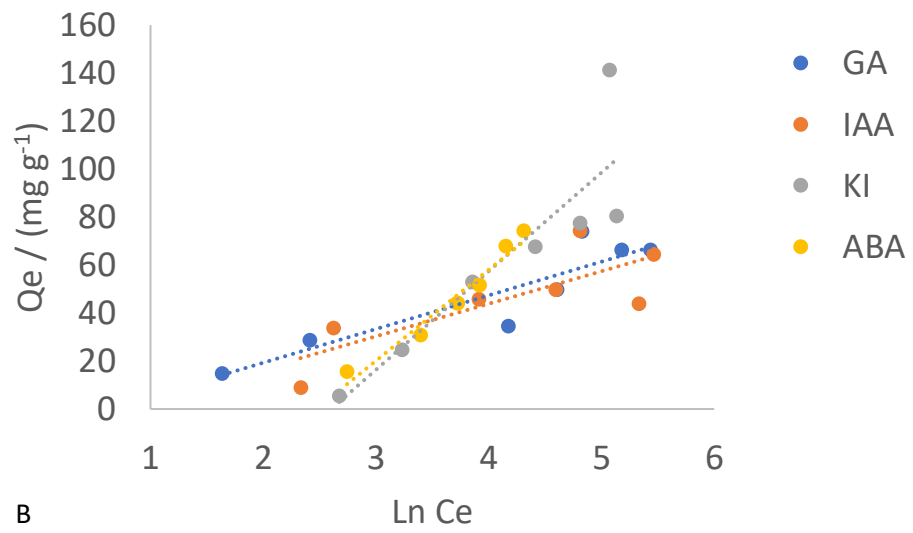
Figure 41. Model of Temkin, note the multilayer and heterogenous surface.

Table 20. Modelling of the Temkin isotherm. (2 repetitions)

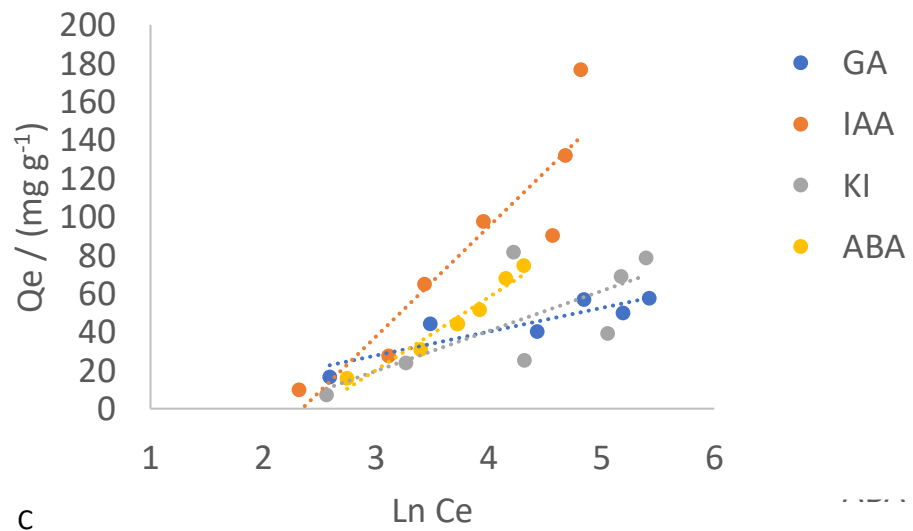
Temkin			
Material	Hormone	E (kJ mol ⁻¹)	R ²
AC	GA	22.0 ± 0.2	0.95 ± 0.15
	IAA	28.5 ± 0.3	0.81 ± 0.15
	KI	1.2 ± 0.1	0.24 ± 0.02
	ABA	3.3 ± 0.7	0.91 ± 0.20
A300	GA	15.6 ± 0.5	0.90 ± 0.01
	IAA	19 ± 2	0.91 ± 0.12
	KI	34.6 ± 0.5	0.99 ± 0.02
	ABA	38.6 ± 0.6	0.98 ± 0.00
A500	GA	12.5 ± 0.5	0.89 ± 0.01
	IAA	42 ± 5	0.94 ± 0.22
	KI	37 ± 3	0.93 ± 0.12
	ABA	22 ± 2	0.95 ± 0.08
A800	GA	27.7 ± 0.1	0.91 ± 0.19
	IAA	37 ± 4.0	0.91 ± 0.06
	KI	26.5 ± 0.3	0.91 ± 0.12
	ABA	43.0 ± 0.8	0.98 ± 0.11



A



B



C

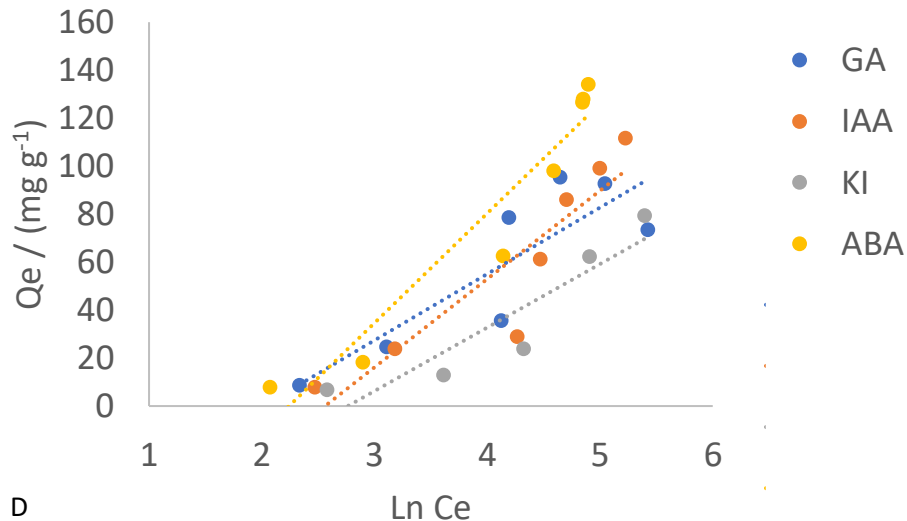


Figure 42. Temkin Isotherm for all tested hormones and materials. A. AC, B. A300, C. A500, D. A800 (four repetitions).

From the results a few key observations may be made (Table 20 and Figure 42). One is that bar a few exceptions all the Starbons show a strong fit to this isotherm with all bioactives tested. Activated carbon also shows a close fit particularly with the larger molecular weight molecules GA and ABA. Overall this suggests that the surface of the materials tested are highly heterogeneous with the Starbons showing more heterogeneity compared to the AC. The correlation was also increased compared to the Freundlich isotherm which would indicate that the heat of adsorption is a constant. Looking at energy of adsorption there is no clear trend observable, but some difference could be seen. The energy for adsorption of KI and ABA was very low on AC compared to the Starbon material suggesting that there was a considerable difference between the materials affecting the adsorption.

3.2.10 Dubinin Radushkevich isotherm

The equation proposed by Dubinin and Radushkevich (Equation 15) is used to describe adsorption onto porous solids, using the assumption there is no homogeneous surface of the adsorbent and that the microporosity can be examined. This model is primarily used to help understand the microporosity of the material which is an important factor with all the materials tested. The Dubinin-Radushkevich isotherm states that due to adsorption occurring

simultaneously in all pores it can be used to estimate the energy of adsorption.^{124,125} The Dubinin-Radushkevich isotherm is an amendment to the Dubinin-Astro isotherm which works to help explain microporosity found within the material. The version of Dubinin-Radushkevich isotherm used in this project is designed on the assumption that there is a gaussian distribution of micropores. Amendments to the isotherm are possible to improve fitting however for the sake of consistency all materials and bioactives have been fitted to one version of the Dubinin-Radushkevich isotherm. Another benefit of the Dubinin-Radushkevich isotherm model is that it can be used to help determine the pore size distribution of the micropores dependent on the trend line shape (Figure 43).

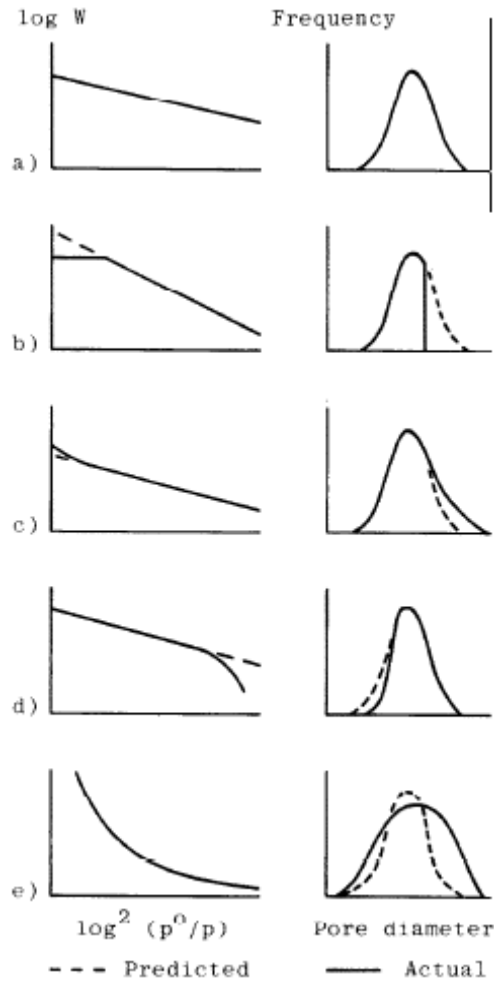


Figure 43. Pore distribution as theorised by the Dubinin-Radushkevich isotherm. (One variation of the isotherm model).¹²⁶

The equation is written as:

Equation 15. Dubinin Radushkevich equation

$$Q_e = Q_m - K' \epsilon e^{(RT \ln(1 + \frac{1}{C_e}))^2}$$

ϵ = the Polanyi potential, is equal to:

Equation 16, Polanyi potential equation

$$\epsilon = RT \ln(1 + \frac{1}{C_e})$$

Q_m = the monolayer saturation capacity ($L g^{-1}$)

R = the gas constant (8.314 J mol⁻¹ K⁻¹)

K' = the constant of adsorption energy which gives the mean free energy of adsorption per molecule of adsorbate when it is transferred to the surface of the solid from the solution and can be calculated from the following relationship:²²

$$E = \frac{1}{\sqrt{2K'}}$$

The mean adsorption energy (E) gives information about chemical and physisorption, where low values of E indicates physisorption of the adsorbate.¹²⁷ higher values (8+) indicates stronger bonding including ion transfer and chemisorption, though this does not take into account the potential for a multilayer forming which can affect the results.^{128,125}

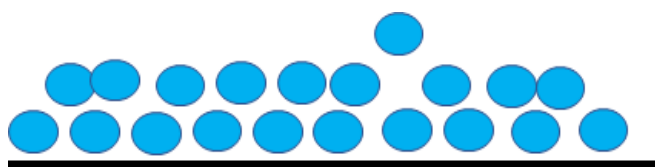
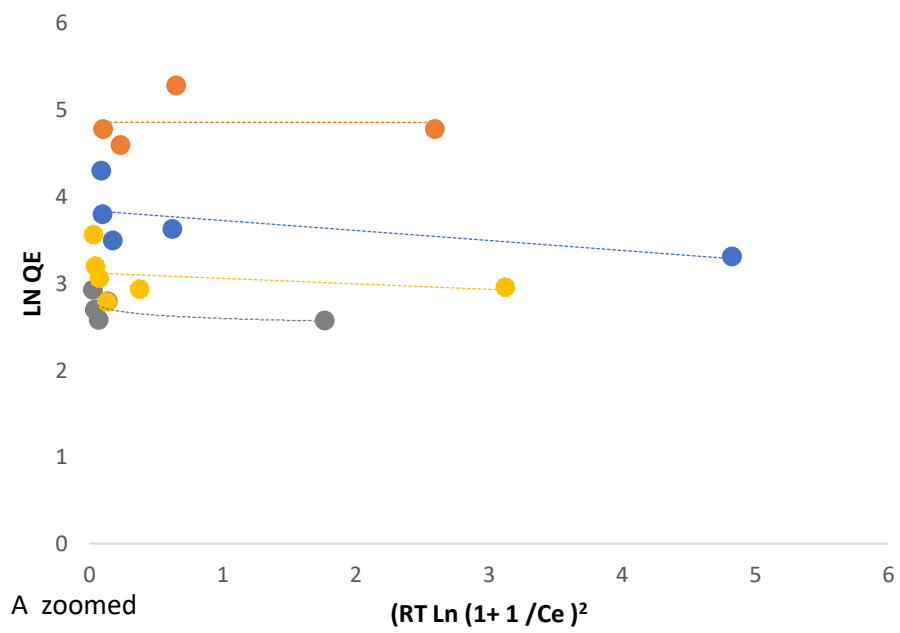
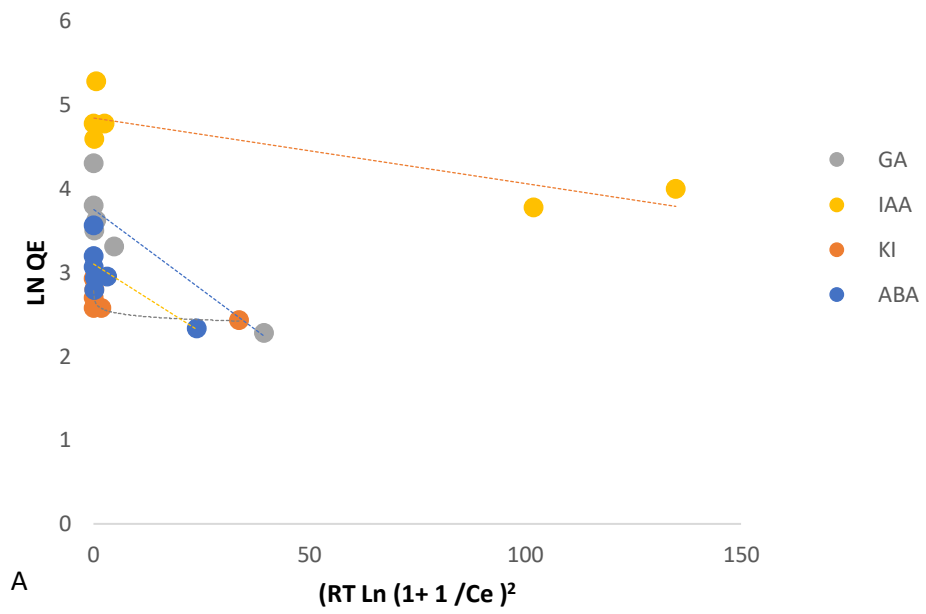
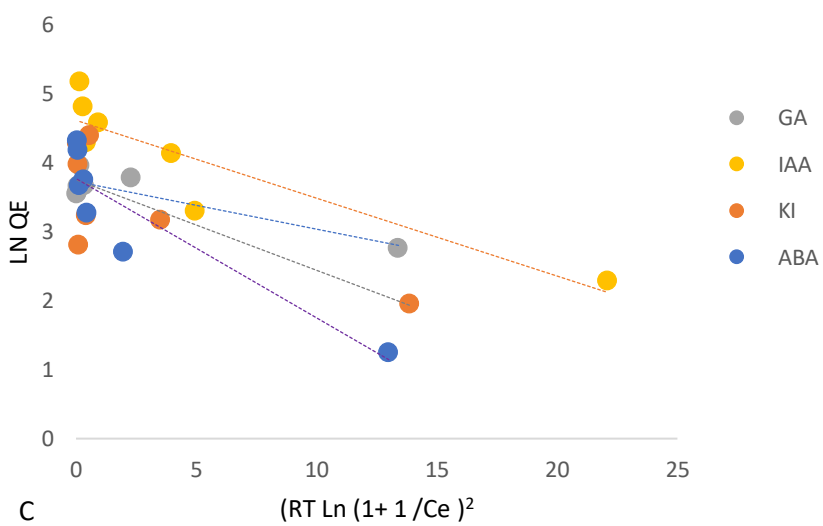
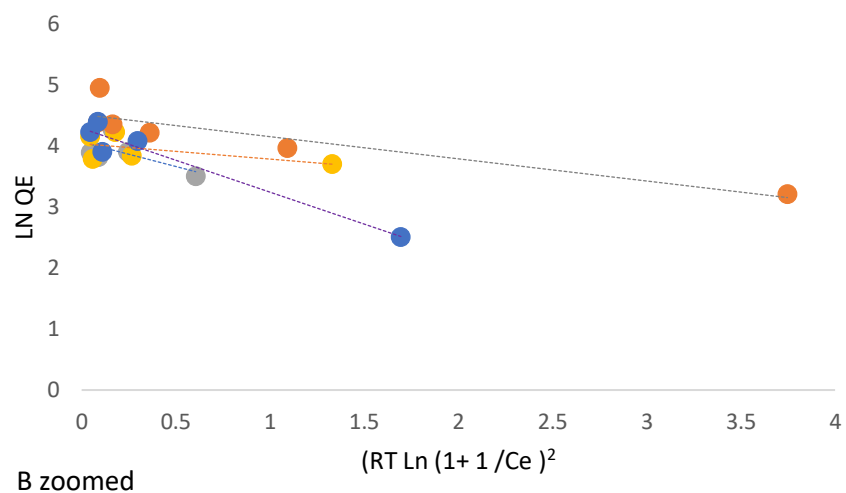
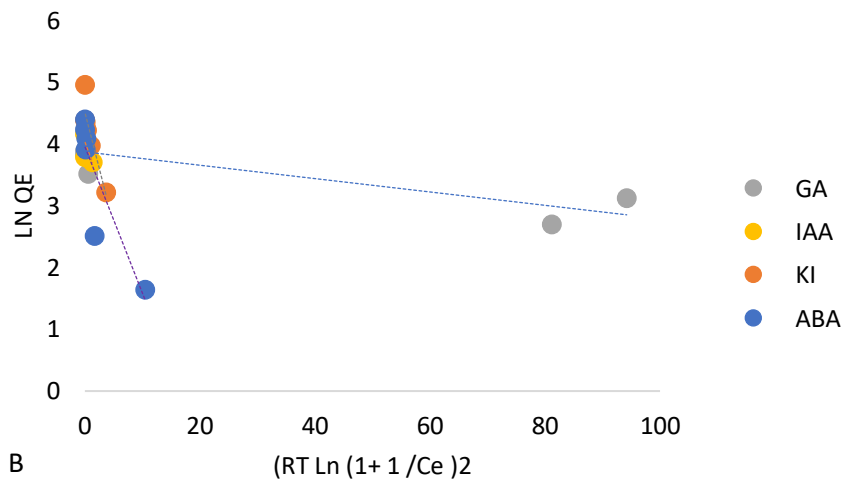


Figure 44. Model of the Dubinin-Radushkevich isotherm. Note the homogenous surface and multilayer formed.

Table 21. Modelling of the Dubinin Radushkevich isotherm (2 repetitions)

D-R			
Material	Hormone	E (kJ mol ⁻¹)	R ²
AC	GA	1.73	0.98 ± 0.02
	IAA	7.18	0.75 ± 0.01
	KI	2.24	0.55 ± 0.00
	ABA	2.80	0.89 ± 0.00
A300	GA	6.80	0.87 ± 0.10
	IAA	1.40	0.75 ± 0.02
	KI	1.17	0.94 ± 0.00
	ABA	0.77	0.98 ± 0.01
A500	GA	2.67	0.81 ± 0.04
	IAA	2.11	0.85 ± 0.09
	KI	1.95	0.79 ± 0.15
	ABA	0.02	0.91 ± 0.04
A800	GA	2.49	0.94 ± 0.07
	IAA	0.40	0.95 ± 0.05
	KI	0.75	0.73 ± 0.01
	ABA	11.79	0.92 ± 0.20





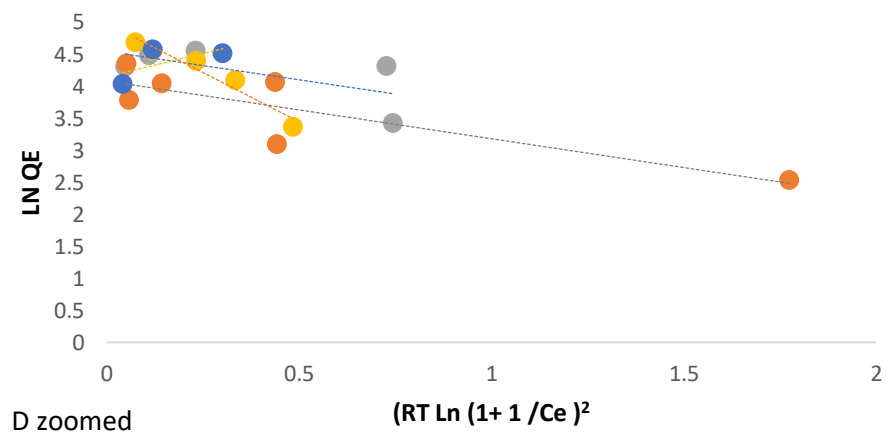
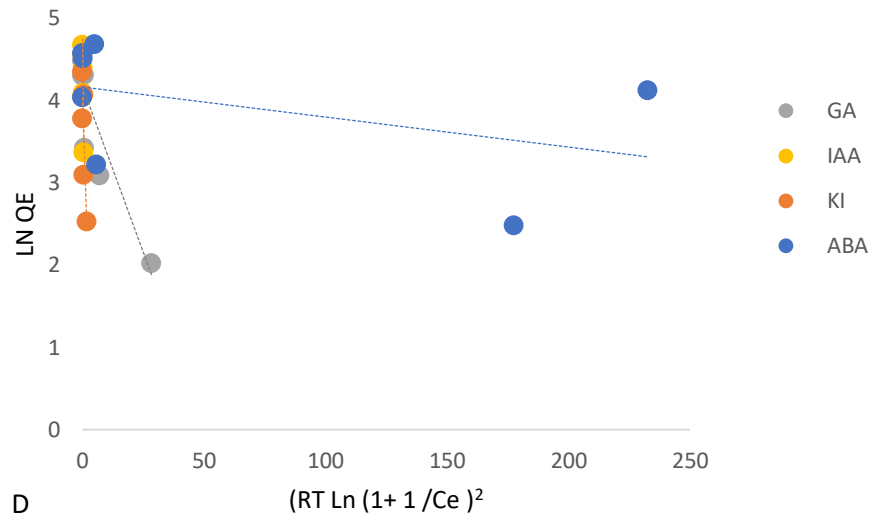
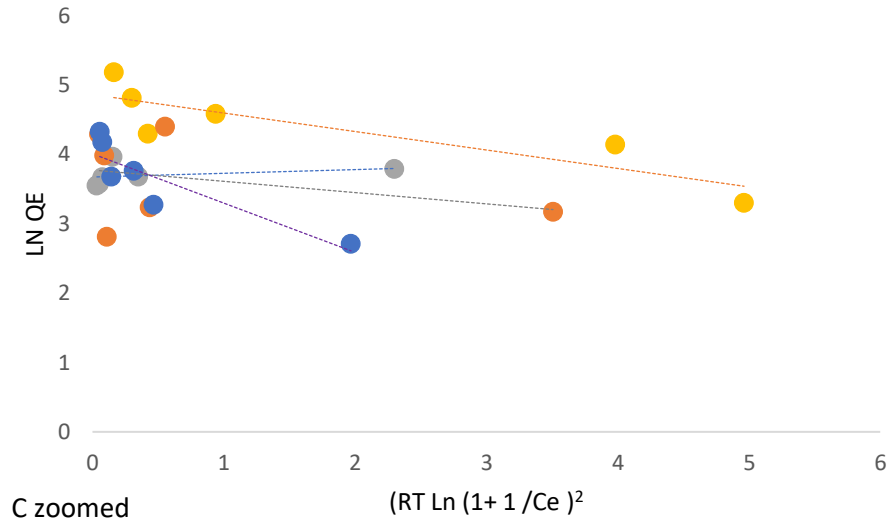


Figure 45. Dubinin Radushkevich Isotherm for all tested hormones and materials showing full set of data and zoomed in of initial points.

Based on the results it shows that a close fit was observed in most cases (Table 21 and Figure 45). Most bioactives bar KI fit the model for AC. Starbon A300 shows a closer fit for all the bioactives particularly KI and ABA. The bioactives show a close fit with A500 and A800 though again KI shows a lower fit than the other tested bioactives. This close fit shows three things, one simply confirms there is a mix of mesoporous and microporous material and the microporous is in a high enough quantity to be analysed. Two is that at these higher temperatures of carbonisation the adsorption is occurring on a more heterogeneous surface and that the microporosity is also increasing confirming what data discussed earlier. Finally, this close fitting means that the microporosity is a gaussian fit so most of the micropores are within a set range in size rather than a wider distribution in size.

One thing of note is that in the E value (energy of adsorption) are low indicating that that the hormones are adsorbing via physisorption and other weak interactions. This is in line with the results obtained from the Freundlich results earlier which indicated weak interactions during adsorption. Abscisic acid does show a high E value when testing with A800 suggesting stronger interactions with the Starbon surface.

As discussed earlier by observing the value trend line the microporosity can be analysed. Based on the trend line and results a few things could be determined about the pore size distribution. It can also be observed with AC, A300 and A500 to a less degree, that the lower values show that there may be a second trend line forming at a steeper angle than calculated. This means that the distribution is shifted towards the left with an increase in smaller micropores with a steeper curve indicating a greater shift to these smaller micropores. With AC, it was noted all bar KI showed this peak with a smaller than expected distribution. Starbon A300 shows this same peak but to a lesser degree whilst also on the zoomed in data shows a slight curve down at the high values, this means that the gaussian distribution is much more pronounced than expected resulting in micropores which are all very similar size to one another. Starbon A800 does not show this steep increase at the

smaller pores but still shows a high fit to the model meaning that higher carbonisation the micropores fit the gaussian model of micropore distribution.

3.2.11

3.2.12 Thermodynamic study of adsorption

To further understand the adsorption process occurring between the hormones tested and the Starbon material. Thermodynamic experiments can occur to evaluate the thermodynamic parameters. To calculate the thermodynamic parameters the Van't Hoff equation was used;

Equation 3: the Van't Hoff equation

$$\ln k = \frac{\Delta S}{R} - \frac{\Delta H}{RT}$$

Where k = the equilibrium constant at

T = temperature (K)

R = the gas constant

ΔH = Change in enthalpy

ΔS = Change in entropy

The Gibbs free energy was also calculated to determine the adsorption feasibility:

Equation 17. Gibbs free energy.

$$\Delta G = -RT \ln k$$

Or

Equation 18. Alternative for Gibbs free energy.

$$\Delta G = \Delta H - T\Delta S$$

A positive value of ΔH would indicate an endothermic reaction is taking place which implies that adsorption would increase as temperature increases. As previously discussed in 3.2.3 in all cases of adsorption studied followed the pseudo second order model and all evidence showed a multistage process. In

a liquid/solid interface this multi-step is the removal of adsorbed solvent molecules (in this case water) followed by the adsorption of the adsorbate molecules. If the experiment showed an endothermic reaction then it suggests that the adsorbate-adsorbent interaction is weak, and that the energy required to desorb the water molecules is larger than that released by the adsorbate-adsorbent interaction. The other possible explanation is that the intra particle diffusion step of the sorption process is highly endothermic. If ΔH is negative than the adsorption process is exothermic and means that the energy released during adsorption is much higher than then the energy required to break the water-adsorbent bonds.

As temperature increases it would be expected that overall entropy also increases, not only due to increased energy put into the mix but also as the sorption process takes place water molecules are desorbed from the solid back into the solution. From the ΔS values it becomes possible to start understanding the likely orientations of the compounds as they interact with the adsorbent. Higher levels of ΔS would indicate that more water is being desorbed off the surface to allow adsorption of the adsorbate suggesting that the adsorbate is adsorbing at multiple points along the surface rather than at one point on the end of the adsorbate. If ΔS is found to be negative than it means that the adsorption process is reducing overall entropy in the system due to forming an associative complex with the adsorbent. This would also mean that there is no change to the internal structure of the adsorbent during the adsorption process.^{118,129,130} The adsorption process is an inherently exothermic process as the adsorbate and adsorbent interact.³³ A negative entropy also indicates that the degrees of freedom when adsorbed are reduced compared to how it was in the solution. For example, a free-flowing adsorbate molecule would have three degrees of freedom but when adsorbed this would be reduced which would further decrease entropy. This would also need to take into account solvent ordering and rearrangement also as potentially affecting the overall adsorption process.

Finally, ΔG can be used to determine if the adsorption that takes place is spontaneous or not. If ΔG is negative it means that the adsorption process is

favoured, and the material is thermodynamically favoured to remain adsorbed to the material, however if ΔG is positive than energy is required for the adsorption to take place and remain adsorbed meaning that the adsorption process is disfavoured resulting in desorption being the favoured process. As such temperature plays an important factor in the adsorption process as ΔG must remain negative for adsorption to remain spontaneous. The tables below show the results for each hormone on the selected material. (see Section 2.2.14 for experimental details). All results below assume per mole of plant hormone.

Table 22. Thermodynamic parameters of Gibberellic acid.

Material	Temp / k	Ln K	$\Delta G / \text{kJ mol}^{-1}$	$\Delta H / \text{kJ mol}^{-1}$	$\Delta S / \text{J mol}^{-1} \text{K}^{-1}$	R^2
AC	298	-0.41	1.02	-59 ± 3	-200 ± 10	0.98 ± 0.02
	308	-1.08	2.77			
	318	-1.92	5.06			
A300	298	-0.54	1.34	-13.9 ± 1.0	-51.0 ± 1.8	0.92 ± 0.02
	308	-0.63	1.62			
	318	-0.77	2.03			
A500	298	-0.67	1.67	-25.4 ± 0.6	-90.5 ± 1.9	0.93 ± 0.05
	308	-1.07	2.75			
	318	-1.35	3.58			
A800	298	-0.46	1.14	-42 ± 8	-145.1 ± 1.6	0.92 ± 0.01
	308	-1.09	2.79			
	318	-1.66	4.38			

From the results several trends can be observed (Table 22). All experiments show that the Gibbs free energy is positive and increases as temperature increases, and that as temperature of carbonisation increases so too does the increase observed for Gibbs free energy. This means that the adsorption process is non-spontaneous requiring energy for adsorption to take place. Enthalpy and entropy was found to be negative in all cases meaning that the adsorption process is both exothermic and reduces overall entropy. The trend

observed suggests that as microporosity increases the greater the change in entropy and enthalpy will be observed.

Table 23. Thermodynamic parameters of Indole-3-acetic acid.

IAA	T / K	Ln K	$\Delta G / \text{kJ mol}^{-1}$	$\Delta H / \text{kJ mol}^{-1}$	$\Delta S / \text{J mol}^{-1} \text{K}^{-1}$	r^2
AC	298	-0.83	2.05	-26 ± 2	-133 ± 7	0.88 ± 0.16
	308	-0.55	1.41			
	318	-0.25	0.67			
A300	298	-0.58	1.45	-53.9 ± 1.6	-100 ± 9	0.95 ± 0.27
	308	-0.70	1.80			
	318	-1.59	4.19			
A500	298	-0.66	1.62	-21.0 ± 1.9	$-176.0 \pm$ 1.5	0.84 ± 0.05
	308	-0.85	2.17			
	318	-1.16	3.07			
A800	298	-0.68	1.69	-54 ± 5	$-133.7 \pm$ 0.6	0.94 ± 0.17
	308	-1.18	3.03			
	318	-1.99	5.25			

The results seen in Table 23 show that the Starbons show negative enthalpy and entropy with a positive value for the Gibbs free energy. It's also interesting to see that there is no clear trend in the calculated entropy or enthalpy values for the Starbons material, in fact the results for A300 and A800 are very similar which would suggest that adsorption is not dependent on the changing porosity or surface chemistry of the Starbons.

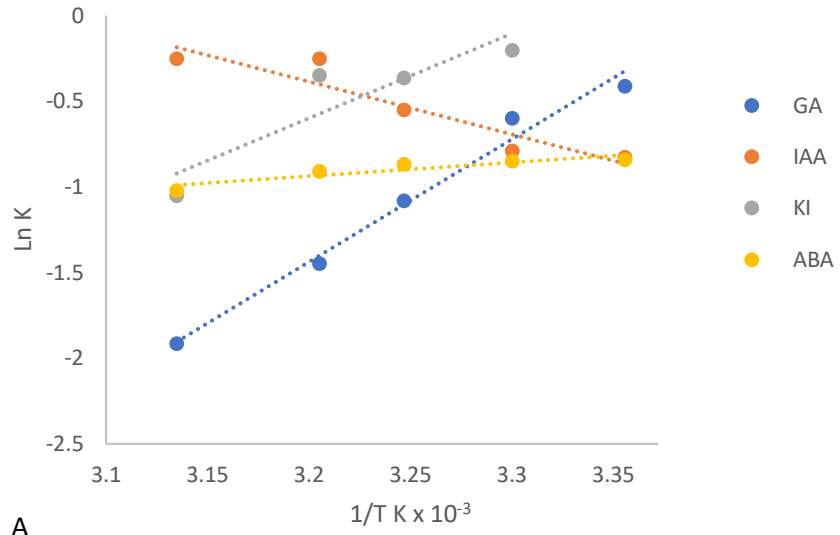
Table 24. Thermodynamic parameters of Kinetin.

KI	T / K	Ln K	$\Delta G / \text{kJ mol}^{-1}$	$\Delta H / \text{kJ mol}^{-1}$	$\Delta S / \text{J mol}^{-1} \text{K}^{-1}$	R ²
AC	298	-1.16	2.89	-38 ± 2	-126 ± 7	0.72 ± 0.05
	308	-0.60	1.55			
	318	-1.05	2.79			
A300	298	-0.42	1.05	-26.9 ± 0.4	-93 ± 2	0.87 ± 0.02
	308	-0.62	1.59			
	318	-1.14	3.01			
A500	298	-0.44	1.08	-37.5 ± 0.5	-129 ± 5	0.92 ± 0.09
	308	-0.91	2.34			
	318	-1.39	3.69			
A800	298	-0.47	1.16	-59.9 ± 0.7	-204 ± 2	0.95 ± 0.02
	308	-1.09	2.80			
	318	-2.05	5.42			

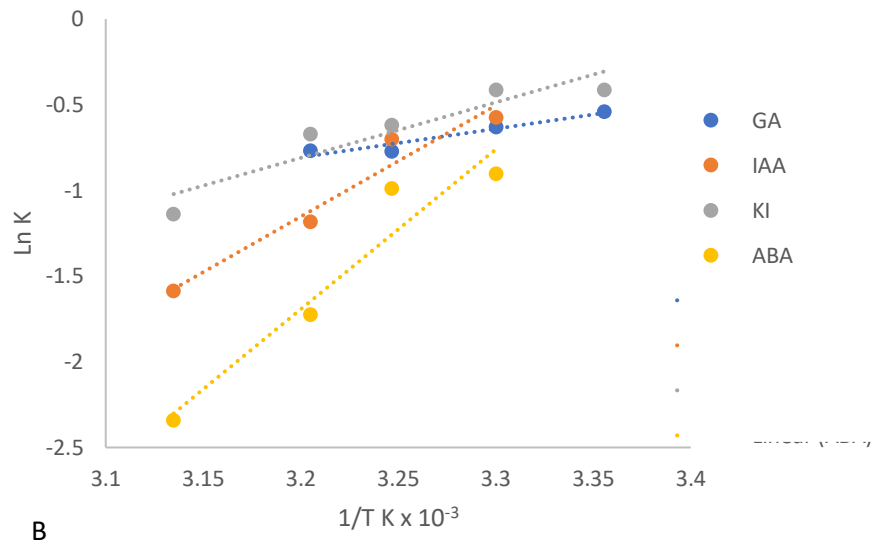
The results for KI in Table 24 show a similar trend to GA shown earlier in Table 22. The Gibbs free energy was found to increase as temperature of carbonisation increased, the change in entropy and enthalpy also increased. Activated carbon however compared to the gibberellic acid results was found to have results like the A500 results with A800 showing a greater change in enthalpy and entropy. This means that while the porosity is a major factor in the adsorption process there is an additional factor which Starbons possess that the AC does not which causes a greater change in entropy and enthalpy, with the most likely reason being the oxygenated functional groups found on the Starbon materials.

Table 25. Thermodynamic parameters of abscisic acid.

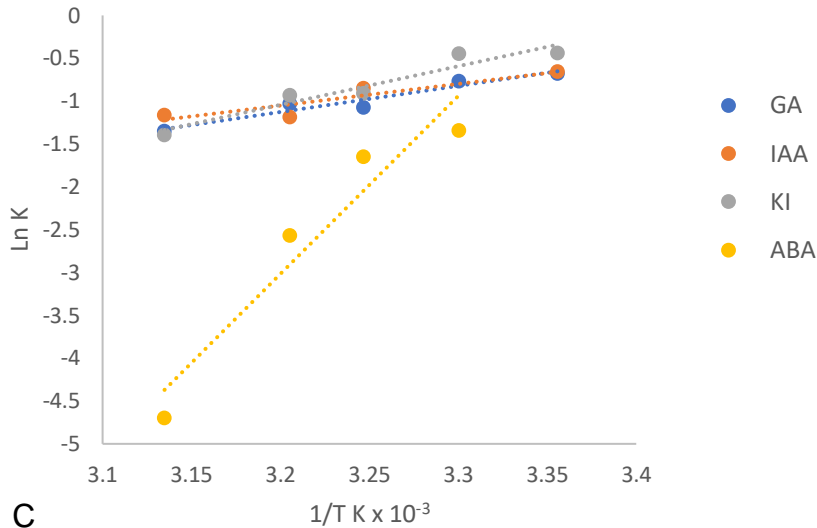
ABA	T / K	Ln K	$\Delta G / \text{kJ mol}^{-1}$	$\Delta H / \text{kJ mol}^{-1}$	$\Delta S / \text{mol}^{-1} \text{K}^{-1}$	r^2
AC	298	-0.84	2.09	-6.6 ± 1.2	-29.0 ± 0.4	0.83 ± 0.06
	308	-0.87	2.22			
	318	-1.02	2.71			
A300	298	-0.90	2.28	-77.6 ± 1.0	-262 ± 3	0.93 ± 0.10
	308	-0.99	2.53			
	318	-2.34	6.19			
A500	298	-1.35	3.36	-124 ± 2	-443 ± 6	0.92 ± 0.01
	308	-1.65	4.22			
	318	-4.69	12.41			
A800	298	-0.81	2.00	-146.0 ± 1.6	-491 ± 6	0.95 ± 0.04
	308	-1.77	4.53			
	318	-3.94	10.43			



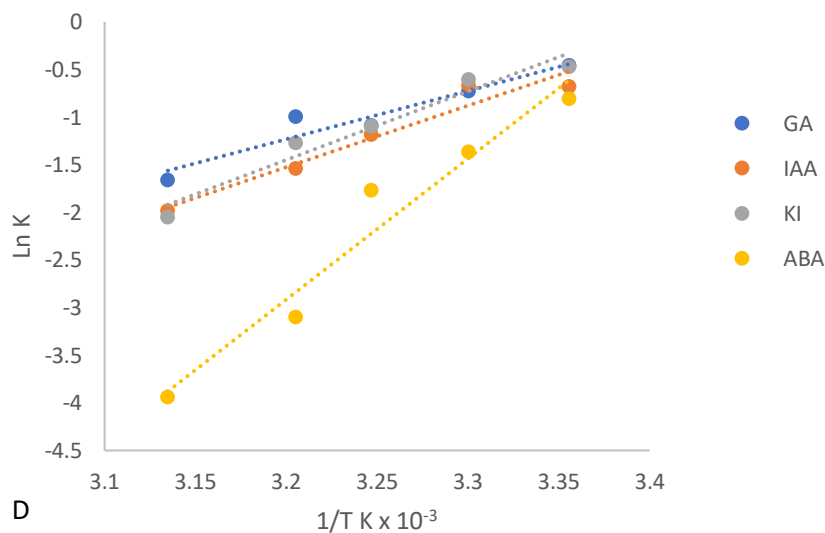
A



B



C



D

Figure 46. Thermodynamics for all tested hormones and materials. A. AC. B. A300. C. A500 and D. A800 (average over four repetitions).

Results for ABA when adsorbed onto each material (Table 25). One thing that is noticed in all experiments conducted was that ΔG was positive meaning that the adsorption process is not favoured. In most cases ΔG increases as temperature increases showing that at higher temperatures overall desorption increases. This is interesting as it would mean that desorption should be the favoured process for the hormones. The change in enthalpy suggests that there is stronger than expected bonding occurring during the adsorption process. However, it has been established that chemisorption does not take

place so the values for the change in enthalpy most likely indicates that there are strong interactions as the ABA forms a multilayer along the surface of the material. Results in section 3.3 show that adsorption not only takes place but desorption either does not take place or occurs in low quantities. As such, to understand this a regression was done to determine at what temperature the equilibrium was achieved for ΔG (e.g. the T at which $\Delta G = 0$) as seen below (Table 26) this is not a wholly accurate representation but allows the closest approximation. The results below show that most of cases the adsorption experiments take place below the equilibrium point at which adsorption takes place resulting in adsorption being spontaneous and favoured. There are a few anomalous results observed such IAA with AC showed a temperature at 323 K which is the highest temperature recorded which would mean that in the adsorption experiments conducted IAA will be strongly adsorbed to the surface. Another result is ABA with AC which showed a temperature of 239 K implying that desorption is highly favoured for abscisic acid on AC. Finally, with the Starbons IAA, KI and ABA all have very similar equilibrium points with no real trend observed but with temperatures above the experimental temperature conducted. Gibberellic acid however, showed that both A300 and A800 show equilibrium temperatures below the experimental temperature which would mean that desorption is favoured for GA, this however is not observed with the A800 material which is now above the experimental temperature.

Table 26. Equilibrium point of ΔG .

Material	Hormone	ΔG equilibrium point / K
AC	GA	294
	IAA	323
	KI	294
	ABA	239
A300	GA	284
	IAA	297
	KI	292
	ABA	297
A500	GA	282
	IAA	293
	KI	293
	ABA	294
A800	GA	294
	IAA	296
	KI	295
	ABA	295

3.2.13 Intermolecular forces of bioactives

It was important that not only were the kinetic and thermodynamic parameters be tested but also their physical properties be examined to understand how this might affect the adsorption and desorption properties. Bioactive physical properties were calculated using the program Chembiodraw Ultra 3D using the molecular modelling version 2, (MM2) as the force field model. ⁴²

Table 27. Computational analysis (MM2) of bioactives tested. (taking averages over the entire structure)

Interactions (kcal / mol)	GA	IAA	KI	ABA
Stretch	2.65	0.53	0.54	1.83
Bend	17.86	8.27	15.39	7.94
Stretch-bend	0.18	-0.04	-0.06	0.55
Torsion	19.64	-8.00	1.67	9.25
Non-bonded	-18.93	-4.49	-2.43	-6.72
Van der Waals	9.38	18.91	17.83	4.97
Dipole/Dipole	0.69	5.41	22.83	1.10
Total energy	2.65	20.59	55.77	18.92

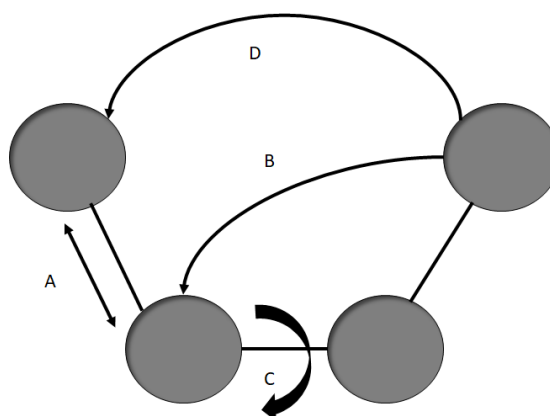


Figure 47. Potential energy interactions, A. Bond stretching, B. Bend stretching, C. Torsion and D non-bonded interactions.

Table 27 and Figure 47 above, show the calculated values of the plant hormones tested with the total potential energy within the molecule along with an explanation for some of the interactions. These values were determined via ChemBiodraw Ultra 3D and have not been identified experimentally. The stretching energy is the interaction between two adjacent atoms and how far they can extend and contract before the bond is broken. Bend stretching otherwise known as angle stretching is the interaction between a chain of atoms and showed the interaction between terminal atoms, showing how close they can interact or move apart. Torsion is the energy for a bond to twist so

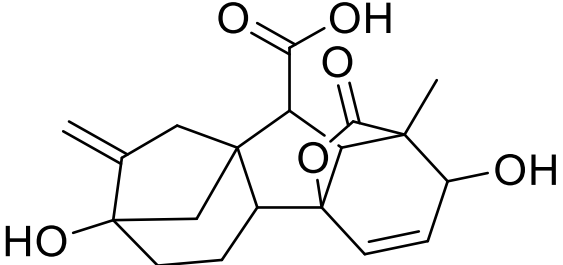
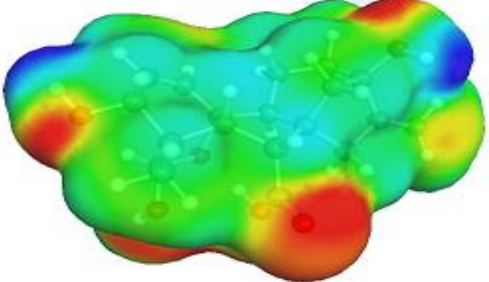
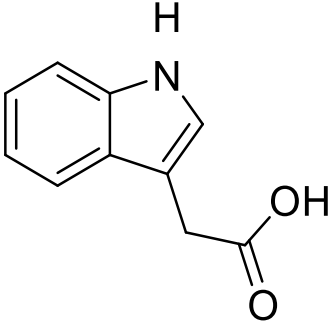
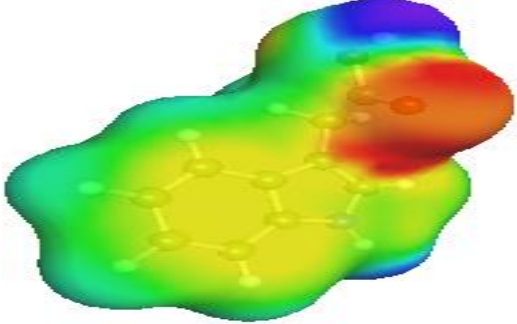
that non-adjacent atoms may line up cleanly. Stretch, bend, stretch-bend, torsion and non-bonded energy primarily affect bond-ordering and bond lengths. This means it is useful in understanding the structure and internal bonding but not useful in how it affects interactions outside of the internal structure.

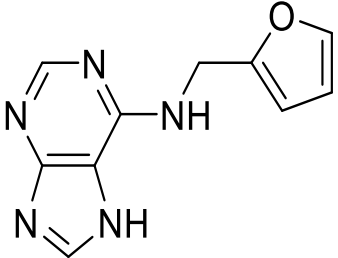
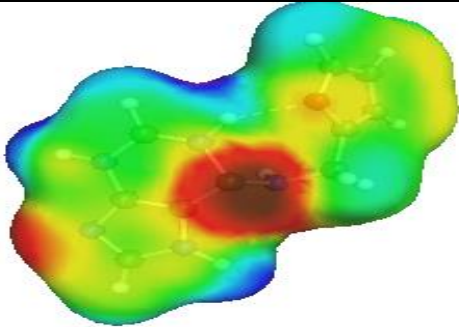
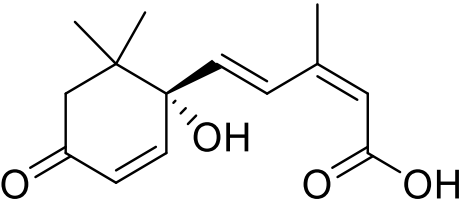
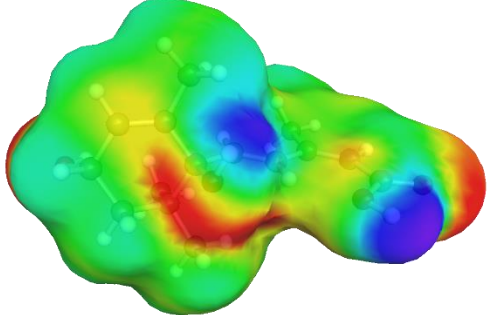
To start understanding the effects of molecular interaction and how that may affect adsorption and desorption non-bonding, dipole to dipole and Van der Waals forces were examined. Non-bonded interactions showed the energies between non-adjacent atoms and the generally repulsive interactions before them. Dipole-Dipole interactions is the attractive forces between opposing dipolar forces such as hydrogen bonding and finally, van der Waals forces which shows the attractive forces as affected by distance.

Table 27 shows that GA has the lowest calculated total energy with IAA and ABA showing similar values to one another and KI showing the highest potential energy. Dipole to dipole interaction showed similar results with GA showing the lowest value followed by ABA, IAA and finally with the highest value KI showing the strong dipole-dipole interactions of KI compared to the other tested bio actives. Finally, looking at the van der Waals forces showed a change in the trends previously observed with ABA showing the lowest values followed by GA and both IAA and KI showing similar interaction energies. This would suggest that KI would have a strong potential interaction with other molecules as would IAA to a less degree. This is further evidence that multilayer forms (as shown in Section 3.2.3) due to the increased intermolecular forces between molecules which would promote multilayer formation to occur. This information was then compared to Table 28 which looked at specific functional groups within the structure to get a greater understanding of the bioactive molecules. Gibberellic acid shows that while it had the lowest overall energy it was found to have the greatest number of electronegative functional groups which would have a significant effect during adsorption and during interaction with the solvent if a polar solvent was used such as water. Indole 3 acetic acid and KI both consist of an aromatic planar structure which allows for the potential of pi-pi stacking which would potentially

increase adsorption capabilities along with interaction with higher temperature Starbons due to their increasingly aromatic characterisation. They both contain electronegative functional groups that are found away from the aromatic ring which will interact with the environment affecting adsorption and desorption, it is interesting to note though that the total intramolecular energies between the molecules are very different though primarily due to a much greater dipole to dipole interaction with KI which will result in a greater interaction with the environment. Finally, ABA was found to have similar intermolecular forces compared to IAA though with higher torsional forces calculated, structurally though ABA did not contain an aromatic ring and was found to have several electronegative and electron rich functional groups that would influence the adsorption and desorption capabilities.

Table 28. Electronic surface mapping and structure correlation

Plant hormone	Structure	Electron density Red – Electron rich Blue – Electron poor	Functionalities and discussion
Gibberellic Acid	 <p>The chemical structure of Gibberellic Acid is a complex polycyclic molecule. It features a central ring system with several substituents: a methyl group, a hydroxyl group (-OH), a carboxylic acid group (-COOH), and another hydroxyl group. The structure is highly branched and contains multiple oxygen atoms.</p>	 <p>The 3D electron density map of Gibberellic Acid shows a complex, multi-lobed surface. The color scale ranges from blue (electron poor) to red (electron rich). The most electron-rich regions (red) are located around the carboxylic acid group and the two hydroxyl groups, indicating high electron density in these functional groups.</p>	<p>9 possible conformers observed. A carboxylic acid group along with 2 alcohol groups allow easy hydrogen bonding. The area around the carboxylic acid and alcohol groups are electron rich. Several branching functional groups results in many points for interaction.</p>
Indole-3-acetic acid	 <p>The chemical structure of Indole-3-acetic acid consists of an indole ring system (a benzene ring fused to a pyrrole ring) with an acetic acid group (-CH₂-COOH) attached to the 3-position of the indole ring.</p>	 <p>The 3D electron density map of Indole-3-acetic acid shows a relatively smooth surface with a prominent red region (electron rich) around the carboxylic acid group and the aromatic ring. A blue region (electron poor) is visible around the pyrrole nitrogen atom.</p>	<p>4 possible conformers. Electron poor area around the pyrrole group and the electron rich and poor areas around the carboxylic acid. Most likely reactive functional group is the carboxylic acid along with aromatic ring. Most likely reactive functional group is the carboxylic acid along with aromatic ring. Planar structure also allows stacking.</p>

<p>Kinetin</p>			<p>7 conformers were calculated. Many areas are electron poor including the aromatic ring and part of the pyrrole ring, with the aniline functional group and part of the pyrrole being electron rich.</p>
<p>Abscisic acid</p>			<p>8 conformers were calculated. 3 key points of electron rich are noted at the carboxylic acid, alcohol and aldehyde functional groups. Electron poor areas are offshoots of the electron rich areas.</p>

3.3 Adsorption and desorption Studies

In addition to understanding the physical properties of the surface of Starbon materials, it is also important to understand their desorption capabilities. Analysis of the Starbon materials was conducted over the course of multiple washings to not only determine if desorption could occur, but also if there was a consistent rate of desorption. A high capacity for adsorption is required to promote the removal of bioactives from the environment that may detrimentally affect seed germination, including plant growth inhibitors such as abscisic acid and herbicides. Following this methodology has resulted in increased seed germination and survival rates in less than ideal conditions.^{131,132}

However, it is less common to use desorption of selected compounds to improve germination for a variety of reasons. Normally, bio actives designed to improve initial seed germination are applied directly to the seed before pelletisation takes place. Starbons, due to their mesoporous nature, have the potential for consistent desorption of these bioactives onto the seed. This is not currently possible with AC and other microporous materials, which typically have high adsorption capacity and low desorption capabilities due to their primarily microporous nature preventing high levels of desorption.

The process of adsorption and desorption on the surface of Starbons has been discussed earlier (section 3.1.11). Before considering the desorption capability of the Starbons, it is vital to also further consider the environment that the Starbons will be acting as a seed coating component. The adsorption process of the seed coating components and selected bioactives is done within an industrial environment in an agitated setting (as discussed in section 1.2.4) where the seed coating components and selected bioactives would be deposited onto the seed as the adsorbate moves through it. Desorption of the selected bioactives however, takes place within the ground, specifically soil and this is a very different environment.

Soil as a material is comprised of porous materials (normally a combination of silica and macroporous carbonaceous material, with the pores normally containing a mix of gases and liquids (usually air and water)).^{133,134} The movement of water is dependent on the permeability of the soil, with slow

movements of water around the plant-soil interface known as the rhizosphere. The flow of water can even become static as the water reaches saturation point and the pull of gravity is no longer great enough to move the water downwards through the soil.^{135,136} When in soil, it becomes difficult to control the environment around the seeds and the impact of water on the seed coating. Differences and varieties in soil environments must also be considered. One such example includes karst environments, which consist of stony and thin soil, which consequently creates fissures and a random distribution of large pores, thus resulting in a rapid flow of water into the bedrock. Britain itself has 27 recorded varieties of soil, with the most common being defined officially as “Slowly permeable seasonally wet slightly acid but base-rich loamy and clay soils”.¹³⁷ These differing soil conditions and the potential for a continuous flow or static environment at the rhizosphere is one of the primary factors that may affect desorption and adsorption on the seed coatings. It is therefore important that seed coating components are designed to improve seed germination under multiple conditions, and that the desorption capabilities in both a flowing and static environment over time is analysed.

As such an experiment was devised to observe the adsorption and desorption capabilities of the materials with selected plant hormones. By examining the desorption process over multiple washings, the consistency of desorption was analysed, and the total desorption capability determined. Activated Carbon and three varieties of Starbon were tested (A300, A500 and A800) to allow for clear comparison. Three solvent washes were tested using water, ethanol and a 50:50 mix of each to determine how the change in solvent polarity and functionality may affect desorption. This way it would be possible to determine which materials would show a consistent level of desorption with the selected plant hormones. The figures below (Figures 49 – 60) show an inlet with a magnified level of desorption to allow clearer comparison between the experiments.

3.3.1 Adsorption and desorption on commercial activated carbon

Testing with AC was used as the control due to its already predominant use as a seed coating component and its microporous nature should result in a

low but observable level of desorption. Each graph below contains an insert to show a magnified view when desorption was low.

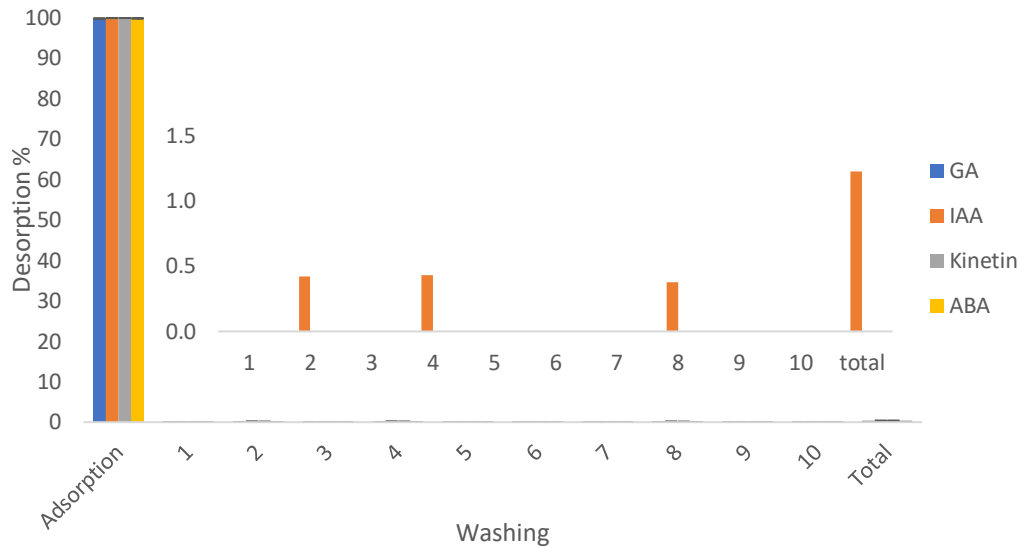


Figure 48. Adsorption and desorption of plant hormones through AC in water over the course of 10 washings. (Results show average over 4 repetitions).

High levels of adsorption for AC for all plant hormones were observed showing 100 % adsorption in all cases (Figure 48). Gibberellic acid, KI and ABA showed no signs of desorption. Indole-3-acetic acid did show low levels of desorption (1.4 %). When desorption was recorded it was found to be at an intermittent rate and was inconsistent, making it difficult to predict how desorption would occur in real world conditions.

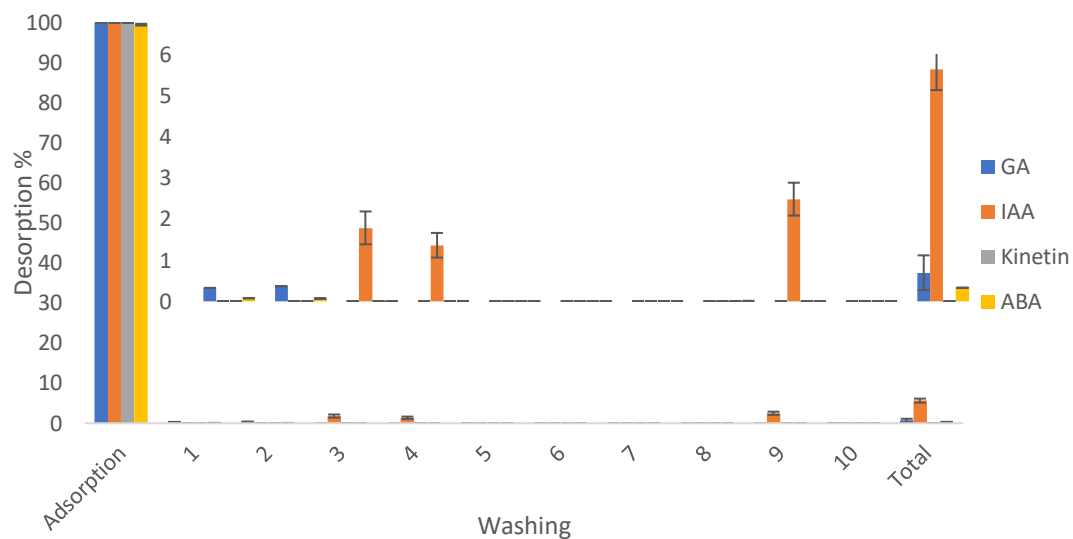


Figure 49. Adsorption and desorption of plant hormones through activated carbon in ethanol. (Results show average over 4 repetitions)

When ethanol was used as elution solvent, adsorption results were similar, as all plant hormones showed high adsorption (Figure 49). With regards to desorption, IAA desorbed from activated carbon at a total approx. 6% throughout the whole experiment and GA and ABA desorbed by approx. 2% and 0.5%, respectively, over two washings. Kinetin did not desorb at all. Overall, this showed that ethanol is a more effective solvent for desorption of certain plant hormones.

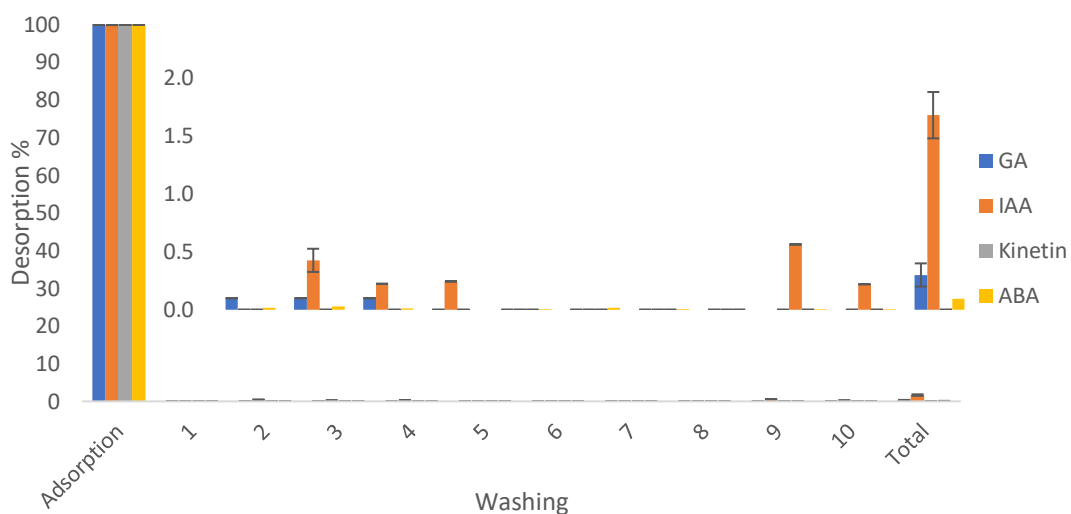


Figure 50. Adsorption and desorption of plant hormones through activated carbon in mixed solvents (water and ethanol in a 50:50 mix. (Results show average over 4 repetitions)

When an equivolume of ethanol and water was use, there was no significant change in desorption (Figure 50). Gibberellic acid desorbed over the first three washings with a total desorption <0.5 %. Again, IAA showed the highest total desorption, but was again inconsistent over the washes. Kinetin did not desorb from the material. Abscisic acid however showed very low levels of desorption consistently over the course of the experiment, though with still a total desorption <0.5 %.

All desorption experiments showed that all plants hormones successfully adsorbed onto commercial AC, but that there was little desorption for any of the hormones, with different solvents other than water required to increase desorption levels (Figure 48, Figure 49 and Figure 50). This suggests that the hormones have a strong interaction with the surface, and the hydrophobic nature of the material significantly reduced the possible interaction between the surface and water. Another explanation is that the hormones adsorbed inside the microporous material, fill the pores blocking them. This prevents further diffusion out of the pores preventing desorption from occurring.

3.3.2 Adsorption and desorption on Starbon A300

Starbon A300 was tested first as it had been determined that it had the largest mesopores (over 25nm in diameter) so would potentially show the highest levels of desorption.

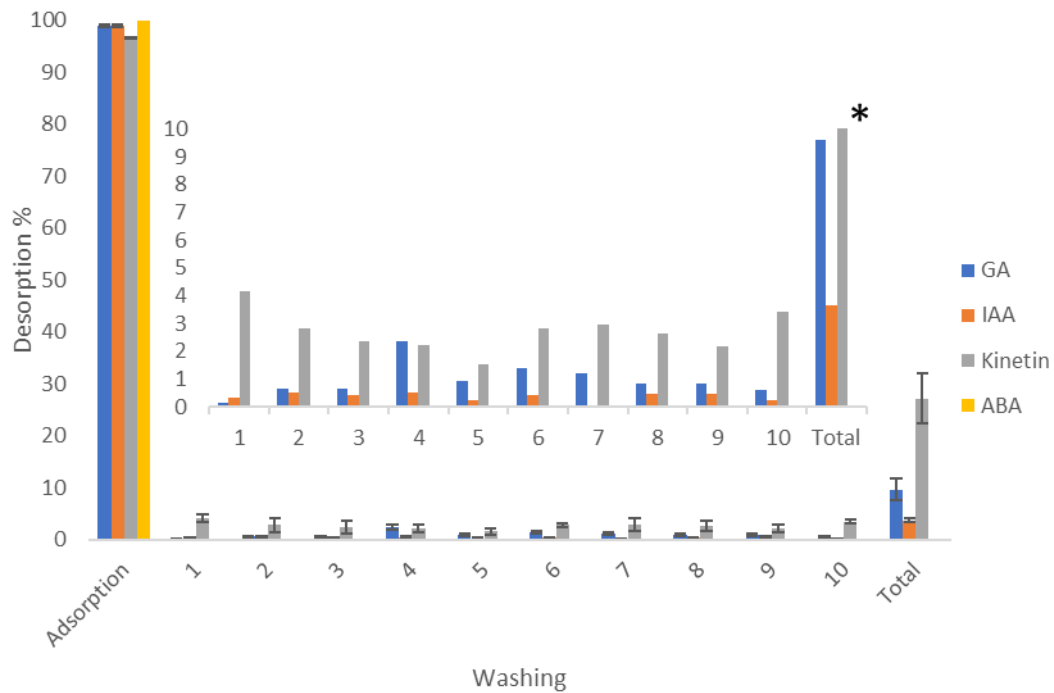


Figure 51. Adsorption and desorption of plant hormones through A300 in water. (Results show average over 4 repetitions). *indicates that the bar continues off the insert

Unlike activated carbon, desorption was observed with all plant hormones tested, with KI desorbing over 25 % (Figure 51). Indole-3-acetic acid showed very low levels of consistent desorption (roughly 0.3 % per wash) during the washings. Gibberellic acid also showed consistent desorption (roughly 0.9 % per wash) but with a greater total desorption of >10%. Abscisic acid showed the lowest levels of desorption with < 1% total desorption.

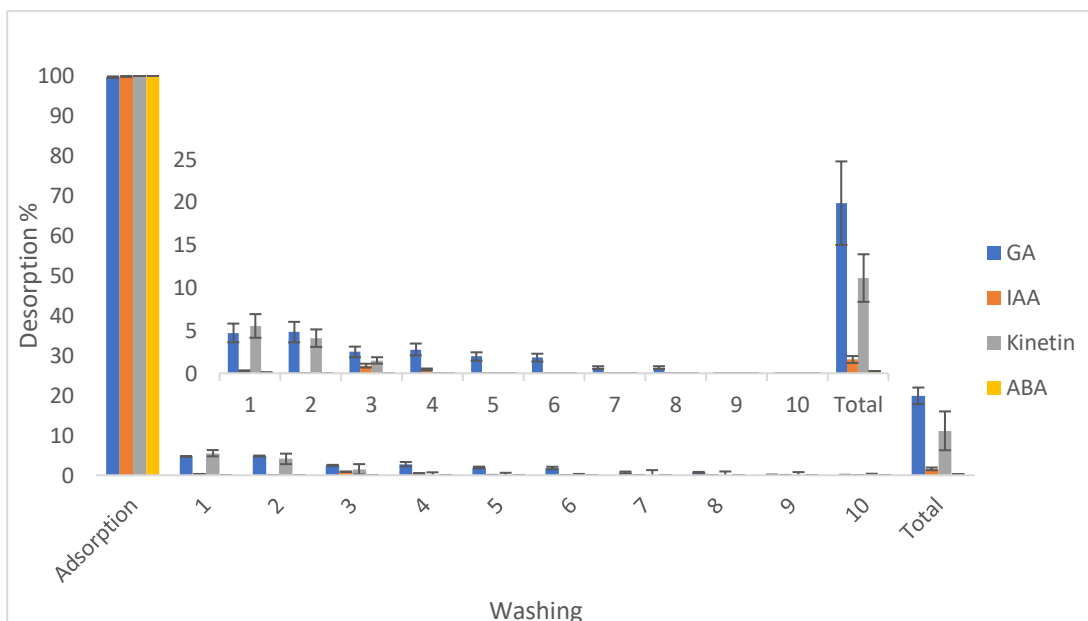


Figure 52. Adsorption and desorption of plant hormones through A300 in ethanol. (Results show average over 4 repetitions)

Significant differences were observed when the solvent was changed from water to ethanol, as desorption solvent, for Starbon A300 (Figure 52). Indole-3-acetic acid showed a low level inconsistent desorption (2%). Kinetin and GA both showed higher initial desorption (roughly 5 %) with low desorption in each consequent wash. Kinetin and GA only showed desorption in the first three and eight washes respectively, with GA desorbing from the material by over 20% in total. Abscisic acid again showed very low levels of total desorption, with < 1% desorbed recorded per solvent wash.

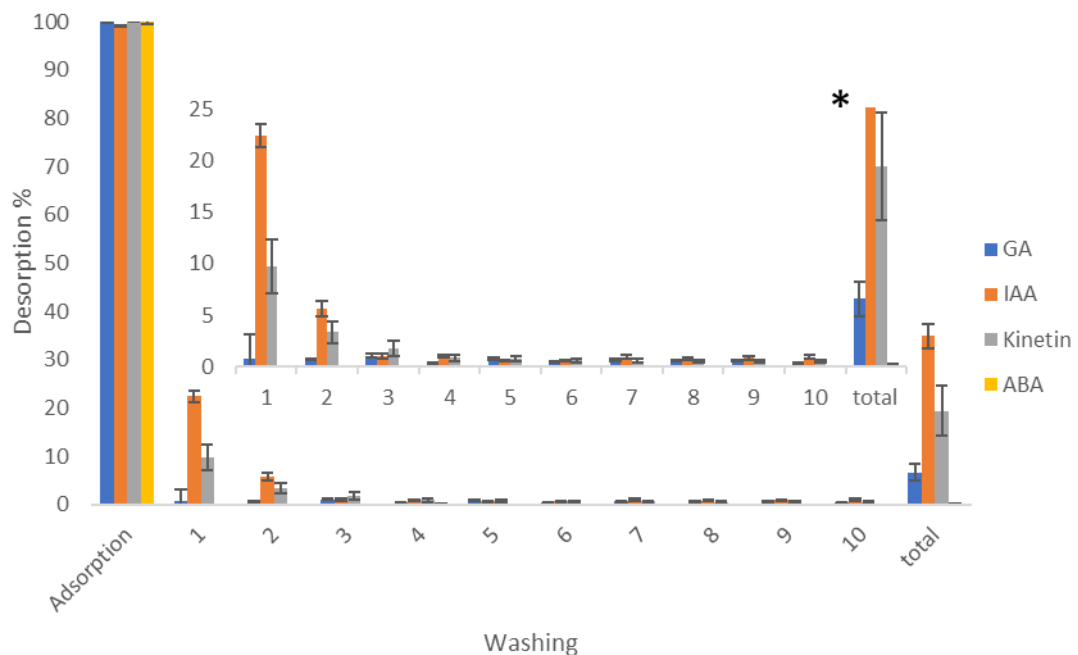


Figure 53. Adsorption and desorption of plant hormones through A300 in mixed solvents (water and ethanol 50:50 mix). (Results show average over 4 repetitions) *indicates that the bar continues off the insert

When the washing solvent was changed to a mixture, unusual results were observed (Figure 53) and were significantly different to when water (Figure 51) and ethanol (Figure 52) were used. Adsorption of all the hormones remained high (> 95%). Indole-3-acetic acid shows the greatest amount of desorption, approx. 25%, and GA shows the poorest desorption of the plant growth promoters at < 10%. Kinetin showed a total desorption of around 20%, in between what was observed in previous experiments (between 10 and 30 %) Abscisic acid again showed low and inconsistent desorption over the course of washing. Unlike the ethanol solvent experiment (Figure 52) all materials showed consistent desorption.

By comparing all of the experiments (Figure 51, Figure 52 and Figure 53), it was clear that Starbon A300 showed similar results to AC, with a very high adsorption rate of over 95% for all hormones. Testing with water solvent (Figure 51) showed low levels of desorption for the hormones, except for KI. This indicates that water may be a poor solvent to desorb large amounts of the

tested plant hormones. Despite its poor performance, it was important to test this solvent, as it would be the primary solvent the material would interact with in nature. Though future experiments with A500 and A800 may change this hypothesis. It was also noted that ABA showed very poor desorption in all cases observed. This is important as ABA is a plant growth inhibitor so low levels of desorption are required to ensure that improved germination may occur.

3.3.3 Adsorption and desorption on Starbon A500

Testing with A500 took place to compare to other tested Starbons and AC.

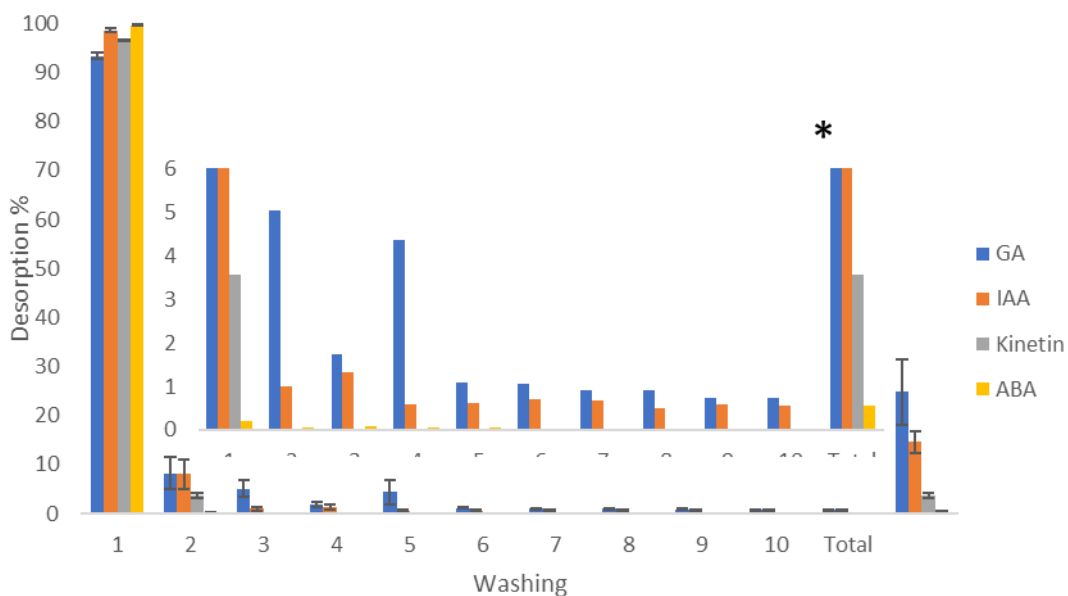


Figure 54. Adsorption and desorption of hormones through A500 in water. (Results show average over 4 repetitions) *indicates that the bar continues off the insert

Adsorption of all plant hormones on A500 remains consistently high and showed the highest levels of desorption reported using water so far (Figure 54). The highest recorded desorption occurred with gibberellic acid, which desorbed by over 20% in total, with most of the material desorbing over the first four washings. Indole-3-acetic acid desorbed < 1% in each washing after the initial washing (6 %) and KI showed no desorption at all after the first washing. Abscisic acid showed a low and consistent desorption over the

course of the washes (less than 0.5% in each wash). This overall highlighted that although Starbon materials show slightly less absorption of materials compared to commercial AC, the former (Starbon) showed a much more consistent desorption.

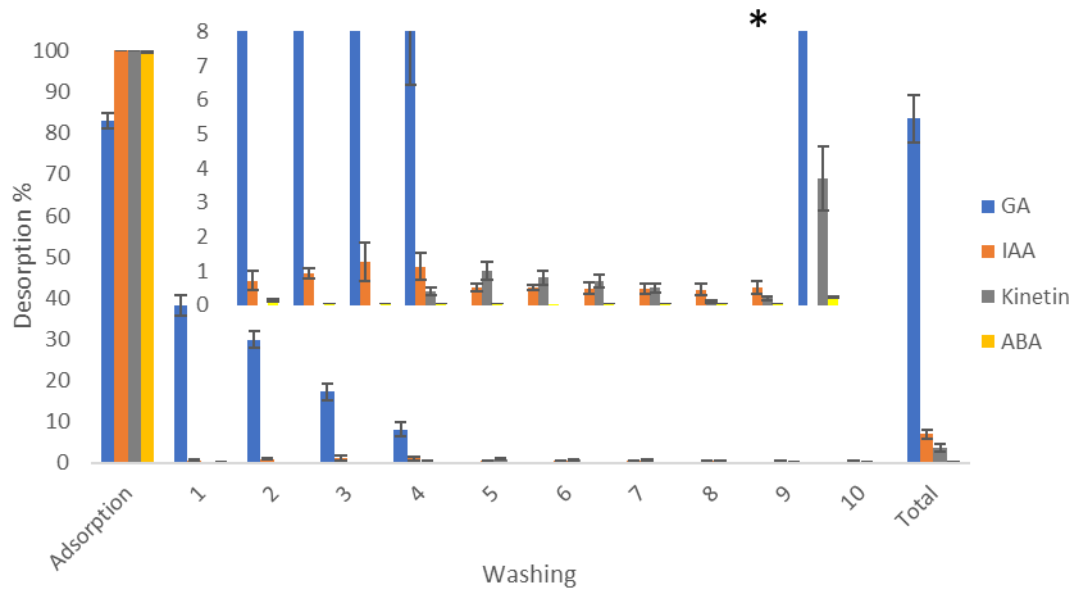


Figure 55. Adsorption and desorption of hormones through A500 in ethanol. (Results show average over 4 repetitions) *indicates that the bar continues off the insert

Three distinct forms of desorption were observed when ethanol was used as solvent (Figure 55). Gibberellic acid fully desorbed over the course of the first four washings, which was not observed in previous experiments. Indole-3-acetic acid showed a consistent desorption of approx.1% per washing. Kinetin however, showed only started desorbing after the fourth solvent wash, with a total desorption of 5 %. Abscisic acid showed inconsistent desorption over all washings, with a total desorption of <0.5 %.

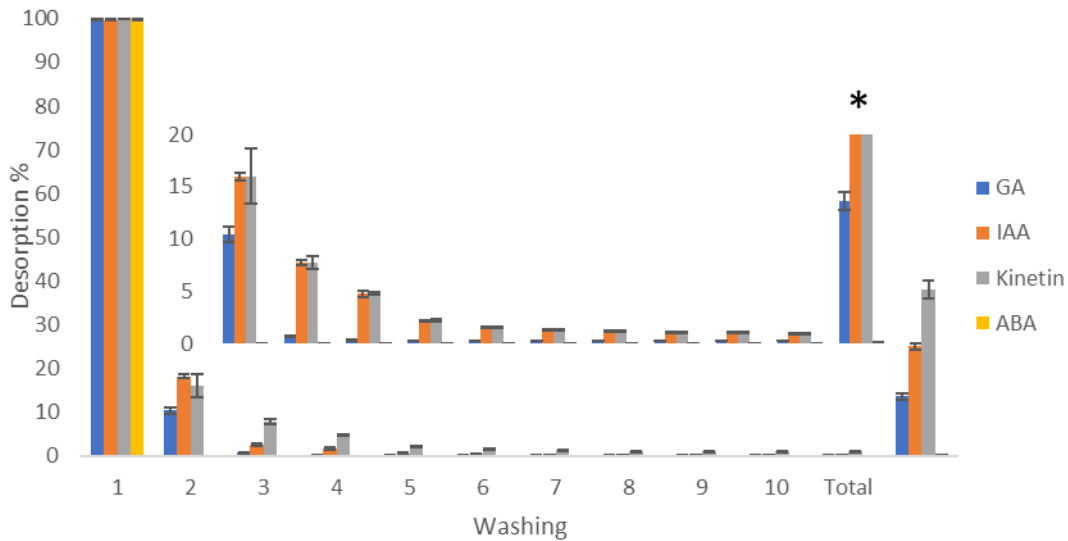


Figure 56. Adsorption and desorption of hormones through A500 in mixed solvents. (Results show average over 4 repetitions) *indicates that the bar continues off the insert

Kinetin shows the greatest total desorption recorded for all the hormones in this experiment, with a total desorption over 30% (Figure 56). It can clearly be seen with all hormones, that there is a steady decline of desorption from the initial washing until the last wash for all plant growth promoters. Abscisic acid again showed the lowest overall desorption at < 1% per wash.

Overall, Starbon A500 material showed more efficient desorption than activated carbon and A300 (Figure 54, Figure 55 and Figure 56). Desorption was also more consistent with regards to GA and IAA through all washes. Abscisic acid initially absorbs extremely well but showed the poorest desorption capability of all the plant hormones. Therefore, this set of experiments illustrated that A500 could be successfully used as a seed coating component.

3.3.4 Adsorption and desorption on Starbon A800

Final adsorption and desorption experiments used A800 as the tested material.

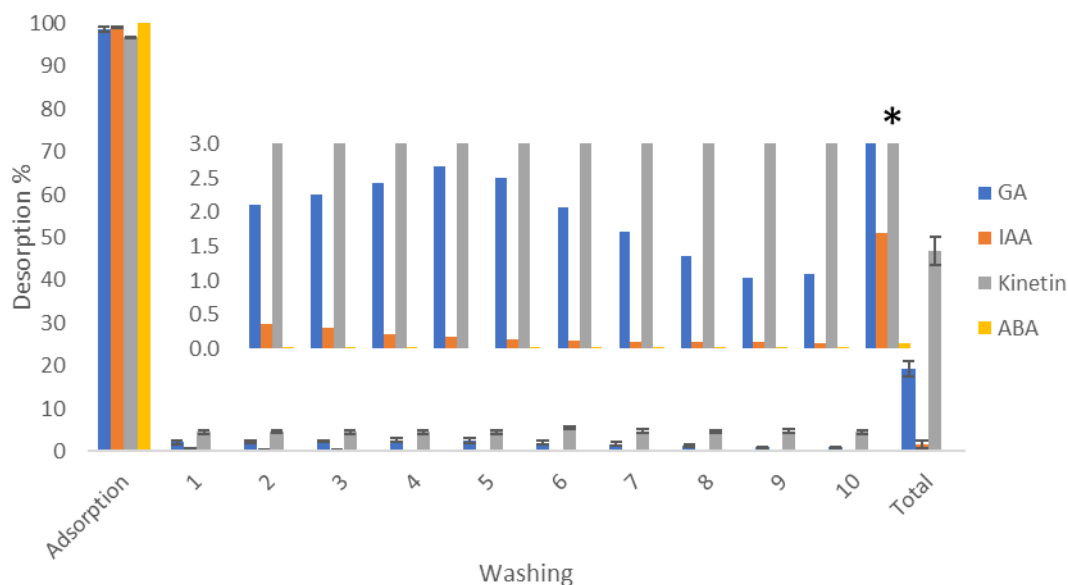


Figure 57. Adsorption and desorption of hormones through A800 in water. (Results show average over 4 repetitions). *indicates that the bar continues off the insert

When Starbon A800 was analysed, desorption again was observed for some plant hormones (Figure 57). Gibberellic acid initially showed a steady desorption of approx 2% per washing. Before dropping to eventually 1 % after washing 4 Indole-3-acetic acid showed a low rate of desorption at < 1% after each wash for the plant growth promoters, and KI showed the highest total desorption with over 30% desorbed and a consistent desorption of 3 % per wash. Finally, ABA desorbed very poorly, with only 0.2 % (or even none desorbing) after all washes.

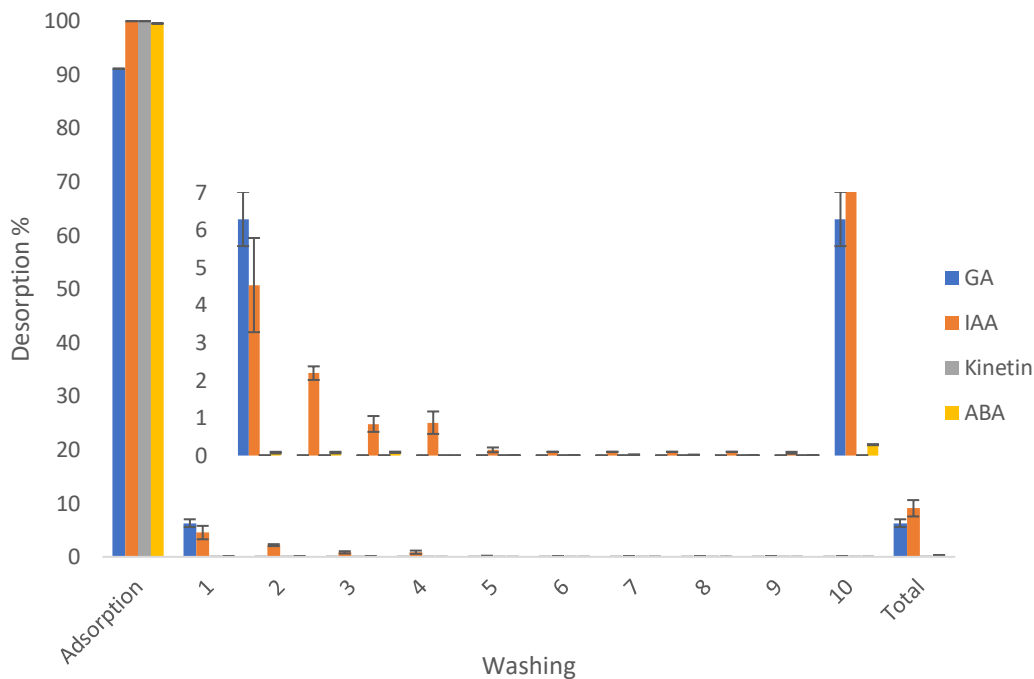


Figure 58. Adsorption and desorption of hormones through A800 in ethanol. (Results show average over 4 repetitions).

Desorption of plant hormones from A800 using ethanol was less compared using water (Figure 58). Gibberellic acid only showed some desorption (8 %) on the first washing, and KI did not desorb at all. Indole-3-acetic acid desorbed from Starbon A800, however it rapidly dropped to a desorption of approx. 0.1 % after five washes and is the only plant growth promotor to show consistent desorption for each washing. Abscisic acid once again showed poor but consistent desorption at < 0.1 % per wash.

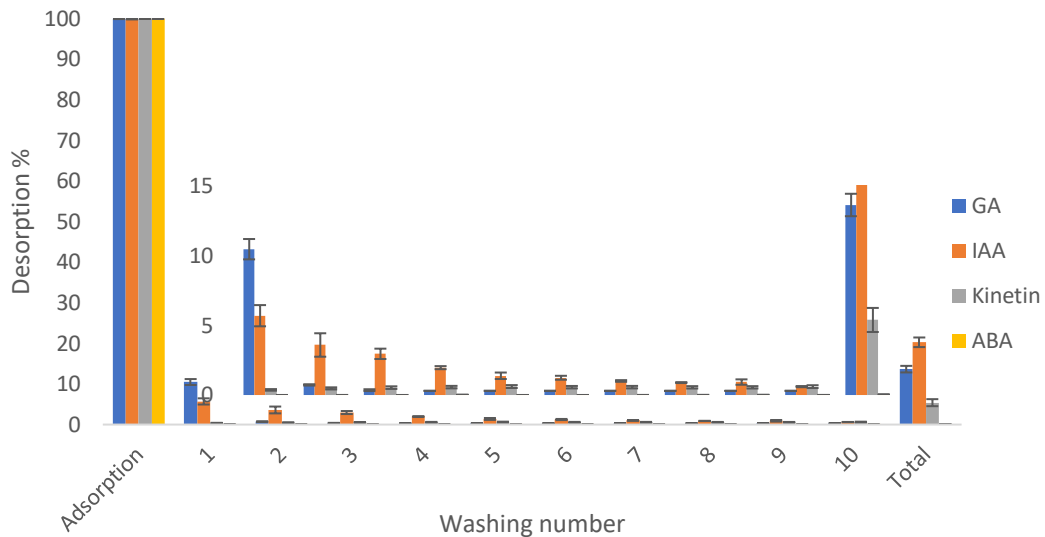


Figure 59. Adsorption and desorption of hormones through A800 in mixed solvents (water and ethanol 50:50 mix). (Results show average over 4 repetitions)

For equivolume ethanol/water, desorption remained low at < 20% for each hormone (Figure 59). Gibberellic acid showed the largest initial desorption but then rapidly drops to < 0.5 % after the first wash. Kinetin showed a consistent desorption of < 1 % in all washings, and IAA showed a steady decrease in desorption throughout the experiment from 5 % to less than 1 % per wash by the 10th washing.

On comparing the results obtained from Starbon A800 (Figure 57, Figure 58 and Figure 59) to other Starbon materials, A800 showed similar results to A500 in desorption, adsorption results were higher for A800, as consistent desorption was observed for all plant hormones tested. The only exception is the water washing results from A500, which showed greater desorption. With all results considered, A800 may be the better material for desorbing plant growth promoters, because water is the primary solvent used for agri-resilience picking a material that shows great desorption in water is therefore ideal.

3.3.5 In flow and static desorption of leachates

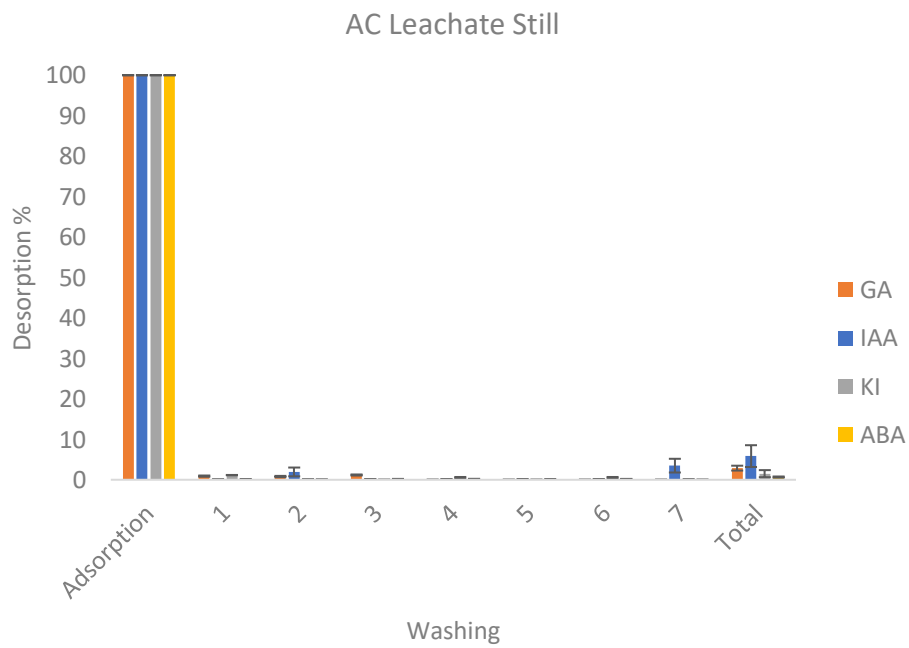
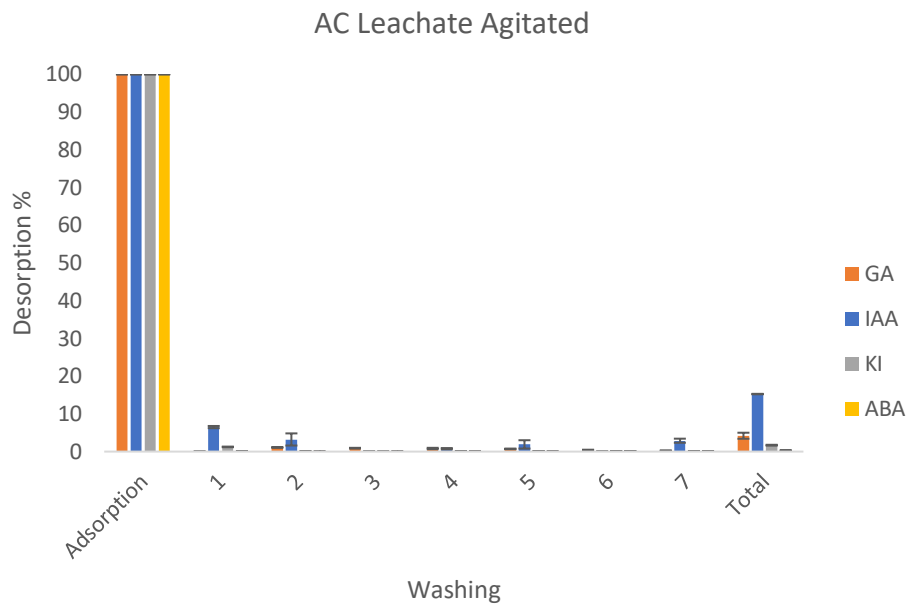
To determine how Starbons would be affected by real life environmental conditions, it was necessary to examine how desorption may be affected by both a static flow of water and agitated conditions. In real world conditions,

seed coating contact with water is not at a steady rate of flow but is either in a static environment of still water or flowing water.

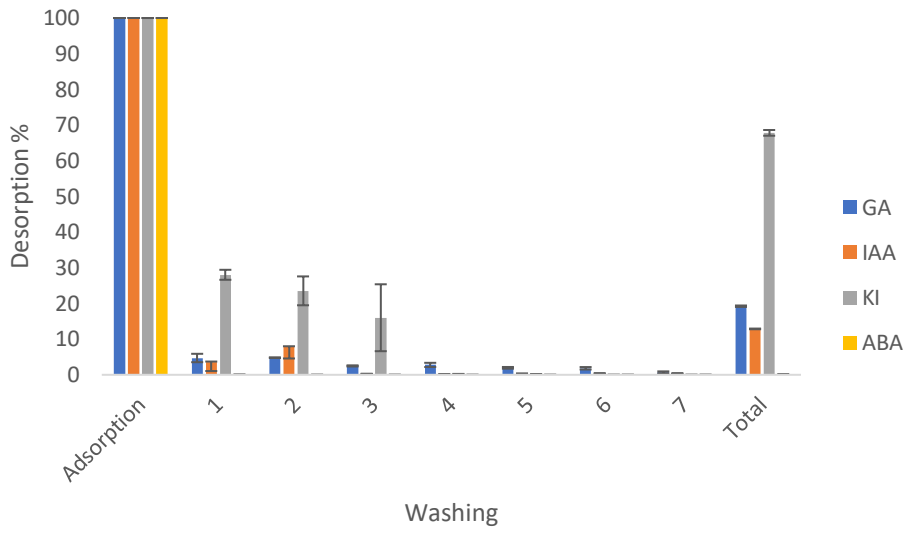
Mimicking real life environmental conditions was best performed by analysing the differences in the total desorption of plant hormones from each material, over the course of seven washings over seven days, with one experiment allowing to settle and the other being continuously agitated (Figure 60). Akin to previous experiments, high adsorption was observed for all plant hormones, with close to total adsorption for all materials before desorption was analysed. Overall desorption of the hormones from each material was greater during the agitated water experiments than the still water experiments. Initial washings during the agitated experiment showed desorption results similar to those observed in previous experiments (for example Figure 57). A800 gave the highest total desorption (nearly 100%) during the agitated experiments and 80% in the still water experiments. These desorption results were considerably higher than observed in previous experiments, though this experiment was with multiple washings with a greater total volume of material over a longer period, so this was to be expected.

All Starbon materials showed a higher total of desorption of the hormone than commercial activated carbon by the end of the agitated and static experiments, highlighting that Starbon material can consistently desorb greater amount of plant hormones regardless of carbonisation temperature. Pleasingly, all Starbon materials can reach high levels of desorption if given enough time and or washes. Starbon A800 showed the greatest amount of desorption, with a consistent desorption of over 10% with each wash, after each wash. Desorption of plant hormones could therefore be controlled over a prolonged period using Starbon A800. All other Starbon materials showed consistent desorption, but to less extent than A800, with some washings showing very low levels of desorption, e.g., A300, when agitated showed a total desorption of GA of 20% compared to the nearly 100% with A800. Overall, all Starbons outperformed the AC which showed total desorption of less than 5% with the plant growth promoters in each case. These results show that Starbons offer a significant advantage if used as a seed coating component over AC as they

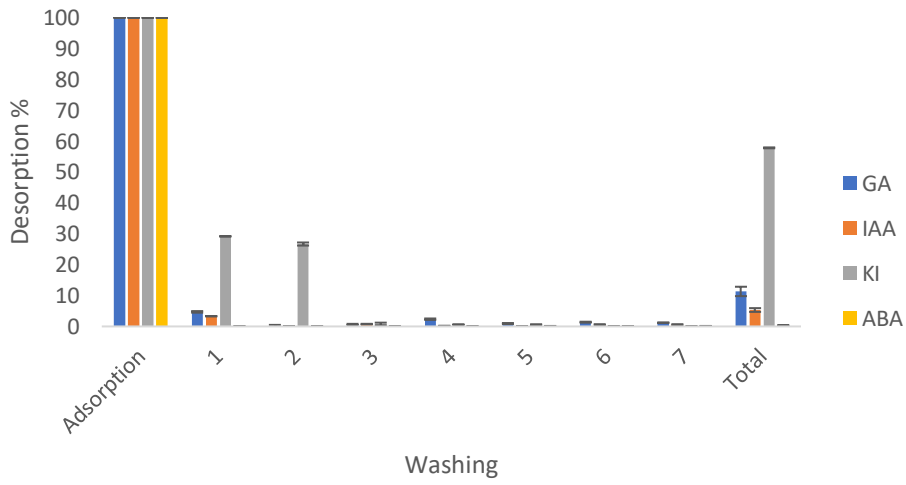
can desorb considerably greater amounts of plant growth promoters which may be able to significantly improve plant germination.



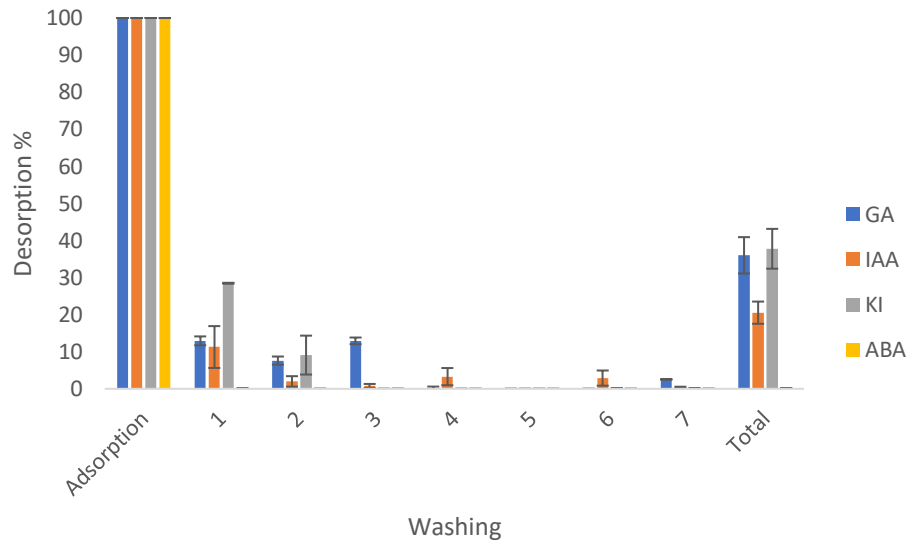
A300 Leachate Agitated



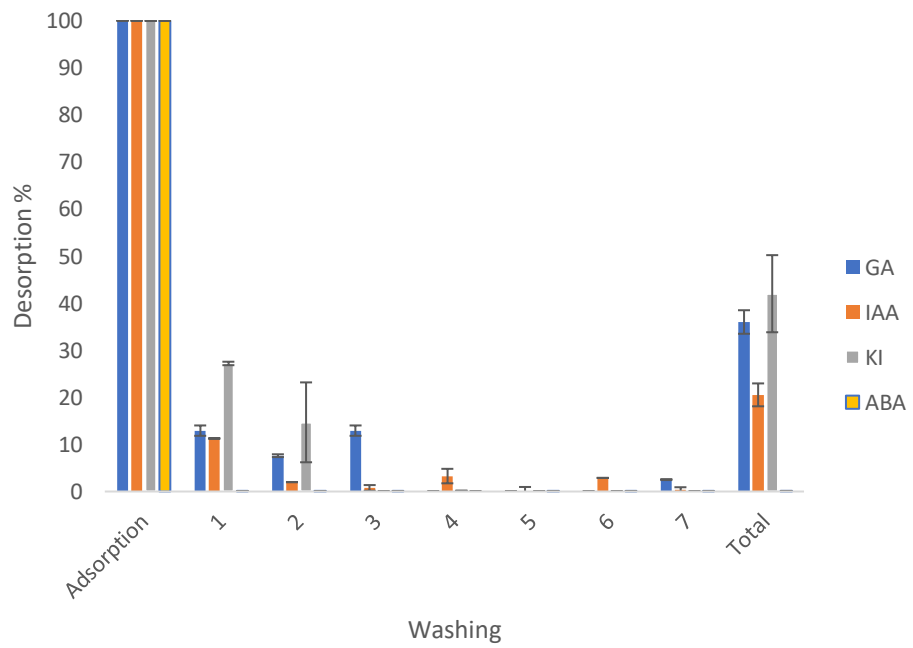
A300 Leachate Still



A500 Leachate Agitated



A500 Leachate Still



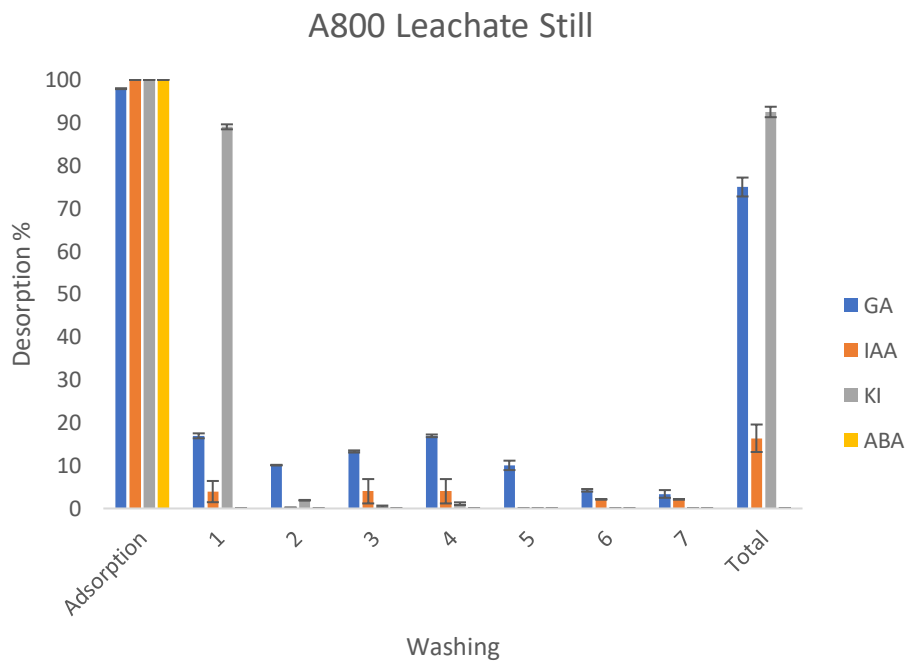
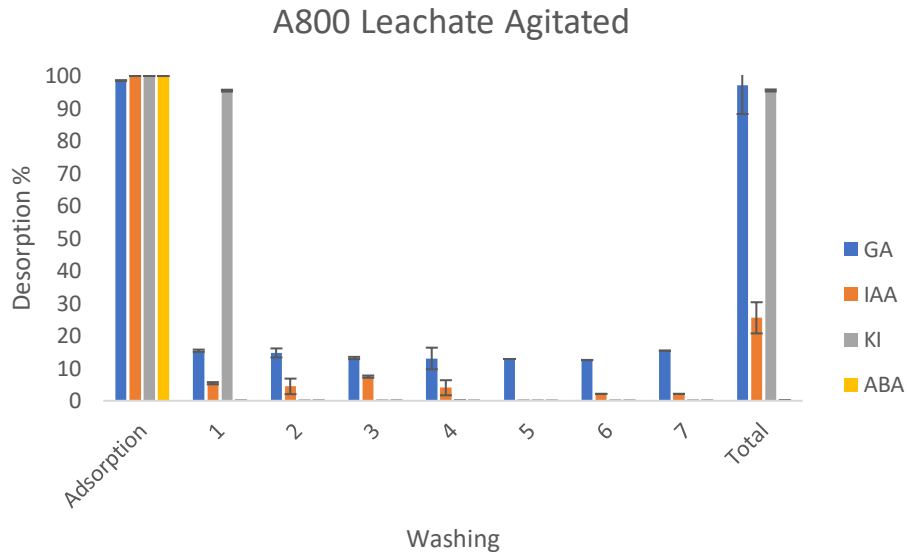


Figure 60. Long term leachate experiment with both agitated and still conditions.

Overall, results show similar trends to those seen previously (Figure 48, Figure 51, Figure 54 and Figure 57) with a much greater overall desorption being observed (Figure 60). In all cases, the agitated experiments showed the highest total desorption for all hormones compared to the still experiments. Interestingly, lower levels of desorption were observed with AC, compared to all the Starbons materials, as all Starbons showed < 10% desorption over 7

washes, whereas AC showed less than 5 % desorption over 7 washes. This does show that desorption does occur for all materials but on a much longer timescale for AC than Starbons. Time of desorption is an important factor to consider, as seed coating materials would be used over a day - week timeframe. The desorption experiments indicate that AC could successfully desorb some of the necessary plant hormones within this timeframe, though Starbons would also desorb the hormones over a quicker time period. It was also observed with A800, that KI shows almost complete desorption (95 %) after the first washing 24 hours into the experiment when agitated. These results were expected as previous results showed that A800 could desorb large amounts (< 75 %) of both GA and KI. Interestingly, as GA showed consistent desorption of approx. 15 % per wash, and KI showed around 90 % desorption in the first wash, with then very low desorption (> 5 %) over consequent washes. This indicates that the majority of KI is not strongly adsorbed to the surface and as such can desorb. The remaining washes show little to no desorption suggesting that the remaining KI material is either strongly adsorbed or remains the micropores, meaning they are unlikely to desorb easily.

3.3.6 Water holding capacity (WHC) and Water retention value (WRV)

Water holding capacity (WHC) and water retention value (WRV) are significant (important to consider) in soil and agricultural sciences, because they ensure germination occurs. There are three key stages in the drainage of water:

1. saturation the solid is saturated - with water and reaches maximum storage capacity;
2. Field capacity – gravitational filtration occurs removing most of the water with the remaining water within the solid (aka WHC), and;
3. Wilting point - the point when all available water has been removed from the solid and thus can no longer sustain a plant (aka WRV).

The WHC value (Equation 6) is important to determine how much water could be retained within the seed coating, and thus could filter out from the material and interact with the environment:

Equation 6. Water holding and retention capacity

$$WHC = \frac{m1}{m2} - 1$$

M1 = wet mass g

M2 = mass after gravimetric filtration g

Table 29. Water holding capacity (WHC) of selected materials.

Material	WHC g g ⁻¹
AC	0.52 ± 0.05
A300	1.25 ± 0.03
A500	0.96 ± 0.08
A800	0.96 ± 0.04

The WHC (g g⁻¹) of commercial activated carbon with respect to Starbon materials (A300, A500 and A800) are listed in Table 29. Commercial activated carbon shows the lowest capacity to hold water at 0.52 g g⁻¹ of water, which could be expected as AC is a hydrophobic material and is therefore unlikely to retain water. Starbon A300 shows the highest WHC value, retaining 1.25 g g⁻¹ of water. Starbon A500 and A800 show similar

results with a WHC of 0.96 g g⁻¹. These results (Table 29) show that while the Starbons become more hydrophobic at higher carbonisation temperatures, the WHC value does not change significantly between the materials.

Water retention value (WRV) is an important characteristic to consider when trying to promote seed germination.^{138,139} If, the soil in question cannot retain water easily, then more water must be added in order for the seed to germinate at all.

There are several methods to improve the WRV in a natural environment and thus improve overall seed germination. One method is to use a seed coating which contains a material that can improve the water holding capacity around the seed e.g. biomass, biochar etc.^{80,140,141} Another method is to mix the soil with materials which improve the overall water holding capacity within the soil itself, thus changing the environment where seeds are planted.¹⁴² The higher the WRV, the greater the retention of water and the overall swelling of the seed coating.

$$WRV = \frac{m1}{m2} - 1$$

M1 = centrifuged wet mass g

M2 = dry mass g

Table 30. Water retention value (WRV) of selected materials.

Material	WRV g g⁻¹
AC	0.01 ± 0.00
A300	0.14 ± 0.02
A500	0.12 ± 0.01
A800	0.01 ± 0.00

The WRV are listed in Table 30 which shows that commercial activated carbon and A800 have very similar WHC results, showing that while the WHC (Table 29) suggests that A800 may retain significantly more water (0.98 g/g⁻¹) upon heating much of this water is removed from the Starbon. Both A300 and A500 had a WRV of approx. 0.1 g/g⁻¹, and thus can retain approx. 10% of their dry

mass in water. Overall these results show that the Starbons can initially hold a large amount of water, with all Starbons able to retain water which equates to over 90 % of their total mass. This water retention drops significantly for the WRV with a greater drop as the Starbons become more hydrophobic in nature with A800 retaining less than A300 (Table 30). This suggests that overall as the temperature of carbonisation increases so too does the overall hydrophobicity of the material.

3.3.7 Extended study: influence of seed exudates

Seeds as living organisms produce a wide variety of chemicals which may aid or inhibit their own growth or germination. Starbons have shown the ability to potentially improve seed germination by adsorbing plant growth inhibitors and retaining them whilst desorbing selected plant growth promoters. However, while these experiments focused on understanding the adsorption and desorption of a variety of plant growth inhibitors and promoters, seeds produce a wide variety of plant hormones depending on the conditions of environment and germination stage of the seed. The question therefore, is whether these bioactive compounds can be tested and analysed to determine the adsorption and desorption of the adsorbate materials when there is a wide variety of plant hormones.

In addition to gibberellic acid, IAA, KI and ABA a variety of plant hormones (see Figure 61) were selected based on their abundance and relative importance during seed germination, namely:

- i. Salicylic acid (SA), a phenolic compound normally produced as a stress hormone during initial germination to promote growth as a survival mechanism,^{143–145}
- ii. Jasmonic acid (JA), a compound used as a regulator in pest control but has a “antagonistic” effect with salicylic acid which can affect plant germination if either is produced in the presence of others,^{146,147} and;
- iii. Zeatin (ZE), a cytokinetin from the same family as KI was selected. Zeatin has promotes the growth of auxiliary roots and budding rather than growth within all cells.^{148–150}

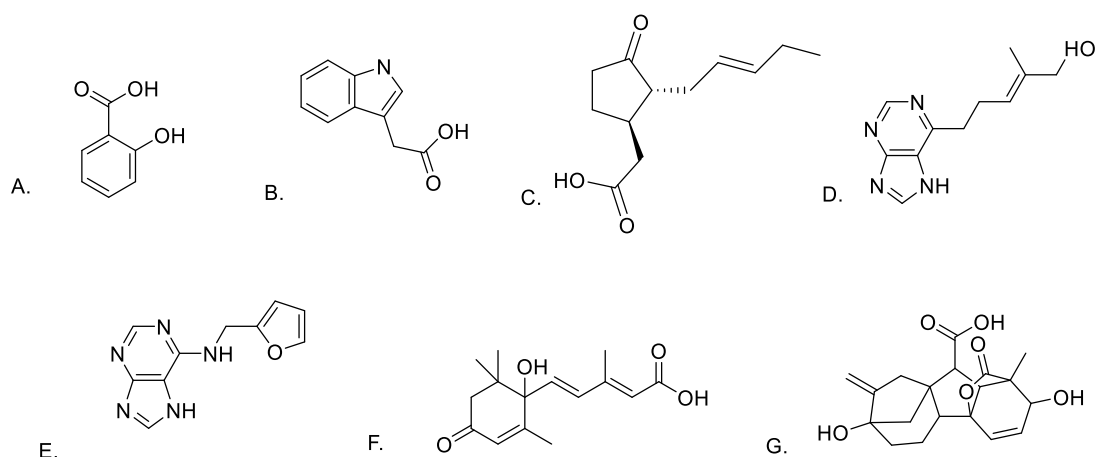


Figure 61. A. Plant exudates tested. A. Salicylic acid. B. Indole-3-acetic acid. C. Jasmonic acid. D. Zeatin. E. Kinetin. F. Abscisic acid and G. Gibberellic acid.

Initial stress tests (as described in Section 2.2.19) showed, as expected, a multitude of components within the exudate. However, it was noted that the results were found to be on a spectrum between two extreme cases (Figure 62 with a breakdown of key peaks found in the appendix Figure 83). One set of results showed low quantities of plant growth inhibitors such as SA and ABA, along with much higher quantities of plant growth promoters such as GA. This suggests that some batches of seeds are germinating even under the stressful conditions applied to them and releasing these plant growth promoters. The other example shows GA in low quantities and SA and ABA in much higher quantities along with IAA. This is likely from highly stressed seeds, as SA is a stress induced hormone (at this point in germination) and as such is likely to be produced in greater quantities during this experiment while GA would most likely not be released in high quantities as it would be required for seed germination under less stressful conditions. The total results can be observed below with a breakdown of the tested plant hormones in Table 31.

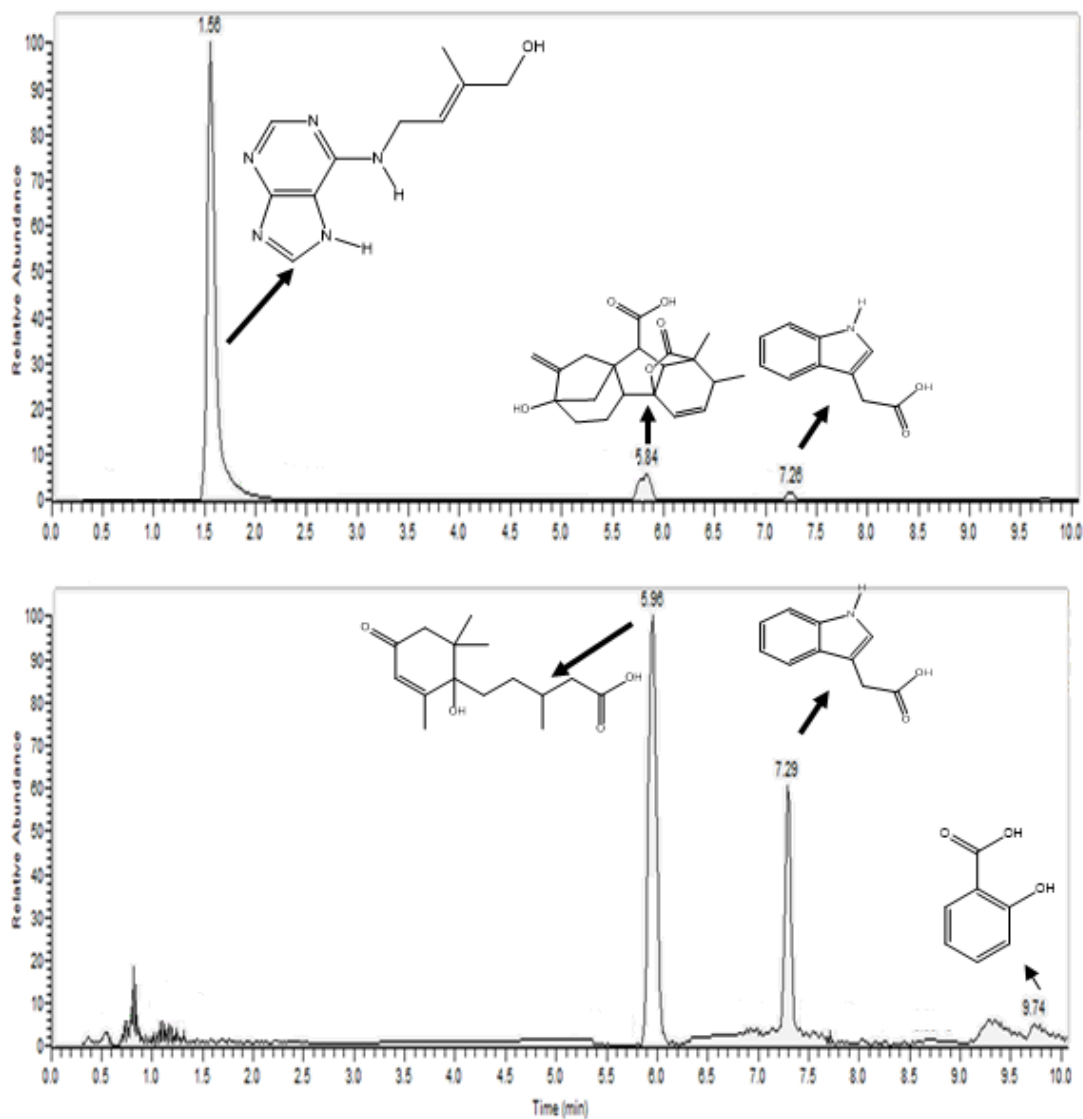


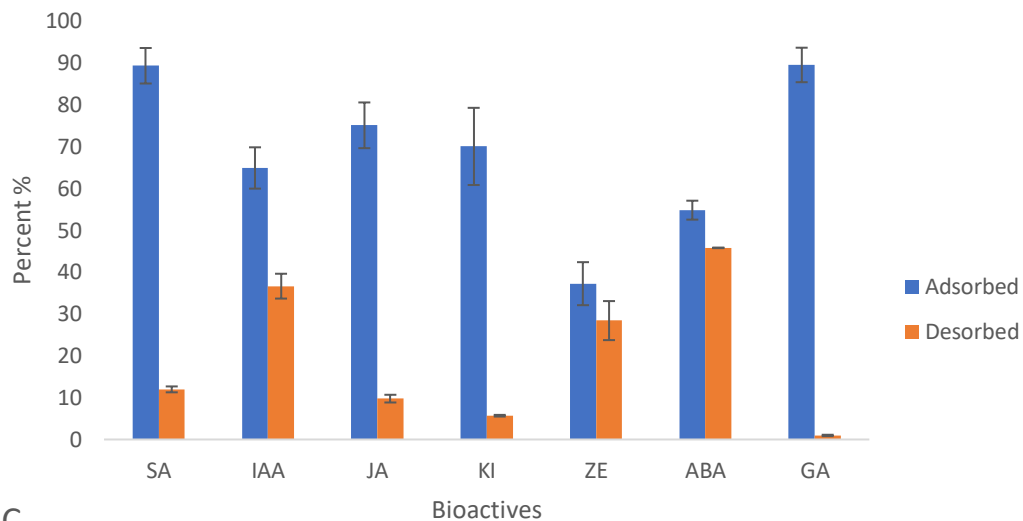
Figure 62. LC-MS of two separate tomato seed batches.

The results were analysed qualitatively by peak area to determine relative adsorption and desorption with an average calculated over four repetitions (Table 31 and Figure 62).

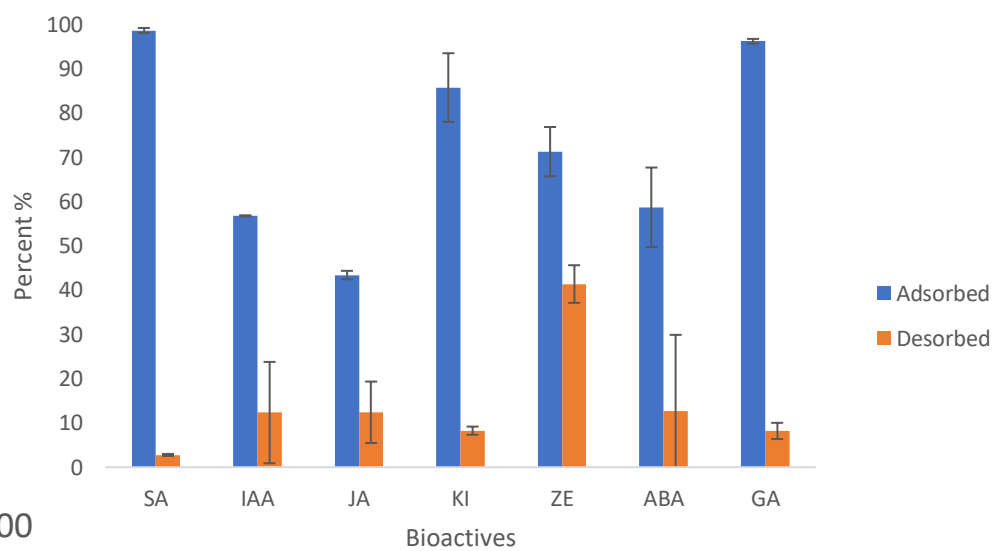
Table 31. LC-MS adsorption and desorption results for tomato seeds. (relative desorption shown not total desorption)

AC	Molecular weight g mol⁻¹	Average adsorption %	Standard error	Average desorption%	Standard error
SA	138.1	89.4	4.2	12.0	0.7
IAA	175.2	64.9	4.9	36.7	3.0
JA	210.3	75.1	5.5	9.8	0.9
KI	215.2	70.1	9.2	5.7	0.2
ZE	219.3	37.2	5.1	28.4	4.7
ABA	264.3	54.8	2.3	45.8	0.1
GA	346.4	89.5	4.1	1.0	0.2
A300		Average adsorption	Standard error	Average desorption	Standard error
SA	138.1	98.6	0.6	2.8	0.2
IAA	175.2	56.8	0.1	12.3	11.4
JA	210.3	43.4	0.9	12.4	6.9
KI	215.2	85.7	7.8	8.2	0.9
ZE	219.3	71.3	5.6	41.4	25.3
ABA	264.3	58.7	9.0	12.6	17.3
GA	346.4	96.2	0.5	8.2	1.8
A500		Average adsorption	Standard error	Average desorption	Standard error
SA	138.1	92.0	0.9	36.8	3.5
IAA	175.2	54.2	10.0	29.7	7.7
JA	210.3	40.4	0.8	16.1	1.1
KI	215.2	70.2	10.7	28.3	4.2
ZE	219.3	48.8	8.3	86.1	9.1
ABA	264.3	54.0	5.4	27.2	3.3
GA	346.4	61.1	8.1	58.4	8.6

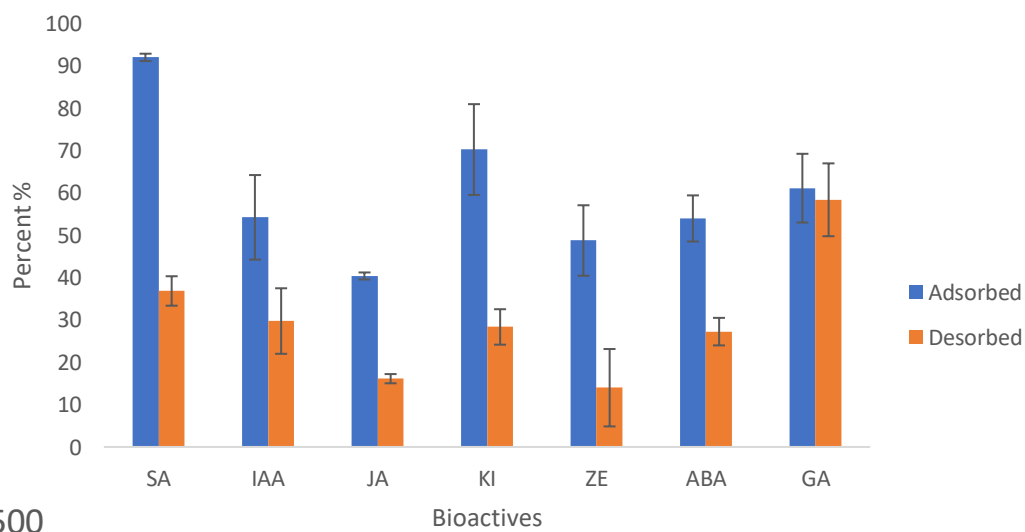
A800		Average adsorption	Standard error	Average desorption%	Standard error
SA	138.1	91.5	4.7	3.0	0.6
IAA	175.2	58.5	7.6	41.7	9.0
JA	210.3	65.2	6.8	43.8	6.7
KI	215.2	92.1	2.3	5.3	0.8
ZE	219.3	63.9	2.7	45.7	4.6
ABA	264.3	59.9	2.7	14.6	2.1
GA	346.4	96.2	1.9	23.8	1.0



AC



A300



A500

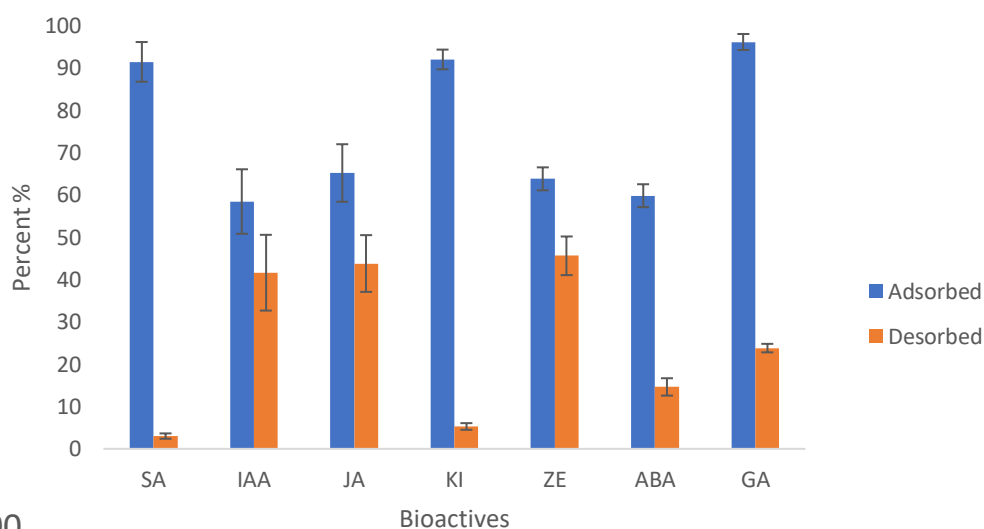


Figure 63. Adsorption and desorption of bioactives via LCMS (results over 4 repetitions).

Based on the results (Table 31 and Figure 63) some preliminary observations can be made. Salicylic acid showed among the highest levels of adsorption in each experiment along with KI and GA. As GA was the largest molecule (by molecular weight), and SA the smallest (by molecular weight) adsorption was not dependent on molecule size and that the only material to adsorb over 50% of the selected bioactives in all cases was A800. However, desorption data shows less observable trend. Interestingly, commercial AC does show levels of desorption which were not observed in previous experiments though still at low levels compared to Starbon materials, except for ABA and ZE which showed higher levels of desorption. It is important to note that the amounts of plant hormone produced and analysed in this study are much lower than the amounts used in the previous adsorption desorption experiments (nanogram scale rather than microgram scale). This would indicate that under real world conditions, commercial AC would probably also show desorption of these bioactives and potentially affect plant germination. ZE showed high levels of desorption but lower levels of adsorption in all cases. This is very different to KI which as mentioned earlier on most cases shows high levels of adsorption but low levels of desorption. In all experiments KI showed lower levels of desorption than ZE, even though they are both structurally very similar (Figure 61) This may mean that the functional group difference between KI and ZE is

responsible for differences in desorption. Kinetin comprises a furan ring while as ZE contains an alcohol group. This would reduce the potential for stacking with ZE and increase the potential interaction with the water solvent which would influence desorption.

Gibberellic acid and some of the other acidic bioactives (IAA and JA but not SA) were found with AC and A300 to have very low desorption levels but was observed to show much higher levels of desorption with A500 and A800. This is interesting as it would be expected that these acidic hormones would have a stronger interaction with the more basic surface of A500 and A800, however as the hormones are bound via physisorption (Section 3.2.6) it would mean that while surface pH has an effect on interaction there are additional factors which are affecting desorption. An example of this is that while some of the acids show increased desorption with A500 and A800, other acidic hormones show lower levels of desorption such as SA.

3.4 Batch germination testing

In previous sections, experiments were conducted to investigate the physical process of adsorption and desorption of bioactives from Starbons, and the difference between Starbons and AC. From this, it was shown that Starbons have the potential to act as a seed coating component. The next step was to take what was learnt and have it applied to biological testing to determine if Starbons can be used to improve germination of seeds and if so understand why.

3.4.1 Plant hormone testing (tomato seeds)

Plant hormones have an important effect on seed germination and growth. To test how effective the materials are when they are doped with plant growth promoters, it was necessary to run experiments to determine a dosage which would result in a clear difference compared to a control group. Gibberellic acid was selected as the hormone to be tested for these experiments due to research showing it should have the most substantial effect overall on the initial seed germination of the hormones tested.^{151,152} testing was completed by determining the rate of seed germination. Testing was discussed earlier in section 2.2.20 and uses a petri dish containing a sample of material separated

from the seeds using filter paper. The initial dosages tested were a set of concentrations ranging from low amounts to improve flowering (emergence of leaves), to concentrations over the recommended dosage to improve seed germination, to ensure a clear difference in germination could be observed.¹⁵³ For the purposes of this experiment the GA was mixed with the water added to the seeds (Figure 64 and Table 32). Future experiments will have the materials doped with the gibberellic acid beforehand.

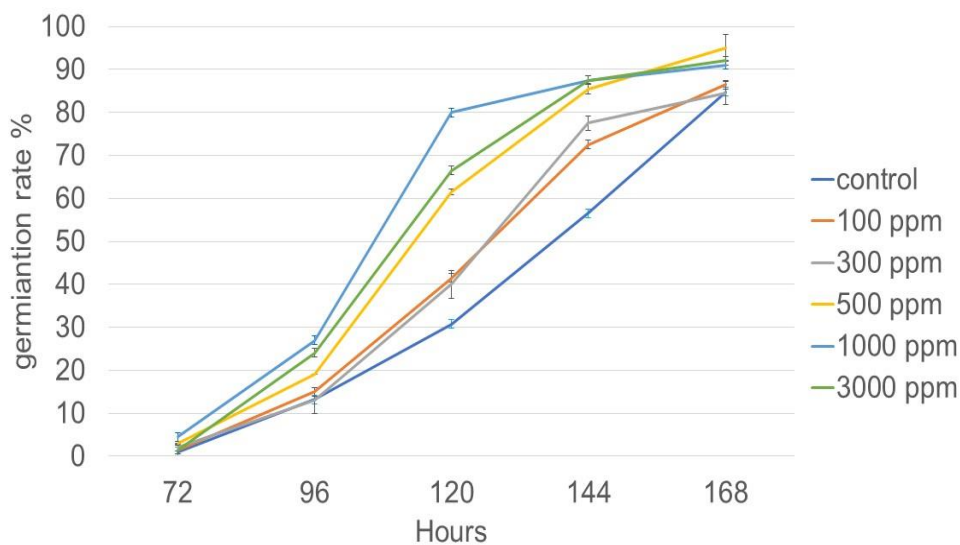


Figure 64. Germination rate of tomato seeds with increasing doses of Gibberellic acid.

Table 32. T50 % values for increasing dosages of Gibberellic acid.

Concentration of GA / mg / L	T 50% / hours
Control	137 ± 9
100	126 ± 1
300	124 ± 2
500	115 ± 2
1000	108 ± 3
3000	112 ± 4

As shown by the data tabulated in Table 32 and plotted in Figure 64, the use of GA had an influence over the germination rates of the tomato seeds with a noticeable difference observed from the lowest amount of 100 ppm per seed compared to the control. The control achieved T50% after 130 h, with the lower dosages of the GA achieving T50% at around 125 h. The higher concentrations (500-3000 mg/L) achieved T50% at an earlier time of between 108 and 115 h with 1000 ppm having the fastest germination rate. The clearest spread of results was seen at 120 h in which all experiments containing GA showed a total germination of at least 10% higher than the control experiment. The results for 1000 ppm per seed showed an increased germination total of 50% over the control group. By the end of the experiment it could be seen that two groups of results can be observed.

The control group and the lowest dosages of the gibberellic acid showed a similar total germination of roughly 84% while as the higher dosages of gibberellic acid show total germination of around 90%. While total germination was not statistically significant at the end of the experiment it would be interesting to observe the difference in crop quality if examined for longer periods. A visual representation of germination is shown in Figure 65.

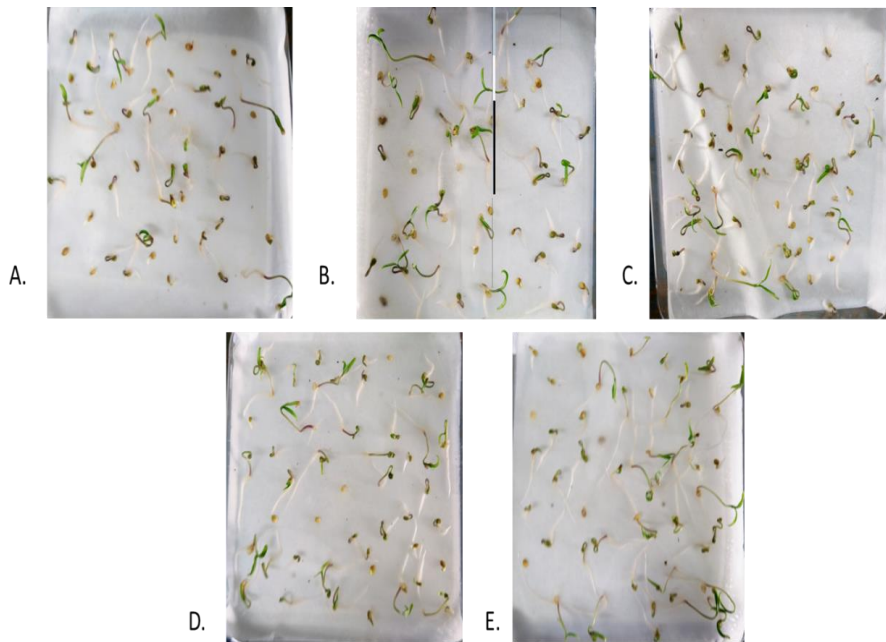


Figure 65. Seed germination when doped with GA after 168 hours. A. 100 mg / L, B. 300 mg / L, C. 500 mg / L, D. 1000 mg / L and E. 3000 mg / L.

While the statistical results of germination time were analysed, information was also being obtained by visual analysis. Germination is the first step in the seed's overall growth, it is important not only to determine when they germinate but also to observe how quickly they then move into the later stages of plant growth and if the use of Starbons may affect this later growth or influence the seeds own biology. Photographs were taken at each seed counting to determine what, if any, differences there were between each experiment. Figure 65 shows that the observed number of green shoots increases as the concentration of GA increases with the greatest increase being observed on average around 500 – 1000 mg L⁻¹. The relative similarities of the seeds between each sample tray show slight flowering of green leaves and root length and were all a similar shape with all roots being a single tail with very little “frittering” off it. This suggests that the addition of the GA has only improved the initial rate of germination of the seeds but has not significantly advanced the rate of further flowering. The image of 100 mg L⁻¹ (Figure 65) show a similar number of green shoots as 300 mg L⁻¹. From the results it was decided that future experiments would use 100 mg L⁻¹ as this would clearly highlight any changes to the rate of seed germination due to the

inclusion of the doped Starbons while ensuring that 100% of the GA would be adsorbed on the adsorbate material.

3.4.2 Lettuce seed germination

Lettuce is known as a fast germinator and to ensure clear results were obtained the experiment would last for 84 h with a counting occurring every 12 hours.

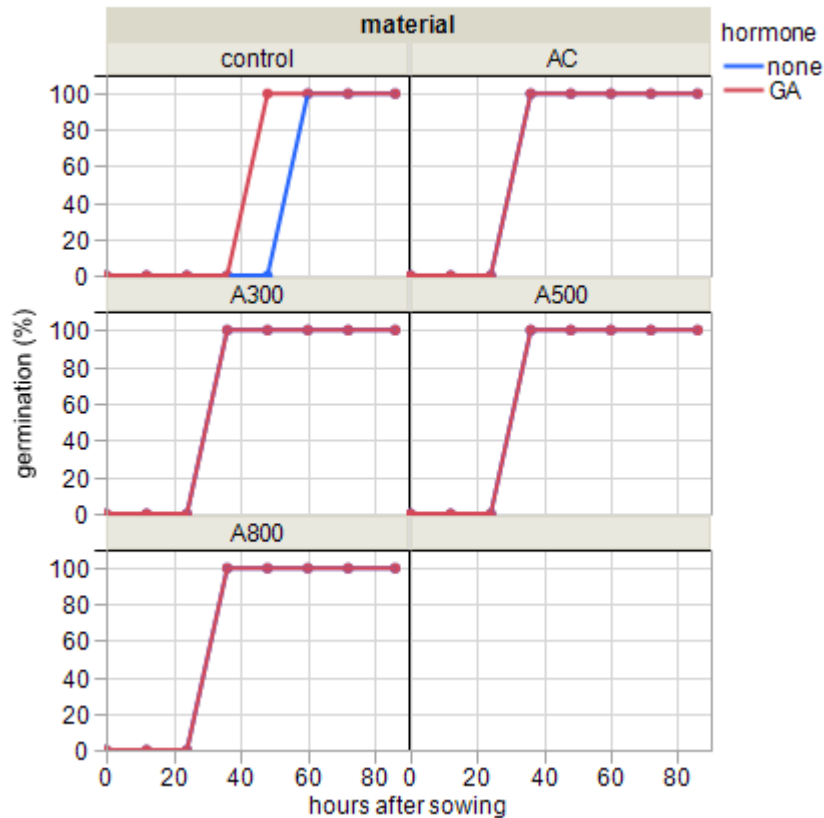


Figure 66. Total germination of lettuce seeds with both doped materials and non-doped materials over 86 hours. (8 sets of 50 seeds per experiment). Note the overlap for all Starbon results.

As shown by the results represented in Figure 66, lettuce seeds germinated quickly (within 36 h) with no deviation between each batch. All experiments with material showed an exact overlap between the doped and non-doped experiments. The control group showed 100% germination after 60 h, all groups tested with the materials showed complete germination occurring 24 h earlier, at 36 h. The T50% of the experiments with material is calculated at 30 h with the control at around 55 h into the experiment. Though, this is merely a

statistical estimate due to the large difference in germination between the 24 and 36 h counting. Unfortunately, due to the lack in variation between each result it is impossible to draw any significant conclusions from this data. The main points that can be concluded are that both the addition of gibberellic acid and the use of materials does improve overall germination rates. For the non-doped materials, they are used in the removal of plant growth inhibitors released by the seeds such as ABA. This removal of the plant growth inhibitors from the environment therefore promotes germination. Doped materials work to not only have the same benefits of the non-doped materials but also desorb and release plant growth promoters initially doped onto the Starbon. The use of doped materials however did not significantly improve overall germination based on the results. The similarities between each result show that the removal of plant growth inhibitors is important but as observed with the controlled doping experiment the presence of GA also has a similar effect on germination. Due to the sensitivity of the germination bays used to analyse the seeds testing more often than every 12 h often would have a detrimental effect on the seed germination and skew the results. As the germination bays are highly calibrated to remain at a set temperature, light level and humidity regular checking of the bay can have a significant impact on these levels which requires time to reset again, as such checking once every 12 h reduces this risk.

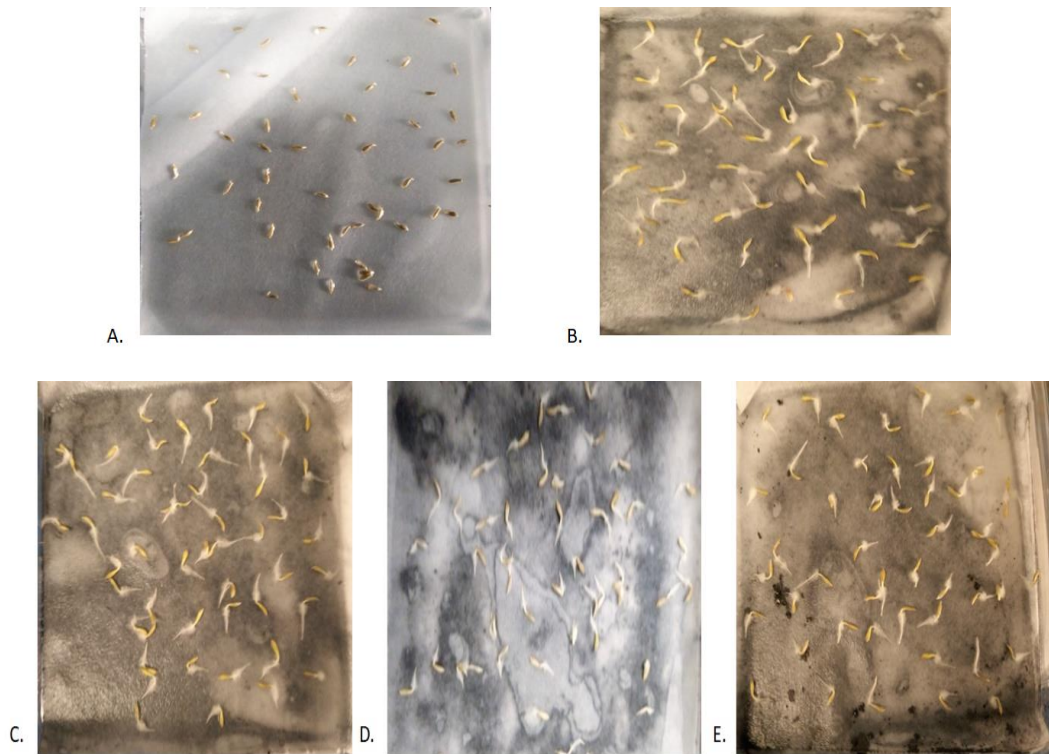


Figure 67. Lettuce seedling germination testing of control after 48 hours, AC, A300, A500 and A800 after 48 hours.

A visual representation (Figure 67) allows a comparison of the lettuce seeds after 100% germination. It is possible to see the radicles with the materials experiments, but not for the control group.

Due to the lack of variation observed in the results with doped materials further images were taken after the original time of 86 hours. Images were taken after seven days to determine if any if any observable variation would be observed at a later stage of the plants life, additional differences could be observed as the seeds continued to germinate and take root. By the end of the 168-hour period there were clear differences visible in the shoots and roots of the examined seeds (Figure 68).

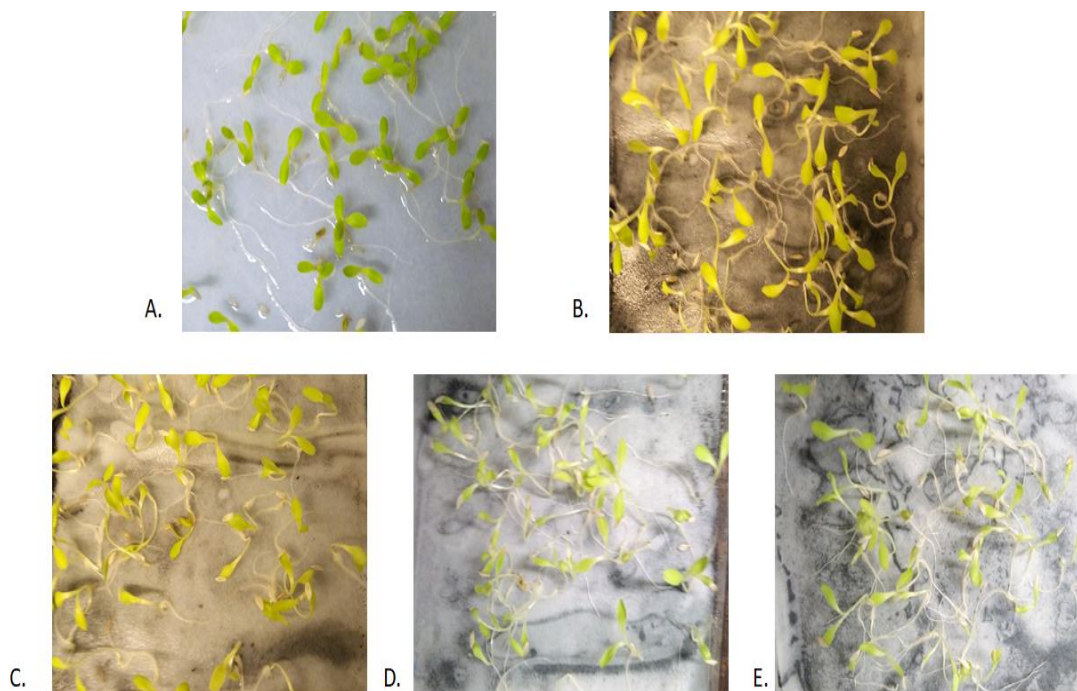


Figure 68. Lettuce seedlings germinated with doped materials at seven days
 A. Control, B. Activated carbon, C. A300, D. A500 and E. A500.

Visual inspection (Figure 68) showed that the control group to have dark green leaves growing and shorter root lengths than those observed with doped materials. The Starbon materials were found to produce much thinner, longer radicles and the leaves on the shoots were larger and of a paler, green colour than the other tested seeds. Activated carbon produced shoots which were darker than the Starbons but with roots longer than the control group. Based on desorption effects (Section 3.3) Starbons all desorbed significantly more GA than AC which desorbed little to no GA. The change in shoots and roots with Starbons is therefore attributed to the increased desorption of GA, resulting in a clear difference in using Starbon materials and AC. However, to more closely analyse the changes and determine that there has been a change, a more in-depth investigation would be required to fully examine the seedling and root differences.

3.4.3 Tomato seed germination

Tomato seed germination showed variation in germination times for each set resulting in a greater spread of results. This increased variance is expected in biological testing more than chemical testing due the inclusion of biological

organisms (e.g. seeds) which may have differences in their makeup. As such, all results for tomato seed testing includes are marked to show the variation that may occur and to identify any anomalous results. Due to slower germination compared to lettuce seeds the observation period was 168 h with counting's every 24 h (Figure 69).

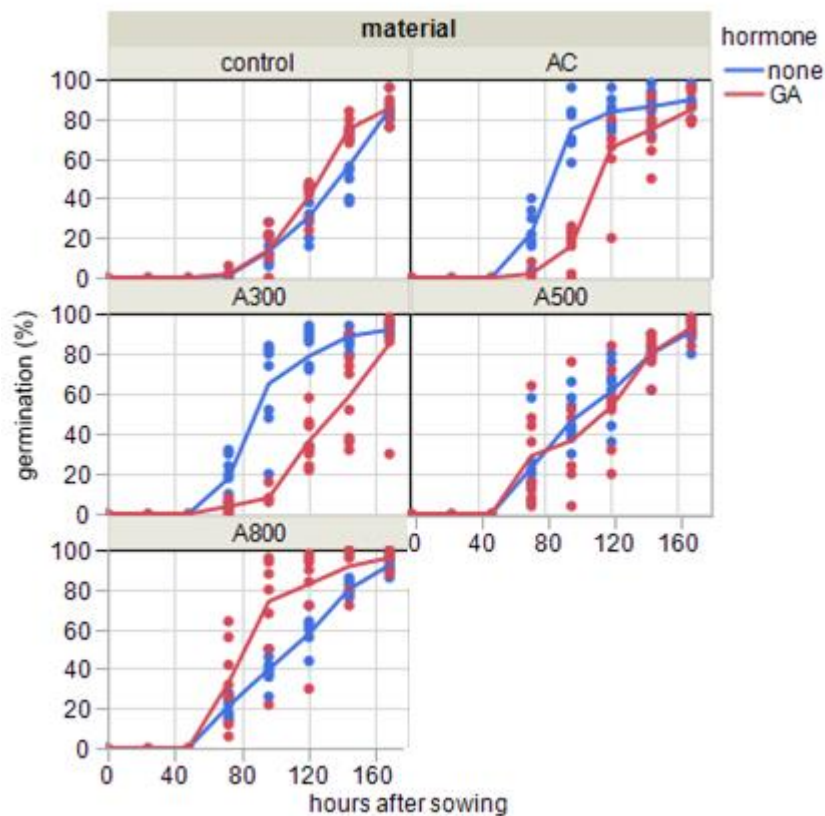


Figure 69. Total germination of tomato seeds with both doped materials and non-doped materials over 168 hours. (8 repeats per experiment)

There is a clear difference between the Starbon materials and the control (no material), and between doped and non-doped materials (Figure 69). The control group compared to some of the Starbon materials show an improvement when GA was added to the experiment. T50% for the control was 130 h into the experiment. All experiments with non-doped materials were found to achieve T50% at an earlier time with all but A800 reaching a T50% between 80 and 100 h. Starbon A800 however, was found to be slightly slower with germination at around 105 hours.

A greater variation of results was observed with doped material which was not seen with the doped control group due to potential uneven access to GA. The control group had GA added to the surface via the addition of water resulting in equal access to all seeds. With the doped materials however, the material could not be set up in an even distribution across the surface which resulted in a potential concentration gradient where some seeds were closer to the material and by extension the GA than others.

Table 33. T50% points of tomato seeds with doped and non-doped material.

Material	T50% /h	
	Non-doped	doped
Control	137 ± 3	126 ± 1
AC	84 ± 2	112 ± 1
A300	88 ± 7	134 ± 5
A500	101 ± 6	91 ± 7
A800	109 ± 3	81 ± 7

Results show that there is a 15-h improvement with the control group when GA is included with T50% being achieved at an earlier time (Table 33). Both A300 and commercial AC report an increase in the time required to achieve the T50% of the seeds when the material has been doped. The T50% for both materials increases by over 20 h showing a significant decrease in effectiveness although T50% is still lower than the initial control results. There are possible explanations for this decrease; activated carbon is primarily microporous and therefore has a high surface area allowing high levels of adsorption. However as shown earlier (Section 3.3.1), AC has the lowest desorption rate of GA for the materials tested with less than 1% desorbed over 10 washings. This means that the addition of GA reduces the available surface area for adsorption of plant growth inhibitors.

Starbon A300 also showed differences between the doped and non-doped material. Based on the shape of the germination curve and T50% the non-doped material showed a fit like AC, the doped material showed a much more linear growth with a large spread of results, the T50% point was seen to have significantly shifted by nearly 46 h later than the non-doped, the largest change in time recorded. Thus, the addition of GA significantly reduces the

effectiveness of the Starbon material. The reasoning for this is that A300 has the lowest recorded adsorption capacity of GA lowest overall surface area compared to the other tested materials (section 3.1.11). In previous experiments, GA was recorded to very slowly desorb off A300 with circa 10% desorption after 10 washing (section 3.3.2) meaning that when the GA is initially adsorbed most of the adsorbate surface is covered reducing the potential surface area for adsorption of the plant growth inhibitors while desorbing more slowly reducing the overall effectiveness. This has a greater impact than observed with AC, attributed to its much lower surface area available for adsorption. From that the difference between the non-doped and the doped results, it can be seen the doped material results in a decrease in the time for T50%. There was a decrease of 10 h in the T50% though with the errors there was a slight overlap which does reduce the statistical difference. However, with the doped material there is an anomalous set of results which skews the fitted line to a lower point. If, this point is removed, then the line would more show a lower T50% of 84 h which is a significant decrease in germination time. However, further testing is needed to justify deletion of this data point.

Adsorption capacity and results from (section 3.3.3) showed A500 desorbs approximately 30% of the gibberellic acid over 10 washes the highest recorded desorption of GA of the materials tested. Over the course of the experiment it shows that the A500 is desorbing the GA from its surface promoting germination while also having sufficient surface area and adsorption capacity to adsorb plant growth inhibitors further improving germination times.

The results for A800 show a marked difference compared to the other materials. The non-doped material showed a 25-h slower germination rate compared to AC but T50% was achieved 28 h earlier than the control. This was unexpected as due to its similarity to AC (surface area and hydrophobicity, etc), it was thought A800 would show similar rates of germination. An explanation for this is that due to the desorption effects previously discussed (Section 3.3.4), it is known that A800 does allow desorption of hormones showing 20% desorption over 10 washings, In this case, one of two things may be happening either:

- i. There is less desorption of the plant growth inhibitors though this is unlikely as A800 was found to have the highest surface area for adsorption of the Starbon materials, or;
- ii. Desorption of the plant growth inhibitors is occurring back into the environment. The doped material showed a clear improvement over the non-doped material.

Based on previous data regarding adsorption capacity and surface area it is known that A800 has comparable surface area to AC (Section 3.1.11), A800 readily desorbs gibberellic acid over a long period of time. It is interesting to note that in this case the doped results achieve T50% at the earliest time of all experiments conducted, even earlier than non-doped activated carbon though the error does show an overlap with doped A500. The material is both able to adsorb the plant growth inhibitors but while simultaneously desorbing gibberellic acid, improving seed germination.

Overall the results suggest the hypothesis that there are two competing factors affecting germination. The first is the ability to adsorb plant growth inhibitors from the environment. This ability increases with surface area and therefore activated carbon and A800 have the highest adsorption capacity. The second factor is the ability to desorb the plant growth promoters into the environment, promoting seed germination. Doping materials reduces the efficacy of the adsorption capacity by lowering surface area, reducing the adsorption of growth inhibitors released by the seed. For doped A300 and AC this desorption factor is poor, showing reduced available adsorption capacity meaning an adsorption capacity resulting in poor germination. With non-doped however the high adsorption capacity and low desorption means plant growth inhibitors are adsorbed well, aiding growth.

For A500 and A800, the adsorption capacity is high, but desorption factor is also increased. This means with non-doped material while much of the plant growth inhibitors are adsorbed some may be released back into the environment slowing germination as observed with A500 and A800. However, when doped the increased desorption factor means that plant growth promoters are released into the environment in greater quantities and overall

adsorption capacity remains high, resulting in the shift between germination rates between A800 doped and non-doped results.

The most important thing to note overall though is that doped A800 showed the shortest time to T50%. However, when looking at the standard error it shows that there is overlap with doped A500 and non-doped A800. This means that until further experiments can be done to clearly show the statistical differences between the materials, on an industrial level AC would be the most effective material from these results.

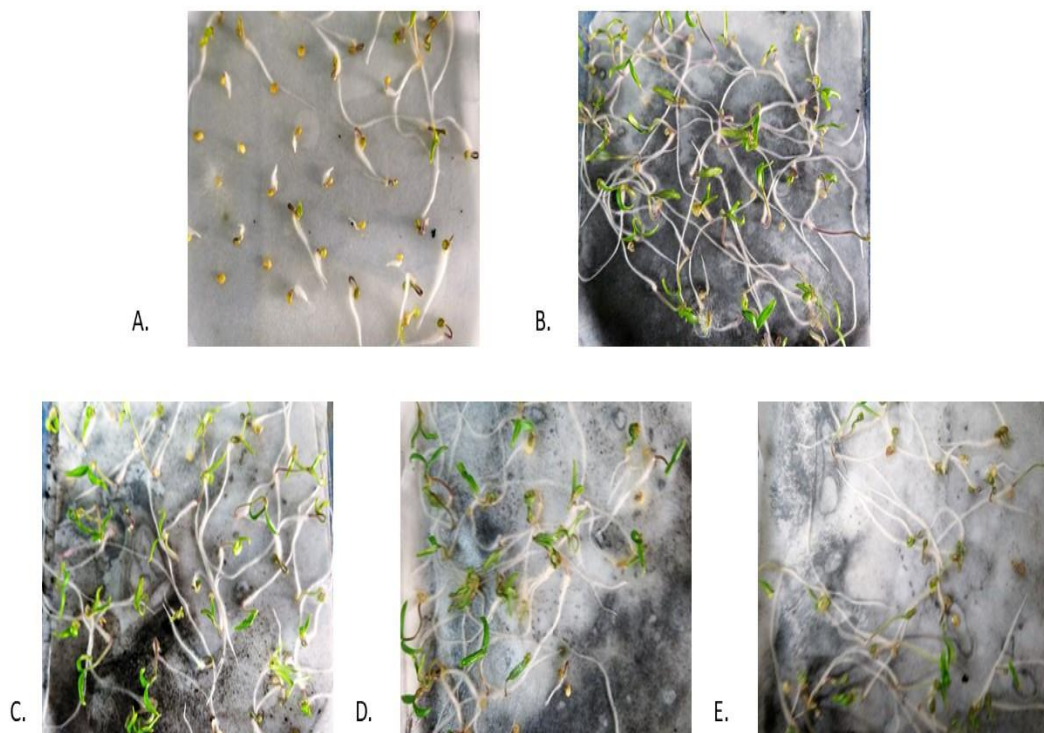


Figure 70. Tomato seedlings with non-doped materials at 7 days A. Control, B. Activated carbon, C. A300, D. A500 and E. A500.

Significant differences in the stages of germination between the control group and those with materials present were observed (Figure 70). While high levels of germination have occurred for each experiment, the seeds without material were at an earlier stage of growth. The control group had relatively short root

lengths along with very few of the seeds showing flowering of green leaves, compared to the seeds with Starbon material which had longer root lengths and a much greater proportion of the seeds had developed green leaves (control shows between 1-10 mm, Starbon materials have over 25 mm in all cases). This results in two conclusions, either the faster germination of the material seeds resulted in an advanced stage of germination, though keeping the control group an additional 72 hours did not show results that would be expected of this was the case. The other option is that the material is resulting in the removal of plant growth inhibitors in the environment which allows a much faster germination and growth rate. This is the most likely reason why there is such a clear difference between the control group and the other experiments.

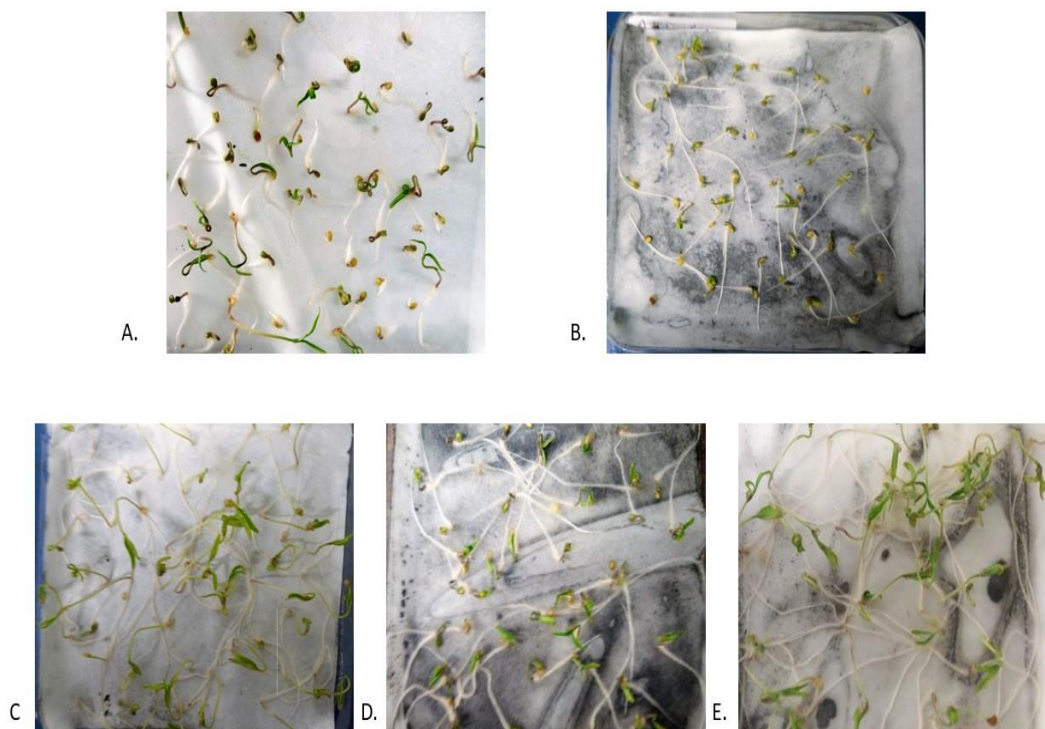


Figure 71. Tomato seedlings with doped materials at 7 days A. Control, B. Activated carbon, C. A300, D. A500 and E. A800.

Compared to the previous control group there is more flowering of leaves suggesting an increased germination rate which is in line with the results for T50% (Figure 71). It could also be seen that both AC and A300 show lower levels of germination with shorter root lengths and less flowering of leaves

which would be expected based on the results observed (later T50% time than the non-doped results). Starbon A500 and A800, showed greater germination than seen in Figure 70 with a clear increase in the germination rates of the leaves and longer root lengths on top of improved germination rates as expected as the doped results show an earlier T50 % time than the non-doped results.

3.4.4 Tomato seed germination using Starch and A00

At this point the working hypothesis is that the ability for the seed coating components to improve seed germination is dependent on the ability of the material to adsorb plant growth inhibitors and to desorb plant growth promoters. To test this hypothesis an experiment was designed to repeat the tomato germination experiment but using materials that would have a significantly different porosity, a lower surface area and different surface chemistry.

Alginic acid was selected since it is the precursor material for Starbons tested. Alginic acid was also selected as its surface area and pore volume was significantly lower than the Starbons tested. Starbon A00 was selected due to its decreased surface area compared to the Starbon materials tested along with a slightly differently surface chemistry with an increased number of oxygen based functional groups (Table 34)

Table 34. Porosity comparison between AC, A300, A00, alginic acid (AA)

	AC	A300	A00	AA
BET surface area (m² / g)	526	402	227	-
Langmuir surface area (m² / g)	730	674	454	0.49
Micropore area (m² / g)	497	125	145	-
Micropore volume (cm³ / g)	0.24	0.05	0.06	-
Mesopore volume (cm³ / g)	0.04	1.22	0.64	-
Ratio of micro to mesopore	1:0.16	1:25	1:10.66	-
Mesoporosity factors (%)	14.00	96.00	90.14	-
(Mesopores / total pores * 100)				
Average adsorption pore diameter (nm)	2.1	10.1	12.3	-

Literature data for Alginic acid porosity was used due to the difficulty analysing with present methods (Table 34).¹⁵⁴ There are clear differences in porosity between AA, A00 and the tested AC and A300. The starch was reported to have a low overall surface area and make up of micro and mesopores. From the data the AA was primarily macroporous with few micropores, A00 however, showed that the micropore volume was slightly higher than for A300 but with roughly half the volume of mesopores. It suggests that during carbonisation the macropores degrade forming mesopores before these pores degrade further into micropores at higher carbonisation temperatures.

Starbon A00 and AA were used in the same seed germination testing as used in previous experiments to determine how such a change in porosity and surface chemistry may affect seed germination (Figure 72 and Table 35).

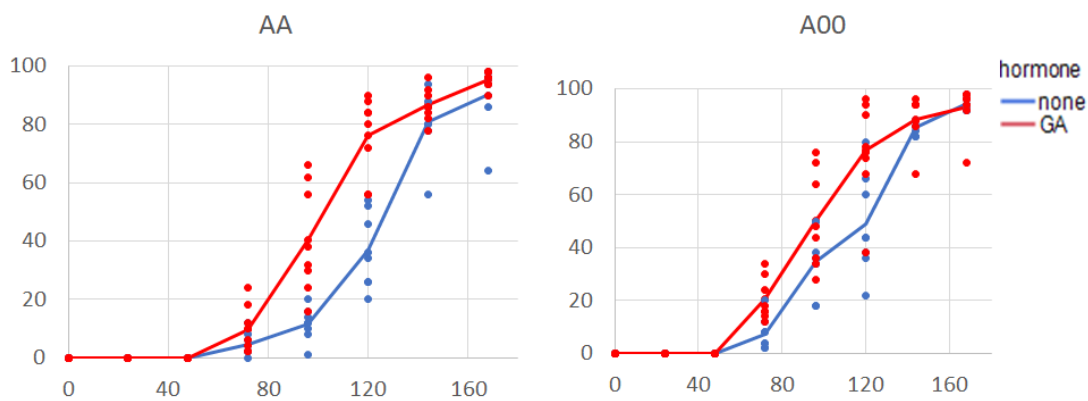


Figure 72. Total Germination of tomato seedlings with both doped materials and non-doped materials over 7 days. (8 sets per experiment)

Table 35. T50 % of all tomato seeds with all tested materials.

Material	T50 % / hours	
	Non-doped	doped
Control	137 ± 3	126 ± 1
AC	84 ± 2	112 ± 1
A300	88 ± 7	134 ± 5
A500	101 ± 6	91 ± 7
A800	109 ± 3	81 ± 7
AA	127 ± 2	102 ± 3
A00	120 ± 4	95 ± 4

The AA experiment shows a difference between the doped and non-doped conditions (Figure 72). Alginic acid was found to provide a slight improvement over the control experiment though it showed a further improvement in germination time when doped. The A00 material showed a slight improvement when doped, over its non-doped material though this effect was less pronounced than observed with AA. These results show that the inclusion of the material does improve the germination rate though the overall surface area and by extension the ability to adsorb plant growth inhibitors appears to have a significant effect on seed germination time. It also suggests that the surface chemistry may also influence seed germination though it is difficult to prove with the non-doped results, with surface chemistry likely having a greater effect when the material is doped due to the desorption affects though overall adsorption capacity is the most important factor overall.

Comparing the information between Table 35 and Figure 72, clear comparisons can be made. The experiment with the AA showed that there is improvement over the control group with T50 % being achieved with a 15-hour difference between the two when not doped. When doped there was a 25-hour improvement in the T50 % for the AA suggesting that the doped material was desorbing whilst also effectively adsorbing plant growth inhibitors, though the T50 % results were still not as effective than most of the other materials. With A00 there were significant differences between the doped and non-doped materials. The non-doped A00 reached T50 % at 120 hours which was the slowest of the Starbon materials tested though earlier than both AA and the control experiment. However, based on the error results it shows that there was an anomalous set of results which skewed the T50 % to a later time. However, T50 % was only 19 hours faster than the control group and 31 hours slower than A300. There was also a recorded improvement between the doped and non-doped material. Overall this showed that adsorption capacity and by extension surface area had a significant effect on the germination rate with the ability to desorb effecting the doped results to a significant degree. These results show that overall Starbons are highly effective at improving

germination rate and A800 was found to result in the fastest germination times when doped.

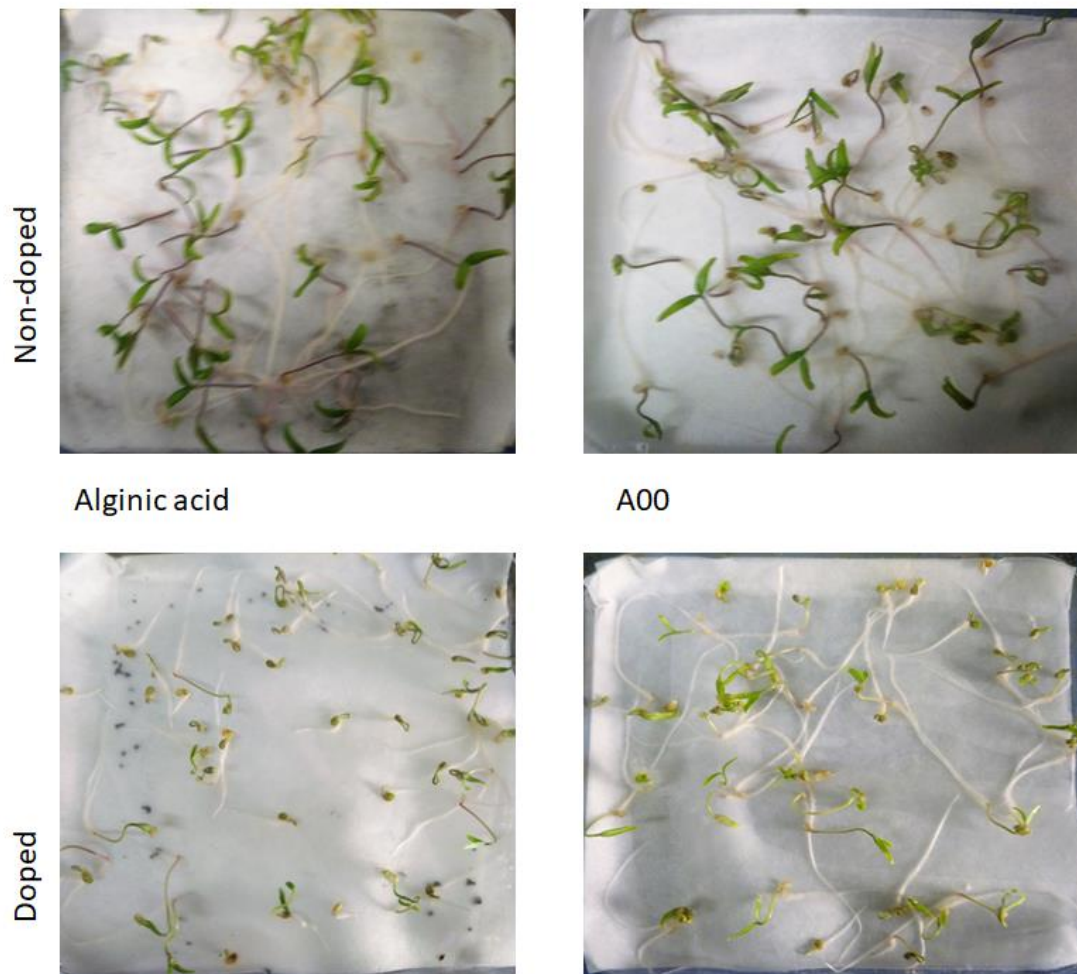


Figure 73. Tomato seedlings after 7 days for non-doped and doped Starch and A00.

There are significant visual differences between the doped and non-doped seeds (Figure 73). The non-doped materials show that most of seeds are germinating with dark green foliage being observed. In comparison, when looking at the doped materials A00 results in seeds which, while showing foliage with most of seeds, are paler green and with smaller foliage similar to previous results (Figure 71). This showed that the GA has been desorbed from the A00 and is affecting the seeds germination. With AA, germination has taken place but with less developed foliage and root length showing that the seeds are at an earlier stage of germination then observed with the non-doped materials with less foliage being observed.

Overall these results further add credence to the hypothesis that for an effective seed coating the primary factor is a high overall surface area and ability to adsorb plant growth inhibitors as observed with the AC showing the shortest time to T50 %. The second factor is the ability to desorb plant growth promoters.

3.4.5 Statistical analysis of tomato seed germination

When doing biological testing it is not only important to look at the results obtained such as the T50% value but also to determine the statistical variations between the experiments. During biological testing one of the most commonly used methodologies is known as the analysis of variance (ANOVA) which looks to determine if there is a clear statistical difference between the values obtained. Once differences between each point has been calculated a further post-test can be done to differentiate between the different results to determine similarities between the materials and the doping experiments.^{155,156}

ANOVA compares the statistical means of a group and determines whether they are equal and if there is a significant difference between them. This is very important within biological systems due to the large number of experiments and samples that must be taken to clearly see how variables may affect the system. The use of ANOVA allows a consolidation of all this data making it easier to observe similarities and differences. A null hypothesis is used to determine if the variables have affected the result. If a null hypothesis has been disproven, then it shows that the working hypothesis is correct.

One-way ANOVA is used when there is one independent variable being tested. One-way ANOVA works on the following hypothesis;

- Normal distribution of the population from which the samples are drawn.
- Measurement of the dependent variable is at interval or ratio level.
- Two or more than two categorical independent groups in an independent variable.
- Independence of samples
- Homogeneity of the variance of the population.

Within this project one-way ANOVA was used to test the use of Starbon materials and the inclusion of GA to the solution. The hypothesis used was that the inclusion of the materials or GA would influence the T50 % and overall final germination. The null hypothesis was that the inclusion of material or GA did not influence the results.

To determine if a variable follows the null hypothesis or not, an “F” test is conducted from the ANOVA. The “F” test runs a test statistical analysis under the null hypothesis where F crit is derived from the scaled sums of squares reflecting the variability and the F value is calculated via

Equation 19. "F" critical test

$$F = \frac{\textit{explained variance}}{\textit{unexplained variencce}}$$

If the calculated F value is found to be greater than the F crit value, then the variable does not follow the null hypothesis. However, this does not mean that it follows the initial hypothesis as additional factors may be affecting the results. This issue can be reduced depending on the experimental procedure followed. The “p” value is a measure of the significance level of the results obtained and are compared to a set “α” level. In the case of this project “α” was set to 0.05 which is the commonly selected value. If the “p” value is below “α” than it can be assumed that sufficient evidence has been collected to accept the results. If the “p” value is above “α” than it means that there are insufficient data points to accept the conclusion obtained.

Statistical analysis showed that the results of the final germination fit into the null hypothesis for all experiments. Showing that by the end of the experiment the inclusion of material did not affect the final germination results. Results do show however, that the null hypothesis was not followed when looking at the T50% time meaning that the inclusion of material or the addition of GA into the control group does likely influence the time to achieve the T50 %.

Table 36. One-way factor ANOVA of T50% for both material testing and control doping.

<i>Source of Variation</i>	<i>SS</i>	<i>df</i>	<i>MS</i>	<i>F</i>	<i>P-value</i>	<i>F crit</i>
Doping	16113.18	6	2685.53	12.1213	1.11E-08	2.265567

Statistical results, comparing the F crit to the “F” value show that in both cases the “F” value is higher meaning the null hypothesis has been disproven (

Table 36). The p value in both cases is below the “ α ” meaning the results can be accepted and do not require additional data points.

One issue with this analysis is that it does not distinguish the differences between each material tested. To do that a post-hoc t test can be conducted which distinguishes between each combination of material to determine which materials show a similar mean to one another. If this is the case, then it means that statistically these grouped results are similar to one another, though these results can have a false positivity result which was taken into during the experiment.

Table 37. Post hoc t test of non-doped materials.(each letter indicates a group of similar data)

material	post hoc t-test
control	A
AC	B
A300	B, C, D
A500	C, D, E
A800	C, D, E
AA	F
A00	C, D, E

From the control group, results show that no other result was comparable to it meaning that based on previous data the addition of material does have a significant effect on T50 % time (in this case improving it) (Table 37). Activated carbon was found to be have similar results to A300 and no other material. Starbon 300 however shows comparable results to AC, A500 and A800. Both

A500 and A800 though show the same results being comparable to A300, A500, A800 and A00. This shows that the Starbon materials are statistically all comparable to one another with only A300 showing a change with it not being comparable to A00 but is with AC. Finally, AA was found not to be comparable to any other material tested.

To analyse multiple variables such as both the material used and doping with GA a more complex form of ANOVA is required. In this project two-way ANOVA with replication was selected since this method specialises in systems with two variables (material and GA) and requires multiple repetitions which has been conducted over the course of this project.

Table 38. Two-way ANOVA of doped materials.

<i>Source of Variation</i>	<i>df</i>	<i>F</i>	<i>P-value</i>	<i>F crit</i>
Material	6	17.5	2.69E-11	2.27
Doping	1	14.2	0.00169	4.494

Results show that as with earlier experiments that the F value shows that the null hypothesis has failed (Table 38). It shows that the effect of the material and doping does influence the T50 %. The “P” value shows that sufficient data has been obtained to accept the results. However, as before, the results are complex and it is important to compare these results to the post hoc T-test in (Table 39).

Table 39. Post hoc t-test of doped materials.

<i>material</i>	<i>post hoc t-test</i>
control	A
AC	B
A300	A
A500	B, C
A800	C
AA	C
A00	C

The materials are differentiated into groups with similarities in T50% (Table 39). The data shows that both the control group and A300 are one group with

similar results which indicates that A300 is as effective as the control group once doping occurs. Activated carbon and A500 were also like one another even though AC had a slower T50% time compared to the non-doped experiments and A500 improved. Starbon 500, A800, AA and A00 all show similarities for the T50 % and all show a significant improvement over the control and AC. The Statistical data shows that overall the inclusion of material and doping does have a significant effect on the speed of germination but not the overall germination of the seeds based on this experiment. To test that a new experiment would have to be devised to observe the long-term effects as the plants grow. It was also observed that with the doping effects the Starbon materials except for A300 show similar results to the precursor materials and all were more effective than doped AC.

4 Summary and future work

Activated carbon shows high microporosity along with the highest recorded surface area of all the materials, but also low levels of mesoporosity. For the Starbon materials, microporosity was found to increase as temperature of carbonisation increased though never to a similar level as the tested AC, as all retain a mesoporous nature. Adsorption capacity was found to increase with increasing surface area, with the bioactives varying in overall capacity with ABA showing the best levels of adsorption with all materials and GA showing the lowest levels. Inductively Coupled Plasma and XPS show that within the Starbons materials tested, additional elements other than carbon, hydrogen and oxygen were detected in particular calcium and sodium. This was expected as all materials tested come from biomass containing such impurities. Surface imaging showed that the particle size and surfaces differ for Starbons compared to the AC, in particular A300 which showed that it was not fully carbonised. Starbon materials functional groups on the material surface were analysed via XPS showing that as carbonisation temperature increased there was a decrease in the oxygen based functional groups along with an increase in carbon based functional groups particularly π - π^* and C=C bonding.

In terms of further analysis of the Starbon surface, the most effective method would be to use computational modelling such to analyse the surface of the material and create a model for points of interaction and the likely surface structure of the material along with adsorption sites could be created. From this it would then be possible to simulate how different bioactives adsorb onto the surface and how monolayers and multilayers form.

Several conclusions can be made about the porosity and interaction between the bioactives and materials. It was noted that the adsorption process in all cases followed the pseudo second order reaction with a multi-step reaction forming a multi-layer. All interactions show physisorption occurring with the adsorbates with the rate determining step for A500 and A800 in most cases being pore diffusion. There are clear differences observed in the adsorption isotherms between AC, A300 and the higher temperature Starbons with the higher temperature Starbons showing a closer fit to the Bangham equation

and Dubinin Radushkevich equation. Finally, in most cases it was observed that the desorption process is thermodynamically favoured at higher temperatures and that adsorption would be thermodynamically favoured at lower temperatures including the temperatures that future experiments would be conducted at.

Other models could be investigated to further improve the modelling at the surface, such as the film-pore diffusion model. This model describes adsorption occurring via adsorption through film mass transfer and intraparticle diffusion to the sorption sites meaning that internal and external mass transfer is the rate determining step. The model is as an extension to the unreacted core theory and was proposed by the teams of Spahn and Brauch (Figure 74).^{19,157}

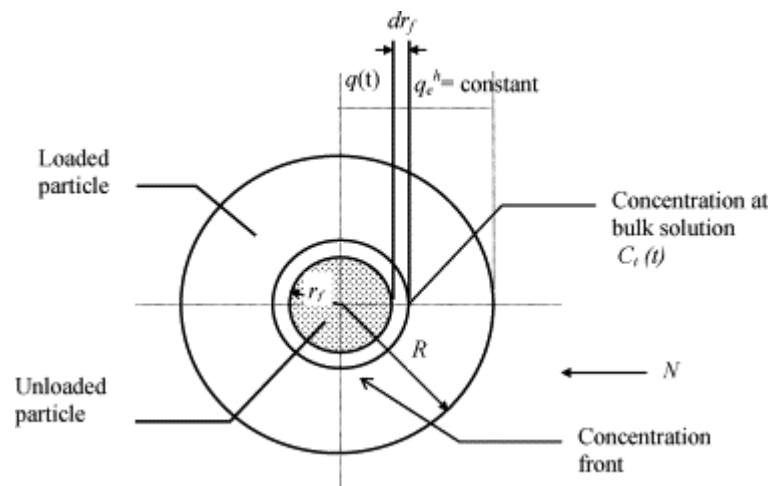


Figure 74. A conceptual model of the film-pore diffusion.¹⁵⁷

The film-pore diffusion model works on the following assumptions;

- Transfer of the adsorbate within the adsorbent is due to molecular diffusion.
- Equilibrium occurs between the solution within the pores and the adsorption site – assumes the flow of the solution into the pores is much faster than the rate of uptake.
- The concentration of the adsorbate is negligible within the solution as to be ignored.

However, for an accurate measurement from this model particle size would need to be determined. As such computational modelling could also be used to determine average particle size.

Starbons showed considerably more potential compared to AC with regards to both desorption capabilities and control of desorption. Desorption studies of each Starbon material showed differing levels of desorption depending on the hormone being tested. Gibberellic acid was found to have increased desorption as the temperature of carbonisation increased, whereas IAA showed the lowest desorption level of the tested plant growth promoters. Kinetin showed low levels of desorption with A500 and increased desorption levels with A300 and A800. Abscisic acid was found to be readily adsorbed in all cases but showed very low levels of desorption with every material tested. These results show that certain compounds can readily remain adsorbed onto carbonaceous materials, whilst others are removed by desorption. It is important that plant growth inhibitors remain adsorbed to the surface of the material, because if Starbons are to be used within a seed coating, it is vital that they retain plant growth inhibitors and desorb the promoters.

Water retention experiments show that Starbons can initially hold roughly their own weight in water, whereas AC could only hold half its mass. With regards to retention, however, it was observed that AC and A800 did not retain water while A300 and A500 could retain low levels of water for longer periods of time.

With regards to LCMS consistently higher levels of adsorption and lower levels of desorption were observed for the lower molecular weight compounds compared to the higher molecular weight molecules. This is due to their ability to pass through smaller pores so can adsorb deeper within the material. Finally, it was noticed that the standard error was high for several results. This was expected and is explained due to the use of biological organisms which results in a high degree of variance to obtain the bioactives for analysis.

Future work would be to expand this experiment to look at additional bioactives such as methyl jasmonate. Other ideas would be to analyse additional samples to allow for quantitative analysis and testing with multiple varieties of seeds. Finally, additional experiments could be conducted with structurally

similar derivatives of bioactives such as ABA to see how the change in functional groups may affect the adsorption and desorption properties (Figure 75).

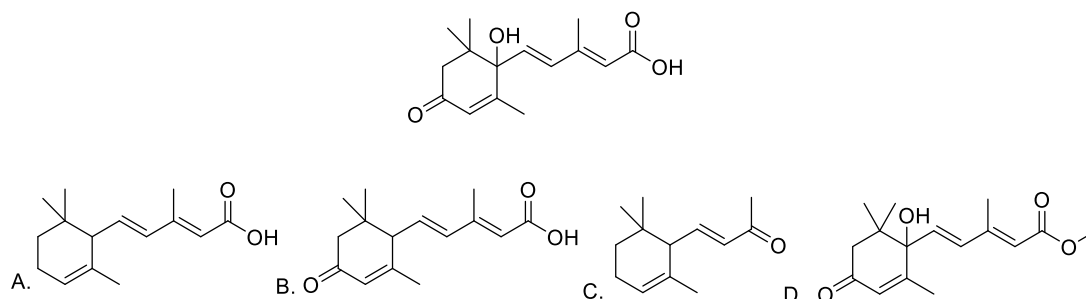


Figure 75. Four derivatives of abscisic acid, A. α-ionylidene acetic acid, B. 1-deoxy- ABA, C. α-ionone and D. ABA methyl ester.

It is important to note that only one hormone was studied in batch germination testing rather than a formulation of bioactives that would more likely be used if on an industrial scale. If this experiment would be taken further, it would be important to look at selecting a mix of plant growth promoters to improve germination rather than one promoter. Another important aspect of this experimental series is that they were conducted under laboratory conditions and to take this further testing under real world conditions with a sample crop would be required.

5 Conclusions

This project has aimed to understand the overall surface and adsorption properties of Starbon materials and how they may be used as a seed coating component to improve germination. An in-depth analysis of the Starbon material showed that it was highly mesoporous with increasing hydrophobicity as the material was carbonised at higher temperatures. The surface was found to have increasing basicity as carbonisation temperature increased. Kinetic studies of adsorption show that all Starbons follow the pseudo second order for adsorption forming a multilayer on the surface. Further experimentation show adsorption is due to physisorption with the rate determining step for adsorption due to pore diffusion. Adsorption and desorption studies showed that AC shows high levels off adsorption but low levels of desorption while as all Starbons showed high levels of adsorption and controllable desorption with

A500 and A800 showing the highest level of desorption over a longer period. Liquid chromatography mass spectrometry show that all materials show low levels of desorption of plant hormones though with Starbons showing higher levels of desorption. Comparisons were made with structurally similar compounds including ZE and KI to understand how variations in chemical functionality may affect adsorption and desorption. Finally, germination studies were conducted to examine if Starbons can improve germination times. The results show that while AC was the most effective non-doped material, A800 was the most effective when testing with pre-doped GA.

In conclusion results show that Starbons can be used as a seed coating component to improve germination times though additional testing may require in field testing to confirm the overall effectiveness of the Starbon materials.

6 Appendix

Table 40. ICP analysis of Alginic acid. (Values below 1 ppm not included).

Analysis	Result (ppm)
Al	9.80
As	1.07
Ba	49.35
Ca	3,978
Cr	4.48
Cu	3.37
Fe	62.65
K	419.05
La	2.97
Mg	65.42
Mn	1.86
Na	5,172
Ni	1.17
P	87.41
S	1448
Si	41.61
Sr	123.8
Ti	4.34

Table 41. ICP analysis of Starbon precursor. (Values below 1 ppm not included).

Analysis	Result (ppm)
Al	135.5
Ba	43.7
Ca	116,700
Cr	1.62
Cu	4.62
Fe	114.1
K	78.76
La	8.35
Mg	174.2
Mn	6.74
Na	517.2
P	92.13
S	345
Si	104.1
Sr	143.6
Ti	8.42
Zn	1.18
Zr	1.44

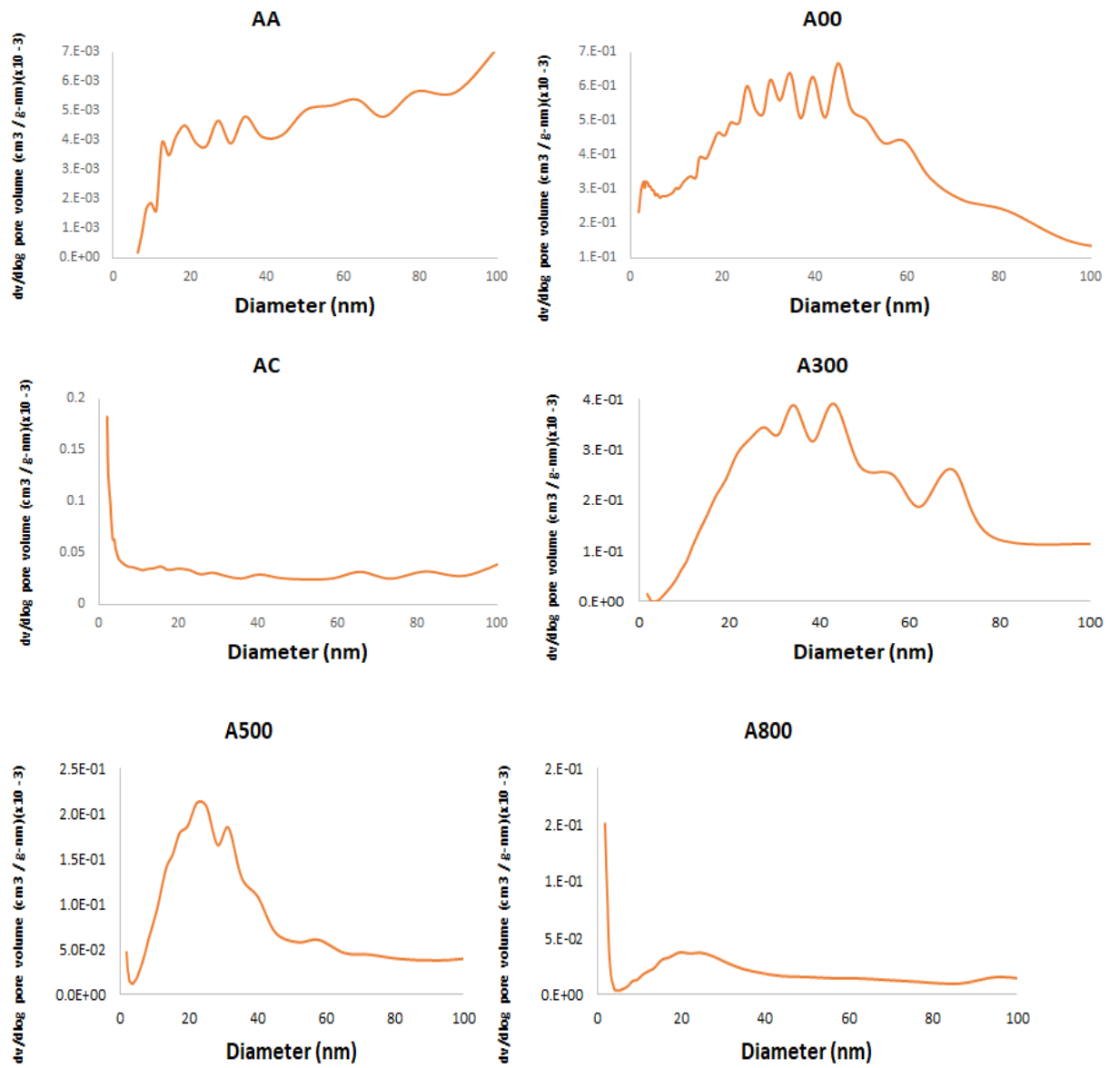
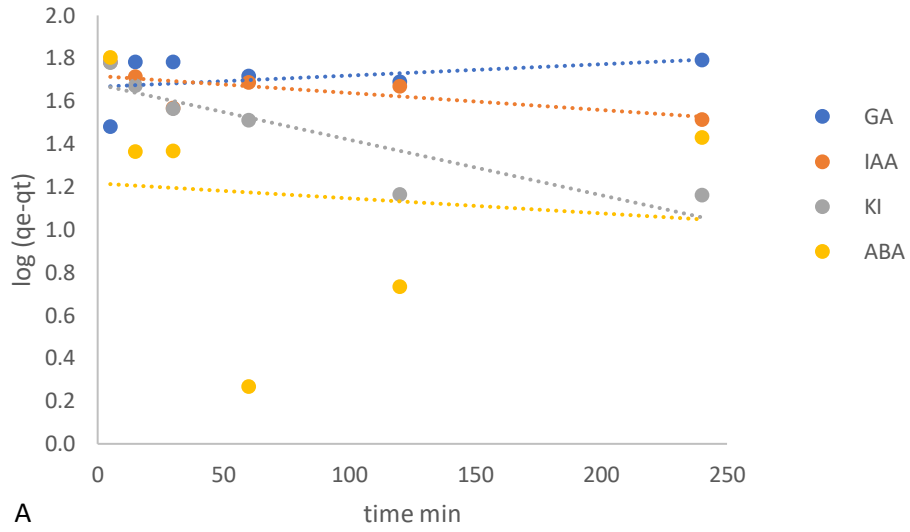
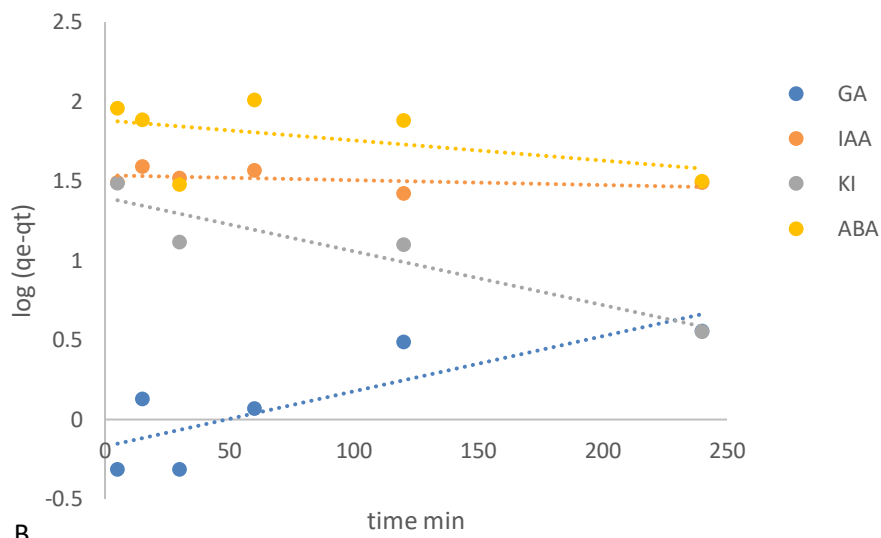


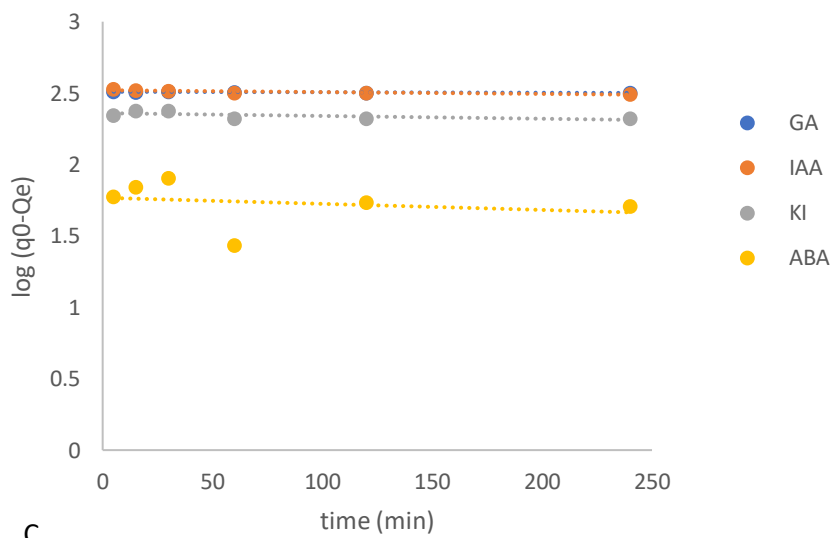
Figure 76. Pore distribution of AC and Starbon materials.



A



B



C

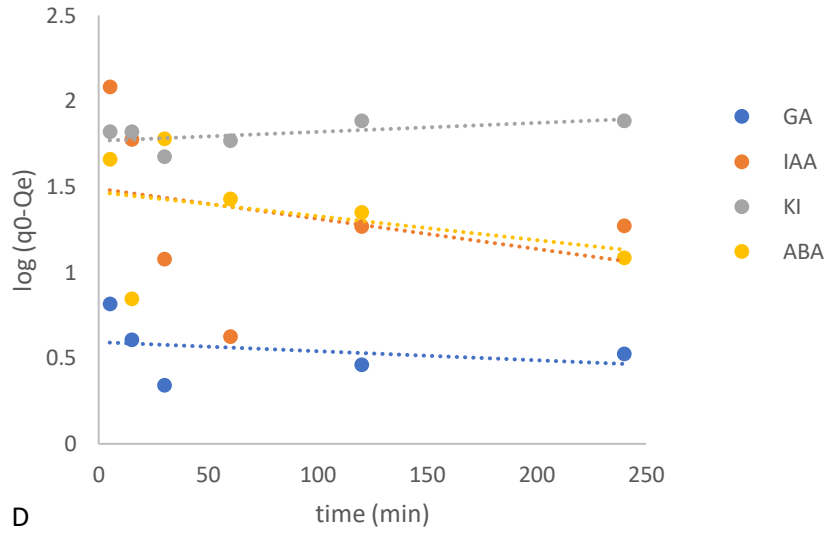
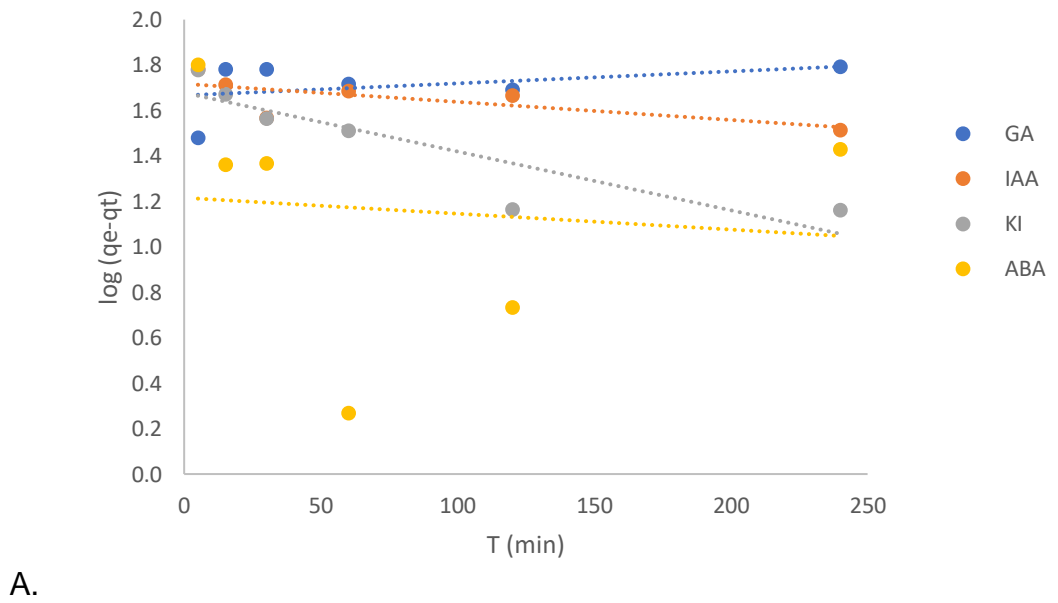
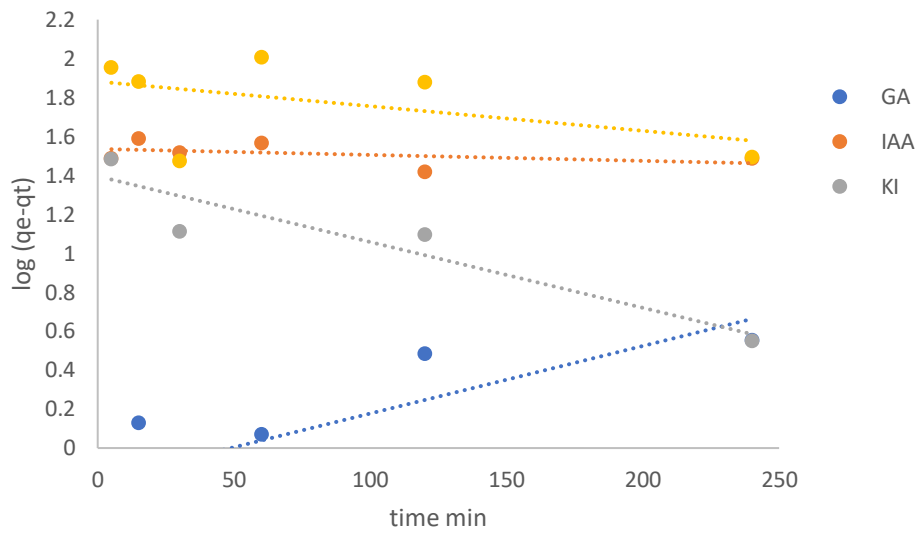
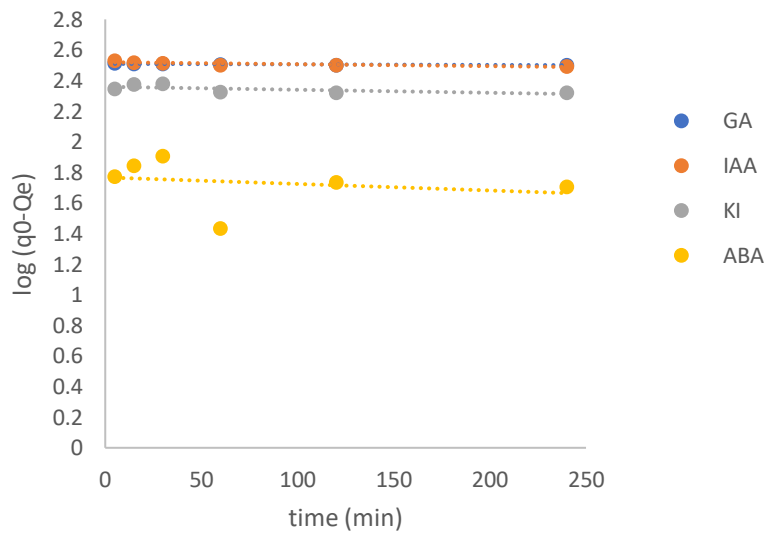


Figure 77. Pseudo first order reaction for all tested materials and hormones. A. AC, B. A300, C. A500, D. A800. (four repetitions)

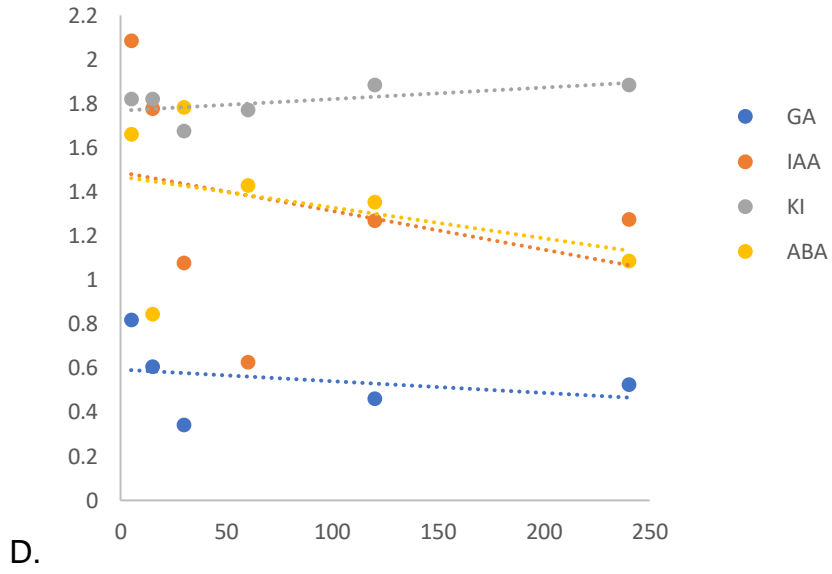




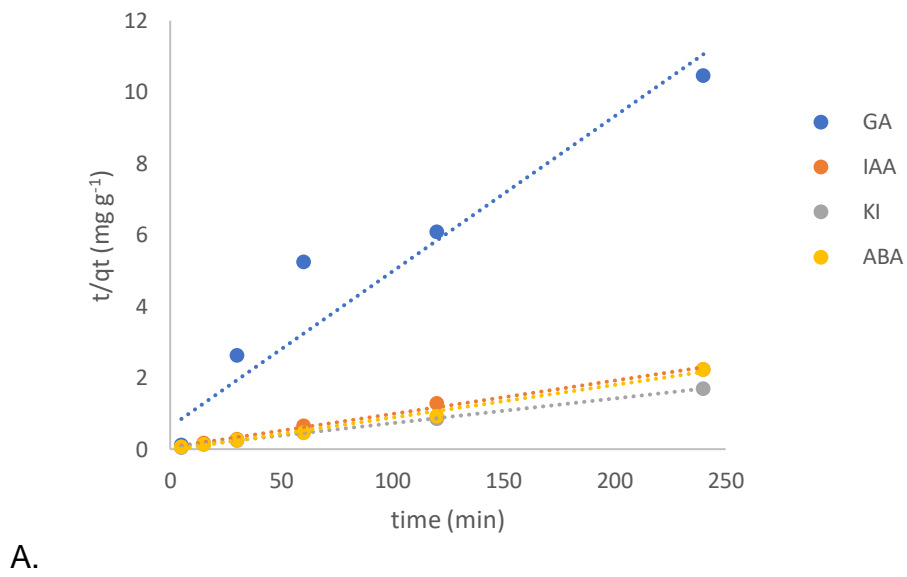
B.

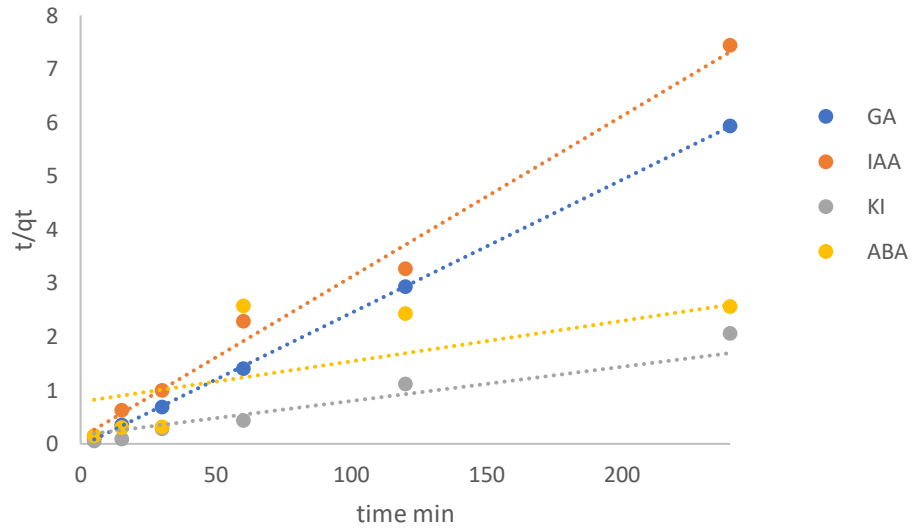


C.

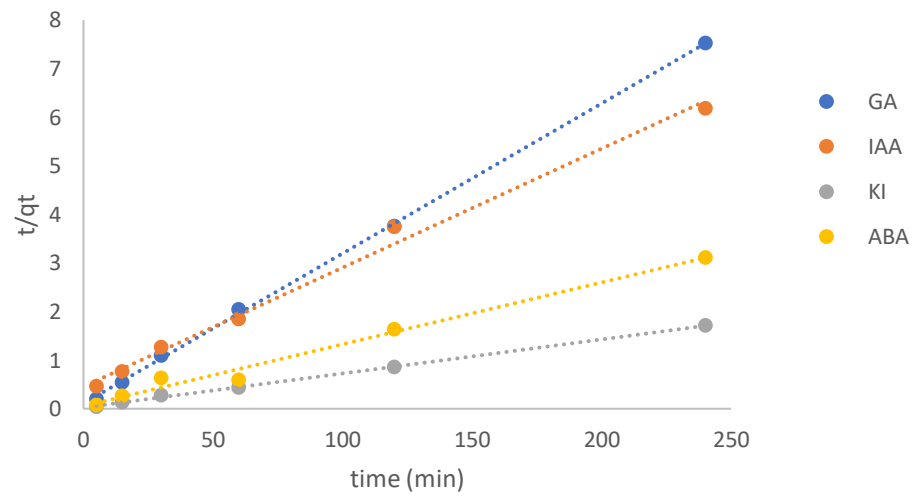


Pseudo first order for A. AC, B. A300, C. A500 and D. A800

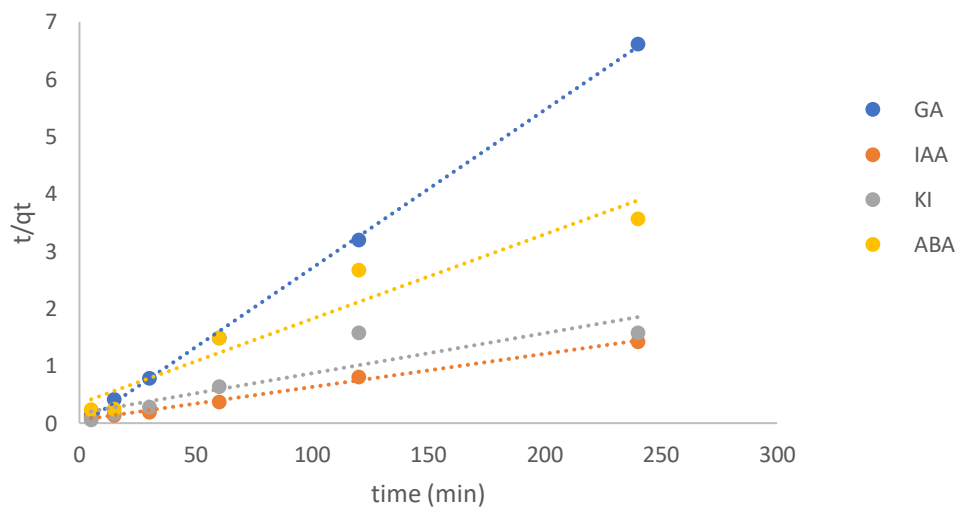




B.

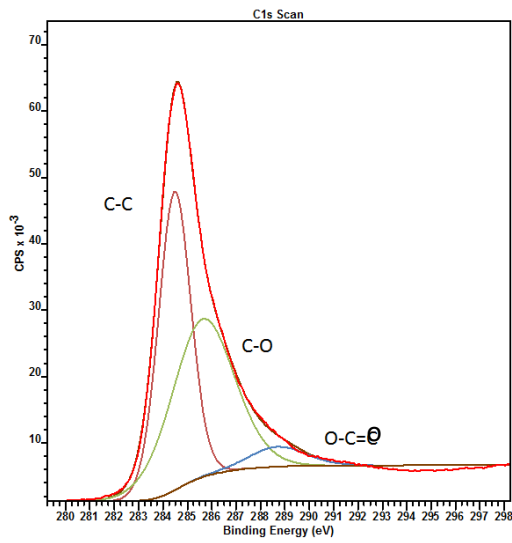


C.

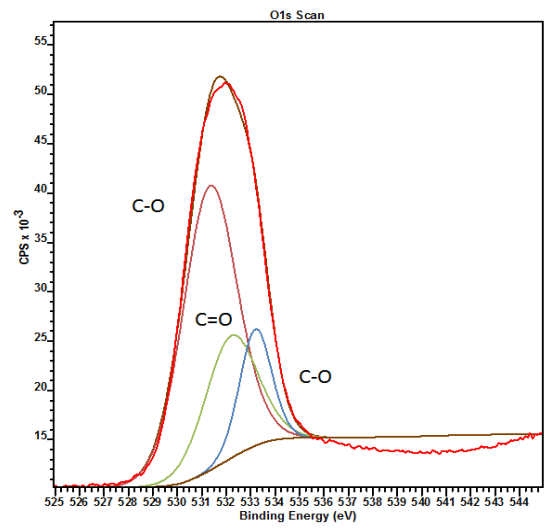


D.

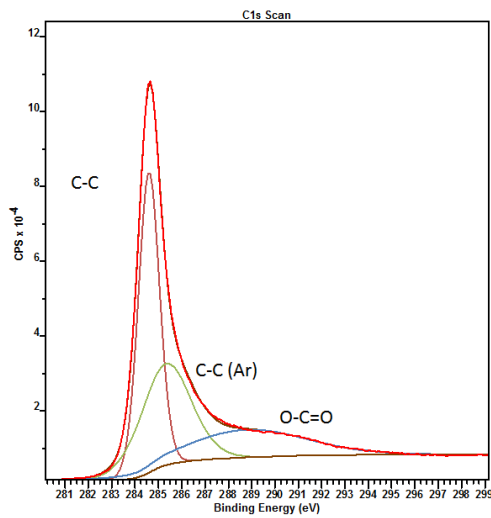
Pseudo second order for A. AC, B. A300, C. A500 and D. A800



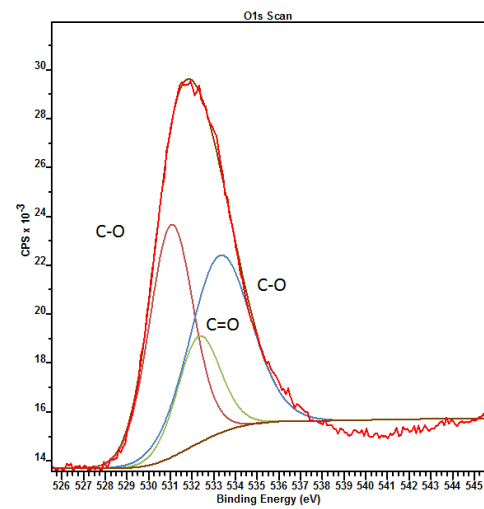
A) Carbon XPS of A300



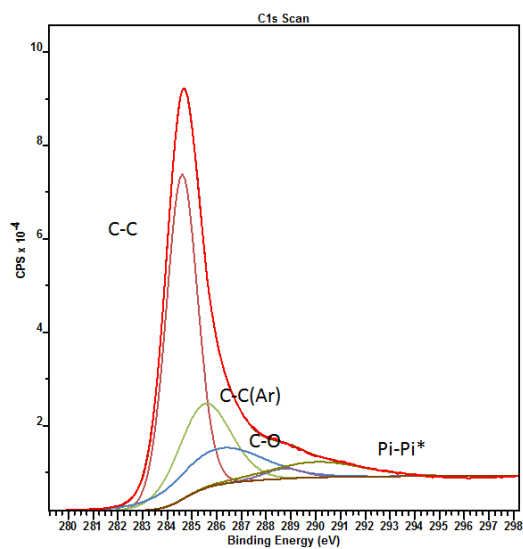
B) Oxygen XPS of A300



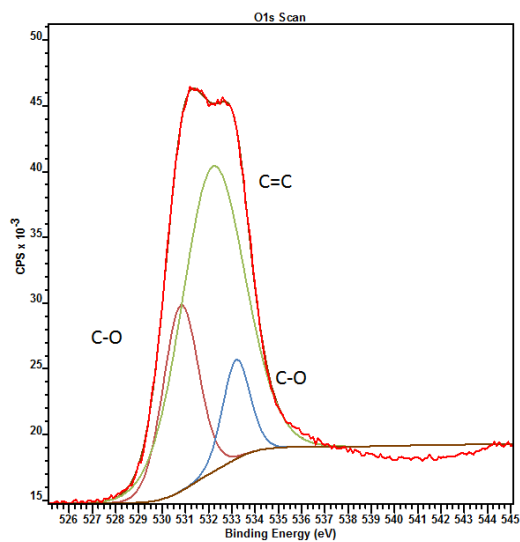
C) Carbon XPS of A500



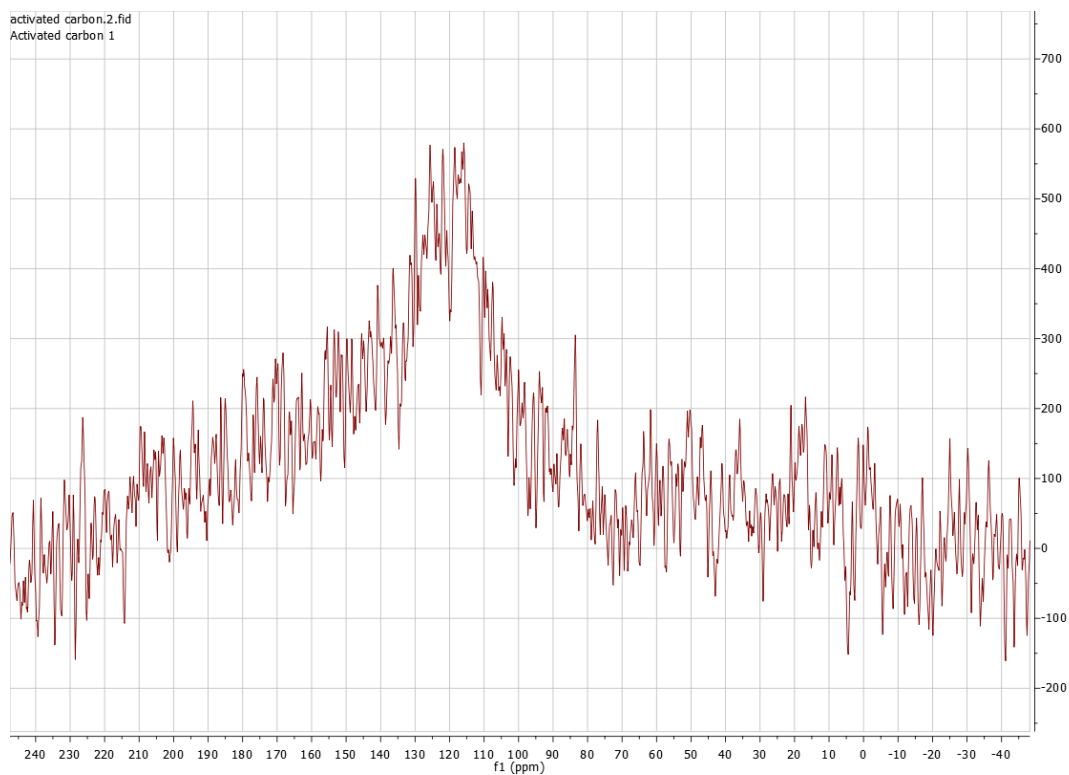
D) Oxygen XPS of A500



E) Carbon XPS of A800

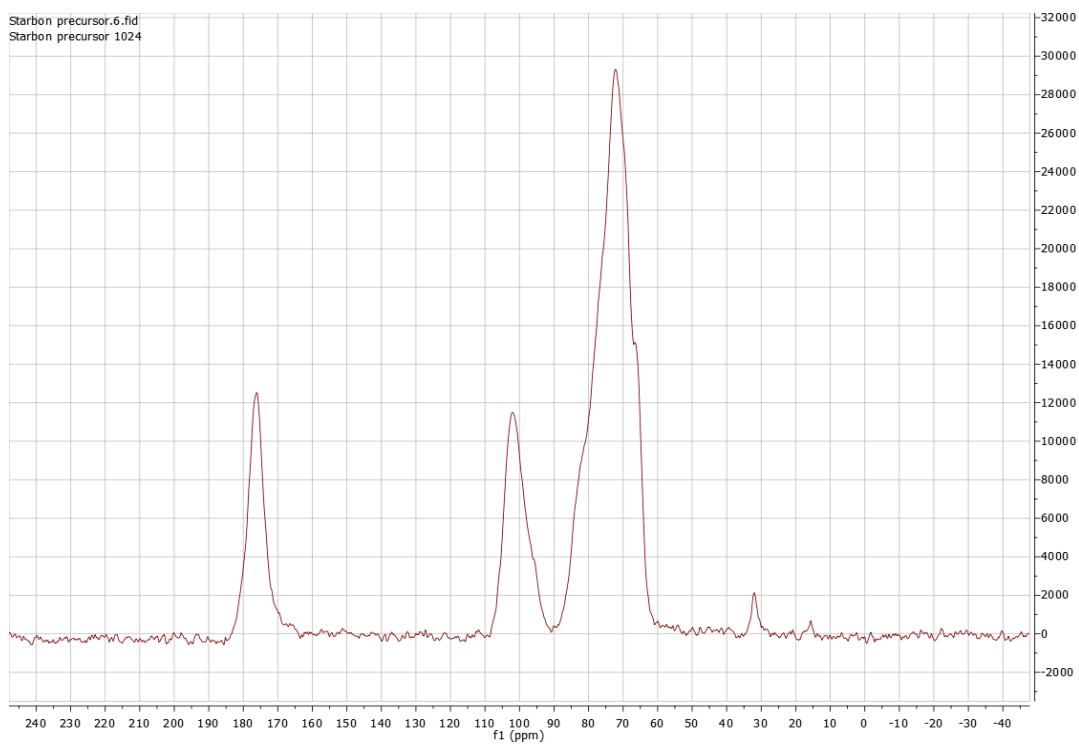


F) Oxygen XPS of A800



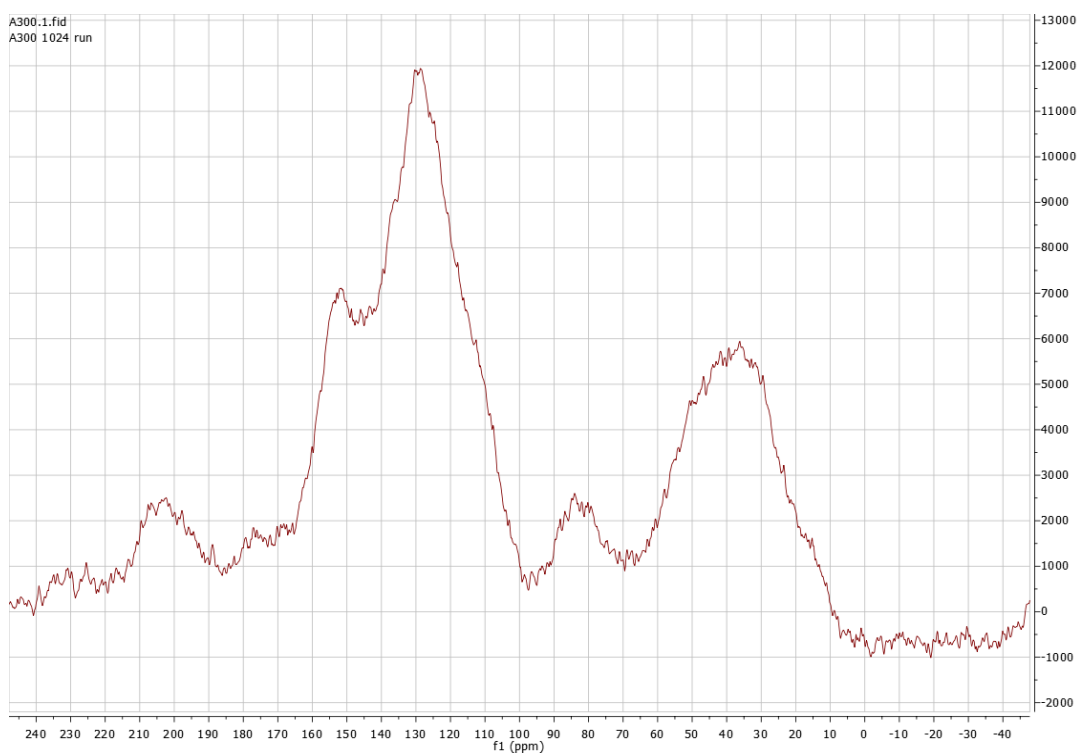
Activated carbon: ¹³C NMR δ 120

Figure 78. ¹³C NMR of AC.



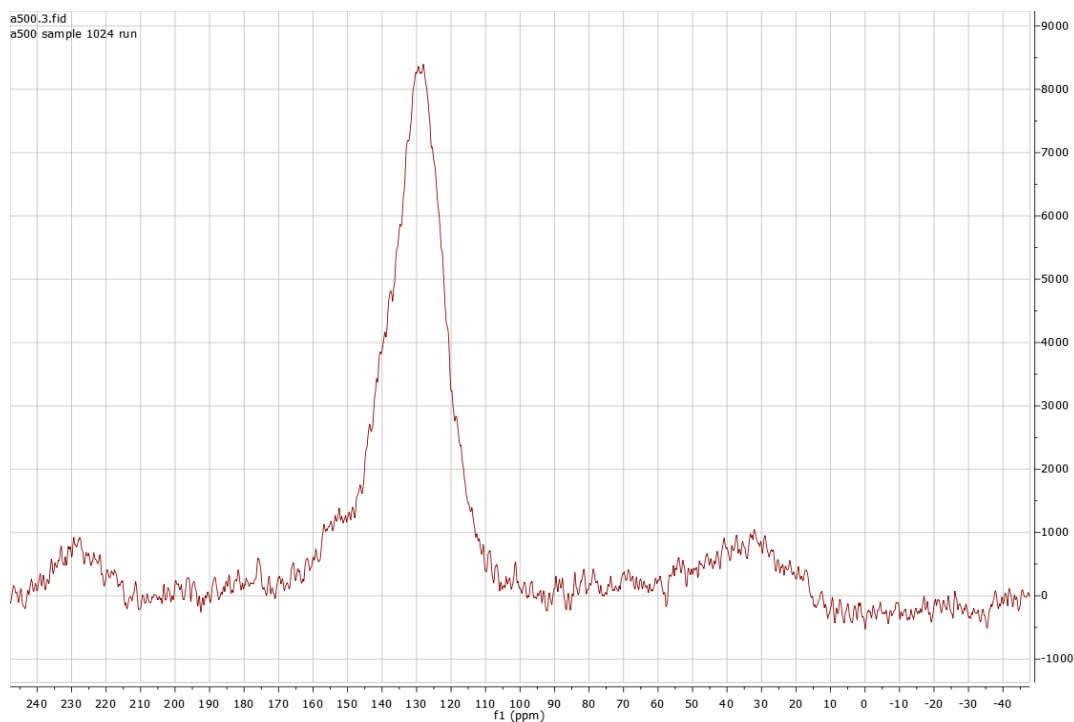
Starbon A00: ^{13}C NMR δ 17, 33, 70, 104, 176

Figure 79. ^{13}C NMR of A00.



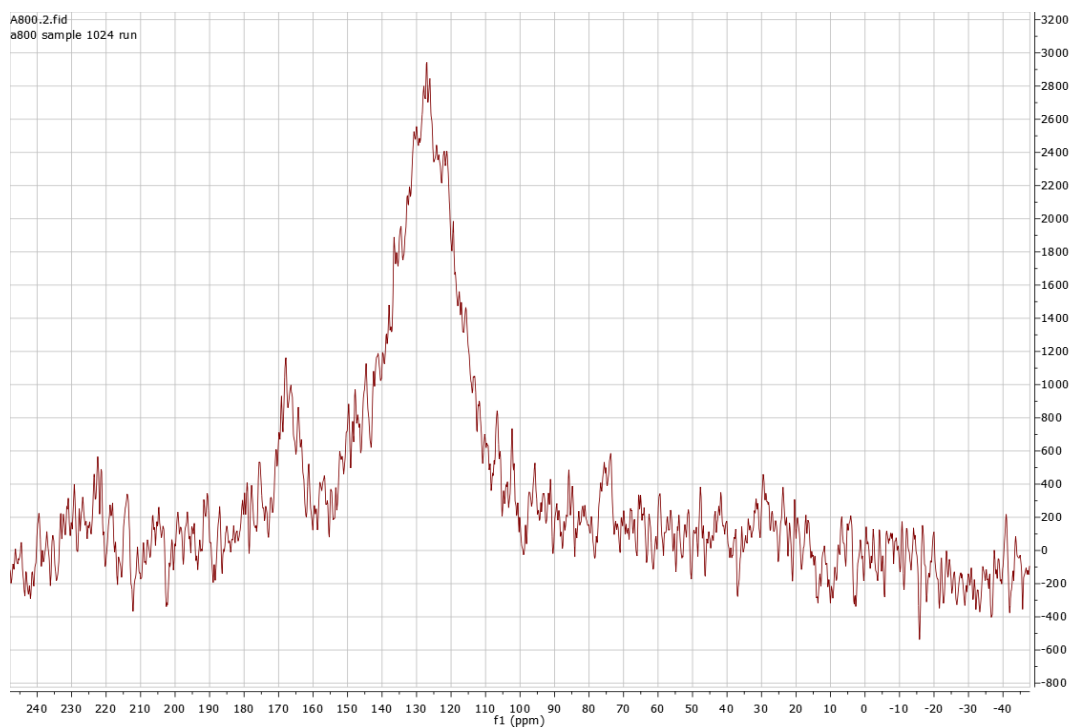
Starbon A300: ^{13}C NMR δ 17, 32-48, 80-85, 130, 151, 205

Figure 80. ^{13}C NMR of A300.



Starbon A500: ^{13}C NMR δ 32, 129, 230

Figure 81. C13 NMR of A500.



Starbon A800: ^{13}C NMR δ 128, 165

Figure 82. C13 NMR of A800.

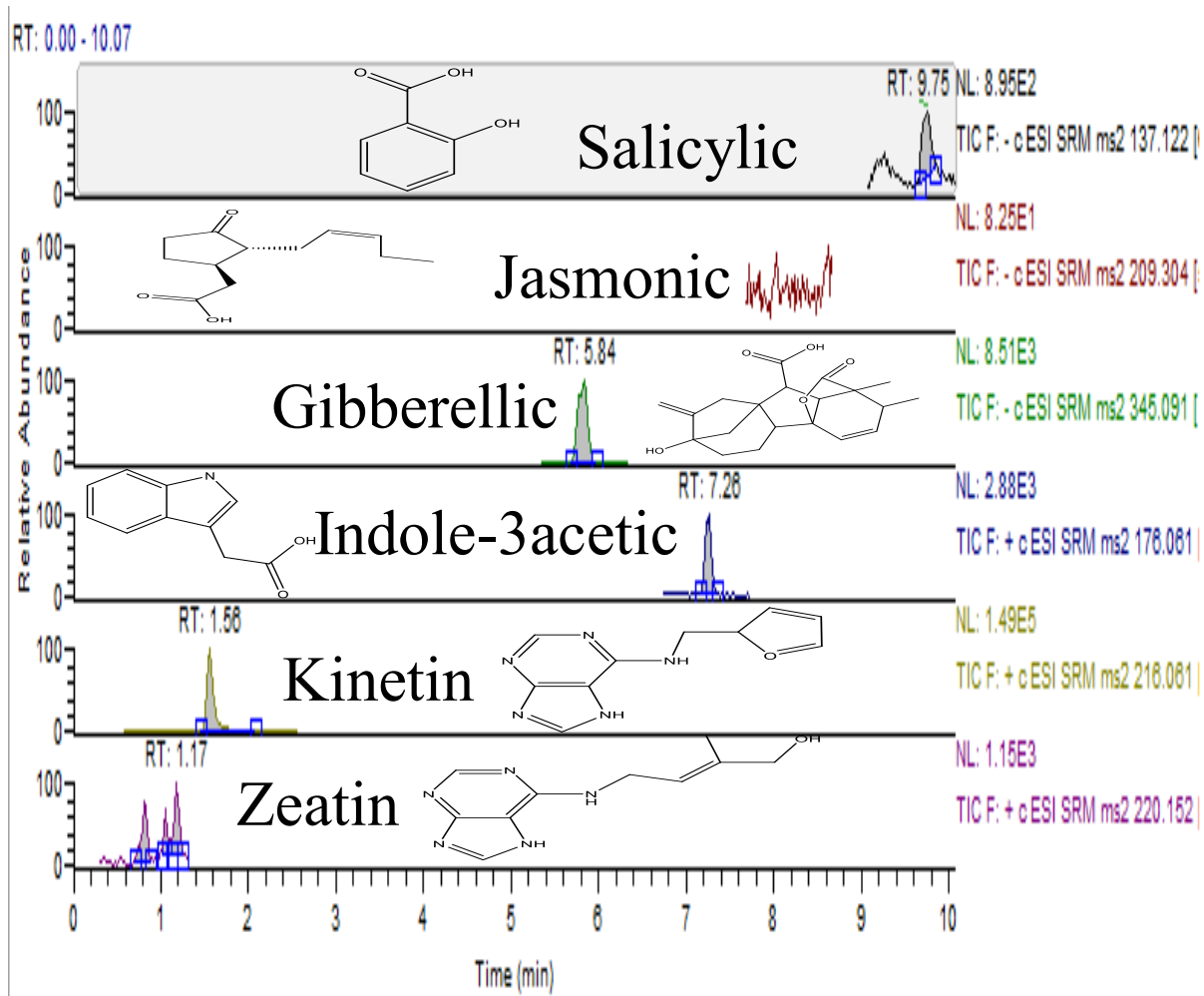


Figure 83. Identification of key plant hormone peaks

7 Abbreviations

- μL Microliter
- A00 Starbons produced from Alginic acid before carbonisation
- A300 Starbons produced from Alginic acid carbonised at 300 °C
- A500 Starbons produced from Alginic acid carbonised at 500 °C
- A800 Starbons produced from Alginic acid carbonised at 800 °C
- AA Alginic acid
- ABA Abscisic acid
- AC Activated carbon
- ANOVA Analysis of variance
- BET Bruauer Emmett Teller
- E Energy (kJ mol)
- GA Gibberellic acid
- HPLC High performance liquid chromatography
- IAA Indole-3-acetic acid
- ICP Inductively charged plasma
- JA Jasmonic acid
- KI Kinetin
- kV Kilo volt
- L Litre
- LC-MS Liquid chromatography mass spectrometry
- mA Milli amp
- mg Milligrams
- MM2 Molecular mechanics
- ppm Parts per million
- SA Salicylic acid
- SEM Scanning electron microscopy
- Starbons Starbons©
- TEM Transmission electron microscopy
- TGA Thermogravimetric analysis

- UV-vis Ultraviolet visible spectroscopy
- XPS X-Ray photoelectron spectroscopy
- ZE Zeatin

8 References

Parts of this work has been published in the work “Kinetic and Desorption Study of Selected Bioactive Compounds on Mesoporous Starbons: A Comparison with Microporous-Activated Carbon” *ACS Omega* 2018, **3**, 12, 18361-18369

- 1 P. Gerland, A. E. Raftery, H. Sevčiková, N. Li, D. Gu, T. Spoorenberg, L. Alkema, B. K. Fosdick, J. Chunn, N. Lalic, G. Bay, T. Buettner, G. K. Heilig and J. Wilmoth, *Science*, 2014, **346**, 234–7.
- 2 <http://www.un.org/sustainabledevelopment/sustainable-development-goals/>, (accessed 16 March 2016).
- 3 A. Ghosh, V. J. Singh, S. Gampala and S. K. Chakraborti, *Environ. Ecol.*, 2016, **34**, 2088–2092.
- 4 M. D. Madsen, K. W. Davies, C. S. Boyd, J. D. Kerby and T. J. Svejcar, *Restor. Ecol.*, 2016, **24**, 77–84.
- 5 J. M. Scott, *J. Crop Prod.*, 2008, **1**, 197–220.
- 6 http://wildweb.co.za/CLIENTS/AdvanceSeed/seed_coating.php (accessed 22.02.2016).
- 7 US pat, US4779376, 1986.
- 8 US pat. US20050004299A1, US20050004299A1, 2004.
- 9 US pat, US5623781A, US5623781A, 1997.
- 10 US pat, US4802305, 1989.
- 11 STARBONS®: Preparation, applications and transition from laboratory curiosity to scalable product, <http://www.nsti.org/procs/Nanotech2011v3/11/W5.162>, (accessed 17 May 2016).
- 12 H. L. Parker, A. J. Hunt, V. L. Budarin, P. S. Shuttleworth, K. L. Miller and J. H. Clark, in *RSC Advances*, 2012, vol. 2, p. 8992.
- 13 A. Muñoz García, A. J. Hunt, V. L. Budarin, H. L. Parker, P. S. Shuttleworth, G. J. Ellis and J. H. Clark, in *Green Chem.*, Royal Society of Chemistry, 2015, vol. 17, pp. 2146–2149.
- 14 P. S. Shuttleworth, V. Budarin, R. J. White, V. M. Gun'ko, R. Luque and J. H. Clark, *Chemistry*, 2013, **19**, 9351–7.
- 15 V. Budarin, J. H. Clark, J. J. E. Hardy, R. Luque, K. Milkowski, S. J. Tavener and A. J. Wilson, in *Angewandte Chemie*, 2006, vol. 118, pp. 3866–3870.
- 16 L. Pereira, *J. Liq. Chromatogr. Relat. Technol.*, 2008, **31**, 1687–1731.

- 17 A. M. Aljeboree, A. N. Alshirifi and A. F. Alkaim, in *Arabian Journal of Chemistry*, King Saud University, 2014, vol. 1, pp. 1–13.
- 18 Y. Aldegs, M. Elbarghouthi, A. Elsheikh and G. Walker, *Dye. Pigment.*, 2008, **77**, 16–23.
- 19 K. Choy, J. F. Porter and G. Mckay, *Adsorption*, 2001, **7**, 231–247.
- 20 A. Dada, Olalekan, A. M. Olatunya and Dada, in *IOSR Journal of Applied Chemistry*, vol. 3, pp. 2278–5736.
- 21 A. Lecloux and J. . Pirard, *J. Colloid Interface Sci.*, 1979, **70**, 265–281.
- 22 Younghun Kim, Changmook Kim, Inhee Choi, A. Selvaraj Rengaraj and J. Yi, *Environ. Sci. Technol.*, 2004, **38**, 924–931.
- 23 T. Horikawa, D. D. Do and D. Nicholson, *Adv. Colloid Interface Sci.*, 2011, **169**, 40–58.
- 24 A. Delavari and R. Baltus, *Membranes (Basel)*, 2017, **7**, 42.
- 25 K. S. W. Sing, in *Pure and Applied Chemistry*, 1985, vol. 57, pp. 603–619.
- 26 R. Zsigmondy, *Zeitschrift für Anorg. Chemie*, 1911, **71**, 356–377.
- 27 M. M. Dubinin, I. T. Erashko, O. Kadlec, V. I. Ulin, A. M. Voloshchuk and P. P. Zolotarev, *Carbon N. Y.*, 1975, **13**, 193–200.
- 28 O. Hamdaoui and E. Naffrechoux, in *Journal of Hazardous Materials*, 2007, vol. 147, pp. 381–394.
- 29 J. H. de Boer, in *The Structure and properties of porous materials*, ed. London, Butterworths, v10 edn., 1958, p. 68.
- 30 D.Do, in *Adsorption Analysis: Equilibria and Kinetics*, 1998, pp. 337–414.
- 31 A. Da, Browski, P. Podkocielny and E. Al, *Chemosphere*, 2005, **58**, 1049–1070.
- 32 Y. C. Wong, Y. S. Szeto, A. W. H. Cheung and G. McKay, *Langmuir*, 2003, **19**, 7888–7894.
- 33 V. C. Srivastava, M. M. Swamy, I. D. Mall, B. Prasad and I. M. Mishra, *Colloids Surfaces A Physicochem. Eng. Asp.*, 2006, **272**, 89–104.
- 34 R. J. White, V. Budarin, R. Luque, J. H. Clark and D. J. Macquarrie, *Chem. Soc. Rev.*, 2009, **38**, 3401–18.
- 35 H. L. Parker, PhD thesis, University of York, 2013.
- 36 A. Borisova, PhD thesis, University of York, 2015.
- 37 K. H. Ku, J. M. Shin, D. Klinger, S. G. Jang, R. C. Hayward, C. J. Hawker and B. J. Kim, *ACS Nano*, 2016, **10**, 5243–5251.
- 38 F. A. Nichols, *J. Nucl. Mater.*, 1969, **30**, 143–165.

- 39 A. A. and T. V. Kenneth R. Hall, Lee C. Eagleton, *Ind. Eng. Chem. Fundamen*, 1966, **5**, 212–223.
- 40 P. Schneider, *Appl. Catal. A Gen.*, 1995, **129**, 157–165.
- 41 S. Liu, *J. Colloid Interface Sci.*, 2015, **450**, 224–238.
- 42 W. D. Cornell, P. Cieplak, C. I. Bayly, I. R. Gould, K. M. Merz, D. M. Ferguson, D. C. Spellmeyer, T. Fox, J. W. Caldwell and P. A. Kollman, *J. Am. Chem. Soc.*, 1995, **117**, 5179–5197.
- 43 J. Björk, F. Hanke, C.-A. Palma, P. Samori, M. Cecchini and M. Persson, *J. Phys. Chem. Lett.*, 2010, **1**, 3407–3412.
- 44 Y. Ho and G. Mckay, *Process Saf. Enviromental Prot.*, 1998, **76**, 332–340.
- 45 C. Aharoni and M. Ungarish, *J. Chem. Soc.*, 1977, **73**, 456.
- 46 G. J. Leigh, in *Catalysts for Nitrogen Fixation*, Springer Netherlands, Dordrecht, 2004, pp. 33–54.
- 47 T. Kandemir, M. E. Schuster, A. Senyshyn, M. Behrens and R. Schlögl, *Angew. Chemie Int. Ed.*, 2013, **52**, 12723–12726.
- 48 S. Alberti, G. J. A. A. Soler-Illia and O. Azzaroni, *Chem. Commun. (Camb)*., 2015, **51**, 6050–75.
- 49 H. Spahn and E. U. Schlünder, *Chem. Eng. Sci.*, 1975, **30**, 529–537.
- 50 Chi-Wai Hui, A. Buning Chen and G. McKay*, *Langmuir*, 2003, 4188–4196.
- 51 <https://greenrushedaily.com/cultivation/germinating-cannabis-seeds/>(accessed 12/01/2019),.
- 52 G. Réidei, *Bibliogr. Genet.*, 1970, **20**, 1–151.
- 53 D. De Vleeschauwer, J. Xu and M. HÄfte, *Front. Plant Sci.*, , DOI:10.3389/fpls.2014.00611.
- 54 C. Vanhee, G. Zapotoczny, D. Masquelier, M. Ghislain and H. Batoko, *Plant Cell*, 2011, **23**, 785–805.
- 55 Inna Punda, *Sugar Beet White Sugar*, FAO Investment Centre Division, 1st edn., 2009.
- 56 L. Cox, W. C. Koskinen and P. Y. Yen, *J. Agric. Food Chem.*, 1997, 1468–1472.
- 57 M. Miransari and D. L. Smith, in *Environmental and Experimental Botany*, Elsevier B.V., 2014, vol. 99, pp. 110–121.
- 58 J. D. Bewley, *Plant Cell Am. Soc. Plant Physiol.*, 1997, **9**, 1055–1.
- 59 A. G. Taylor and G. E. Harman, in *Annual Review of Phytopathology*, 1990, vol. 28, pp. 321–339.
- 60 Y. Liu, PhD thesis, Hunan Agricultural University, 1996.

- 61 S. Scheffknecht, R. Mammerler, S. Steinkellner and H. Vierheilig, *Mycorrhiza*, 2006, **16**, 365–370.
- 62 H. H. Zhu and Q. Yao, *J. Phytopathol.*, 2004, **152**, 537–542.
- 63 US pat, US4249343A, 1979.
- 64 J. M. Scott, *Adv. Agron.*, 1989, **42**, 43–83.
- 65 M. Black and J. D. Bewley, in *Seed technology and its biological basis*, Sheffield Academic Press, 2000, pp. 257–287.
- 66 S. Pedrini, D. J. Merritt, J. Stevens and K. Dixon, *Trends Plant Sci.*, 2017, **22**, 106–116.
- 67 P. Halmer, *Acta Hortic.*, 2008, **0**, 17–26.
- 68 S. Sedagathoor, *Acta Hortic.*, 2008, **0**, 27–31.
- 69 M. D. Madsen, K. W. Davies, D. L. Mummey and T. J. Svejcar, *Rangel. Ecol. Manag.*, 2014, **67**, 61–67.
- 70 Abscisic Acid, Ethylene, and Nontraditional Hormones, <https://www.boundless.com/biology/textbooks/boundless-biology-textbook/plant-form-and-physiology-30/plant-sensory-systems-and-responses-184/abscisic-acid-ethylene-and-nontraditional-hormones-705-11930/>, (accessed 26 October 2015).
- 71 M. J. Chrispeels and J. E. Varner, *PLANT Physiol.*, 1967, **42**, 398–406.
- 72 Y. Huang, S. Cai, L. Ye, H. Hu, C. Li and G. Zhang, *Food Chem.*, 2016, **192**, 928–933.
- 73 W. M. Gray, *PLoS Biol.*, 2004, **2**, E311.
- 74 C. O. Miller, F. Skoog, M. H. Von Saltza and F. M. Strong, in *J. Amer. Ghent. Soc.*, 1955, vol. 77, p. 1392.
- 75 G. E. Budge, D. Garthwaite, A. Crowe, N. D. Boatman, K. S. Delaplane, M. A. Brown, H. H. Thygesen and S. Pietravalle, *Sci. Rep.*, 2015, **5**, 12574.
- 76 US pat, US20090093365, 2009.
- 77 US pat, US6329319, 2001.
- 78 US pat, US7003914, 2006.
- 79 A. Servin, W. Elmer, A. Mukherjee, R. De la Torre-Roche, H. Hamdi, J. C. White, P. Bindraban and C. Dimkpa, *J. Nanoparticle Res.*, 2015, **17**, 92.
- 80 M. I. Williams, R. K. Dumroese, D. S. Page-Dumroese and S. P. Hardegree, *J. Arid Environ.*, 2016, **125**, 8–15.
- 81 A. Campos, C. Silva-Neto, A. Seleguini and P. Fernandes, *Sci. Agropecu.*, 2016, **6**, 325–328.
- 82 L. Gorim and F. Asch, *Funct. Plant Biol.*, 2015, **42**, 209.

- 83 US pat, US8551917, 2013.
- 84 M. D. Madsen, K. W. Davies, D. L. Mummey and T. J. Svejcar, *Rangel. Ecol. Manag.*, 2014, **67**, 61–67.
- 85 P. T. Anastas, *ChemSusChem*, 2009, **2**, 391–392.
- 86 M. J. Mulvihill, E. S. Beach, J. B. Zimmerman and P. T. Anastas, *Annu. Rev. Environ. Resour.*, 2011, **36**, 271–293.
- 87 W. Libbrecht, A. Verberckmoes, J. W. Thybaut, P. Van Der Voort and J. De Clercq, *Langmuir*, 2017, **33**, 6769–6777.
- 88 G. Sethia and A. Sayari, *Carbon N. Y.*, 2016, **99**, 289–294.
- 89 F. Wang, Y. Qiu, B.-J. Wang, H.-L. Wang and Y.-T. Long, *RSC Adv.*, 2016, **6**, 100519–100525.
- 90 Y. Cheng, X. Zeng, D. Cheng, X. Xu, X. Zhang, R.-X. Zhuo and F. He, *Colloids Surfaces B Biointerfaces*.
- 91 A. S. Marriott, A. J. Hunt, E. Bergström, J. Thomas-Oates and J. H. Clark, *J. Anal. Appl. Pyrolysis*, 2016, **121**, 62–66.
- 92 A. K. Bajpai and M. Rajpoot, in *Journal of Scientific and Industrial Research*, 1999, vol. 58, pp. 844–860.
- 93 J. L. Figueiredo, *J. Mater. Chem. A*, 2013, **1**, 9351.
- 94 W. Yang, Queens university, 2016.
- 95 M. Enterría and J. L. Figueiredo, *Carbon N. Y.*, 2016, **108**, 79–102.
- 96 J. Rivera-Utrilla, I. Bautista-Toledo, M. A. Ferro-García and C. Moreno-Castilla, *J. Chem. Technol. Biotechnol.*, 2001, **76**, 1209–1215.
- 97 D. K. Heyse, in *Practice*, 2003, vol. 1, p. 36.
- 98 L. Li, P. A. Quinlivan and D. R. U. Knappe, in *Carbon*, 2002, vol. 40, pp. 2085–2100.
- 99 J. Rivera-Utrilla, I. Bautista-Toledo, M. A. Ferro-García and C. Moreno-Castilla, *J. Chem. Technol. Biotechnol.*, 2001, **76**, 1209–1215.
- 100 N. Mu'azu, N. Jarrah, M. Zubair and O. Alagha, *Int. J. Environ. Res. Public Health*, 2017, **14**, 1094.
- 101 Y. Bulut and H. Aydın, *Desalination*, 2006, **194**, 259–267.
- 102 M. SAÑ NCHÉZ-POLO AND J. RIVERA-UTRILLA, *Environ. Sci. Technol.*, 2002, 3850–3854.
- 103 S. L. Goertzen, K. D. Thériault, A. M. Oickle, A. C. Tarasuk and H. A. Andreas, *Carbon N. Y.*, 2010, **48**, 1252–1261.
- 104 A. M. Oickle, S. L. Goertzen, K. R. Hopper, Y. O. Abdalla and H. A. Andreas, *Carbon N. Y.*, 2010, **48**, 3313–3322.
- 105 A. Contescu, C. Contescu, K. Putyera and J. A. Schwarz, *Carbon N. Y.*,

- 1997, **35**, 83–94.
- 106 A. Contescu, C. Contescu, K. Putyera and J. A. Schwarz, *Carbon N. Y.*, 1997, **35**, 83–94.
- 107 H. P. Boehm, *Carbon N. Y.*, 1994, **32**, 759–769.
- 108 V. Fierro, V. Torné-Fernández, D. Montané and A. Celzard, in *Microporous and Mesoporous Materials*, 2008, vol. 111, pp. 276–284.
- 109 G. Limousin, J.-P. Gaudet, L. Charlet, S. Szenknect, V. Barthès and M. Krimissa, *Appl. Geochemistry*, 2007, **22**, 249–275.
- 110 T. Yavini, T. D. Yavini, M. H. Yunusa, K. G. Atiku, A. A. Musa and P. K. Ruth, *J. Fundam. Appl. Sci.*, 2017, **9**, 354–377.
- 111 C. Tien and B. V. Ramarao, in *Separation Science and Technology*, Taylor & Francis, 2016, vol. 00, pp. 1–12.
- 112 J. Simonin, *Chem. Eng. J.*, 2016, **300**, 254–263.
- 113 Y. S. Ho and G. McKay, *Pseudo-second order model for sorption processes*, 1999, vol. 34.
- 114 Y. S. Ho and G. McKay, *Process Biochem.*, 1999, **34**, 451–465.
- 115 S. J. Allen, G. McKay and J. F. Porter, *J. Colloid Interface Sci.*, 2004, **280**, 322–33.
- 116 Y.-S. S. Ho, *J. Hazard. Mater.*, 2006, **136**, 681–689.
- 117 R. K. Chakrapani C, Babu C, Vani K, *E-Journal Chem.*, 2010, **7**, 419–427.
- 118 S. M. Yakout and E. Elsherif, *Carbon – Sci. Tech*, 2010, **1**, 144–153.
- 119 C. Wu, L. Tseng and S. Juang, *Chem. Eng. J.*, 2009, **150**, 366–373.
- 120 Y. Liu and L. Shen, *Langmuir*, 2008, **24**, 11625–11630.
- 121 H. L. Parker, V. L. Budarin, J. H. Clark and A. J. Hunt, *ACS Sustain. Chem. Eng.*, 2013, **1**, 1311–1318.
- 122 K. Y. Foo and B. H. Hameed, *Chem. Eng. J.*, 2010, **156**, 2–10.
- 123 J. H. C. A. Basar, *Mater*, 2006, **135**, 232–241.
- 124 X. Chen and Xunjun, *Information*, 2015, **6**, 14–22.
- 125 C. Nguyen and D. Do, *Carbon N. Y.*, 2001, **39**, 1327–1336.
- 126 B. J. Marsh, H.; Rand, *Colloid Interface Sci*, 1970, **33**, 101.
- 127 D. D. Do and C. Nguyen, *Carbon N. Y.*, 2000, 894–896.
- 128 D.D.Do, in *Adsorption analysis: Equilibria and kinetics*, 1998, pp. 337–679.
- 129 P. Saha and S. Chowdhury, in *Thermodynamics*, InTech, 2011, pp. 349–359.

- 130 Y. Xu and B. Chen, *Bioresour. Technol.*, 2013, **146**, 485–93.
- 131 E. Fortunati, G. Giovanale, F. Luzi, A. Mazzaglia, J. Kenny, L. Torre and G. Balestra, *Coatings*, 2017, **7**, 196.
- 132 R. V. L. Joosen, J. Kodde, L. A. J. Willems, W. Ligterink, L. H. W. Van Der Plas and H. W. M. Hilhorst, in *Plant Journal*, 2010, vol. 62, pp. 148–159.
- 133 P. Benard, E. Kroener, P. Vontobel, A. Kaestner and A. Carminati, *Adv. Water Resour.*, 2016, **95**, 190–198.
- 134 K. Kaiser and G. Guggenberger, *Eur. J. Soil Sci.*, 2003, **54**, 219–236.
- 135 J.-Y. Parlange, *Geophys. Surv.*, 1974, **1**, 357–387.
- 136 I. Gaurav Society of Agricultural Research Information Centre (Hisar, F. M. Nezhad and A. R. Golparvar, *Res. Crop.*, 2017, **18**, 340–342.
- 137 <http://www.landis.org.uk/soilscapes/soilguide.cfm> (accessed 30 August 2017).
- 138 S. pulp paper and board testing Committee, 2000, vol. 0, pp. 1–5.
- 139 A. Hunt, *Adv. Water Resour.*, 2004, **27**, 175–183.
- 140 E. Forgács, *J. Chromatogr. A*, 2002, **975**, 229–243.
- 141 D. Y. Wang, D. H. Yan, X. S. Song and H. Wang, *Adv. Mater. Res.*, 2014, **941–944**, 952–955.
- 142 C. J. Barrow, *Appl. Geogr.*, 2012, **34**, 21–28.
- 143 J. Malamy, J. P. Carr, D. F. Klessig and I. Raskin, *Science (80-.)*, 1990, **250**, 1002–1004.
- 144 J. Lee, J. Nam, H. C. Park, G. Na, K. Miura, J. B. Jin, C. Y. Yoo, D. Baek, D. H. Kim, J. C. Jeong, D. Kim, S. Y. Lee, D. E. Salt, T. Mengiste, Q. Gong, S. Ma, H. J. Bohnert, S.-S. Kwak, R. A. Bressan, P. M. Hasegawa and D.-J. Yun, *Plant J.*, 2006, **49**, 79–90.
- 145 J. Malamy and D. F. Klessig, *Plant J.*, 1992, **2**, 643–654.
- 146 R. A. Creelman and J. E. Mullet, *Annu. Rev. Plant Physiol. Plant Mol. Biol.*, 1997, **48**, 355–381.
- 147 B. Kucera, M. A. Cohn and et al, *Seed Sci. Res.*, 2005, **15**, 281–307.
- 148 J. Immanen, K. Nieminen and E. Al, *Curr. Biol.*, 2016, **1**, 1–8.
- 149 Synthesis and Biological Activity of New Watersoluble Cytokinins, <http://www.tandfonline.com/doi/pdf/10.1271/bbb.57.803>, (accessed 17 December 2015).
- 150 E. Farrow, S. C. Farrow and R. N. Emery, *Farrow and Emery Plant Methods*, 2012, **8**, 42.
- 151 S. Yadav, S. K. Bhatia and M. S. Student, *Int. J. Pure App. Biosci*, 2018, **6**, 1142–1147.

- 152 W. S. Dilip, D. Singh, D. Moharana, S. Rout and S. S. Patra, *J. Sci. Agric.*, 2017, **1**, 62–69.
- 153 N. A. Aziz, N. S. Abdullah, F. Plantation, U. Teknologi, M. Pahang, B. Tun and A. Razak, in *American-Eurasian J. Agric. & Environ. Sci*, 2016, vol. 16, pp. 1378–1382.
- 154 M. Younes, P. Aggett, F. Aguilar, R. Crebelli, M. Filipič, M. J. Frutos, P. Galtier, D. Gott, U. Gundert-Remy, G. G. Kuhnle, C. Lambré, J. Leblanc, I. T. Lillegaard, P. Moldeus, A. Mortensen, A. Oskarsson, I. Stankovic, I. Waalkens-Berendsen, R. A. Woutersen, M. Wright, L. Brimer, O. Lindtner, P. Mosesso, A. Christodoulidou, Z. Horváth, F. Lodi, B. Dusemund and B. Dusemund, *EFSA J.*, 2017, **15**, 1.
- 155 H. J. Keselman, C. J. Huberty, L. M. Lix, S. Olejnik, R. A. Cribbie, B. Donahue, R. K. Kowalchuk, L. L. Lowman, M. D. Petoskey, J. C. Keselman and J. R. Levin, *Rev. Educ. Res.*, 1998, **68**, 350–386.
- 156 T. H. Wonnacott, R. J. Wonnacott and W. John Wiley, *Introductory statistics fifth edition 1 The Nature of Statistics*, Fifth edit.
- 157 S. Y. Quek and B. Al-Duri, *Chem. Eng. Process. Process Intensif.*, 2007, **46**, 477–485.